UNIVERSITAT POLITÈCNICA DE VALÈNCIA

Departamento de Máquinas y Motores Térmicos

DOCTORAL THESIS

"A non-linear quasi-3D model for air management modelling in engines"

Presented by: Mr. Manuel Hernández Marco
Supervised by: Dr. Antonio J. Torregrosa Huguet

in fulfilment of the requirements for the degree of

Doctor of Philosophy

Valencia, May 2018

Doctoral Thesis

"A non-linear quasi-3D model for air management modelling in engines"

Presented by: Mr. Manuel Hernández Marco
Supervised by: Dr. Antonio J. Torregrosa Huguet

THESIS EXAMINERS

Dr. Angelo Onorati
Dr. Gianluca Montenegro
Dr. Jorge Luis Parrondo Gayo

DEFENCE COMMITTEE

Chairman: Dr. Alberto Broatch Jacobi
Secretary: Dr. Francisco Vera García
Member: Dr. Angelo Onorati

Valencia, May 2018

Abstract

Engine modelling has become an essential tool in the design of internal combustion engines, allowing considerable reductions in development time and cost. Classical design methodologies are based on prototype manufacturing and trial-and-error tests, but currently, most of those tests have been replaced by numerical computations, so that only the most promising design options are actually tested on engine bench.

For years, one-dimensional gas dynamics codes in the time domain have offered sufficiently good solutions for modelling both engine performance and intake and exhaust noise. However, for a more demanding level of design, a 1D representation may not be sufficient to describe accurately the flow in certain elements. This is especially important in the case of silencers, where the one-dimensional assumption can only be applied to simple geometries and, even in that case, suitable results can only be obtained for frequencies below the cut-off frequency of higher order modes. In the case of duct junctions, the existence of complex 3D flow structures is what sets the applicability limit for a simple zero-dimensional description. In view of these limitations, the first option would typically be the use of a computational fluid dynamics (CFD) model; however, the application of such a model to a complete intake or exhaust system entails an excessive computational time.

A possible compromise solution is given by quasi-3D models, based on three-dimensional schemes, but with certain simplifications able to significantly reduce the calculation time without excessively affecting the accuracy. Such solutions have become standard in commercial codes and have been successfully applied to silencers with perforated tubes and absorbing material, both in the linear acoustic regime and in real engine conditions, typically non-linear.

The objective of this thesis is the development a new quasi-3D numerical method in a staggered-grid, based on the simplification of the momentum equation, to be included in an existing one-dimensional code. Such method however, is not hassle free. In particular, it is affected by the appearance of non-physical oscillations, specially near significant pressure gradients. From the literature review it is determined that this behaviour is typical among second-order schemes and it can be aggravated by the simplifications adopted. After researching the possible solutions to face this problem, three different flux limiters are developed, based on the MDT (momentum diffusion term), FCT (flux corrected transport) and TVD (total variation diminishing) methodologies. In the case of the two latter methods, its effectiveness is well established for finite

differences schemes, thus defining a clear improving line for quasi-3D models.

Once the numerical method is defined and its stability assured, proper boundary conditions that allow its use must be developed. With this objective, a pressure pulse inlet and an anechoic termination boundary condition are developed, which allow the simulation of an impulse test rig. It should not be forgotten, however, that the ultimate objective is the connection with a one-dimensional code, therefore the compatibility of the quasi-3D numerical method created with the existing one-dimensional methods has to be tested, showing some preliminary results.

Eventually, with a fully operative method, the validation process for the applications which it has been mainly developed for, takes place, namely, mufflers and duct junctions modelling. In the case of mufflers, increasingly complex devices are modelled, from constant section geometries to real geometry systems. The results obtained are validated with both linear and non-linear tools. In the case of duct junctions, the main objective is to establish the potential of the new numerical method against the traditional one-dimensional schemes, consequently, results from both approaches are compared to experimental measures, obtaining promising results.

Resumen

El modelado se ha convertido en los últimos años en una herramienta esencial en el diseño de motores de combustión interna alternativos, ya que permite reducir considerablemente el tiempo y los costes de desarrollo. Las metodologías de diseño clásicas se basan en la fabricación de prototipos y la realización de pruebas de ensayo y error. Actualmente, la mayoría de estas pruebas han sido sustituidas por cálculos numéricos, de modo que sólo las opciones de diseño más prometedoras se prueban en realidad en banco motor.

Durante años, los códigos unidimensionales de dinámica de gases en el dominio del tiempo han sido suficientes para modelar tanto las prestaciones y el consumo del motor como el ruido de admisión y escape. Sin embargo, para un nivel más exigente de diseño, una representación 1D puede no ser suficiente para describir con precisión el flujo en ciertos elementos. Esto es especialmente importante en el caso de silenciadores, donde la hipótesis unidimensional sólo se puede aplicar a geometrías simples e, incluso en ese caso, sólo se pueden obtener resultados adecuados para frecuencias inferiores a la frecuencia de corte de los modos de orden superior. En el caso de las uniones de conductos es la existencia de estructuras tridimensionales de flujo complejas lo que establece el límite de la aplicabilidad de una descripción simple cero-dimensional. En vista de estas limitaciones, la primera opción sería típicamente el uso de un modelo de dinámica de fluidos computacional (CFD); sin embargo, la aplicación de un modelo de este tipo para un sistema de admisión o de escape completo conlleva un tiempo de cálculo excesivo.

Una posible solución de compromiso alternativa viene dada por los modelos cuasi-3D, basados en esquemas tridimensionales, pero con ciertas simplificaciones capaces de reducir significativamente el tiempo de cálculo sin afectar excesivamente a la precisión. Tales soluciones se han convertido en estándar en los códigos comerciales y se han aplicado con éxito a los silenciadores con tubos perforados y materiales absorbentes, tanto para excitaciones acústicas en el régimen lineal como en condiciones reales de motor, típicamente no lineales.

Esta tesis tiene como objetivo el desarrollo de un nuevo método numérico cuasi-3D en una malla escalonada, basado en la simplificación de la ecuación de la cantidad de movimiento, para ser incluido en un código unidimensional existente. Tal método, sin embargo, no está libre de inconvenientes. En particular, se ve afectado por la aparición de oscilaciones no físicas, especialmente en gradientes de presión significativos. De la revisión bibliográfica se determina que este comportamiento es típico en esquemas de segundo orden y se puede ver acentuado por las simplificaciones adoptadas. Tras estudiar las

posibles soluciones aplicables a este problema, se desarrollan tres limitadores de flujo diferentes, basados en las metodologías MDT (momentum diffusion term), FCT (flux corrected transport) y TVD (total variation diminishing). En el caso de los dos últimos métodos, su efectividad está bien establecida para los esquemas de diferencias finitas, lo que define una clara vía de mejora para los modelos cuasi-3D.

Una vez definido el método numérico y asegurada su estabilidad, es necesario desarrollar las condiciones de contorno adecuadas que permitan su utilización. Con este objetivo, se desarrollan las condiciones de pulso de presión de entrada y de extremo anecoico, los cuales permiten simular un banco de impulso. No hay que olvidar, sin embargo, que el objetivo final es la conexión con un código unidimensional, por lo que hay que comprobar que el método numérico cuasi-3D creado es compatible con los unidimensionales existentes, mostrando algunos resultados preliminares.

Finalmente, con el método ya completamente operativo, se procede a su validación en las aplicaciones para las que ha sido diseñado principalmente, las cuales son, modelado de silenciadores y uniones de conductos. Para el caso de los silenciadores, se modelan dispositivos de complejidad creciente, pasando por geometrías de sección constante hasta sistemas con geometrías reales. Los resultados obtenidos se validan con otras herramientas tanto lineales como no lineales. En el caso de las uniones de conductos, el objetivo principal es el de establecer el potencial del nuevo método numérico frente a los tradicionales unidimensionales, por lo que los resultados de ambos se comparan con datos experimentales, obteniendo resultados prometedores.

Resum

El modelatge s'ha convertit en els últims anys en una eina essencial en el disseny de motors de combustió interna alternatius, ja que permet reduir considerablement el temps i els costos de desenvolupament. Les metodologies de disseny clàssiques es basen en la fabricació de prototips i la realització de proves d'assaig i error. Actualment, la majoria d'aquestes proves han sigut substituïdes per càlculs numèrics, de manera que només les opcions de disseny més prometedores es proven en realitat en banc motor.

Durant anys, els codis unidimensionals de dinàmica de gasos en el domini del temps han sigut suficients per a modelar tant les prestacions i el consum del motor com el soroll d'admissió i escapament. No obstant això, per a un nivell més exigent de disseny, una representació 1D pot no ser prou per a descriure amb precisió el flux en certs elements. Açò és especialment important en el cas de silenciadors, on la hipòtesi unidimensional només es pot aplicar a geometries simples i, inclús en eixe cas, només es poden obtindre resultats adequats per a freqüències inferiors a la freqüència de tall dels modes d'orde superior. En el cas de les unions de conductes és l'existència d'estructures tridimensionals de flux complexes el que establix el límit de l'aplicabilitat d'una descripció simple zero-dimensional. En vista d'estes limitacions, la primera opció seria típicament l'ús d'un model de dinàmica de fluids computacional (CFD); no obstant això, l'aplicació d'un model d'aquest tipus per a un sistema d'admissió o de escapament complet comporta un temps de càlcul excessiu.

Una possible solució de compromís alternativa ve donada pels models quasi-3D, basats en esquemes tridimensionals, però amb certes simplificacions capaços de reduir significativament el temps de càlcul sense afectar excessivament la precisió. Tals solucions s'han convertit en estàndard en els codis comercials i s'han aplicat amb èxit als silenciadors amb tubs perforats i materials absorbents, tant per a excitacions acústiques en el règim lineal com en condicions reals de motor, típicament no lineals.

Aquesta tesi té com a objectiu el desenvolupament d'un nou mètode numèric quasi-3D en una malla escalonada, basat en la simplificació de l'equació de la quantitat de moviment, per a ser inclòs en un codi unidimensional existent. Tal mètode, però, no està lliure d'inconvenients. En particular, es veu afectat per l'aparició d'oscil · lacions no físiques, especialment en gradients de pressió significatius. De la revisió bibliogràfica es determina que aquest comportament és típic en esquemes de segon ordre i es pot veure accentuat per les simplificacions adoptades. Després d'estudiar les possibles solucions aplicables a aquest problema, es desenvolupen tres limitadors de flux diferents, basats

en les metodologies MDT (momentum diffusion term) , FCT (flux corrected transport) i TVD (total variation diminishing) . En el cas dels dos últims mètodes, la seua efectivitat està ben establida per als esquemes de diferències finites, la qual cosa definix una clara via de millora per als models quasi-3D.

Una vegada definit el mètode numèric i assegurada la seua estabilitat, és necessari desenvolupar les condicions de contorn adequades que permeten la seua utilització. Amb aquest objectiu, es desenvolupen les condicions de pols de pressió d'entrada i d'extrem anecoic, els quals permeten simular un banc d'impuls. No cal oblidar, però, que l'objectiu final és la connexió amb un codi unidimensional, per la qual cosa cal comprovar que el mètode numèric cuasi-3D creat és compatible amb els unidimensionals existents, mostrant alguns resultats preliminars.

Finalment, amb el mètode ja completament operatiu, es procedix a la seua validació en les aplicacions per a les que ha sigut dissenyat principalment, les quals són, modelatge de silenciadors i unions de conductes. Per al cas dels silenciadors, es modelen dispositius de complexitat creixent, passant per geometries de secció constant fins a sistemes amb geometries reals. Els resultats obtinguts es validen amb altres eines tant lineals com no lineals. En el cas de les unions de conductes, l'objectiu principal és el d'establir el potencial del nou mètode numèric front als unidimensionals tradicionals, per la qual cosa els resultats d'ambdós es comparen amb dades experimentals, obtenint resultats prometedors.

List of publications

This thesis is based on the work contained in the following papers:

[1] A. Torregrosa, A. Broatch, F. Arnau, and M. Hernández. "A non-linear quasi-3D model with Flux-Corrected-Transport for engine gas-exchange modelling." *Journal of Computational and Applied Mathematics* 291 (2016), pp. 103–111

[2] A. Torregrosa, A. Broatch, F. Arnau, and M. Hernández. "On the effect of different flux limiters on the performance of an engine gas exchange gas-dynamic model." *International Journal of Mechanical Sciences* (2017)

[3] A. J. Torregrosa, A. Broatch, L. M. García-Cuevas, and M. Hernández. "A Study of the Transient Response of Duct Junctions: Measurements and Gas-Dynamic Modeling with a Staggered Mesh Finite Volume Approach." *Applied Sciences* 7(5) (2017), p. 480

Division of work between authors

The work leading up to this thesis was done in collaboration with other researchers. The respondent is the co-author of all papers on which this thesis is based, with the author signatures being in order of seniority. The respondent developed the numerical method and performed the models and experimental results post-processing presented here. Methodology and results discussion were performed in collaboration with supervisor, Prof. Torregrosa, as well as with the rest of co-authors. Experimental measurements were not performed by the respondent, and are thus gratefully acknowledged.

Other publications by the respondent

The following are publications in which the respondent has been involved during his doctorate studies, but are not included in the thesis.

[4] J. R. Serrano, F. J. Arnau, J. Martin, M. Hernandez, and B. Lombard. *Analysis of Engine Walls Thermal Insulation: Performance and Emissions.* SAE Technical Paper. 2015

Funding acknowledgements

The respondent wishes to acknowledge the financial support received through contract FPI-S2-2015-1064 of *Programa de Apoyo para la Investigación y Desarrollo* (PAID) of Universitat Politècnica de València.

Acknowledgments

First and foremost, I want to express my gratitude to my supervisor Prof. Torregrosa for his guidance and implication. I am sure this would not have been possible without his support and knowledge. This gratitude is also extended to all the members of CMT-Motores Térmicos for providing the best possible means to complete this work. This includes professors, researchers, technicians, administration staff, specially Amparo, and students that have worked with me, and those who have not, but equally contribute to the research here performed.

Among the researchers group, I am specially grateful to those who share with me this journey, my fellow PhD students, Tarí, Alberto, Ausias, Julián, Pablo, Auñón and Artem, and the students that helped us, like Sergio and Maggie; all of you are the best example of how colleagues can become friends. All journeys have a beginning, and this one started with my final degree project with the help of Dr. Francisco Arnau and Prof. José Ramón Serrano, thank you for introducing me to CMT-Motores Térmicos. Also, I express my gratitude to Dr. Luis Miguel for his insightful computing assistance and for being a example of what a researcher should be. Special thanks as well to Adolfo Guzmán for the experimental measurements, which are all his merit.

I also wish to thank Dr. Robert Fairbrother for welcoming and assisting me during my stay in AVL in Graz, and of course to the rest of workmates who offered me their hospitality, like Sandra, Georg and Eduardo.

Finally, I am grateful to my friends and family for their continuous support, to Luisa, always offering transport to Valencia and even her house for accommodation these last months, and specially, to my parents, Ambrosio and Mari Carmen, always giving more than what they have to assure my future. Thank you.

And, certainly, to the person that has been there every single day long before this started, thank you Mari Carmen, and let us begin this next journey together.

Valencia, 2018

Agradecimientos

En primer lugar, quería expresar mi gratitud a mi supervisor Prof. Torregrosa por su guía e implicación. Estoy seguro de que esto no habría sido posible sin su apoyo y conocimiento. Esta gratitud se extiende también a todos los miembros del CMT-Motores Térmicos por aportar los mejores medios posibles para completar este trabajo. Esto incluye profesores, investigadores, técnicos, personal de administración, especialmente Amparo, y estudiantes que han trabajado conmigo, y aquellos que no, pero igualmente han contribuido a la investigación aquí realizada.

Dentro del grupo de investigación, estoy especialmente agradecido a aquellos que han compartido conmigo este viaje, mis compañeros estudiantes de doctorado, Tarí, Alberto, Ausias, Julián, Pablo, Auñón y Artem, y a los estudiantes que nos ayudaron, como Sergio y Maggie; vosotros sois el mejor ejemplo de cómo compañeros pueden convertirse en amigos. Todos los viajes tienen un principio, y este empezó con mi proyecto final de carrera con la ayuda del Dr. Francisco Arnau y del Prof. José Ramón Serrano, gracias por introducirme al CMT-Motores Térmicos. Además, quería expresar mi gratitud al Dr. Luis Miguel por su ilustrativa asistencia computacional y por ser un ejemplo de cómo debería ser un investigador. Un especial agradecimiento también a Adolfo Guzmán por las medidas experimentales, todas mérito suyo.

También quiero agradecer al Dr. Robert Fairbrother darme la bienvenida y asistirme durante mi estancia en AVL en Graz, y por supuesto al resto de compañeros que me ofrecieron su hospitalidad, como Sandra, Georg y Eduardo.

Finalmente, estoy agradecido a mis amigos y familia por su continuo apoyo, a Luisa, siempre ofreciendo transporte a Valencia e incluso su casa como alojamiento estos últimos meses, y especialmente a mis padres, Ambrosio y Mari Carmen, siempre dando más de lo que tienen para asegurar mi futuro. Gracias.

Y, desde luego, a la persona que ha estado ahí cada día mucho antes de que esto empezase, gracias Mari Carmen, y empecemos este próximo viaje juntos.

Valencia, 2018

"The most important step a man can take. It's not the first one, is it?
It's the next one. Always the next step."

Brandon Sanderson, *Oathbringer (The Stormlight Archive, Book 3)*

Contents

1 Introduction **1**
- 1.1 Motivation . . . 2
- 1.2 Background . . . 4
- 1.3 Main objectives . . . 6
- 1.4 Thesis outline . . . 7
- Chapter 1 bibliography . . . 11

2 Literature review **13**
- 2.1 Introduction . . . 14
- 2.2 Euler equations for gas dynamics . . . 15
- 2.3 Numerical methods . . . 24
- 2.4 Flux limiters . . . 48
- 2.5 Duct junctions . . . 56
- Chapter 2 bibliography . . . 67

3 Numerical method **69**
- 3.1 Introduction . . . 70
- 3.2 Staggered-grid scheme . . . 72
- 3.3 The Courant-Friedrichs-Lewy stability criterion adaptation . . . 76
- 3.4 Momentum diffusion term . . . 77
- 3.5 Flux corrected transport . . . 78
- 3.6 Total variation diminishing . . . 79
- 3.7 Shock-tube problem . . . 82
- 3.8 Summary and conclusions . . . 88
- Chapter 3 bibliography . . . 93

4 Boundary conditions **95**
- 4.1 Introduction . . . 96
- 4.2 Independent boundary conditions . . . 97
- 4.3 One-dimensional collocated scheme connection . . . 100
- 4.4 Preliminary results and discussion . . . 104
- 4.5 Summary and conclusions . . . 108
- Chapter 4 bibliography . . . 111

5 Application to mufflers and other three-dimensional systems 113
5.1 Introduction . . . 114
5.2 Meshing techniques . . . 115
5.3 Linear acoustics . . . 120
5.4 Parallelepiped shape muffler . . . 125
5.5 Reversal chamber . . . 135
5.6 General shape muffler . . . 141
5.7 Summary and conclusions . . . 143
Chapter 5 bibliography . . . 146

6 Application to duct junctions 147
6.1 Introduction . . . 148
6.2 Statement of the validation method . . . 149
6.3 Experimental procedure . . . 151
6.4 1D method with pressure loss-based junction model . . . 153
6.5 Results and discussion . . . 154
6.6 Summary and conclusions . . . 174
Chapter 6 bibliography . . . 176

7 Concluding remarks and future work 177
7.1 Introduction . . . 178
7.2 Main contributions . . . 178
7.3 Limitations . . . 181
7.4 Future work . . . 184
Chapter 7 Bibliography . . . 187

Bibliography 189

List of Tables

3.1 Comparison of the L^2 and L^∞ norms of the deviation between the analytical shock-tube solution and the different correction methods used with 250 cells. 87
3.2 Comparison of the L^2 and L^∞ norms of the deviation between the analytical shock-tube solution and the different correction methods used with 500 cells. 88
3.3 Comparison of the L^2 and L^∞ norms of the deviation between the analytical shock-tube solution and the different correction methods used with 1000 cells. 88

6.1 Values of the mean quadratic error: T-junction. 162
6.2 Values of the mean quadratic error: Y-junction. 163
6.3 Values of the mean quadratic error: T-junction. 170

List of Figures

2.1 Characteristics lines on a general cell for a time step. 30
2.2 Conservative variables and flux in a generic cell. 36
2.3 Leapfrog scheme representation. 38
2.4 Two-step Lax-Wendroff representation. 40
2.5 Constant state data in each cell in a Godunov scheme. 43
2.6 Regions of the Riemann problem for subsonic flow. 46
2.7 Region for TVD flux limiter. 55

3.1 Basic mesh elements, definition of velocity projections and notation of volumes and connectors. 73
3.2 Scheme of the staggered mesh and the associated time marching. 75
3.3 Initial state of the shock-tube problem (a) and scheme of the solution structure after a certain time (b). 83
3.4 Comparison of solutions of the shock-tube problem: analytical, obtained with the original (raw) method and with the momentum diffusion term (MDT). 84
3.5 Comparison of solutions of the shock-tube problem: analytical, obtained with the TVD method and the FCT method. 85
3.6 Effect of the discretization used on the description of the contact discontinuity for the three flux limiters considered: (a) MDT, (b) FCT, (c) TVD. 86

4.1 Shock-tube results with a one-dimensional first order Godunov scheme. 102
4.2 Schematic representation of virtual cells information exchange between one-dimensional and quasi-3D methods meshes. 103
4.3 Plots of the pressure pulse generated and the pressure in the volume following the boundary condition in the mesh. 104
4.4 Plots of the pressure pulse measured and the pressure calculated at the middle of the duct. 105
4.5 Shock-tube results with a staggered grid for the left side and a collocated scheme for the right side. 107
4.6 Detailed contact zone of the shock-tube results with a staggered grid for the left side and a collocated scheme for the right side. 108

5.1 Constant section geometry mesh representation. 118
5.2 Parallel ducts geometry mesh transformation representation. . 119
5.3 Complex geometry mesh importation process representation. . 120
5.4 Schematic representation of a multi-port. 123
5.5 Scattering matrix formulation for 2-port. 124
5.6 Experimental set-up and representation of pressure pulse propagation. 126
5.7 Pressure pulse recorded at first measurement station, and later used as boundary condition for the computations: (a) time domain, (b) frequency domain. 127
5.8 Pressure pulse as recorded at the second (a) and third (b) measurement stations, and results produced by the different methods. 127
5.9 Geometry considered and mesh used. 129
5.10 Pressure pulse transmitted by the chamber, and corresponding transmission loss, produced by the different flux limiters. 130
5.11 Effect of parameter ξ in equation (5.20) on the pressure pulse transmitted by the chamber and the corresponding transmission loss obtained with the TVD method. 132
5.12 Effect of parameter ξ in equation (5.20) on the pressure and velocity results of the shock-tube problem: detail at the contact discontinuity and the shock front. 132
5.13 Effect of parameter ξ in equation (5.20) on the pressure pulse as recorded at the third measurement station. 133
5.14 Geometry with extended ducts considered and mesh used. . . . 134
5.15 Pressure pulse transmitted by the chamber, and corresponding transmission loss, produced by the different flux limiters. 135
5.16 Symmetric reversal chamber representation. 135
5.17 Symmetric reversal chamber schematic representation of the mesh used in the quasi-3D method. 136
5.18 Incident and transmitted pressure pulses in the symmetric reversal chamber and corresponding transmission loss with MDT and a commercial code. 137
5.19 Incident and transmitted pressure pulses in the symmetric reversal chamber and corresponding transmission loss with the different flux limiters. 138
5.20 Skew-symmetric reversal chamber schematic representation of the mesh used in the quasi-3D method. 138

5.21 Incident and transmitted pressure pulses in the skew-symmetric reversal chamber and corresponding transmission loss with MDT and a commercial code. 139
5.22 Incident and transmitted pressure pulses in the skew-symmetric reversal chamber and corresponding transmission loss with the different flux limiters. 139
5.23 Asymmetric reversal chamber schematic representation of the mesh used in the quasi-3D method. 140
5.24 Incident and transmitted pressure pulses in the asymmetric reversal chamber and corresponding transmission loss with MDT and a commercial code. 140
5.25 Incident and transmitted pressure pulses in the asymmetric reversal chamber and corresponding transmission loss with the different flux limiters. 141
5.26 General shape muffler geometry and mesh considered in this section. 142
5.27 Incident and transmitted pressure pulses in the general shape muffler and corresponding transmission loss with MDT and a commercial code. 142
5.28 Incident and transmitted pressure pulses in the general shape muffler and corresponding transmission loss with the different flux limiters. 143

6.1 Junctions considered in the study. 149
6.2 Wave components acting on a multi-port. 150
6.3 Experimental setup used. 152
6.4 Experimental results for the T-junction in the time domain. (a) Excitation at port 1; (b) excitation at port 3. Ports are denoted as in Figure 6.1. 155
6.5 Experimental results for the Y-junction in the time domain. (a) Excitation at port 1; (b) excitation at port 2; (c) excitation at port 3. Ports are denoted as in Figure 6.1. 156
6.6 Experimental results for the T-junction in the frequency domain. (a) Excitation at port 1; (b) excitation at port 3. Ports are denoted as in Figure 6.1. 157
6.7 Experimental results for the Y-junction in the frequency domain. (a) Excitation at port 1; (b) excitation at port 2; (c) excitation at port 3. 158

6.8 Experimental vs. modeled results for the T-junction: raw data (top) and differences (bottom) in the time domain, momentum diffusion term (MDT) method. (a) excitation at port 1; (b) excitation at port 3. 160
6.9 Comparison between the different models for the T-junction: raw data (top) and differences (bottom plots) in the time domain. (a) excitation at port 1; (b) excitation at port 3. 161
6.10 Comparison between the different models considered for the Y-junction (time domain): (a) excitation at port 1; (b) excitation at port 2; (c) excitation at port 3. 164
6.11 Comparison between the experimental results and the different models for the reflection coefficients of the T-junction (frequency domain): (a) excitation at port 1; (b) excitation at port 3. 165
6.12 Comparison between the experimental results and the different models for the transmission coefficients of the T-junction (frequency domain): (a) excitation at port 1, transmission through port 2; (b) excitation at port 1, transmission through port 3; (c) excitation at port 3, transmission through port 1; (d) excitation at port 3, transmission through port 2. 165
6.13 Comparison between the experimental results and the different models for the reflection coefficients of the Y-junction (frequency domain): (a) excitation at port 1; (b) excitation at port 2; (c) excitation at port 3. 166
6.14 Comparison between the experimental results and the different models for the transmission coefficients of the Y-junction (frequency domain): (a) excitation at port 1, transmission through port 2; (b) excitation at port 1 , transmission through port 3; (c) excitation at port 2, transmission through port 1; (d) excitation at port 2, transmission through port 3 (c) excitation at port 3, transmission through port 1; (d) excitation at port 3, transmission through port 2. 168
6.15 Meshes used in the staggered-grid method: (a) a 0D description of the junction; (b) a quasi-3D description. 169
6.16 Influence of the description of the junction in the time domain, MDT method: raw data (top) and differences with measurement (bottom). (a) Excitation at port 1; (b) excitation at port 3. 170

6.17 Influence of the description of the junction on the reflection coefficients (frequency domain), MDT method. (a) Excitation at port 1; (b) excitation at port 3. 171
6.18 Influence of the description of the junction on the transmission coefficients (frequency domain), MDT method. (a) Excitation at port 1, transmission through port 2; (b) excitation at port 1, transmission through port 3; (c) excitation at port 3, transmission through port 1; (d) excitation at port 3, transmission through port 2. 172
6.19 Influence of using a quasi-3D approach for the whole system on the reflection and transmission coefficients (frequency domain). MDT method, excitation at port 1. (a) Reflection at port 1; (b) transmission through port 2; (c) transmission through port 3.173

List of symbols

Latin characters

a	Speed of sound	$m \cdot s^{-1}$
A	Area, non-dimensional speed of sound, wave component	$m^2, -, -$
A_A	Non-dimensional entropy level	$-$
a_A	Entropy level	$m \cdot s^{-1}$
B	Wave component	$-$
c	Wave speed	$m \cdot s^{-1}$
C	Function of the Courant number	$-$
c_p	specific heat capacity at constant pressure	$J \cdot kg^{-1} \cdot K^{-1}$
c_v	specific heat capacity at constant volume	$J \cdot kg^{-1} \cdot K^{-1}$
D	Equivalent or hydraulic diameter	m
E	Total internal energy	$kg \cdot m^2 \cdot s^{-2}$
e	Specific internal energy	$m^2 \cdot s^{-2}$
f	Frequency, wall friction factor	s^{-1}
G	Function of gradients (TVD)	$-$
H	Total enthalpy	$kg \cdot m^2 \cdot s^{-2}$
h	Specific enthalpy	$m^2 \cdot s^{-2}$
K	Total pressure loss coefficient	$-$
L	Length, mathematics norm	$m, -$
l	Characteristic length	m
M	Mach number	$-$
$\dot{m}$	Mass flow rate	$kg \cdot s^{-1}$
N	Total number	$-$
p	Pressure	$kg \cdot m^{-1} \cdot s^{-2}$
q	Heat transfer rate per unit of mass	$m^2 \cdot s^{-2}$
$\dot{Q}$	Heat flow	$kgm^2 \cdot s^{-3}$
R	Specific gas constant, reflection coefficient	$J \cdot kg^{-1} \cdot K^{-1}, -$
r	Radio, function of gradients (TVD)	$-$
S	Cross section	m^2
s	Entropy, sign	$kg \cdot m^2 \cdot s^{-2} K^{-1}, -$
T	Temperature, transmission coefficient	$K, -$
u	Flow velocity	$m \cdot s^{-1}$
U	Non-dimensional flow speed	$-$

V	Volume	m^3
v	Mass velocity	$kg \cdot s^{-1}$
$\dot{W}$	Power	$kg \cdot m^2 \cdot s^{-3}$
Z	Acoustic impedance	$Pa \cdot s \cdot m^{-3}$

Greek characters

∇	Gradient	$-$
$\nabla\cdot$	Divergence	$-$
α	Lerat-Peret method parameter	$-$
β	Lerat-Peret method parameter, characteristic	$-$
γ	Ratio of specific heats	$-$
Δ	Increment	$-$
ε	Momentum diffusion coefficient	$-$
ζ	Entropy function	$-$
θ	Angle between duct branches, diffusive function	$rad, -$
ϑ	FCT factor	$-$
λ	Eigenvalue, characteristic	$-$
ν	Courant number	$-$
ξ	TVD factor	$-$
π	Pi number	$-$
ρ	Density	$kg \cdot m^{-3}$
τ_w	Shear stress	$N \cdot m^{-2}$
Υ	Entropy flux	$-$
ϕ	Flux limiter function	$-$
Ψ	Anti-diffusion function	$-$
ψ	Limiter function of gradients (TVD)	$-$
ω	Angular frequency	$rad \cdot s^{-1}$

Vector and matrices

A	Jacobian matrix, anti-diffusion operator, left network matrix
B	Right network matrix
C	Source terms vector
Cn	Connectors orientation matrix
D	Diffusive operator
e	Right eigenvector
F	Flux terms vector
G	G matrix of Q3D method
S	Scattering matrix
U	Velocity terms vector
V	Primitive variables vector
W	State vector

Sub- and Superscripts

0	Stagnation, mean value
$+$	Forward
$-$	Backward
c	Connector variable
i	Cell position
in	Inlet, inflow
L	Left
max	Maximum value
n	Current time step, normal projection
$n+1$	Following time step
out	Outlet, outflow
R	Right, Riemann problem solution average
ref	Reference value

Acronyms

0D	Zero-dimensional
1D	One-dimensional
2D	Two-dimensional
3D	Three-dimensional
CFD	Computational fluid-dynamics
CFL	Courant–Friedrichs–Lewy condition
CO	Carbon monoxide
ENO	Essentially non-oscillatory
FCT	Flux corrected transport
HIL	Hardware in the loop
ICE	Internal combustion engine
MDT	Momentum diffusion term
MUSCL	Monotonic upstream centred scheme for conservation laws
NOx	Nitrogen oxides
PDE	Partial differential equations
PPM	Parabolic piece-wise method
Q3D	Quasi-three-dimensional
Quasi-3D	Quasi-three-dimensional
TL	Transmission loss
TVD	Total variation diminishing

Chapter 1

Introduction

Contents

1.1 Motivation **2**
1.2 Background **4**
1.3 Main objectives **6**
1.4 Thesis outline **7**
Chapter 1 bibliography **11**

1.1 Motivation

As a consequence of the need of reducing the development time and costs associated with the design of intake and exhaust systems for reciprocating internal combustion engines, engine modelling has become an essential engineering tool. Trial-and-error-based design methodologies are still in use, but most of the tests previously performed on prototypes in the early design stages have currently been replaced by numerical computations, and only the most promising solutions are tested in order to fix the final product.

It is important to notice one of the main rules when modelling, and it is that there will always be a trade-off between potential accuracy and computational cost. This means that more complex models will be able to bring a more accurate prediction, but the computational time needed for that solution will also highly increase. This situation emphasises the importance of selecting the proper model according to the state of the design and the accuracy required. Using always the more accurate tools will heavily increase the cost of the design in time and resources when in early stages an approximation would have been enough, and abusing the fastest tools will usually result in a product lacking the precision to be competitive.

According to the grade of complexity of the computational methods commonly used by manufactures, they are usually classified as:

- Look-up tables-based methods. They use a large database to obtain the outputs of the problem. They are fast, but they have a low accuracy and very low time-resolution. They can be used in real time models or as a first step in the design process and they need the use of the experience of the engineers.
- Mean value engine models. Slightly slower and used in the second phase of the design or for hardware in the loop (HIL) applications. They are able to produce cycle-averaged results.
- Filling and emptying models. They are based on modelling the momentum conservation between elements instead of simulating it. It is still possible to use them in real time and they have time resolutions of the order of the crank angle. Their non-linear acoustic performance only reaches low frequencies.
- One-dimensional methods. They simulate the momentum conservation equation in a single direction so they are able to predict the wave dynamic behaviour of the system. Although their computational cost is

still low, a lot of simplifications are needed to use them in real time, so they are usually the core of more sophisticated tools along with other models and they are used in the optimization process. They have a better time resolution and the non linear acoustic performance is usually limited to 1 kHz.

- Quasi-3D methods. The philosophy of these methods is to adopt some simplifications to model a particular problem in a way that the accuracy does not suffer too much while drastically improving the computational cost when compared to the full three-dimensional model. The simplification adopted will depend on the problem that the model is applied to and the objective is to improve the results that a one-dimensional model would offer with a similar or only slightly higher computational cost.

- Three-dimensional methods or computational fluid dynamics (CFD) methods. They simulate as much phenomena as possible, only modelling some aspects, such as turbulence. As the computation power increases, it is possible to even simulate the largest turbulent structures for some cases. However, their computational cost is so high that they cannot even be considered until the final stages of the design, when the highest accuracy is needed.

Typically, fast and suitable solutions for modelling both engine performance and intake and exhaust noise have been provided by one-dimensional time domain gas-dynamic codes [5]. The assumption of one-dimensional wave action is legitimate in most of the ducts used in engine intake and exhaust systems, at least in passenger car applications, where duct diameters are relatively small. However, certain elements, most notably duct junctions and intake and exhaust silencers, may exhibit noticeable three-dimensional effects, so that a one-dimensional flow representation would be insufficiently accurate unless a very rough description of such elements were acceptable in the problem under study.

In the case of duct junctions [6] it is the occurrence of complex three-dimensional flow structures what sets the limits for the applicability of simple zero-dimensional descriptions [3]. In the case of silencers, the one-dimensional assumption can only be applied to very simple geometries [7] but, even in simple cases such as expansion chambers and Herschel-Quincke tubes, the results are not in general acceptable for frequencies above the cut-on frequency of transversal modes [8]. This represents a serious drawback, especially in the case of the intake system, where underhood packaging necessities give rise to

airbox and silencer geometries with low cut-on frequencies, thus impeding a proper assessment even of the low frequency intake noise.

An obvious way to overcome these limitations is the use of computational fluid dynamics (CFD) models; however, the computation time required by their use in a complete intake or exhaust system is excessive. An alternative is provided by using a three-dimensional model only locally, precisely for those elements exhibiting significant three-dimensional effects. This can be achieved by coupling the one-dimensional and three-dimensional models [9], although the proper convergence of the coupling procedure may still imply a considerable computational cost [10].

Finally, quasi-3D staggered-mesh finite volume models [11] provide a suitable compromise between the quality of the solution and the computational cost when addressing the prediction of wave dynamics in intake and exhaust systems of internal combustion engines and, in particular, of the effects produced by complex elements. These models have lately become standard in commercial codes, either as the core of the whole computation [12, 13], or used locally for complex elements exhibiting significant three-dimensional features [14]. Thus, the model will have the benefits of a one-dimensional tool when a one-dimensional mesh is used, either because higher accuracy is not required at the moment or because no three-dimensional effects are expected, and then in any moment, a three-dimensional mesh may be used to improve the acoustic behaviour prediction where needed. When approached in such a way, quasi-3D methods can be regarded as a natural evolution of purely one-dimensional models.

1.2 Background

The here presented work is part of a series of tasks considered for the process of continuous improvements of a complete one-dimensional wave action model developed in the University Institute of Investigation CMT-Motores Térmicos in Universitat Politècnica de València.

The program was first conceived by Corberán [15] in 1984 with the method of characteristics as the technique to solve hyperbolic partial differential equations systems, based on the formulation suggested by Benson [16].

In a later stage, it was proposed the substitution of the method of characteristics by one of the more conservative and faster finite difference methods that were being developed at that time. Among the diverse possible schemes and after a comparative research performed in 1993 by Desantes, Chust and

Llorens [17], it was concluded that the best options were the second order two-step Lax-Wendroff and McCormack methods.

Nowadays, the model calculates the evolution of the flow inside the intake and exhaust ducts with the finite differences Lax-Wendroff method, only using the method of characteristics in the boundary conditions. However, another work under development aimed at improving the program has been proposed to substitute the above mentioned methods by finite volumes MUSCL technique (monotonic upstream centred scheme for conservation laws), a more modern and conservative scheme.

Besides the evolution of the one-dimensional fluid-dynamic methods, some other sub-models have been added for other systems. To name some of them, cylinder and plenum make use of a zero-dimensional filling and emptying models [15, 18], the turbine boundary condition [19, 20] or the heat transfer in ducts by Reyes [21], with improvements by Serrano [22] and Galindo *et al.* [23]. After the thesis of Galindo [24], the model started to be able to calculate transient load simulations with a set of theoretical and experimental works [25, 26, 27, 22]. It was precisely in these transient simulations where some problems with the conservation of some properties were detected, specially in conical ducts, encouraging the consideration of using a new numerical method.

Ultimately, the program was not able to compete with other codes based on a finite volume method, more stable and conservative, which where also able to bring a better approximation to a thee-dimensional system in non-linear acoustics. Therefore, a set of improvements were considered with the purpose of making the program competitive enhancing its accuracy, computational cost and overall performance. One of the suggested proposals consisted in developing a tool that will expand the non-linear acoustics prediction capabilities of the program. It had to be able to take into account three-dimensional effects that may appear in more complex devices, such as mufflers or other after-treatment systems, effects that are impossible to model with a classical one-dimensional approach. This new feature will not only increase the maximum frequency for which the method is reliable, but it can also be exploited in other parts of the simulation where the exact direction of the flow might be important, with special interest in duct junctions. On the other hand, the calculation time should not be severely increased, keeping it within the one-dimensional methods standards.

After analysing recent work in the field and the favoured solutions adopted by the main engine simulation programs of the market [28], along with how these possibilities would interact with the rest of the work lines being devel-

oped, focusing on the compatibility between them, it was concluded that a finite volume staggered-grid quasi-3D method should be implemented. Consequently, the work here presented was performed, including from the proposal of the numerical method and the adaptation of the flux limiters needed, to an extensive validation process, while showing the potential and possible applications of the method.

1.3 Main objectives

The main objective of the present work is the development of a fluid-dynamic quasi-3D numerical method that can be connected to a one-dimensional wave action model to improve the non-linear acoustical predictions by adding the capability of simulating three dimensional effects, all that while keeping a low computational cost, comparable to the original one-dimensional method. This general objective can be divided in sub-objectives.

- Extensive review of the existing one-dimensional models in engine simulation and the evolution of the diverse techniques developed to better comprehend the one-dimensional modelling approach in engine simulation. This knowledge will also be useful to consider adapting some of the most successful techniques and implement them in a way that facilitates the connection between codes.
- Development of the quasi-3D numerical method, with special emphasis on the flux limiters. The numerical method will be used in three-dimensional systems, but contrary to a regular CFD method, the calculation time required has to be low enough, around the order of magnitude of one-dimensional methods. To achieve this, some simplifications in the calculation approach of the governing equations will have to be performed, as long as new inaccuracies and instabilities of the method are avoided. It is at this point when choosing the suitable existing flux limiters and performing a proper adaptation to the three-dimensional case becomes a critical issue.
- The validation method is also crucial in the development of a new numerical method; therefore, a wide set of systems will be subjected to tests in order to validate the applicability and accuracy of the method. For this step, a meshing technique that fulfils the requirements of the numerical methods needs to be created as well, at least for the less complex systems.

- Eventually, the quasi-3D numerical method is intended to be added to the one-dimensional based scheme for fluid-dynamics used in OpenWAM. In consequence, a connection with the one-dimensional code as a boundary condition should be presented, or at least, some tests with preliminary results that assure that said connection is attainable without sacrificing accuracy in the final results.

1.4 Thesis outline

After this introduction, constituting chapter 1, the remainder of this thesis is organized in the following manner. Chapter 2 presents a comprehensive literature review focusing first on the governing equations for fluid-dynamics and its formulation, followed by a study of the main lines in which the one-dimensional engine modelling has evolved from its origin. The objective of this detailed review, covering even the first finite difference methods developed circa 1930, is on one hand to have a wider point of view when developing the quasi-3D method and its flux limiters, since most of the issues than may appear during that process were already faced and solved in the bibliography, or at least previous approaches might be key for solving a newly found problem. On the other hand, the literature review has been structured in a way that it can be also used as an anthology of one-dimensional engine modelling or as an introduction to this kind of numerical methods.

Chapter 3 is dedicated to the explanation of the numerical method in which this work is based. First, the type of mesh that the method uses, known as staggered grid mesh, it is explained. Then, how the discretization of the governing equations has been performed and where are they solved. In these sections it is also explained the main simplification that the method assumes in order to reduce the calculation time needed, establishing the quasi-3D method. After that, the development of the three flux limiters used in the method is detailed and they are tested by applying them to the well-known shock-tube problem, a standard first validation in one-dimensional numerical methods.

Chapter 4 is dedicated to the boundary conditions that the numerical method will need to be able to solve. This includes stand-alone boundary conditions based on the Method of Characteristics, like an incident pulse or an anechoic termination, and more importantly, the conception of the connection with the one-dimensional program in which the method is planned to be included. In this regard, some preliminary results are shown to check the capabilities and feasibility of the connection between numerical schemes, using

a first order Godunov scheme for a collocated mesh as a representative of a modern one-dimensional method.

Chapter 5 presents the main validation process that has been performed. A set of different mufflers and other three-dimensional devices have been modelled and simulated using the quasi-3D numerical method and the results obtained have been compared with different tools in order to validate the time-domain and non-linear acoustics capabilities of the method. The performance of the different flux limiters was also compared in every device to determine which one might be more suitable depending on the kind of simulation. Furthermore, a simple meshing technique and a linear acoustics tool, used in this chapter, are described.

Chapter 6 explores a different application of the quasi-3D method in which it is used locally to model duct junctions. Duct junction modelling, although they are not a typical three-dimensional device, also present an important influence in their performance and prediction capabilities depending on the direction of the flow. The proposed application is presented as an alternative to the usual models widely used in one-dimensional codes, offering higher accuracy, versatility and an easier set-up, since it does not need any experimental parameter. With this purpose, the results obtained with the quasi-3D method and a zero-dimensional approach are compared with experimental measurements.

Chapter 7 summarises the main findings and contributions of this Ph.D. dissertation, presenting the main conclusions reached through the analysis of the results obtained, as well as the limitations of the model and the recommendations for future work that could improve it.

Chapter 1 Bibliography

[3] A. J. Torregrosa, A. Broatch, L. M. García-Cuevas, and M. Hernández. "A Study of the Transient Response of Duct Junctions: Measurements and Gas-Dynamic Modeling with a Staggered Mesh Finite Volume Approach." *Applied Sciences* 7(5) (2017), p. 480 (cit. on pp. xi, 3, 181).

[5] D. E. Winterbone and R. J. Pearson. *Design techniques for engine manifolds: wave action methods for IC engines*. Professional Engineering Publishing, 1999 (cit. on pp. 3, 31, 56, 70).

[6] F. Payri, E. Reyes, and J. Galindo. "Analysis and modeling of the fluid-dynamic effects in branched exhaust junctions of ICE." *Journal*

of engineering for gas turbines and power 123(1) (2001), pp. 197–203 (cit. on pp. 3, 56, 70).

[7] F. Payri, A. Torregrosa, and M. Chust. "Application of MacCormack schemes to IC engine exhaust noise prediction." *Journal of Sound and Vibration* 195(5) (1996), pp. 757–773 (cit. on pp. 3, 70).

[8] A. Broatch, J. Serrano, F. Arnau, and D. Moya. "Time-domain computation of muffler frequency response: comparison of different numerical schemes." *Journal of sound and vibration* 305(1) (2007), pp. 333–347 (cit. on pp. 3, 70).

[9] G. Montenegro and A. Onorati. "A coupled 1D-multiD nonlinear simulation of IC engine silencers with perforates and sound-absorbing material." *SAE International Journal of Passenger Cars-Mechanical Systems* 2(2009-01-0305) (2009), pp. 482–494 (cit. on pp. 4, 70).

[10] J. Galindo, A. Tiseira, P. Fajardo, and R. Navarro. "Coupling methodology of 1D finite difference and 3D finite volume CFD codes based on the Method of Characteristics." *Mathematical and Computer Modelling* 54(7) (2011), pp. 1738–1746 (cit. on pp. 4, 70, 101).

[11] G. Montenegro, A. Onorati, and A. Della Torre. "The prediction of silencer acoustical performances by 1D, 1D–3D and quasi-3D non-linear approaches." *Computers & Fluids* 71 (2013), pp. 208–223 (cit. on pp. 4, 59, 72, 151).

[12] T. Morel, J. Silvestri, K.-A. Goerg, and R. Jebasinski. *Modeling of engine exhaust acoustics*. SAE Technical Paper 1999-01-1665. 1999 (cit. on pp. 4, 59, 70, 72).

[13] S. M. Sapsford, V. C. Richards, D. R. Amlee, T. Morel, and M. T. Chappell. *Exhaust system evaluation and design by non-linear modeling*. SAE Technical Paper 920686. 1992 (cit. on pp. 4, 59, 72, 122).

[14] G. Montenegro, A. Della Torre, A. Onorati, R. Fairbrother, and A. Dolinar. *Development and application of 3D generic cells to the acoustic modelling of exhaust systems*. SAE Technical Paper 2011-01-1526. 2011 (cit. on pp. 4, 59).

[15] J. Corberán. "Contribución al modelado del proceso de renovación de la carga en motores de combustión interna alternativos." PhD thesis. Tesis Doctoral, Universidad Politécnica de Valencia, 1984 (cit. on pp. 4, 5).

[16] R. S. Benson. *Thermodynamics and Gas Dynamics of Internal Combustion Engines*. Cambridge University Press, 1982 (cit. on pp. 4, 25, 57).

[17] J. Desantes, M. Chust, and J. Llorens. "Análisis comparativo de métodos numéricos para la resolución del flujo no estacionario en colectores de motores de combustión interna alternativos." In: *II Congreso de Métodos Numéricos en Ingeniería, F. Ambarina and M. Casteleiro, eds., c SEMNI*. 1993 (cit. on p. 5).

[18] F. Payri, J. Desantes, and J. Corberán. "A quasi-steady model on gas exchange process, some results." *Motor Sympo'88* (1988) (cit. on p. 5).

[19] F. Payri, J. Benajes, and M. Reyes. "Modelling of supercharger turbines in internal-combustion engines." *International Journal of Mechanical Sciences* 38(8) (1996), pp. 853–869 (cit. on p. 5).

[20] F. Payri, J. Galindo, and J. Serrano. "Variable geometry turbine modelling and control for turbocharged Diesel engine transient operation." In: *Thermo-and Fluid-dynamic Processes in Diesel Engines: Selected Papers from the THIESEL 2000 Conference Held in Valencia, Spain, September 13-15, 2000*. Springer Verlag. 2002, p. 189 (cit. on p. 5).

[21] M. Reyes. "Contribución al Modelado del Proceso de Transferencia de calor en Colectores de Escape de Motores Alternativos." PhD thesis. Tesis Doctoral, Universidad Politécnica de Valencia, 1993 (cit. on p. 5).

[22] J. Serrano. "Análisis y modelado del transitorio de carga en motores turboalimentados de encendido por compresión." PhD thesis. PhD thesis, Universidad Politécnica de Valencia, Spain, 1999 (cit. on p. 5).

[23] J. Galindo, J. Serrano, H. Climent, and F. Arnau. "New one-dimensional fluid-dynamic model for automotive intercoolers." In: *Proceedings of EAEC 8th European Automotive Congress*. 2001 (cit. on p. 5).

[24] J. Galindo. "Diseño de uniones de colectores de escape de motores alternativos." PhD thesis. 1998 (cit. on p. 5).

[25] J. Benajes, J. Lujan, V. Bermudez, and J. Serrano. "Modelling of turbocharged diesel engines in transient operation. Part 1: insight into the relevant physical phenomena." *Proceedings of the type of Mechanical Engineers, Part D: Journal of Automobile Engineering* 216(5) (2002), pp. 431–441 (cit. on p. 5).

[26] F. Payri, J. Benajes, J. Galindo, and J. Serrano. "Modelling of turbocharged diesel engines in transient operation. Part 2: wave action models for calculating the transient operation in a high speed direct injection engine." *Proceedings of the type of Mechanical Engineers, Part D: Journal of Automobile Engineering* 216(6) (2002), pp. 479–493 (cit. on p. 5).

[27] F. Payri, E. Reyes, and J. Serrano. *A model for load transients of turbocharged diesel engines*. SAE Technical Paper 1999-01-0225. 1999 (cit. on p. 5).

[28] G. Montenegro, A. Della Torre, A. Onorati, and R. Fairbrother. "A nonlinear Quasi-3D approach for the modeling of mufflers with perforated elements and sound-absorbing material." *Advances in Acoustics and Vibration* 2013 (2013) (cit. on pp. 5, 70–72, 76, 78, 90, 179).

Chapter 2

Literature review

Contents

2.1 Introduction **14**
2.2 Euler equations for gas dynamics **15**
2.2.1 Mass conservation equation 15
2.2.2 Momentum conservation equation 17
2.2.3 Energy conservation equation 18
2.2.4 Closure of the equations 20
2.2.5 Conservative law form of the Euler equations . . . 21
2.2.6 Three-dimensional Euler equations 23
2.3 Numerical methods **24**
2.3.1 Method of Characteristics 25
2.3.2 The Courant-Friedrichs-Lewy stability criterion . . 31
2.3.3 The entropy condition 33
2.3.4 Conservative centred schemes 34
2.3.5 Upwind schemes and Riemann solvers 41
2.4 Flux limiters **48**
2.4.1 Flux Corrected Transport (FCT) 50
2.4.2 Total Variation Diminishing (TVD) 52
2.4.3 Other high resolution schemes 54
2.5 Duct junctions **56**
Chapter 2 bibliography **67**

2.1 Introduction

Nowadays, the research involving internal combustion engines, ICE, is heavily focused on reducing the pollutant emissions in order to fulfil the increasingly restrictive regulations such as the European norm Euro VI [29, 30] while maintaining the engine performance and reducing the fuel consumption. Although most of the efforts are headed to reduce the most hazardous emissions, such as NOx or CO, the rest of emissions have to be kept under control as well. The way to achieve this consists in performing a set of simulations with the proper tools to model the diverse physical phenomena present in the engine until the design requirements are met. Besides, experimental tests have to be performed, first to complement the models that need measured data, and finally to verify the simulated results. How efficient and reliable the models are is hence a critical point in the design process.

Among the engine emissions, acoustic emissions will be usually the main focus of this work. Traditionally, one-dimensional models have been accurate enough to model the whole engine, including its acoustic behaviour. However, as increasingly complex devices are needed to reduce pollutant emissions, such as catalyst bricks or particle filters, and mufflers need to have more complex geometries, the three-dimensional effects start to be important, making the one-dimensional models insufficient for acoustics. Surely, three-dimensional models come to mind as an alternative, but a complete 3D simulation drastically increases the computational time needed, usually becoming a non-viable option. Finally, a compromise solution is offered by quasi-3D models, which are able to simulate three-dimensional geometries, but by using some simplifications, need a much lower computational time, ideally comparable to a one-dimensional tool.

In this chapter, a literature review of the most relevant work about gas-dynamic engine simulation is presented, focusing on one-dimensional methods, as a way to understand the precedents that lead to the creation of a quasi-3D model. First the governing equations are explained as the base of the method, then a brief description of the main one-dimensional techniques and their evolution is given, getting more into detail in the flux limiters, since some of them will later be adapted to the quasi-3D method. Finally, a brief literature review of duct junctions is presented, since they are also an interesting problem where three-dimensional effect are often relevant.

2.2 Euler equations for gas dynamics

The fundamental conservation equations studied in this chapter are the so-called Euler Equations. They define the conservation of mass, momentum and energy for a control volume. A conservation law establish that the rate of change of a conserved flow property in a fixed volume depends only on the flux of the property through the boundary of the volume and the change of that property due to internal sources.

The Euler Equations are actually a simplified case of the general Navier-Stokes equations. These last equations take also into account the viscous interactions of the fluid and, therefore, the resulting flux depends not only on the conservative variables, but also on their gradients. As a consequence, the partial differential equations system does not behave as an hyperbolic system, considerably increasing the complexity of its resolution. This simplification adopted in the Euler Equations does not affect the solution to a large extent since in the gas flowing through engines the viscous forces are generally negligible, except in the boundary layer, where they can be modelled with a friction term.

In order to understand the physical meaning of the three conservation equations that govern the fluid-dynamic behaviour of a gas inside the ducts of an internal combustion engine, the three equations will be developed first in its more traditional and simple one-dimensional form [31, 32, 33]. This will make mathematical development easier to follow and to visualize. Eventually, the equations will be extended to the three-dimensional form.

2.2.1 Mass conservation equation

The density of the gas in a determined point x of the duct in time t is denote by $\rho(x,t)$. The total mass per surface unit between two points x_1 and x_2 can be defined with the following expression

$$(\text{Mass in } [x_1, x_2] \text{ for time } t) \int_{x_1}^{x_2} \rho(x,t)\mathrm{d}x \tag{2.1}$$

Assuming impermeable walls and that there is nothing that destroys mass, then the quantity of mass in the gap represented in equation (2.1) depends only on the flow along time in sections x_1 and x_2. If $u(x,t)$ represents the velocity of the flow in section x and at time t, the mass flow per surface unit can be represented as

$$(\text{Mass flow in } (x,t)) : \rho(x,t)u(x,t) \tag{2.2}$$

With this approach, the mass variation in $[x_1, x_2]$ along time depends on the mass that goes in or out in that portion of the duct across their sides. Therefore, it can be written as

$$\frac{\mathrm{d}}{\mathrm{d}t}\int_{x_1}^{x_2} \rho(x,t)\mathrm{d}x = \rho(x_1,t)u(x_1,t) - \rho(x_2,t)u(x_2,t) \tag{2.3}$$

Equation (2.3) is known as the integral form of the conservation equation, being in this case the mass conservation equation.

Knowing the mass in the portion $[x_1, x_2]$ at time t_1, it is possible to know its value at time $t_2 > t_1$ by integrating equation (2.3) in time, resulting in the following expression

$$\int_{x_1}^{x_2} \rho(x,t_2)\mathrm{d}x = \int_{x_1}^{x_2} \rho(x,t_1)\mathrm{d}x + \int_{x_1}^{x_2} \rho(x_1,t)u(x_1,t)\mathrm{d}t - \int_{x_1}^{x_2} \rho(x_2,t)u(x_2,t)\mathrm{d}t \tag{2.4}$$

Knowing that

$$\rho(x,t_2) - \rho(x,t_1) = \int_{x_1}^{x_2} \frac{\partial}{\partial t}\rho(x,t)\mathrm{d}x \tag{2.5}$$

and that

$$\rho(x_2,t)u(x_2,t) - \rho(x_1,t)u(x_1,t) = \int_{x_1}^{x_2} \frac{\partial}{\partial t}(\rho(x,t)u(x,t))\mathrm{d}x \tag{2.6}$$

after substituting into equation (2.4) the following is obtained

$$\int_{t_1}^{t_2}\int_{x_1}^{x_2} \left(\frac{\partial}{\partial t}\rho(x,t) + \frac{\partial}{\partial x}\left(\rho(x,t)u(x,t)\right)\right)\mathrm{d}x\mathrm{d}t = 0 \tag{2.7}$$

If both $\rho(x,t)$ and $u(x,t)$ are differentiable functions in the interval, it is possible to assume that the term of the equation inside the integral is also zero. With this assumption the following is obtained:

$$\frac{\partial \rho}{\partial t} + \frac{\partial(\rho u)}{\partial x} = 0 \tag{2.8}$$

This equation (2.8) is known as the differential form of the conservation law, in this case, of the mass conservation equation. This equation can be written in a more general form when the section is also considered. Since the

conservation dictates that the rate of change of mass within a control volume of length dx and cross-section S is equal to the net mass flow rate through the element, the mass conservation equation can be expressed as

$$\frac{\partial(\rho S \mathrm{d}x)}{\partial t} + \frac{\partial(\rho u S)}{\partial x}\mathrm{d}x = 0 \tag{2.9}$$

2.2.2 Momentum conservation equation

The momentum equation adds the requirement that the sum of the pressure forces and the shear forces located in the surface of the control volume equals the sum of the rate of change of momentum in the control volume and the net flux of momentum across the surface. The resultant force on the volume can be expressed with two terms. The first one represents the difference in the pressure forces across the end sections of the of the control volume and, for a one-dimensional case, it is given by the product of the gradient of the force by the length of the element.

$$-\frac{\partial(pS)}{\partial x}\mathrm{d}x \tag{2.10}$$

The second term represents the pressure on the sides of the control volume, which once again for a one-dimensional case, produces a force in the x-direction given by:

$$p\frac{\mathrm{d}S}{\mathrm{d}x}\mathrm{d}x \tag{2.11}$$

The negative sign in the term (2.10) comes from the convention that the forces in the x-direction are accounted as positive. Also, for engine models, in the pipes and other fluid-dynamic elements it can be assumed that their geometry do not change with time (except cylinders, which are usually modelled as zero-dimensional elements), so that the area of the elements is only a function of x.

The shear forces on the control volume are due to the friction between the flow and the duct walls and can be modelled as a shear stress, τ_w, opposing the fluid motion. For a one-dimensional infinitesimal control volume, the surface force is given by

$$-\pi D \tau_w \mathrm{d}x \tag{2.12}$$

where D is the equivalent or hydraulic diameter of the element. The shear stress can be expressed in therms of the element wall friction factor, f, as

$$\tau_w = \frac{1}{2}\rho u^2 f \tag{2.13}$$

In this way, the surface force on the control volume can be represented as

$$-\frac{1}{2}\rho u^2 f \pi D \mathrm{d}x \tag{2.14}$$

In one-dimensional fluid-dynamic models this term accounts for all the effects of viscous forces, giving as a result an essentially inviscid character for the governing equations.

The rate of change of momentum inside the control volume can be expressed as

$$\frac{\partial(u\rho S \mathrm{d}x)}{\partial t} \tag{2.15}$$

and the net flux of momentum across the control volume faces is given by

$$\frac{\partial(\rho S u^2)}{\partial x}\mathrm{d}x \tag{2.16}$$

Hence the momentum conservation equation is finally expressed as

$$-\frac{\partial(pS)}{\partial x}\mathrm{d}x + p\frac{\mathrm{d}S}{\mathrm{d}x}\mathrm{d}x - \frac{1}{2}\rho u^2 f \pi D \mathrm{d}x = \frac{\partial(u\rho S \mathrm{d}x)}{\partial t} + \frac{\partial(\rho S u^2)}{\partial x}\mathrm{d}x \tag{2.17}$$

2.2.3 Energy conservation equation

The energy equation comes directly from applying the First Law of Thermodynamics to the control volume, which results in

$$\dot{Q} - \dot{W}_s = \frac{\partial E_0}{\partial t} + \frac{\partial H_0}{\partial x}\mathrm{d}x \tag{2.18}$$

Here, E_0 is the total stagnation internal energy of the control volume and H_0 is the total stagnation enthalpy. Equation 2.18 can also be written in terms of the specific stagnation internal energy and specific stagnation enthalpy, resulting in

$$\dot{Q} - \dot{W}_s = \frac{\partial(e_0 \rho S \mathrm{d}x)}{\partial t} + \frac{\partial(h_0 \rho S u)}{\partial x}\mathrm{d}x \tag{2.19}$$

where e_0 is the specific stagnation internal energy, defined as

$$e_0 = e + \frac{1}{2}u^2 \tag{2.20}$$

and h_0 is the stagnation enthalpy of the fluid, which can also be related to the stagnation internal energy by

$$h_0 = e_0 + \frac{p}{\rho} \tag{2.21}$$

Regarding the remaining terms of equation 2.18, the work done by or on the system, $\dot{W}_s$, is zero for gas flow in a duct, and generally the only source that is taken into account is the heat transfer from the gas to the element walls, or vice versa. In order to incorporate it to the energy equation, the heat transfer rate per unit of mass is denoted as q. Using the convention that heat transfer is positive into the control volume, the total heat transfer from or to the volume is

$$q\rho S\mathrm{d}x \tag{2.22}$$

Considering the above terms, the energy equation eventually takes the following form

$$q\rho S\mathrm{d}x = \frac{\partial(e_0\rho S\mathrm{d}x)}{\partial t} + \frac{\partial(h_0\rho S u)}{\partial x}\mathrm{d}x \tag{2.23}$$

To summarize, the governing equations for the one-dimensional flow of a compressible fluid in a duct with area variation, wall friction, and heat transfer result in the following set of non-linear hyperbolic partial differential equation

Mass conservation

$$\frac{\partial(\rho S)}{\partial t} + \frac{\partial(\rho u S)}{\partial x} = 0 \tag{2.24}$$

Momentum conservation

$$\frac{\partial(\rho u S)}{\partial t} + \frac{\partial(\rho u^2 + p)S}{\partial x} - p\frac{\mathrm{d}S}{\mathrm{d}x} + \frac{1}{2}\rho u^2 f\pi D = 0 \tag{2.25}$$

Energy conservation

$$\frac{\partial(\rho e_0 S)}{\partial t} + \frac{\partial(\rho u h_0 S)}{\partial x} - \rho q S = 0 \tag{2.26}$$

2.2.4 Closure of the equations

After setting the three governing equations, the number or unknown variables is, in fact, four, ρ, u, p and e_0. This means that a further relationship between them is needed in order to close the problem. The best candidate for this task is a state equation, and for gases in engines, the *ideal gas* state equation is usually the preferable solution

$$p = \rho RT \tag{2.27}$$

This simple relationship between the fluid-dynamic variables is usually sufficiently accurate, buy it is possible to use a more complex state equation if desired. The ideal gas state equation introduces however a new variable, the gas temperature T, but has the benefit of enabling the internal energy and enthalpy of the gas to be written as a function of the temperature alone. If the fluid is considered to be a *perfect gas*, both the internal energy and the enthalpy are directly proportional to the gas temperature

$$e = c_v T \tag{2.28}$$

and

$$h = c_p T \tag{2.29}$$

where c_v represents the specific heat capacity at constant volume and c_p, the specific heat capacity at constant pressure, which can be expressed in terms of the ratio of specific heats, γ, as

$$\gamma = \frac{c_p}{c_v} \tag{2.30}$$

and also in terms of the specific gas constant with

$$R = c_p - c_v \tag{2.31}$$

Considering the above relationships, the specific internal energy can be expressed as

$$e = \frac{RT}{\gamma - 1} = \frac{p}{\rho(\gamma - 1)} \tag{2.32}$$

and the specific enthalpy is given by

$$h = c_p T = \frac{\gamma RT}{\gamma - 1} = \frac{\gamma p}{\rho(\gamma - 1)} \tag{2.33}$$

Some other magnitudes worth mentioning are the speed of sound, which will be denoted as a and calculated as

$$a = \sqrt{\gamma RT} \tag{2.34}$$

and the Mach number, which represents the relationship between speed of the flow and the speed of sound as follows

$$M = \frac{u}{a} \tag{2.35}$$

The case of $M < 1$ is referred to as subsonic flow, while for $M > 1$ one has supersonic flow and, when $M = 1$, sonic flow.

Finally, the entropy, s, can be written as:

$$s = c_v \ln\left(\frac{p}{\rho^\gamma}\right) \tag{2.36}$$

2.2.5 Conservative law form of the Euler equations

Expanding and rearranging the governing equations (2.24) to (2.26), they can be expressed as

$$\frac{\partial(\rho)}{\partial t} + \frac{\partial(\rho u)}{\partial x} + \frac{\rho u}{S}\frac{\mathrm{d}S}{\mathrm{d}x} = 0 \tag{2.37}$$

$$\frac{\partial(\rho u)}{\partial t} + \frac{\partial(\rho u^2 + p)}{\partial x} - \frac{\rho u^2}{S}\frac{\mathrm{d}S}{\mathrm{d}x} + \rho G = 0 \tag{2.38}$$

$$\frac{\partial(\rho e_0)}{\partial t} + \frac{\partial(\rho u h_0)}{\partial x} + \frac{\rho u h_0}{S}\frac{\mathrm{d}S}{\mathrm{d}x} - \rho q = 0 \tag{2.39}$$

where

$$G = \frac{1}{2} u|u| f \frac{4}{D} \tag{2.40}$$

here, the term $u|u|$ is used to ensure that the element wall friction always opposes the direction of fluid motion.

From equations (2.37) to (2.39), it is easy to identify that the main variables are differentiated with respect to time, the fluxes of these variables are

differentiated with respect x, and finally the source terms complete the equations. This identification of variables leads naturally to the symbolic vector form of the system of equations as

$$\frac{\partial \mathbf{W}}{\partial t} + \frac{\partial \mathbf{F}(\mathbf{W})}{\partial x} + \mathbf{C}_1(\mathbf{W}) + \mathbf{C}_2(\mathbf{W}) = 0 \tag{2.41}$$

where the different vectors of the system are written as

$$\begin{aligned} \mathbf{W} &= \begin{bmatrix} \rho \\ \rho u \\ \rho e_0 \end{bmatrix}, & \mathbf{F}(\mathbf{W}) &= \begin{bmatrix} \rho u \\ \rho u^2 + p \\ \rho u h_0 \end{bmatrix} \\ \mathbf{C}_1(\mathbf{W}) &= \begin{bmatrix} \rho u \\ \rho u^2 \\ \rho u h_0 \end{bmatrix} \frac{1}{S}\frac{\mathrm{d}S}{\mathrm{d}x}, & \mathbf{C}_2(\mathbf{W}) &= \begin{bmatrix} 0 \\ \rho G \\ -\rho q \end{bmatrix} \end{aligned} \tag{2.42}$$

When there is no section variation through the element, wall friction nor heat transfer, equations (2.41) reduce to

$$\frac{\partial \mathbf{W}}{\partial t} + \frac{\partial \mathbf{F}(\mathbf{W})}{\partial x} = 0 \tag{2.43}$$

and are known as *homentropic one-dimensional Euler equations*. The representation of equations (2.41) is referred to as the *conservation law form* since it can be obtained directly from the integral conservation equations of mass, momentum and energy applied to a fixed control volume. However, these equations can be expressed in a even more conservative form, as proposed by Gascón [34], by including the cross-sectional area of the elements in the differential terms

$$\frac{\partial \mathbf{W}'}{\partial t} + \frac{\partial \mathbf{F}'(\mathbf{W}')}{\partial x} + \mathbf{C}' = 0 \tag{2.44}$$

where

$$\begin{aligned} \mathbf{W}' &= \begin{bmatrix} \rho S \\ \rho u S \\ \rho e_0 S \end{bmatrix}, \mathbf{F}'(\mathbf{W}') = \begin{bmatrix} \rho u S \\ \rho(u^2 + p)S \\ \rho u h_0 S \end{bmatrix} \\ \mathbf{C}'_1(\mathbf{W}') &= \begin{bmatrix} 0 \\ -p\frac{\mathrm{d}S}{\mathrm{d}x} \\ 0 \end{bmatrix}, \mathbf{C}'_2(\mathbf{W}') = \begin{bmatrix} 0 \\ \rho G S \\ -\rho q S \end{bmatrix} \end{aligned} \tag{2.45}$$

With this form or the equation system vectors, the cross-section variation only affects the momentum conservation equation, as indicated by the

corresponding term in $\mathbf{C}_1$ being different from zero, representing the forces that the walls exert on the fluid at the points where there are cross-section changes. The mass conservation equation, on the other hand, is now strictly homogeneous since it does not contain any source term. This form of the governing equations also gives the advantage of conserving mass in pipes of varying cross-sectional area when numerical methods which use flux limiter functions are used in order to achieve second-order accuracy (Corberán and Gascón [35, 36], Liu *et al.* [37]). For all these reasons, it is usually recommended that equations (2.44) and (2.45) are used as the starting point for algorithms used in one-dimensional wave-action simulation models for ducts.

2.2.6 Three-dimensional Euler equations

Following a similar development as in section 2.2, the Euler equations in Cartesian coordinates for three-dimensional flow of a compressible fluid, neglecting source terms, can be written as follows

$$\frac{\partial \mathbf{W}}{\partial t} + \frac{\partial \mathbf{F}}{\partial x} + \frac{\partial \mathbf{G}}{\partial y} + \frac{\partial \mathbf{H}}{\partial z} = 0 \tag{2.46}$$

where

$$\begin{gathered} \mathbf{W} = \begin{bmatrix} \rho \\ \rho u \\ \rho v \\ \rho w \\ \rho e_0 \end{bmatrix}, \mathbf{F} = \begin{bmatrix} \rho u \\ \rho u^2 + p \\ \rho uv \\ \rho uw \\ \rho u h_0 \end{bmatrix} \\ \mathbf{G} = \begin{bmatrix} \rho v \\ \rho uv \\ \rho v^2 + p \\ \rho vw \\ \rho v h_0 \end{bmatrix}, \mathbf{H} = \begin{bmatrix} \rho w \\ \rho uw \\ \rho vw \\ \rho w^2 + p \\ \rho w h_0 \end{bmatrix} \end{gathered} \tag{2.47}$$

The elements of the state vector $\mathbf{W}$, define the mass per unit volume, or density, ρ, in the first row of the equations, giving the mass conservation equation. The second, third and fourth row give the momentum equations in the three spatial coordinates, with the momentum per unit of volume also in the three coordinates as conservative variables, $\rho u, \rho v, \rho w$. It is worth mentioning that these three momentum equations are coupled, noticeably increasing the complexity of the resolution of the problem when compared with the one-dimensional case. Finally, the fifth row gives the energy conservation equation,

with the stagnation internal energy per unit of volume, ρe_0, as conservative variable. The specific stagnation enthalpy, h_0, is given by

$$h_0 = h + \frac{u^2}{2} + \frac{v^2}{2} + \frac{w^2}{2} = e + \frac{p}{\rho} + \frac{u^2}{2} + \frac{v^2}{2} + \frac{w^2}{2} = e_0 + \frac{p}{\rho} \tag{2.48}$$

Alternatively, the three-dimensional Euler equations without source terms can be written as the classic three equations for mass, momentum and energy conservation, being the momentum equation a vector equation, as follows

$$\frac{\partial(\rho)}{\partial t} + \nabla \cdot (\rho \mathbf{U}) = 0 \tag{2.49}$$

$$\frac{\partial(\rho \mathbf{U})}{\partial t} + \nabla \cdot (\rho \mathbf{U} \otimes \mathbf{U}) + \nabla p = 0 \tag{2.50}$$

$$\frac{\partial(\rho e_0)}{\partial t} + \nabla \cdot (\rho h_0 \mathbf{U}) = 0 \tag{2.51}$$

where

$$\mathbf{U} = \begin{bmatrix} u \\ v \\ w \end{bmatrix} \tag{2.52}$$

2.3 Numerical methods

In order to solve a partial differential equations system by a numerical method, a discretization of the calculation domain is necessary. This means that such calculation domain has to be represented by nodes in which the solution will be calculated. In the case of the Euler equations for fluid-dynamics, the calculation domain corresponds to the space-time plane. Therefore, for a one-dimensional case, the length of the cells of the mesh will be represented by Δx and the numerical time step, by Δt. On the other hand, x_i would represent the spatial position of the cell i and t_n would represent the time in the integration step n. In a similar fashion, W_i^n will denote the solution calculated by the numerical method in cell i in time step n.

The techniques for the simulation of gas-dynamic processes in engines are considered to have their origin in the use of the graphical Method of Characteristics in the 1950s [38, 39, 40, 41], which evolved into the mesh Method of

Characteristics [16], but was finally displaced by shock-capturing finite differences schemes [42, 43]. Initially, the two-step Lax-Wendroff and McCormack schemes without flux limiters were used, but later the use of non-linear terms for flux limiting became much more common [44, 45]. Finally, some numerical schemes based on Riemann solvers and other high-resolution shock-capturing schemes were developed [35, 46].

In this section the main techniques developed for gas-dynamic modelling will be outlined, starting with the Method of Characteristics. Before describing the main shock-capturing schemes, some stability criterion will be discussed that will help to understand the limitations and evolution of those schemes. Understanding these old one-dimensional techniques is mandatory when developing a new scheme, even when working in a three dimensional model. In traditional schemes it is easier to identify terms and their influence on the solution. Also, knowing the limitations, advantages and disadvantages of the different schemes enables to make better decisions when developing a new one and knowing how some difficulties where solved helps when facing new ones. In later sections it will be explained how some of these one-dimensional finite difference techniques where adapted to a quasi-three dimensional staggered grid scheme to achieve stability in the solution or how the Method of Characteristics is still used for the boundary conditions.

2.3.1 Method of Characteristics

The Method of Characteristics was developed by Riemann [47] as a tool for solving systems of partial differential equations. For simplicity, in this section it will be discussed only the case where there is no heat transfer nor wall friction, so the entropy level of the fluid remains constant, being called *homentropic flow*. The starting point is given by the one dimensional governing equations in non conservative form

$$\frac{\partial \rho}{\partial t} + u\frac{\partial \rho}{\partial x} + \rho\frac{\partial u}{\partial x} = 0 \tag{2.53}$$

$$\frac{\partial u}{\partial t} + u\frac{\partial u}{\partial x} + \frac{1}{\rho}\frac{\partial p}{\partial x} = 0 \tag{2.54}$$

$$\frac{\partial e}{\partial t} + u\frac{\partial e}{\partial x} - \frac{p}{\rho^2}\left[\frac{\partial \rho}{\partial t} + u\frac{\partial \rho}{\partial x}\right] = 0 \tag{2.55}$$

For an ideal gas, equation (2.55) becomes

$$\frac{\partial p}{\partial t} + u\frac{\partial p}{\partial x} - a^2\left[\frac{\partial \rho}{\partial t} + u\frac{\partial \rho}{\partial x}\right] = 0 \tag{2.56}$$

Now equations (2.53), (2.54) and (2.56) form a system that can be written in vector form

$$\frac{\partial \mathbf{V}}{\partial t} + \mathbf{A}\frac{\partial \mathbf{V}}{\partial x} = 0 \tag{2.57}$$

where the variables in vector $\mathbf{V}$ (ρ,u and p) are known as *primitive variables* and $\mathbf{A}$ is the Jacobian 3×3 matrix. For a perfect gas, Hirsch [48] defines the Jacobian matrix $\mathbf{A}$ as

$$\mathbf{A} = \begin{bmatrix} 0 & 1 & 0 \\ (\gamma-3)\frac{u^2}{2} & (3-\gamma)u & (\gamma-1) \\ (\gamma-2)\frac{u^3}{2} - \frac{ua^2}{\gamma-1} & \frac{a^2}{\gamma-1} - \frac{u^2}{2}(2\gamma-3) & \gamma u \end{bmatrix} \tag{2.58}$$

The eigenvalues λ_k and right eigenvectors $\mathbf{e}_k$ of $\mathbf{A}$ are

$$\begin{aligned} \lambda_1 = u + a, \quad e_1 &= \begin{bmatrix} 1 \\ u + a \\ \frac{a^2}{\gamma-1} + \frac{u^2}{2} + ua \end{bmatrix} \\ \lambda_2 = u - a, \quad e_2 &= \begin{bmatrix} 1 \\ u - a \\ \frac{a^2}{\gamma-1} + \frac{u^2}{2} - ua \end{bmatrix} \\ \lambda_3 = u, \qquad\quad e_3 &= \begin{bmatrix} 1 \\ u \\ \frac{u^2}{2} \end{bmatrix} \end{aligned} \tag{2.59}$$

Given that the eigenvalues are real and the eigenvectors are linearly independent, the system of equations (2.57) is said to be *hyperbolic*.

In order to make more evident the wave-like nature of the flow, equations (2.53), (2.54) and (2.56) can be manipulated and simplified until obtaining the following equations

$$\frac{\partial p}{\partial t} + (u+a)\frac{\partial p}{\partial x} + \rho a\left[\frac{\partial u}{\partial t} + (u+a)\frac{\partial u}{\partial x}\right] = 0 \tag{2.60}$$

$$\frac{\partial p}{\partial t} + (u-a)\frac{\partial p}{\partial x} + \rho a\left[\frac{\partial u}{\partial t} + (u-a)\frac{\partial u}{\partial x}\right] = 0 \tag{2.61}$$

This expressions along with the energy equation (2.56) can be transformed from partial differential equations with respect to time and space, into ordinary

differential equations with respect to time with the relationship between time and space defined by the lines

$$\frac{\mathrm{d}x}{\mathrm{d}t} = u \pm a \tag{2.62}$$

for equations (2.60) and (2.61). These equations represents the speed of propagation of the signals or disturbances through the gas at the local speed of sound relative to the gas velocity, $u \pm a$. This disturbance is called wave characteristic and has an effect in pressure, temperature, density and velocity. Similarly,

$$\frac{\mathrm{d}x}{\mathrm{d}t} = u \tag{2.63}$$

for equation (2.56). In this case, this equation represents disturbances propagating at the local fluid velocity, u, which is usually called pathline characteristic and affects the gas temperature and composition. With these characteristic lines, the resulting total differentials would be:

$$\frac{\mathrm{d}p}{\mathrm{d}t} = \frac{\partial p}{\partial t} \pm (u \pm a)\frac{\partial p}{\partial x} \tag{2.64}$$

$$\frac{\mathrm{d}u}{\mathrm{d}t} = \frac{\partial u}{\partial t} \pm (u \pm a)\frac{\partial u}{\partial x} \tag{2.65}$$

$$\frac{\mathrm{d}p}{\mathrm{d}t} = \frac{\partial p}{\partial t} + u\frac{\partial p}{\partial x} \tag{2.66}$$

$$\frac{\mathrm{d}\rho}{\mathrm{d}t} = \frac{\partial \rho}{\partial t} + u\frac{\partial \rho}{\partial x} \tag{2.67}$$

which can be used again in equations (2.53), (2.54) and (2.56) to obtain the *compatibility relationships*

$$\frac{\mathrm{d}p}{\mathrm{d}t} \pm \rho a \frac{\mathrm{d}u}{\mathrm{d}t} = 0 \tag{2.68}$$

where pressure and velocity of the gas along the characteristic line of equation (2.62) are related, and

$$\frac{\mathrm{d}p}{\mathrm{d}t} - a^2 \frac{\mathrm{d}\rho}{\mathrm{d}t} = 0 \tag{2.69}$$

where pressure and density of the gas along the characteristic line of equation (2.63) are related. Finally, equation (2.69) can be written as follows

$$a^2 = \frac{\mathrm{d}p}{\mathrm{d}\rho} = \left(\frac{\mathrm{d}p}{\mathrm{d}\rho}\right)_s \tag{2.70}$$

which is actually the isentropic relationship for the speed of sound.

According to the Second Law of Thermodynamics

$$T\mathrm{d}s = \mathrm{d}h - \frac{\mathrm{d}p}{\rho} \tag{2.71}$$

and since the homentropic process is considered, $\mathrm{d}s = 0$, which gives

$$\mathrm{d}p = \rho \mathrm{d}h \tag{2.72}$$

The enthalpy of a perfect gas is expressed as

$$h = c_p T = \frac{\gamma RT}{\gamma - 1} = \frac{a^2}{\gamma - 1} \tag{2.73}$$

and once differentiated with respect to a, gives

$$\mathrm{d}h = \frac{2a}{\gamma - 1}\mathrm{d}a \tag{2.74}$$

Equations (2.72) and (2.74) can be substituted into the compatibility relationship represented by equation (2.68), resulting in

$$\mathrm{d}a \pm \frac{\gamma - 1}{2}\mathrm{d}u = 0 \tag{2.75}$$

With these equations it is possible to relate a and u along the path of the characteristic line given by equation (2.62). Therefore, two relationships between a and u can be obtained, since there is a rightward and a leftward propagating wave. For the rightward one, propagating from point 1 to 2 along the wave, the integration of equation (2.75) gives

$$\int_1^2 \mathrm{d}a + \frac{\gamma - 1}{2}\int_1^2 \mathrm{d}u = 0 \tag{2.76}$$

which results in

$$a_2 - a1 + \frac{\gamma - 1}{2}(u_2 - u_1) = 0 \tag{2.77}$$

This equation can be rearranged as follows

$$a_2 + \frac{\gamma - 1}{2}u_2 = a_1 + \frac{\gamma - 1}{2}u_1 \tag{2.78}$$

At this point, the parameter λ (do not confuse with the eigenvalues) is defined as

$$\lambda = a + \frac{\gamma - 1}{2} u \tag{2.79}$$

which will be constant along the characteristic line, so that

$$\lambda_2 = \lambda_1 \tag{2.80}$$

Following the same process for the leftward propagating wave, it is obtained

$$a_2 - \frac{\gamma - 1}{2} u_2 = a_1 - \frac{\gamma - 1}{2} u_1 \tag{2.81}$$

where now the parameter β, defined as

$$\beta = a - \frac{\gamma - 1}{2} u \tag{2.82}$$

will be constant along the characteristic line, so that

$$\beta_2 = \beta_1 \tag{2.83}$$

The parameters λ and β are called *Riemann invariants* for homentropic flow, or *Riemann variables* in non-homentropic flow, since in that case these quantities are not constant along the characteristic line. Both the velocity u and the speed of sound a can be obtained from the Riemann invariants by adding and subtracting equations (2.79) and (2.82), resulting in

$$a = \frac{\lambda + \beta}{2} \tag{2.84}$$

$$u = \frac{\lambda - \beta}{\gamma - 1} \tag{2.85}$$

In order to further understand the physical meaning of the characteristic lines and the numerical scheme that can be exploited by using the Riemann invariants or variables, Figure 2.1 shows schematically a one dimensional grid where the variables of cell i are calculated for the next time step $n + 1$ from the value of the Riemann invariants in points L and R at time n. As the figure shows, the rightward wave travels at a speed $a + u$ from point L at time step n, while the leftward wave travels at a speed $a - u$ from point R also at time step n, and both waves arrives at point i at time step $n + 1$.

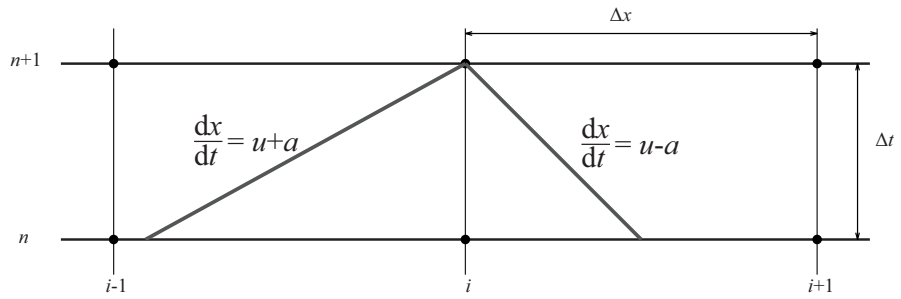

Figure 2.1: Characteristics lines on a general cell for a time step.

Adopting this notation the point 1 of the integration will become point L or R at time step n, and the point 2 will become point i at time step $n+1$. Hence the rightward wave is expressed as follows

$$a_i^{n+1} + \frac{\gamma-1}{2} u_i^{n+1} = a_L^n + \frac{\gamma-1}{2} u_L^n \tag{2.86}$$

or

$$\lambda_i^{n+1} = \lambda_L^n \tag{2.87}$$

where the subscript denotes spatial position and the superscript, time step. Similarly, for the leftward wave it is obtained

$$a_i^{n+1} - \frac{\gamma-1}{2} u_i^{n+1} = a_R^n - \frac{\gamma-1}{2} u_R^n \tag{2.88}$$

or

$$\beta_i^{n+1} = \beta_R^n \tag{2.89}$$

Assuming that all the variables are known at time step n, the value of point L is the linear interpolation of the values of the velocity u and the speed of sound a between points $i-1$ and i at time step n. The same procedure can be use to obtain point R from u and a between points i and $i+1$, achieving thus first-order spacial accuracy.

In the case of non-homentropic flow, the same procedure is followed, including the linear interpolation, but the inclusion of wall friction, heat transfer and section variation modifies the Riemann invariants, changing is value as they propagate, being called then Riemann variables. This makes the formulation

much more complicated and adds a new variable, which depends on the entropy level and travels at the same velocity of the flow. The formulation of the non-homentropic flow case can be found in [5] for more details.

2.3.2 The Courant-Friedrichs-Lewy stability criterion

One of the first papers about finite difference methods for partial differential equations (PDEs) was written in 1928 by Courant, Friedrichs and Lewy [49]. They used finite difference methods as an analytical tool to prove the existence of a solution to certain PDEs. The main goal was to define a series of approximated solutions, proving their convergence as the mesh size is reduced and then show that the limit of the function has to satisfy the PDE, existing thus a solution.

While performing these convergence tests, they demonstrated a stability condition that was necessary for every numerical method. That condition was that the dependency domain of the finite difference method must include the dependency domain of the PDE, at least in the limit when Δx and Δt tend to 0. This stability condition is known as the CFL condition.

The dependency domain $D(\bar{x}, \bar{t})$ of a PDE is defined as a group of points whose initial values $w_0(x)$ affect the solution in $\bar{x}$ and $\bar{t}$. In the case of a hyperbolic system of equations, such points are represented by the following expression

$$D(\bar{x}, \bar{t}) = \left[(\bar{x} - \lambda_1 \bar{t}), (\bar{x} - \lambda_2 \bar{t}), \cdots, (\bar{x} - \lambda_m \bar{t})\right] \tag{2.90}$$

where λ_p are the eigenvalues of the Jacobian matrix of the system and m is the number of equations of the system.

Consider a three-point numerical scheme so that the value of $\mathbf{W}_{\Delta x}(x_j, t_n)$ depends in t_{n-1} on points x_{i+q}, where $q = -1, 0, 1$. Similarly, in t_{n-2} it will depend on points x_{i+q}, where this time $q = -2, -1, 0, 1, 2$. Therefore, going back in time until $t = 0$, the solution in x_j and t_n will depend on points x_{i+q}, where $q = -n, \cdots, n$. Hence the dependency domain of that numerical scheme satisfies

$$D_{\Delta x}(x_j, t_n) \subset \{x : |x - x_j| \leqslant n\Delta x\} \tag{2.91}$$

For a determined fixed point $(\bar{x}, \bar{t})$ it results in

$$D_{\Delta x}(\bar{x}, \bar{t}) \subset \left\{x : |x - \bar{x}| \leqslant (\bar{t}/\Delta t)\Delta x\right\} \tag{2.92}$$

if the mesh is refined keeping constant the ratio $\Delta t/\Delta x = r$, this domain can be expressed in the limit when $\Delta x \to 0$ as:

$$D_0(\bar{x}, \bar{t}) = \{x : |x - \bar{x}| \leqslant \bar{t}/r\} \tag{2.93}$$

The CFL condition requires that

$$D(\bar{x}, \bar{t}) \subset D_0(\bar{x}, \bar{t}) \tag{2.94}$$

By substituting the points of the dependency domain of the PDE in equation (2.93) it is obtained that the following inequality needs to be fulfilled

$$\left|(\bar{x} - \lambda_p \bar{t}) - \bar{x}\right| \leqslant \bar{t}/r \tag{2.95}$$

Therefore, operating and rearranging

$$\left|\frac{\lambda_p \Delta t}{\Delta x}\right| \leqslant 1 \tag{2.96}$$

for each eigenvalue λ of the Jacobian matrix.

The CFL condition is a necessary condition for the stability of the calculation method, but it is not a sufficient condition. It is a necessary condition because if the requirement (2.94) is not met, then there would be points in the real domain that do not belong to the numerical domain. A change in the initial value of some of those points would affect the real solution, but not the numerical solution, therefore, the latter could not converge for every initial value.

The quantity ν is known as the Courant number

$$\nu = \max \left|\frac{\lambda_p \Delta t}{\Delta x}\right| \tag{2.97}$$

For a three-point centred numerical method to be stable it is a necessary condition that the Courant number is lower than 1, $\nu < 1$.

From a physical point of view, the eigenvalues of the Jacobian matrix represent the speed in which the information of the different magnitudes travels, hence, the meaning of the CFL condition of equation (2.96) can be summarized as the condition that the calculation cannot advance faster than information in the fluid. In other words, trying to use a Δt higher than the one indicated by the CFL condition will result in a calculation of the properties of a point before the physical information of the adjacent cells could reach it, obtaining thus an unpredictable result.

2.3.3 The entropy condition

The Euler equations system admits non-differentiable solutions, i.e. discontinuities. From the mathematics point of view, this discontinuities do not satisfy the differential equations of the system, but they are a valid solution for the integral form of the conservation equations.

Nonetheless, the fact that discontinuous solutions exist does not imply that all of them have a physical meaning. Therefore, a criterion is required to identify which of the possible solutions is the correct one from the physical point of view.

According to the Second Law of Thermodynamics it can be deduced that both entropy and entropy flux can be expressed as a function of the conservative variables. Changes in entropy only occur due to entropy flux, except in shock waves. This means that, except in shock waves, entropy will not be created nor destroyed, or expressed as an equation

$$\frac{\partial(\rho s)}{\partial t} + \frac{\partial(\rho u s)}{\partial x} = 0 \tag{2.98}$$

Across a shock wave though, entropy increases, which means that the entropy variation will be higher than the variation produced by the entropy flux. Again, in equation form

$$\frac{\partial(\rho s)}{\partial t} + \frac{\partial(\rho u s)}{\partial x} > 0 \tag{2.99}$$

Based on the statement of the Second Law of Thermodynamics, only compression shock waves are possible, since expansion shock waves would imply negative entropy, which is physically impossible in a real flow. Due to the fact that in the Euler equations there are no dissipative mechanisms, such as viscosity, a new condition to the system needs to be added, which will assure that the correct physical solution is chosen. This condition is called *entropy condition*.

A detailed analysis of the entropy condition based on the properties of the one-dimensional hyperbolic conservation laws was performed by Lax [50], where, as a summary, a conservative laws system with an entropy function $\zeta(\mathbf{W})$ is considered such as:

- ζ is a concave function of $\mathbf{W}$, for instance, $\zeta_{WW} < 0$
- ζ satisfies the expression $\zeta_W \cdot \mathbf{F_W} = \Upsilon_W$

where Υ is called entropy flux. Note that the notation used here for partial derivatives indicates the variable with respect it is differentiated with the subscript.

The solutions that converge to the differential form of the conservation equations are called weak solutions, and they satisfy

$$\frac{\partial \zeta(\mathbf{W})}{\partial t} + \frac{\partial \zeta(\mathbf{W})}{\partial x} \geqslant 0 \tag{2.100}$$

This inequality is the so called entropy condition. Given the following conservative scheme

$$\mathbf{W}_i^{n+1} = \mathbf{W}_i^n - \frac{\Delta t}{\Delta x}\left(\hat{\mathbf{F}}_{i+\frac{1}{2}} - \hat{\mathbf{F}}_{i-\frac{1}{2}}\right) \tag{2.101}$$

where $\hat{\mathbf{F}}$ is a continuous function called numerical flux.

$$\hat{\mathbf{F}}_{i+\frac{1}{2}} = \hat{\mathbf{F}}\left(\mathbf{W}_{i-k+1}^n, \ldots, \mathbf{W}_{i+k}^n\right) \tag{2.102}$$

This conservative scheme is consistent with the entropy condition if the following expression is satisfied:

$$\zeta(\mathbf{W}_i^{n+1}) \geqslant \zeta(\mathbf{W}_i^n) - \frac{\Delta t}{\Delta x}\left(\boldsymbol{\Upsilon}_{i+\frac{1}{2}} - \boldsymbol{\Upsilon}_{i-\frac{1}{2}}\right) \tag{2.103}$$

It is assumed then that the numerical solution of the system of equations (2.43) converges to a smooth solution when the following conditions are accomplished.

- The total variation of the numerical solution with respect to x is bounded with respect to t, Δt and Δx.
- The numerical solution is consistent with the entropy condition (2.100) for all the entropy functions of (2.43)

The entropy condition implies uniqueness in the solution of the initial value problem.

2.3.4 Conservative centred schemes

A centred scheme is one in which all the variables are calculated in the centre of every cell, as opposed to the staggered grid schemes, where usually scalar and vector variables are separated. Even though the method developed here

is applied to a staggered grid, it is important to understand the roots of the method by the history of the evolution of the main numerical methods developed for fluid-dynamics, which were for the most part applied to centred schemes.

In the early development of the numerical schemes, discontinuities introduced by shock waves and contact surfaces could not be properly represented by the differential form of the governing equations, due to the infinite gradients that would result. This problem was finally solved by using the integral conservation form of the equations, guaranteeing that the mass, momentum and energy are explicitly conserved in the volume, even in the presence of discontinuities.

The integral form of the governing equation can be written as follows

$$\int_x \int_t \left(\frac{\partial \mathbf{W}}{\partial t} + \frac{\partial \mathbf{F}(\mathbf{W})}{\partial x} \right) \mathrm{d}x\mathrm{d}t = 0 \tag{2.104}$$

which, once integrated, gives

$$\left(\mathbf{W}_i^{n+1} - \mathbf{W}_i^n \right) \Delta x + \left(\mathbf{F}_{i+\frac{1}{2}} - \mathbf{F}_{i-\frac{1}{2}} \right) \Delta t = 0 \tag{2.105}$$

Here, $\mathbf{W}_i$ represents the average of the conservative variables along the cell i and can be expressed as

$$\mathbf{W}_i = \frac{1}{\Delta x} \int_{x_{i-1/2}}^{x_{i+1/2}} \mathbf{W}\mathrm{d}x \tag{2.106}$$

and $\mathbf{F}_{i\pm1/2}$ is the average flux through the boundaries of cell i during the interval Δt, as follows

$$\mathbf{F}_{i\pm1/2} = \frac{1}{\Delta t} \int_{t^n}^{t^{n+1}} \mathbf{F}\mathrm{d}t \tag{2.107}$$

In figure 2.2 the placement of the variables $\mathbf{W}_i$ and the flux $\mathbf{F}_{i\pm1/2}$ on a generic cell i is schematically shown .

Equation (2.105) is known as the discrete integral form of the one-dimensional system of the Euler Equations without source term. In this equation, the main unknown quantity is the state vector in the next time step, $\mathbf{W}_i^{n+1}$, which has to be obtained so the calculation can continue in time. Rearranging equation (2.105)

$$\mathbf{W}_i^{n+1} = \mathbf{W}_i^n - \frac{\Delta t}{\Delta x} \left(\mathbf{F}_{i+\frac{1}{2}} - \mathbf{F}_{i-\frac{1}{2}} \right) \tag{2.108}$$

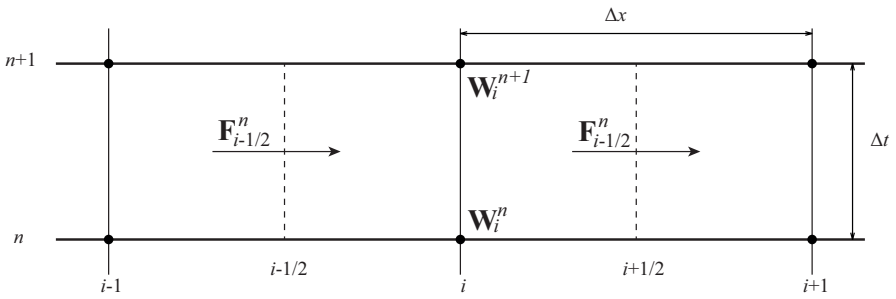

Figure 2.2: Conservative variables and flux in a generic cell.

With equation (2.108), the solution in the time step $n+1$ can be calculated from the values of the solution in the previous time step n and the flux between cells, which would have been calculated in the same way as before or come directly from the initial values of the problem. The only issue that has to be faced is that the flux is evaluated in the boundaries of the cells, but the values of the main variables in that position are unknown, since they are only calculated in the centre of each cell. Therefore, for the numerical method to be usable, this flux has to be estimated as accurately as possible using the values of the variables in the centre of the cell. This estimated flux will be denoted as $\hat{\mathbf{F}}$ and how it is calculated will be the main difference between the different one-dimensional centred schemes developed.

Lax-Friedrichs scheme

This scheme starts from the most simple way to estimate the flux, which is assuming that it will be the average value of the flux evaluated in the two nearest cells

$$\hat{\mathbf{F}}_{i+\frac{1}{2}}^n = \frac{1}{2}\left[\mathbf{F}(\mathbf{W}_{i+1}^n) + \mathbf{F}(\mathbf{W}_i^n)\right] \tag{2.109}$$

which will result in the following equation

$$\mathbf{W}_i^{n+1} = \mathbf{W}_i^n - \frac{\Delta t}{2\Delta x}\left(\mathbf{F}_{i+1}^n - \mathbf{F}_{i-1}^n\right) \tag{2.110}$$

However, by using this simple scheme, numerical oscillations appear and grow with every time step, leading to an unstable solution. This issue can be solved by adding a new term to the flux.

$$\hat{\mathbf{F}}_{i+\frac{1}{2}}^n = \frac{1}{2}\left[\mathbf{F}(\mathbf{W}_{i+1}^n) + \mathbf{F}(\mathbf{W}_i^n) - \frac{\Delta x}{\Delta t}\left(\mathbf{W}_{i+1}^n - \mathbf{W}_i^n\right)\right] \tag{2.111}$$

Using this flux expression leads to the Lax-Friedrichs scheme

$$\mathbf{W}_i^{n+1} = \frac{1}{2}\left(\mathbf{W}_i^{n+1} + \mathbf{W}_{i-1}^{n-1}\right) - \frac{\Delta t}{2\Delta x}\left(\mathbf{F}_{i+1}^n - \mathbf{F}_{i-1}^n\right) \tag{2.112}$$

The resulting method has only first-order accuracy, which is the reason why it is hardly ever used, but it is an important scheme since it became the basis for other more accurate methods.

Mid-point leapfrog method

The leapfrog method uses a similar flux function, but averaging of the cell conservative variables in time

$$\hat{\mathbf{F}}_{i+\frac{1}{2}}^n = \frac{1}{2}\left[\mathbf{F}(\mathbf{W}_{i+1}^n) + \mathbf{F}(\mathbf{W}_i^n) - \frac{\Delta x}{\Delta t}\left(\mathbf{W}_i^{n+1} - \mathbf{W}_i^n\right)\right] \tag{2.113}$$

which results in the following equation

$$\mathbf{W}_i^{n+1} = \mathbf{W}_i^{n-1} - \frac{\Delta t}{\Delta x}\left(\mathbf{F}_{i+1}^n - \mathbf{F}_{i-1}^n\right) \tag{2.114}$$

giving a method that uses three time steps simultaneously, which means that it will need initial conditions in two time steps to start the calculation. Another problem associated with this scheme, is that, as shown in figure 2.3, it actually leads to two independent solutions that alternate each time step. This might result in inconsistencies in the solution, or even in two diverging solutions, especially if the initial conditions are not well defined.

Despite these problems, the leapfrog method is the simplest method that gives second-order accuracy in time and space.

Lax-Wendroff method

One of the most important methods for second-order accuracy centred schemes is the Lax-Wendroff method [51]. It is based on the Taylor series expansion of the sate vector $\mathbf{W}$, as follows

$$\mathbf{W}^{n+1} = \mathbf{W}^{n-1} + \frac{\partial \mathbf{W}}{\partial t}\Delta t + \frac{\partial^2 \mathbf{W}}{\partial t^2}\frac{(\Delta t)^2}{2!} + \dots \tag{2.115}$$

It is possible to substitute the differential terms in order to achieve an expression in the same terms as (2.108). First, using the conservative law form of the Euler Equation (2.41) without source terms, it is obtained

$$\frac{\partial \mathbf{W}}{\partial t} = -\frac{\partial \mathbf{F}}{\partial x} \tag{2.116}$$

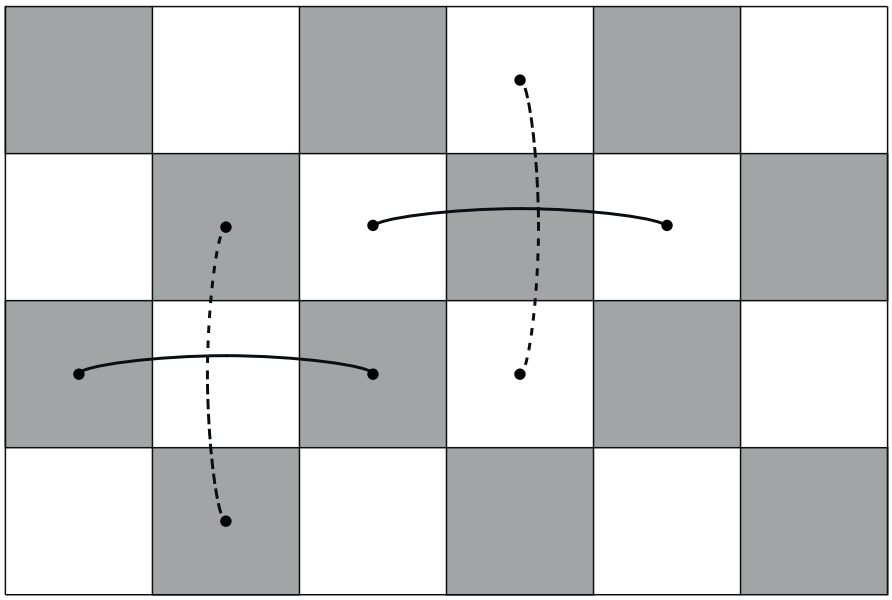

Figure 2.3: Leapfrog scheme representation.

Additionally,

$$\frac{\partial^2 \mathbf{W}}{\partial t^2} = -\frac{\partial}{\partial t}\left(\frac{\partial \mathbf{F}}{\partial x}\right) = -\frac{\partial}{\partial x}\left(\frac{\partial \mathbf{F}}{\partial t}\right) \tag{2.117}$$

which can also be expanded

$$\frac{\partial \mathbf{F}}{\partial t} = \frac{\partial \mathbf{F}}{\partial \mathbf{W}}\frac{\partial \mathbf{W}}{\partial t} = \frac{\partial \mathbf{F}}{\partial \mathbf{W}}\left(-\frac{\partial \mathbf{F}}{\partial x}\right) = -\mathbf{A}\frac{\partial \mathbf{F}}{\partial x} \tag{2.118}$$

where, once again, $\mathbf{A}$ is the Jacobian matrix of the system. Substituting equation (2.118) into equation (2.117) gives

$$\frac{\partial^2 \mathbf{W}}{\partial t^2} = -\frac{\partial}{\partial x}\left(\frac{\partial \mathbf{F}}{\partial t}\right) = \frac{\partial}{\partial x}\left(\mathbf{A}\frac{\partial \mathbf{F}}{\partial x}\right) \tag{2.119}$$

And substituting now equations (2.116) and (2.119) into equation (2.115) gives the following expression

$$\mathbf{W}^{n+1} = \mathbf{W}^{n-1} - \frac{\partial \mathbf{F}}{\partial x}\Delta t + \frac{\partial}{\partial x}\left(\mathbf{A}\frac{\partial \mathbf{F}}{\partial x}\right)\partial(\Delta t)^2 2! + O(\Delta t)^3 \tag{2.120}$$

After operating, it is possible to obtain an explicit scheme with second-order accuracy in time and space with the following flux term:

$$\hat{\mathbf{F}}^n_{i+\frac{1}{2}} = \mathbf{F}^n_{i+\frac{1}{2}} + \frac{\Delta x}{2}\left.\frac{\partial \mathbf{F}}{\partial t}\right|^n_{i+\frac{1}{2}} = \frac{1}{2}\left[\mathbf{F}^n_i + \mathbf{F}^n_{i+1} - \frac{\Delta t}{\Delta x}\mathbf{A}^n_{i+\frac{1}{2}}\left(\mathbf{F}^n_{i+1} - \mathbf{F}^n_i\right)\right] \tag{2.121}$$

As described above, the Lax-Wendroff method introduces an issue, as it requires the evaluation of the Jacobian matrix each time step for every cell boundary, $\mathbf{A}_{i+1/2}$. To overcome this issue, Richtmyer and Morton [52] proposed a modification of the method to avoid the calculation of the Jacobian matrix, by solving the equation with a two-step approach, retaining thus the second order accuracy. This modification is known as the two-step Lax-Wendroff method and became the base of a family of methods with the form of a predictor-corrector algorithm with explicit time integration. The first step is based on the Lax-Friedrichs method, and the second on a mid-point Leapfrog calculation, as follows:

First step:

$$\mathbf{W}^{n+\frac{1}{2}}_{i+\frac{1}{2}} = \frac{1}{2}\left[\mathbf{W}^n_i + \mathbf{W}^n_{i+1} - \frac{\Delta t}{\Delta x}\left(\mathbf{F}^n_{i+1} - \mathbf{F}^n_i\right)\right] \tag{2.122}$$

$$\mathbf{F}^{n+\frac{1}{2}}_{i+\frac{1}{2}} = \mathbf{F}\left(\mathbf{W}^{n+\frac{1}{2}}_{i+\frac{1}{2}}\right) \tag{2.123}$$

Second step:

$$\mathbf{W}^{n+1}_i = \mathbf{W}^n_i - \frac{\Delta t}{2\Delta x}\left(\mathbf{F}^{n+\frac{1}{2}}_{i+\frac{1}{2}} - \mathbf{F}^{n+\frac{1}{2}}_{i-\frac{1}{2}}\right) \tag{2.124}$$

In the first step, an estimation of the solution at points $i+1/2$ and $n+1/2$ is performed, obtaining thus the flux through the volume during the integration step. These inter-cell fluxes are later used in the second step to calculate the solution at point i and $n+1$. A schematic of the method can be seen in figure 2.4.

MacCormack method

A similar method was developed by McCormack [53], which consisted in a two-step predictor-corrector method. Therefore, in the first step the value of the solution in cell i is predicted for the time step $n+1$, which will be called $\bar{\mathbf{W}}^{n+1}_i$, and in the second step that value is corrected to obtain the final solution. The scheme is defined as:

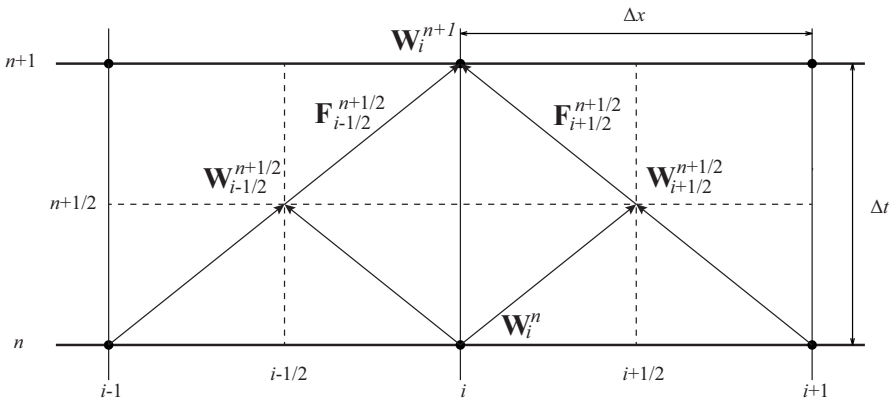

Figure 2.4: Two-step Lax-Wendroff representation.

Predictor step:

$$\bar{\mathbf{W}}_i^{n+1} = \mathbf{W}_i^n - \frac{\Delta t}{2\Delta x}\left(\mathbf{F}_{i+1}^n - \mathbf{F}_i^n\right) \tag{2.125}$$

Corrector step:

$$\mathbf{W}_i^{n+1} = \frac{1}{2}\left[\mathbf{W}_i^n + \bar{\mathbf{W}}_i^{n+1} - \frac{\Delta t}{\Delta x}\left(\bar{\mathbf{F}}_i^{n+1} - \bar{\mathbf{F}}_{i-1}^{n+1}\right)\right] \tag{2.126}$$

resulting as well in an explicit second-order accuracy method.

The S_α^β classification

Lerat and Peyret [54] formulated a general form of two-step predictor-corrector methods in a single scheme with two parameters, α and β. These schemes have the general form:

Predictor step:

$$\mathbf{W}_{i+\alpha}^{n+\beta} = \alpha\mathbf{W}_{i+1}^n + (1-\alpha)\mathbf{W}_i^n - \beta\frac{\Delta t}{2\Delta x}\left(\mathbf{F}_{i+1}^n - \mathbf{F}_i^n\right) \tag{2.127}$$

Corrector step:

$$\mathbf{W}_i^{n+1} = \mathbf{W}_i^n - \frac{\Delta t}{2\beta\Delta x}\left[(\beta-\alpha)\mathbf{F}_{i+1}^n + (2\alpha-1)\mathbf{F}_i^n + (1-\alpha-\beta)\mathbf{F}_{i-1}^n + \mathbf{F}_{i+\alpha}^{n+\beta} - \mathbf{F}_{i-1+\alpha}^{n+\beta}\right] \tag{2.128}$$

The values of α and β define where the predicted variables are evaluated, creating a family of centred second-order accuracy methods called S_α^β family

of Lerat-Peyret. For instance, with the values $\alpha = \beta = 0.5$, the Lax-Wendroff method is obtained, while with the vales $\alpha = 0$ and $\beta = 1$, the McCormack scheme is obtained.

2.3.5 Upwind schemes and Riemann solvers

The numerical methods discussed so far have not taken into account the physical properties of the fluid in the discretization. While centred schemes are symmetrical, upwind schemes are characterised by considering the direction of the propagation of the waves, i.e. distinguishing between upstream and downstream propagation of the information.

One of the first upwind schemes was developed in 1952 by Courant, Isaacson and Rees [55]. They introduced for the first time the physical properties of the flow in the formulation of the discretization of the scheme, which was based on the scalar linear advection equation

$$\frac{\partial w}{\partial t} + a\frac{\partial w}{\partial x} = 0 \tag{2.129}$$

With $a > 0$ the discretization would be

$$w_i^{n+1} = w_i^n - a\frac{\Delta t}{2\Delta x}\left(w_i^n - w_{i-1}^n\right) \tag{2.130}$$

and with $a < 0$

$$w_i^{n+1} = w_i^n - a\frac{\Delta t}{2\Delta x}\left(w_{i+1}^n - w_i^n\right) \tag{2.131}$$

Therefore, the discretization clearly depends on the direction of the propagation of the wave. This scheme is the equivalent to the Method of Characteristics, where the information for the next time step was tracked from the previous one. This scheme also gives better resolution of discontinuities than the Lax-Friedrichs scheme since it is less dissipative. One can define

$$\begin{aligned} a^+ &= \max[a, 0] = \tfrac{1}{2}(a + |a|) \\ a^- &= \min[a, 0] = \tfrac{1}{2}(a - |a|) \end{aligned} \tag{2.132}$$

so that equations (2.130) and (2.131) can be expressed in a single equation as follows

$$w_i^{n+1} = w_i^n - a\frac{\Delta t}{2\Delta x}\left(w_{i+1}^n - w_{i-1}^n\right) + |a|\frac{\Delta t}{2\Delta x}\left(w_{i+1}^n - 2w_i^n + w_{i-1}^n\right) \tag{2.133}$$

This method can be extended to the Euler equations system by expressing it in matrix form and operating (Jacobian matrix diagonalisation and change of variable), resulting in

$$\mathbf{W}_i^{n+1} = \mathbf{W}_i^n - a\frac{\Delta t}{2\Delta x}\left(\mathbf{F}_{i+1}^n - \mathbf{F}_{i-1}^n\right) + |\mathbf{A}|\frac{\Delta t}{2\Delta x}\left(\mathbf{W}_{i+1}^n - 2\mathbf{W}_i^n + \mathbf{W}_{i-1}^n\right) \tag{2.134}$$

In the non-linear case, these schemes require the evaluation of the Jacobian matrix $\mathbf{A}_{i+1/2}$.

This method still remains being first-order accuracy, but modern upwind schemes were later developed in the form of Riemann solvers and extended to higher-order accuracy. Regarding how the upwind direction should be determined, two approaches were established: the *flux vector splitting* approach and the *Godunov method*. The former is based on separating positive and negative flux [56] and usually leads to a more simple algorithm. Godunov's method, on the other hand, gives a better resolution of waves and thus it will be discussed in this section.

Godunov's scheme

Godunov's method is the origin of many modern schemes, also known as reconstruction-evolution schemes. It appeared in 1959 when Godunov [57] proposed a way of using the information of the characteristic lines within a conservative scheme. The method consist of three steps. In the first step, Godunov assumed that the initial state vector of each cell could be replaced by an approximated reconstruction of that state vector that remains constant in that cell. This will give as a result a set of piecewise-constant states with discontinuities at each cell interface, i.e., at $x_{i\pm1/2}$, as shown in figure 2.5. Therefore, the second step would be calculating the inter-cell fluxes by solving the Riemann problem that appears in each cell boundary. This is equivalent to solving a set of shock-tube problems, one in each cell interface, which has an analytical solution. Initially, Godunov used the analytical solution to the Riemann problem, but later other authors developed accurate approximated solvers to the Riemann problem with a much lower computational cost. Finally, the third step consist in calculating the solution for the next time step as a new set of constant state vectors for each cell, establishing a new set of Riemann problems for the next time step.

The resulting method gives a first-order scheme with monotonic behaviour, which was also the basis of Godunov's scheme family. This scheme family, as Godunov's method itself, consist of three calculation steps, which can be

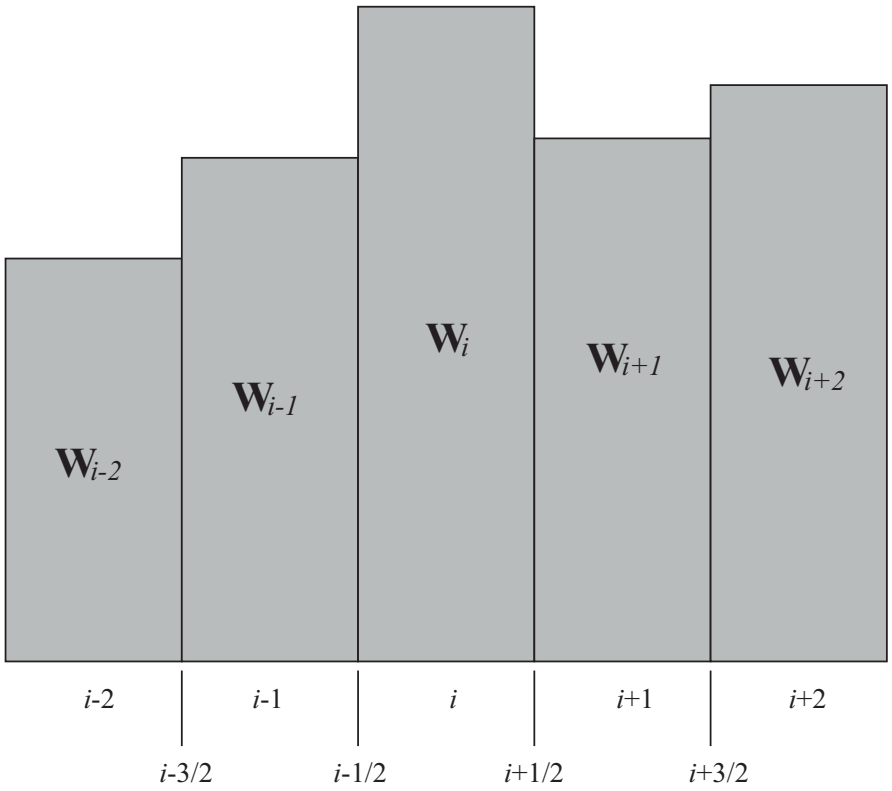

Figure 2.5: Constant state data in each cell in a Godunov scheme.

formulated as follows:

The first step consist in an approximated reconstruction of $\mathbf{W}(x, t_n)$ in the interval $[x_{i-1/2}, x_{i+1/2}[$

$$R(x, \mathbf{W}_i^n) = \hat{\mathbf{W}}_i^n,\ x \in [x_{i-1/2}, x_{i+1/2}[\tag{2.135}$$

Although Godunov used a constant value for the approximated state in each cell, it is possible to use polynomial approximations of the solution, which will increase the order of the scheme to $p + 1$, being p the order of the polynomial approximation.

In the second step the Riemann problems between cells are solved, either with the exact solution or an approximation, taking as initial values

$$\mathbf{W}(x,t_n) = \begin{cases} \hat{\mathbf{W}}_i^n & x < x_{1+\frac{1}{2}} \\ \hat{\mathbf{W}}_{i+1}^n & x > x_{1+\frac{1}{2}} \end{cases} \tag{2.136}$$

Finally, in the third step the solution $\mathbf{W}_i^{n+1}$ is obtained by averaging the solution of the Riemann problem for each cell in t_{n+1}, which is denoted as $\mathbf{W}_n^R(x,t_{n+1})$, as follows

$$\mathbf{W}_i^{n+1} = \frac{1}{\Delta x}\int_{x_{i-1/2}}^{x_{i+1/2}} \mathbf{W}_n^R(x,t_{n+1})\mathrm{d}x \tag{2.137}$$

Considering that the integral includes two different Riemann problems, after some operations, equation (2.137) can be written in conservative form

$$\mathbf{W}_i^{n+1} = \mathbf{W}_i^n + \frac{\Delta t}{\Delta x}\left[\mathbf{F}(\mathbf{W}_n^R(\hat{\mathbf{W}}_i^n, \hat{\mathbf{W}}_{i+1}^n)) - \mathbf{F}(\mathbf{W}_n^R(\hat{\mathbf{W}}_{i-1}^n, \hat{\mathbf{W}}_i^n))\right] \tag{2.138}$$

It is also worth mentioning that Godunov's method leads to a finite volume mesh in a natural way, since state vectors remain constant in each cell, and it also facilitates the calculation of the following time step, since it is calculated directly from the solution of the current time step, as opposed to the Method of Characteristics, where backward tracing of the characteristic lines was needed.

Roe's Riemann solver

One of the main issues of Godunov's method is that it needs to calculate the exact solution of the Riemann problem for every cell interface, which is a slow process. In order to reduce the computational cost, Roe [58] proposed an alternative approach by calculating an approximated solution of the Riemann problem. After his success, a great number of authors started designing upwind schemes based on approximate Riemann solvers. These schemes also used equation (2.138), but the flux $\hat{\mathbf{F}}_{i\pm1/2}^n(\mathbf{W}_L^n, \mathbf{W}_R^n)$ is calculated by means of a Riemann solver. Note that subscripts L and R denote that the value is evaluated either at the left or the right of the cell interface, and they correspond to points $i-1$, i or $i+1$, depending on which of the two interfaces is being evaluated.

What Roe proposed was replacing the Riemann problem that appears in the second step of Godunov's method by the following approximated linear problem, where in the system of conservation laws $\mathbf{F}$ is a linear function of $\mathbf{W}$

$$\frac{\partial \mathbf{W}(x,t)}{\partial t} + \mathbf{A}(\mathbf{W})\frac{\partial \mathbf{W}(x,t)}{\partial x} = 0 \tag{2.139}$$

where $\mathbf{A}$ is the constant Jacobian matrix and it is imposed that

$$\mathbf{W}(x,t_n) = \begin{cases} \hat{\mathbf{W}}_L^n & x < x_{1+\frac{1}{2}} \\ \hat{\mathbf{W}}_R^n & x > x_{1+\frac{1}{2}} \end{cases} \tag{2.140}$$

The Jacobian matrix has to be evaluated at point $i \pm 1/2$, for what Roe proposed

$$\begin{aligned} \bar{u} &= \frac{u_L\sqrt{\rho_L}+u_R\sqrt{\rho_R}}{\sqrt{\rho_L}} \\ \bar{h} &= \frac{h_L\sqrt{\rho_L}+h_R\sqrt{\rho_R}}{\sqrt{\rho_L}} \\ \bar{a} &= \sqrt{(\gamma-1)\left(\bar{h}-\tfrac{1}{2}\bar{u}^2\right)} \\ \bar{\rho} &= \sqrt{\rho_L\rho R} \end{aligned} \tag{2.141}$$

for the Jacobian matrix, the eigenvalues and the eigenvectors.

Lastly, the intercell flow set out by Roe is defined as

$$\hat{\mathbf{F}}^n_{i+\frac{1}{2}} = \frac{1}{2}\left(\mathbf{F}(\mathbf{W}_L^n) + \mathbf{F}(\mathbf{W}_R^n)\right) - \frac{1}{2}\left|\mathbf{A}^n_{i+\frac{1}{2}}\right|\left(\mathbf{W}_L^n + \mathbf{W}_R^n\right) \tag{2.142}$$

Harten-Lax-van Leer (HLL) Riemann solver

Harten *et al.* [59] proposed a different approach to solve the Riemann problem. Their idea was to use a simplified wave structure of the Riemann problem and solve it to get an approximation of the inter-cell flux. Figure 2.6 shows the usual four regions that appear in a general Riemann problem for subsonic flow, simplifying the rarefaction wave to a single line. Therefore, four states can be distinguished, separated by the wave lines. The simplification adopted by the HLL Riemann solver consists of assuming that there is no contact surface, so that the central state is $\mathbf{W}^* = \mathbf{W}_L^* = \mathbf{W}_R^*$.

With this assumption, the integral form of the Euler equations can be solved for the left control volume, giving

$$\mathbf{W}^* = \mathbf{W}_L + \frac{\mathbf{F}^* - \mathbf{F}_L}{c_L} \tag{2.143}$$

and for the right control volume

$$\mathbf{W}^* = \mathbf{W}_R + \frac{\mathbf{F}^* - \mathbf{F}_R}{c_R} \tag{2.144}$$

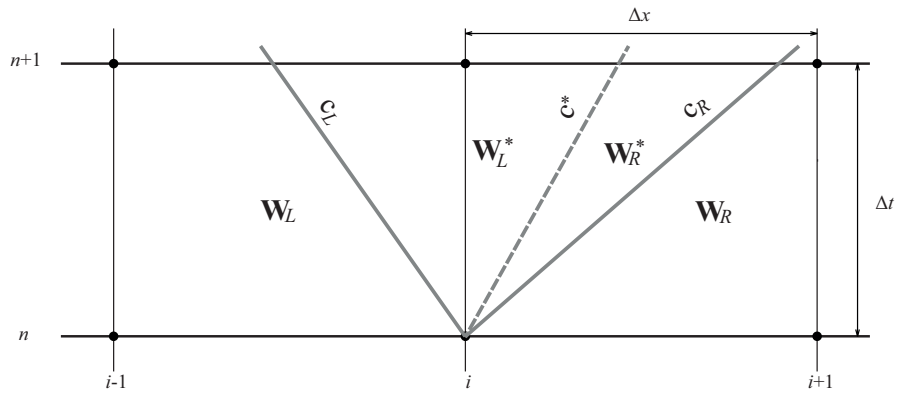

Figure 2.6: Regions of the Riemann problem for subsonic flow.

The state vector $\mathbf{W}^*$ expression can be obtained from equations (2.143) and (2.144)

$$\mathbf{W}^* = \frac{c_R\mathbf{W}_R - c_L\mathbf{W}_L - (\mathbf{F}_R - \mathbf{F}_L)}{c_R - c_L} \tag{2.145}$$

Similarly, the flux function $\mathbf{F}^*$ can be obtained as

$$\mathbf{F}^* = \frac{c_R\mathbf{F}_L - c_L\mathbf{F}_R + c_Lc_R(\mathbf{W}_R - \mathbf{W}_L)}{c_R - c_L} \tag{2.146}$$

eventually giving the inter-cell flux expression used in a Godunov's scheme, as in equation (2.138)

$$\hat{\mathbf{F}}_{i+\frac{1}{2}} = \begin{cases} \mathbf{F}_L & c_L > 0 \\ \mathbf{F}^* = \mathbf{F}_R + c_R(\mathbf{W}^* - \mathbf{W}_R) & c_L \leqslant 0 \leqslant c_R \\ \mathbf{F}_R & c_R > 0 \end{cases} \tag{2.147}$$

where $c_L > 0$ and c_R represent the cases of supersonic flow to the right and to the left, respectively, since in that case both wave lines would be on the same side.

Regarding the estimation of the wave lines c_L and c_R, there are several possibilities, being the most simple

$$c_L = u_L - a_L,\ c_R = u_R + a_R \tag{2.148}$$

or, using the expression suggested by Roe in equation (2.141),

$$c_L = \bar{u}_L - \bar{a}_L,\ c_R = \bar{u}_R + \bar{a}_R \tag{2.149}$$

Both of those approximations were proposed by Davis [60].

The resulting method gives a very efficient inter-cell flux calculation in a very robust numerical method. Its main weakness though appears when calculating a contact surface region in the solution, where the results will be too diffusive, which on the other hand can be expected when considering that the simplification adopted was precisely ignoring the contact surface in the Riemann problem.

HLLC Riemann solver

With the objective of improving the HLL Riemann solver, Toro *et al.* [61] proposed adding a third wave, which can be understood as an approximation of the contact surface. This wave, therefore, is located between the two waves considered in the HLL method and propagates at a speed u^*. This scheme would fully correspond to figure 2.6, where four different states appear. Solving the integral Euler equations for the left control volume in this case gives

$$\mathbf{F}_L^* = \mathbf{F}_L + c_L(\mathbf{W}_L^* - \mathbf{W}_L) \tag{2.150}$$

and for the right control volume

$$\mathbf{F}_R^* = \mathbf{F}_R + c_R(\mathbf{W}_R^* - \mathbf{W}_R) \tag{2.151}$$

where the only unknown values are $\mathbf{W}_L^*$ and $\mathbf{W}_R^*$, besides the flux itself. It is known from the analytical solution of the Riemann problem that in both sides of the contact surface the pressure and velocity of the flow are the same, therefore

$$u^* = u_L^* = u_R^* \tag{2.152}$$

and

$$p^* = p_L^* = p_R^* \tag{2.153}$$

which can be imposed in equations (2.150) and (2.151) to obtain

$$\mathbf{W}_K^* = \rho_K \left(\frac{c_K - u_k}{c_K - u^*}\right) \begin{bmatrix} 1 \\ u^* \\ e_{0K} + (c^* - u_K)\left(c^* + \frac{p_K}{\rho_K(c_K - u_K)}\right) \end{bmatrix} \tag{2.154}$$

where K can be L or R. Now, the only unknown value is c^*, which can be obtain by using equations (2.150) and (2.151) to obtain the pressure at both sides of the contact surface, and then with condition (2.153), combining both pressure expressions to obtain c^* as follows

$$c^* = \frac{p_R - p_L + \rho_L u_L(c_L - u_L) - \rho_R u_R(c_R - u_R)}{\rho_L(c_L - u_L) - \rho_R(c_R - u_R)} \tag{2.155}$$

With this, now W_L^* and W_R^* can be calculated and substituted into equations (2.150) and (2.151) to evaluate the fluxes F_L^* and F_R^* as follows:

$$\hat{\mathbf{F}}_{i+\frac{1}{2}} = \begin{cases} \mathbf{F}_L & c_L > 0 \\ \mathbf{F}_L^* = \mathbf{F}_L + c_L(\mathbf{W}_L^* - \mathbf{W}_L) & c_L \leqslant 0 \leqslant c^* \\ \mathbf{F}_R^* = \mathbf{F}_R + c_R(\mathbf{W}_R^* - \mathbf{W}_R) & c^* \leqslant 0 \leqslant c_R \\ \mathbf{F}_R & c_R > 0 \end{cases} \tag{2.156}$$

After this modification, the resulting method, known as HLLC Riemann solver, manages to keep the advantages of the HLL variant in robustness and efficiency while also bringing a significantly improved resolution around the contact surface. The results obtained by using this method are very similar to the ones obtained using the Godunov method, which uses the exact Riemann solution, but the former is a much more efficient method in terms of computational cost.

2.4 Flux limiters

After the development of the schemes based on Godunov's method, which were still first-order accuracy, the following natural step was to extend them to second-order accuracy. Given the propagation based physics of Godunov's scheme, it could be expected that the robustness of the first-order accuracy solution would be carried to higher-order accuracy numerical methods. However, using this straightforward approach to increase the accuracy of the method proved to bring spurious oscillations into the solution in the regions with high gradients, similarly to the oscillations found in higher-order accuracy methods for finite differences schemes.

The demonstration and formalisation of this problem was rigorously proved by Godunov [57] in what is known as Godunov's theorem. In that theorem he proved that given a first-order accuracy monotonic solution, when trying to expand the scheme to second-order accuracy, the resulting method does

not fulfil the Cauchy inequality, concluding that such scheme cannot exist. In other words, numerical schemes for solving partial differential equations with the property of not generating new extrema (monotonic scheme), can be at most first-order accurate.

It was proposed later the use of non-linear schemes that were high-order accuracy in smooth regions of the solution but that could increase locally the numerical dissipation of the method in the proximity of steep gradients, thus avoiding the development of spurious oscillations. This approach allowed for the appearance of the so called *High-resolution schemes*. Although many different schemes have been developed under this approach, this section will focus on the methods based on *flux limiters*.

In order to easily visualize the flux limiter concept, the one-step Lax-Wendroff scheme can be used on the linear advection equation, giving

$$w_i^{n+1} = w_i^n - \nu \Delta w_{i-\frac{1}{2}}^n - \nu(1-\nu)[(w_{i+1}^n - w_i^n) - (w_i^n - w_{i-1}^n)] \tag{2.157}$$

where $\nu = a\Delta t/\Delta x$. Sweby [62] showed that this second order scheme can be interpreted as the sum of the first-order scheme

$$w_i^{n+1} = w_i^n - \nu \Delta w_{i-\frac{1}{2}}^n \tag{2.158}$$

which corresponds to a Godunov scheme, plus the term

$$-\nu(1-\nu)[(w_{i+1}^n - w_i^n) - (w_i^n - w_{i-1}^n)] \tag{2.159}$$

which can be seen as the anti-diffusive flux. Since the first-order accuracy scheme given by equation (2.158) is known to be free of spurious oscillations, they have to come from the anti-diffusive term. Therefore, following the high-resolution schemes philosophy, this scheme can be modified with a non-linear term able to activate the anti-diffusive term only far away from steep gradients, as follows

$$w_i^{n+1} = w_i^n - \nu \Delta w_{i-\frac{1}{2}}^n - \nu(1-\nu)\phi_i[(w_{i+1}^n - w_i^n) - (w_i^n - w_{i-1}^n)] \tag{2.160}$$

being ϕ the flux limiter. Here, ϕ_i is a function of the solution, as it is non-linear, and it has to be able to measure how smooth the solution is around point i. Therefore, if the solution in the proximity is smooth, the value of ϕ_i should be close to one, resulting in the original Lax-Wendroff scheme. Near

steep gradients however, ϕ_i should be close to zero, going back to first-order accuracy and avoiding numerical oscillations.

Following this criterion, two classes of high-resolution numerical methods can be established: post-processing and pre-processing schemes.

In a post-processing scheme, first the solution is calculated with the appropriate numerical method and then modified with the corresponding flux limiter. Some examples are the flux corrected transport (FCT) schemes or some total variation diminishing (TVD) flux limiters, which will be discussed later.

On the other hand, in a pre-processing scheme the data representation is modified before the solution is updated. Some examples are the MUSCL technique (monotonic upstream centred scheme for conservation laws), the parabolic piece-wise method (PPM) or the essentially non-oscillatory (ENO) schemes.

Given the nature of the numerical method developed in this work, where a three-dimensional staggered grid is used and the momentum equation is simplified to a one-dimensional equation, it is much more suitable using a post-processing scheme, where the flux limiter has just to be added to the original numerical method. Therefore, post-processing schemes will be detailed, while the pre-processing schemes will only be mentioned with a brief description.

2.4.1 Flux Corrected Transport (FCT)

The Flux Corrected Transport method (FCT) [63] is a post-processing scheme that consists of three stages: a transport stage based on the scheme considered, a diffusion stage for reducing the numerical dispersion introduced in the transport stage, and an anti-diffusion stage to restore the accuracy of the scheme at cells with a smooth solution while preserving the diffusion operator accuracy in the vicinity of discontinuities. While the transport stage is defined by the governing equations and their discretization, in the diffusion stage a linear operator is defined that is introduced in the scheme in conservative form and allows to reduce or eliminate any non-physical numerical oscillations produced in the transport stage, thus reducing the accuracy to first order.

The diffusive operator is defined as

$$\mathbf{D}_i(\mathbf{W}) = \theta(\mathbf{W}_{i+1/2}) - \theta(\mathbf{W}_{i-1/2}) \tag{2.161}$$

where

$$\theta(\mathbf{W}_{i+1/2}) = \frac{\vartheta}{4}(\mathbf{W}_{i+1} - \mathbf{W}_i) \tag{2.162}$$

Here, $\mathbf{W}_i$ is the variable computed at cell i in the transport stage, subscripts $i \pm 1/2$ indicate that the variable is evaluated at the midpoint between cells i and $i \pm 1$. The factor ϑ is a positive real number that has to be $\vartheta \geqslant 1/2$ so that instabilities are avoided. The guessed value $\bar{\mathbf{W}}_i$ of the variable $\mathbf{W}_i$ may be computed in two ways: applying diffusion via smoothing, so that:

$$\bar{\mathbf{W}}_i^{n+1} = \mathbf{W}_i^{n+1} + \mathbf{D}_i(\mathbf{W}_i^{n+1}) \tag{2.163}$$

or applying diffusion via damping, in which case one has:

$$\bar{\mathbf{W}}_i^{n+1} = \mathbf{W}_i^{n+1} + \mathbf{D}_i(\mathbf{W}_i^{n}) \tag{2.164}$$

Finally, an anti-diffusion stage is applied, where the accuracy of the scheme used in the transport stage in those cells where the solution is smooth is restored, but preserving the non-oscillatory behaviour of the diffusion operator in the neighbourhood of discontinuities. With this purpose, a non-linear operator A_j is defined as

$$\mathbf{A}_i(\mathbf{W}) = \Psi(\mathbf{W}_{i+1/2}) - \Psi(\mathbf{W}_{i-1/2}) \tag{2.165}$$

Using the anti-diffusive limited flow defined in [64] one has

$$\Psi(\mathbf{W}_{i+\frac{1}{2}}) = s \max\left[0, \min\left(\frac{5}{8}s\Delta\mathbf{W}_{i-\frac{1}{2}}, \frac{1}{8}\left|\Delta\mathbf{W}_{i+\frac{1}{2}}\right|, \frac{5}{8}s\Delta\mathbf{W}_{i+\frac{3}{2}}\right)\right] \tag{2.166}$$

Here, $s = \texttt{sign}(\Delta\mathbf{W}_{i+1/2})$, $\Delta\mathbf{W}_{i-1/2} = \mathbf{W}_i - \mathbf{W}_{i-1}$, $\Delta\mathbf{W}_{i+1/2} = \mathbf{W}_{i+1} - \mathbf{W}_i$ and $\Delta\mathbf{W}_{i+3/2} = \mathbf{W}_{i+2} - \mathbf{W}_{i+1}$. Then, depending on the information used, one can devise three different forms for this step:

- The Naive method

$$\bar{\bar{\mathbf{W}}}_i^{n+1} = \bar{\mathbf{W}}_i^{n+1} + \mathbf{A}_i(\mathbf{W}_i^{n}) \tag{2.167}$$

- The Phoenical method

$$\bar{\bar{\mathbf{W}}}_i^{n+1} = \bar{\mathbf{W}}_i^{n+1} + \mathbf{A}_i(\mathbf{W}_i^{n+1}) \tag{2.168}$$

- The Explicit method

$$\bar{\bar{\mathbf{W}}}_i^{n+1} = \bar{\mathbf{W}}_i^{n+1} + \mathbf{A}_i(\bar{\mathbf{W}}_i^{n+1}) \tag{2.169}$$

As defined, flux correction techniques are conservative at the interior mesh points, since all the corrections are cancelled out along the duct except at the ends, where the anti-diffusion operator can be defined by evaluating the differences present in each case, i.e.:

$$\Psi(\mathbf{W}_{i+\frac{1}{2}}) = s \max\left[0, \min\left(\frac{8}{5} s\Delta\mathbf{W}_{i-\frac{1}{2}}, \frac{1}{8}\left|\Delta\mathbf{W}_{i+\frac{1}{2}}\right|\right)\right] \tag{2.170}$$

for the right end, and

$$\Psi(\mathbf{W}_{i-\frac{1}{2}}) = s \max\left[0, \min\left(\frac{1}{8}\left|\Delta\mathbf{W}_{i-\frac{1}{2}}\right|, \frac{5}{8} s\Delta\mathbf{W}_{i+\frac{1}{2}}\right)\right] \tag{2.171}$$

for the left end.

2.4.2 Total Variation Diminishing (TVD)

The total variation diminishing concept appears from the need of a criterion that allows the design of a numerical scheme that does not suffer from spurious oscillations. For that, some properties have to be fulfilled.

As starting point, consider the initial value problem for a scalar conservation law

$$w_t + f(w)_x = 0,\ w(x,0) = w_0(x),\ -\infty < x < \infty \tag{2.172}$$

where sub-index t and x represent the partial derivative of w with respect to that variable and w_0 is assumed to have bounded total variation. A weak solution to this problem (physical solution) has the so-called monotonicity property, according to which:

- No new local extrema in space is created.
- The value of a local minimum is nondecreasing and the value of a local maximum is nonincreasing.

The total variation of the solution to (2.172) at time t for a continuous and discrete equation is defined as

$$TV = \int \left| \frac{\partial w}{\partial x} \right| \mathrm{d}x,\ TV(w) = \sum_i |w_{i+1} - w_i| \tag{2.173}$$

From the monotonicity property, it follows that the total variation in x of $w(x,t)$ does not increase with t. That is

$$TV(w^{n+1}) \leqslant TV(w^n) \tag{2.174}$$

In order to satisfy the discrete version of the equation (2.173), Harten [65] proposed to consider an explicit finite difference scheme in conservation form, denoted in operator form as

$$w^{n+1} = L \cdot w^n \tag{2.175}$$

Then, the finite difference scheme is *total variation diminishing* (TVD) if for all w of bounded total variation one has:

$$TV(w^{n+1}) = TV(L \cdot w^n) \leqslant TV(w^n) \tag{2.176}$$

In addition, a scheme is called *monotonicity preserving* if the finite difference operator L is monotonicity preserving, i.e., if w is a monotone mesh function, so is $L \cdot w$.

Harten [65] also proved that a monotone scheme is total variation diminishing and that a TVD scheme is monotonicity preserving. Therefore, TVD schemes are intrinsically free from spurious oscillations.

It is usual to write the scheme (2.175) in the form

$$u_i^{n+1} = u_i^n - C_{i-1/2}^- \Delta u_{i-1/2}^n + C_{i+1/2}^+ \Delta u_{i+1/2}^n \tag{2.177}$$

where

$$\Delta u_{i+1/2}^n = u_{i-1}^n - u_i^n \tag{2.178}$$

and

$$C_{i-1/2}^- = C^-(u_{i-2}, u_{i-1}, u_i, u_{i+1}) \tag{2.179}$$

$$C_{i+1/2}^+ = C^+(u_{i-1}, u_i, u_{i+1}, u_{i+2}) \tag{2.180}$$

The choice of $C_{i-1/2}^-$ and $C_{i+1/2}^+$ is not unique. Harten [65] also proved that if the coefficients $C_{j-1/2}^-$ and $C_{j+1/2}^+$ satisfy the inequalities

$$\begin{gathered} C^{-}_{i-1/2} \geqslant 0,\ C^{+}_{i+1/2} \geqslant 0 \\ C^{-}_{i-1/2} + C^{+}_{i+1/2} \leqslant 1 \end{gathered} \tag{2.181}$$

then the scheme (2.177) is total variation diminishing.

With this definition, Sweby [62] developed the general theory of flux limiters that ensure a TVD scheme. At the beginning of this section a flux limiter was applied to the Lax-Wendroff discretization of the advection equation, giving the scheme represented by equation (2.160), where ϕ was the flux limiter. This flux limiter can be a function of successive gradients, r, expressed as

$$\phi_i = \phi(r_i) \tag{2.182}$$

where

$$r_i = \frac{\Delta w^n_{i-1/2}}{\Delta w^n_{i+1/2}} \tag{2.183}$$

The objective is to find the range of values that the function ϕ can adopt which results in a scheme with the TVD property. Sweby [62] was able to find the region where $\phi(r)$ must lie so that the resulting second order scheme is TVD by choosing the following values for $C^{-}_{i-1/2}$ and $C^{+}_{i+1/2}$

$$C^{-}_{i-1/2} = \nu\left[1 + \frac{1}{2}(1-\nu)\left(\frac{\phi(r_i)}{r_i} - \phi(ri-1)\right)\right],\ C^{+}_{i+1/2} = 0 \tag{2.184}$$

and using the known values used for the flux limiter to obtain a Lax-Wendroff scheme, $\phi(r) = 1$, and a Warming and Beam upwind scheme, $\phi(r) = r$, as delimiters for that region. Figure 2.7 shows the region where $\phi(r)$ must lie to obtain a second order TVD scheme.

In section 3.6 the Davis TVD scheme will be detailed, along with its adaptation to a staggered-grid mesh method.

2.4.3 Other high resolution schemes

In addition to the numerical methods described in this section, a lot of different work lines have been developed in fluid-dynamic simulation, but since they are not essential for understanding the numerical method developed in chapter 3, they will not be detailed here. However, it is worth at least enumerate the main ones in this section to complete the literature review and to provide a hint for future work.

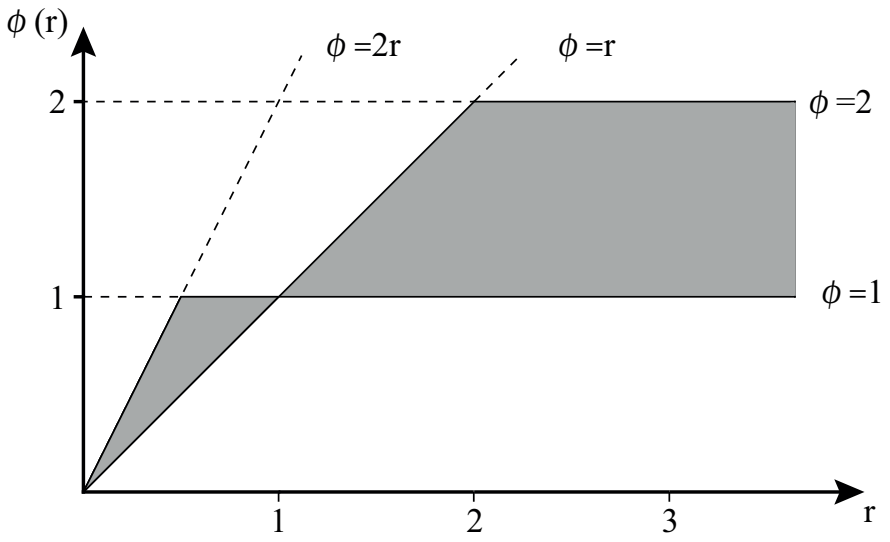

Figure 2.7: Region for TVD flux limiter.

Firstly, an interesting type of scheme are the self-adjusting hybrid schemes. The basis of these schemes is the combination of two different fluxes depending on the circumstances, for example combining the flux of the Roe scheme and the Lax-Wendroff scheme. In order to do this, a parameter is defined that depends on the gradients in the solution, favouring one flux or the other. Some important schemes within this family were proposed by Harten and Zwas [66, 67], Harten [68] or Jameson [69, 70].

Another important family of numerical methods are the second order Godunov schemes. From the original Godunov's method, Van Leer [71] proposed using linear approximations to achieve second-order accuracy. Besides, by limiting the slopes of those approximations for each component, the scheme can be TVD. These Godunov's schemes with linear approximations belong to the pre-processing schemes family, since they modify the data representation before updating the solution, and are known as MUSCL (Monotonic Upstream-centred Scheme for Conservation Laws). Goodman and LeVeque [72] proposed one of these schemes with a scalar approximation but with a linear interpolation for the numerical flux. Other MUSCL methods were proposed by Davis [73] and Colella [74].

Later, Colella and Woodward [75] replaced the linear functions for piecewise parabolic functions, giving this method the name PPM (Piecewise Parabolic

Method) and improving the accuracy of the MUSCL schemes by increasing its order. Other high-order methods were developed by Coquel and LeFloch [76].

Lastly, Harten and Osher [77] presented a family of high-order non-oscillatory schemes, known as ENO (Essentially Non-Oscillatory) schemes, with the objective of reducing the number of local extrema in the numerical solution. This fact guarantees that monotonic initial solutions lead to monotonic results, but as opposed to the TVD schemes, the local extrema values can be accentuated if needed.

2.5 Duct junctions

Duct junctions are essential elements of numerous piping systems, including the intake and exhaust systems of reciprocating internal combustion engines. The use of one-dimensional time domain gas-dynamic codes has become commonplace in the numerical study of unsteady flows in such systems, both in terms of their effect on engine performance and on intake and exhaust orifice noise, as stated by Winterbone and Pearson [5]. While assuming one-dimensional wave action may be acceptable when duct diameters are relatively small, as is the case in the majority of the ducts present in engine intake and exhaust systems of passenger car engines, Payri *et al.* [6] proved that in certain elements, and most notably in duct junctions, complex three-dimensional flow structures may occur. Consideration of the effects of such structures on the one-dimensional flow in the adjacent ducts requires the definition of suitable boundary conditions at the junction, usually involving empirical information.

The effects of a junction on the flow in the neighbouring ducts arise in different ways. From the point of view of the passive propagation of small amplitude pressure waves (i.e., in the acoustic range) the effect can be characterized in terms of length corrections, which have been reported to depend on the type of side-branch and the branch width and length by Tang [78], and with a rapid increase in the duct length corrections being associated with the excitation of non-planar higher order modes, which also results in lower sound transmission. This sort of representation has been quite successfully applied by Harrison [79] to the prediction of the effect on intake noise of a multi-pipe junction in the intake manifold. Karlsson and Åbom [80] also reported that for low Strouhal numbers based on the duct diameter, the acoustic transmission properties of T-junctions can be acceptably described by using an incompressible quasi-steady model, the upper limit of the Strouhal number being defined by flow-acoustic interaction effects, which differ significantly between different

flow configurations: waves incident on the junction at the downstream side are attenuated, whereas waves incident at the other branches may be either amplified or attenuated, depending on the Strouhal number, also by Karlsson and Åbom [81]. Desantes *et al.* [82] proved that such flow-acoustic interactions due to the coupling of the flow and the geometry are common to all intake and exhaust system elements.

When the focus is on the effect of the junction on the propagation of finite amplitude pressure waves and the resulting influence on engine performance, different approaches are found in the literature, most of them inspired by the seminal work of Benson [16]. The simplest approach is given by constant pressure models, in which is it assumed that the pressure at the end of all branches of the junction is the same at any time, so that the pressure is assumed to be uniform across the junction. The most comprehensive description of these models is given by Corberán [83], where it was shown that, besides the assumption of uniform pressure, additional closing equations must be added. While the choice of those equations is arbitrary, Corberán [83] also showed that assuming that the total enthalpy for all the outgoing flows is the same provides suitable results.

More elaborated approaches are based on the consideration of the pressure differences existing between the different branches, which are incorporated in a quasi-steady manner, i.e., steady pressure loss coefficients (or more properly, as discussed in detail by Schmandt and Herwig [84], energy change coefficients accounting partly for losses and partly to a mutual energy transfer between the partial flows) are applied at each time step. The solutions proposed differ mainly in the origin of the pressure loss coefficients, in the hypotheses underlying their determination, and in the precise implementation of the solution method.

Regarding the origin of the coefficients, while there have been some attempts to obtain them from computational fluid dynamics (CFD) simulations by Shaw [85], Pérez-García [86] and Naeimi [87], it appears that the results are strongly dependent on the numerical method used, both in the details of the flow and in the overall values of the coefficients obtained, as Sakowitz *et al.* [88] detailed. Therefore, usually the coefficients are either obtained from simple and robust models, or specific measurements are performed in order to characterize the junction under consideration. The most successful example of the first option was probably presented by Bassett *et al.* [89], where a remarkable agreement with experimental results was obtained from a model that extended the previous work performed by Hager [90] and neglected any

effects of mixing losses, compressibility and wall friction. Regarding the experimental characterization, it is usual to consider steady incompressible flow, as Paul *et al.* [91] did, but more recently, Pérez-García *et al.* [92] have reported specific studies accounting for the flow compressibility that suggest that the total pressure loss coefficient is mainly dependent on the Mach number, mass flow rate ratio, and area ratio, and is almost independent of the Reynolds number.

Numerous implementations of the pressure loss model for multi-pipe junctions have been proposed in the literature, comprising implicit time formulations by Peters and Gosman [93] and different explicit solutions, such as the supplier–collector strategy, by Bingham and Blair [94], the branch superposition method by William-Louis[95] and the generalization of the classical approach of Benson presented by Basset *et al.* [96]. The limitations of these approaches lie mainly in the fact that, even if steady flow coefficients contain information on three-dimensional separation effects around the junction, the results will be significant only if quasi-steady flow can be assumed, which requires that mass and energy storage at the junction are very small, which may not be the case in real manifold flows. Additionally, any information regarding the wave refraction characteristics of the junction is lost in the quasi-steady approximation.

Overcoming these limitations requires accounting for the unsteady and multi-dimensional character of the flow at the junction, but without incurring in an excessive computational cost. A suitable solution is thus to include a local multi-dimensional region within an otherwise one-dimensional wave-action engine simulation, as first Pearson *et al.* [97] suggested. In this first approach, an inviscid two-dimensional model was applied to the simulation of shock-wave propagation through different junctions, and the observed evolution of the wave fronts through the junctions and the measured high frequency pressure oscillations induced by the transverse reflections were successfully predicted. However, even if the increase in the computational cost was reasonable, it did not appear to be justified when compared with a conventional quasi-steady pressure loss model, as shown by Basset [98].

It appears, thus, that a full three-dimensional description of the junction should be used in order to describe its unsteady behaviour. Monenegro [99] and Onorati [100] successfully presented such description, reproducing the flow field and the associated non-plane-wave motion. However, even if coarse 3D grids were used in the first simulation cycles that were switched to more refined grids during the last simulation cycles, the computational cost and time may

still be regarded as excessive for the practical design and evaluation of full intake and exhaust systems.

A possible alternative to 1D–3D coupling, which could provide some accountancy for the three-dimensional effects at the junction and which has not been explored in some detail, would be used in the context of a staggered mesh finite volume method, as the one proposed by Montenegro *et al.* [11]. Such methods have become standard in commercial codes, either as the core solver by Morel [12] and Sapsford [13], or used locally for elements exhibiting significant three-dimensional features, such as plenums and mufflers, as performed by Montenegro *et al.* [14]. Typically, when these methods are applied to simple duct junctions, a single volume is used for the junction with appropriate effective areas and characteristic lengths at each connection with the adjacent ducts. As these connections contain information on vector quantities (including the orientation of the branch duct) the momentum equation can be solved, even in an approximate way, so that all the effects of the junction of the flow need not be included through the pressure loss coefficients. Additionally, it would be possible to use a refined mesh locally at the junction, so that a first-order estimate of any three-dimensional features could be obtained.

In chapter 6 it is explored the potential of these ideas as a way to improve the description of the effect of simple duct junctions on an otherwise one-dimensional flow system, specifically as the intake or exhaust of an internal combustion engine.

Chapter 2 Bibliography

[5] D. E. Winterbone and R. J. Pearson. *Design techniques for engine manifolds: wave action methods for IC engines*. Professional Engineering Publishing, 1999 (cit. on pp. 3, 31, 56, 70).

[6] F. Payri, E. Reyes, and J. Galindo. "Analysis and modeling of the fluid-dynamic effects in branched exhaust junctions of ICE." *Journal of engineering for gas turbines and power* 123(1) (2001), pp. 197–203 (cit. on pp. 3, 56, 70).

[11] G. Montenegro, A. Onorati, and A. Della Torre. "The prediction of silencer acoustical performances by 1D, 1D–3D and quasi-3D non-linear approaches." *Computers & Fluids* 71 (2013), pp. 208–223 (cit. on pp. 4, 59, 72, 151).

[12] T. Morel, J. Silvestri, K.-A. Goerg, and R. Jebasinski. *Modeling of engine exhaust acoustics*. SAE Technical Paper 1999-01-1665. 1999 (cit. on pp. 4, 59, 70, 72).

[13] S. M. Sapsford, V. C. Richards, D. R. Amlee, T. Morel, and M. T. Chappell. *Exhaust system evaluation and design by non-linear modeling*. SAE Technical Paper 920686. 1992 (cit. on pp. 4, 59, 72, 122).

[14] G. Montenegro, A. Della Torre, A. Onorati, R. Fairbrother, and A. Dolinar. *Development and application of 3D generic cells to the acoustic modelling of exhaust systems*. SAE Technical Paper 2011-01-1526. 2011 (cit. on pp. 4, 59).

[16] R. S. Benson. *Thermodynamics and Gas Dynamics of Internal Combustion Engines*. Cambridge University Press, 1982 (cit. on pp. 4, 25, 57).

[29] European Parliament, Council of the European Union. "Regulation (EC) No 715/2007 of the European Parliament and of the Council of 20 June 2007 on type approval of motor vehicles with respect to emissions from light passenger and commercial vehicles (Euro 5 and Euro 6) and on access to vehicle repair and maintenance information (Text with EEA relevance)." *Official Journal of the European Union* (50) (June 2007), pp. 1–16 (cit. on p. 14).

[30] European Parliament, Council of the European Union. "Regulation (EC) No 595/2009 of the European Parliament and of the Council of 18 June 2009 on type-approval of motor vehicles and engines with respect to emissions from heavy duty vehicles (Euro VI) and on access to vehicle repair and maintenance information and amending Regulation (EC) No 715/2007 and Directive 2007/46/EC and repealing Directives 80/1269/EEC, 2005/55/EC and 2005/78/EC (Text with EEA relevance)." *Official Journal of the European Union* (52) (July 2009), pp. 1–13 (cit. on p. 14).

[31] H. Daneshyar. *One-Dimensional Compressional Flow*. Peramon Press, 1976 (cit. on p. 15).

[32] D. E. Winterbone and R. J. Pearson. *Theory of engine manifold design: wave action methods for IC engines*. Wiley-Blackwell, 2000 (cit. on p. 15).

[33] F. J. Arnau. *Métodos numéricos para el modelado unidimensional del proceso de renovación de la carga*. Reverté, 2009 (cit. on pp. 15, 80).

[34] M. L. Gascón Martínez. "Estudio de esquemas en diferencias finitas para el cálculo del flujo compresible unidimensional, no estacionario y no isentrópico." PhD thesis. Universitat Politècnica de València, 1995 (cit. on p. 22).

[35] J. Corberán and M. L. Gascón. "New method to calculate unsteady 1-D compressible flow in pipes with variable cross section. Application to the calculation of the flow in intake and exhaust pipes of I. C. engines." *ASME, NEW YORK, NY,(USA).* 23 (1995), pp. 77–87 (cit. on pp. 23, 25).

[36] J. Corberán and M. L. Gascón. "TVD schemes for the calculation of flow in pipes of variable cross-section." *Mathematical and computer modelling* 21(3) (1995), pp. 85–92 (cit. on p. 23).

[37] J. Liu, N. Schorn, C. Schernus, and L. Peng. *Comparison studies on the method of characteristics and finite difference methods for one-dimensional gas flow through IC engine manifold.* SAE Technical Paper 960078. 1996 (cit. on p. 23).

[38] E. Jenny. "Unidimensional transient flow with consideration of friction, heat transfer and change of section." *Brown Boveri Review* 37(11) (1950), p. 447 (cit. on p. 24).

[39] F. Wallace and G. Boxer. "Wave action in diffusers for exhaust-pipe systems, with special reference to the scavenging of two-stroke engines." *Proceedings of the type of Mechanical Engineers* 170(1) (1956), pp. 1131–1156 (cit. on p. 24).

[40] R. Benson. "The Effect of Excess Scavenge Air on the Pressure Drop in the Cylinder of a Two-Stroke Cycle Engine During Exhaust Blow down." *The Aeronautical Journal* 59(539) (1955), pp. 773–778 (cit. on p. 24).

[41] R. Benson and W. Woods. "Wave action in the exhaust system of a supercharged two-stroke-engine model." *International Journal of Mechanical Sciences* 1(2-3) (1960), pp. 253–281 (cit. on p. 24).

[42] G. Zehnder. "Calculating gas flow in pressure-wave machines." *Brown Boveri Review* 58(4-5) (1971), p. 172 (cit. on p. 25).

[43] H. Dwyer, R. Allen, M. Ward, D. Karnopp, and D. Margolis. "Shock capturing finite difference methods for unsteady gas transfer." In: *7th Fluid and PlasmaDynamics Conference.* 1974, p. 521 (cit. on p. 25).

[44] G. Ferrari and A. Onorati. "Determination of silencer performances and radiated noise spectrum by 1-d gas dynamic modelling." In: *VEHICLE AND ENVIRONMENT. 25TH FISITA CONGRESS, BEIJING 1994, VOL 3. TECHNICAL PAPER NO. 945135*. 1994 (cit. on p. 25).

[45] D. Winterbone, R. Pearson, and Y. Zhao. "Numerical simulation of intake and exhaust flows in a high speed multi-cylinder petrol engine using the Lax-Wendroff method." *I Mech E, C* 430 (1991), p. 038 (cit. on p. 25).

[46] A. Onorati and G. Ferrari. *Modeling of 1-D unsteady flows in IC engine pipe systems: numerical methods and transport of chemical species*. SAE Technical Paper 980782. 1998 (cit. on p. 25).

[47] B. Riemann et al. *Über die Fortpflanzung ebener Luftwellen von endlicher Schwingungsweite*. Verlag der Dieterichschen Buchhandlung, 1860 (cit. on p. 25).

[48] C. Hirsch and C. Hirsch. *Fundamentals of numerical discretization*. Wiley, 1988 (cit. on p. 26).

[49] R. Courant, K. Friedrichs, and H. Lewy. "Über die partiellen Differenzengleichungen der mathematischen Physik." *Mathematische annalen* 100(1) (1928), pp. 32–74 (cit. on pp. 31, 76).

[50] P. D. Lax. *Hyperbolic systems of conservation laws and the mathematical theory of shock waves*. SIAM, 1973 (cit. on p. 33).

[51] P. Lax and B. Wendroff. "Systems of conservation laws." *Communications on Pure and Applied mathematics* 13(2) (1960), pp. 217–237 (cit. on p. 37).

[52] R. D. Richtmyer and K. W. Morton. "Difference methods for initial-value problems." *Malabar, Fla.: Krieger Publishing Co.,| c1994, 2nd ed.* (1994) (cit. on p. 39).

[53] R. W. MacCormack. "The effect of viscosity in hypervelocity impact cratering." *Frontiers of Computational Fluid Dynamics* (1969), pp. 27–44 (cit. on p. 39).

[54] A. Lerat and R. Peyret. "Non-centred schemes and shock propagation problems." *Computers and fluids* (1974), pp. 35–52 (cit. on p. 40).

[55] R. Courant, E. Isaacson, and M. Rees. "On the solution of nonlinear hyperbolic differential equations by finite differences." *Communications on Pure and Applied Mathematics* 5(3) (1952), pp. 243–255 (cit. on p. 41).

[56] J. L. Steger and R. Warming. "Flux vector splitting of the inviscid gasdynamic equations with application to finite-difference methods." *Journal of computational physics* 40(2) (1981), pp. 263–293 (cit. on p. 42).

[57] S. K. Godunov. "A difference method for numerical calculation of discontinuous solutions of the equations of hydrodynamics." *Matematicheskii Sbornik* 89(3) (1959), pp. 271–306 (cit. on pp. 42, 48, 179).

[58] P. L. Roe. "Approximate Riemann solvers, parameter vectors, and difference schemes." *Journal of computational physics* 43(2) (1981), pp. 357–372 (cit. on p. 44).

[59] A. Harten, P. D. Lax, and B. v. Leer. "On upstream differencing and Godunov-type schemes for hyperbolic conservation laws." *SIAM review* 25(1) (1983), pp. 35–61 (cit. on p. 45).

[60] S. Davis. "Simplified second-order Godunov-type methods." *SIAM Journal on Scientific and Statistical Computing* 9(3) (1988), pp. 445–473 (cit. on p. 47).

[61] E. F. Toro, M. Spruce, and W. Speares. "Restoration of the contact surface in the HLL-Riemann solver." *Shock waves* 4(1) (1994), pp. 25–34 (cit. on pp. 47, 153).

[62] P. K. Sweby. "High resolution schemes using flux limiters for hyperbolic conservation laws." *SIAM journal on numerical analysis* 21(5) (1984), pp. 995–1011 (cit. on pp. 49, 54, 80).

[63] J. P. Boris and D. L. Book. "Flux-corrected transport. I. SHASTA, a fluid transport algorithm that works." *Journal of computational physics* 11(1) (1973), pp. 38–69 (cit. on pp. 50, 78).

[64] T. Ikeda and T. Nakagawa. "On the SHASTA FCT algorithm for the equation = 0." *Mathematics of Computation* 33(148) (1979), pp. 1157–1169 (cit. on p. 51).

[65] A. Harten. "High resolution schemes for hyperbolic conservation laws." *Journal of computational physics* 49(3) (1983), pp. 357–393 (cit. on pp. 53, 71, 80).

[66] A. Harten and G. Zwas. "Self-adjusting hybrid schemes for shock computations." *Journal of Computational Physics* 9(3) (1972), pp. 568–583 (cit. on p. 55).

[67] A. Harten and G. Zwas. "Switched numerical Shuman filters for shock calculations." *Journal of Engineering Mathematics* 6(2) (1972), pp. 207–216 (cit. on p. 55).

[68] A. Harten. "The artificial compression method for computation of shocks and contact discontinuities. III. Self-adjusting hybrid schemes." *Mathematics of Computation* 32(142) (1978), pp. 363–389 (cit. on p. 55).

[69] A. Jameson. "Steacfy-State Solution of the Euler Equations for Transonic Flow." - (1982) (cit. on p. 55).

[70] A. Jameson, W. Schmidt, E. Turkel, et al. "Numerical solutions of the Euler equations by finite volume methods using Runge-Kutta time-stepping schemes." *AIAA paper* 1259 (1981), p. 1981 (cit. on p. 55).

[71] B. Van Leer. "Towards the ultimate conservative difference scheme I. The quest of monotonicity." In: *Proceedings of the Third International Conference on Numerical Methods in Fluid Mechanics*. Springer. 1973, pp. 163–168 (cit. on p. 55).

[72] J. B. Goodman and R. J. LeVeque. "A geometric approach to high resolution TVD schemes." *SIAM journal on numerical analysis* 25(2) (1988), pp. 268–284 (cit. on p. 55).

[73] S. F. Davis. "A simplified TVD finite difference scheme via artificial viscosity." *SIAM journal on scientific and statistical computing* 8(1) (1987), pp. 1–18 (cit. on pp. 55, 80).

[74] P. Colella. "A direct Eulerian MUSCL scheme for gas dynamics." *SIAM Journal on Scientific and Statistical Computing* 6(1) (1985), pp. 104–117 (cit. on p. 55).

[75] P. Colella and P. R. Woodward. "The piecewise parabolic method (PPM) for gas-dynamical simulations." *Journal of computational physics* 54(1) (1984), pp. 174–201 (cit. on p. 55).

[76] F. Coquel and P. G. LeFloch. "An entropy satisfying MUSCL scheme for systems of conservation laws." *Numerische Mathematik* 74(1) (1996), pp. 1–33 (cit. on p. 56).

[77] A. Harten and S. Osher. "Uniformly high-order accurate nonoscillatory schemes. I." *SIAM Journal on Numerical Analysis* 24(2) (1987), pp. 279–309 (cit. on p. 56).

[78] S. Tang. "Sound transmission characteristics of Tee-junctions and the associated length corrections." *The Journal of the Acoustical Society of America* 115(1) (2004), pp. 218–227 (cit. on p. 56).

[79] M. Harrison, I. De Soto, and P. R. Unzueta. "A linear acoustic model for multi-cylinder IC engine intake manifolds including the effects of the intake throttle." *Journal of Sound and Vibration* 278(4) (2004), pp. 975–1011 (cit. on p. 56).

[80] M. Karlsson and M. Åbom. "Quasi-steady model of the acoustic scattering properties of a T-junction." *Journal of Sound and Vibration* 330(21) (2011), pp. 5131–5137 (cit. on p. 56).

[81] M. Karlsson and M. Åbom. "Aeroacoustics of T-junctions-An experimental investigation." *Journal of Sound and Vibration* 329(10) (2010), pp. 1793–1808 (cit. on p. 57).

[82] J. Desantes, A. Torregrosa, and A. Broatch. "Experiments on flow noise generation in simple exhaust geometries." *Acta Acustica united with Acustica* 87(1) (2001), pp. 46–55 (cit. on p. 57).

[83] J. Corberán. "A new constant pressure model for N-branch junctions." *Proceedings of the type of Mechanical Engineers, Part D: Journal of Automobile Engineering* 206(2) (1992), pp. 117–123 (cit. on pp. 57, 148).

[84] B. Schmandt and H. Herwig. "The head change coefficient for branched flows: Why "losses" due to junctions can be negative." *International Journal of Heat and Fluid Flow* 54 (2015), pp. 268–275 (cit. on pp. 57, 148).

[85] C. Shaw, D. Lee, S. Richardson, and S. Pierson. *Modelling the effect of plenum-runner interface geometry on the flow through an inlet system.* SAE Technical Paper. 2000 (cit. on p. 57).

[86] J. Pérez-García, E. Sanmiguel-Rojas, J. Hernández-Grau, and A. Viedma. "Numerical and experimental investigations on internal compressible flow at T-type junctions." *Experimental thermal and fluid science* 31(1) (2006), pp. 61–74 (cit. on p. 57).

[87] H. Naeimi, G. D. Domiry, M. Gorji, G. Javadirad, and M. Keshavarz. "A parametric design of compact exhaust manifold junction in heavy duty diesel engine using CFD." *Thermal Science* 15(4) (2011), pp. 1023–1033 (cit. on p. 57).

[88] A. Sakowitz, M. Mihaescu, and L. Fuchs. "Turbulent flow mechanisms in mixing T-junctions by Large Eddy Simulations." *International Journal of Heat and Fluid Flow* 45 (2014), pp. 135–146 (cit. on p. 57).

[89] M. Bassett, D. Winterbone, and R. Pearson. "Calculation of steady flow pressure loss coefficients for pipe junctions." *Proceedings of the type of mechanical engineers, part C: Journal of Mechanical Engineering Science* 215(8) (2001), pp. 861–881 (cit. on pp. 57, 150, 153).

[90] W. Hager. "An approximate treatment of flow in branches and bends." *Proceedings of the type of Mechanical Engineers, Part C: Journal of Mechanical Engineering Science* 198(1) (1984), pp. 63–69 (cit. on pp. 57, 150, 153).

[91] J. Paul, A. Selamet, K. Miazgowicz, and K. Tallio. *Combining flow losses at circular T-junctions representative of intake plenum and primary runner interface*. SAE Technical Paper. 2007 (cit. on p. 58).

[92] J. Pérez-García, E. Sanmiguel-Rojas, and A. Viedma. "New coefficient to characterize energy losses in compressible flow at T-junctions." *Applied Mathematical Modelling* 34(12) (2010), pp. 4289–4305 (cit. on p. 58).

[93] B. Peters and A. Gosman. *Numerical simulation of unsteady flow in engine intake manifolds*. SAE Technical Paper 930609. 1993 (cit. on p. 58).

[94] J. Bingham and G. Blair. "An improved branched pipe model for multicylinder automotive engine calculations." *Proceedings of the type of Mechanical Engineers, Part D: Transport Engineering* 199(1) (1985), pp. 65–77 (cit. on p. 58).

[95] M. William-Louis, A. Ould-El-Hadrami, and C. Tournier. "On the calculation of the unsteady compressible flow through an N-branch junction." *Proceedings of the type of Mechanical Engineers, Part C: Journal of Mechanical Engineering Science* 212(1) (1998), pp. 49–56 (cit. on p. 58).

[96] M. Bassett, R. Pearson, N. Fleming, and D. Winterbone. *A multi-pipe junction model for one-dimensional gas-dynamic simulations*. SAE Technical Paper 2003-01-0370. 2003 (cit. on p. 58).

[97] R. Pearson, M. Bassett, P. Batten, D. Winterbone, and N. Weaver. *Multi-dimensional wave propagation in pipe junctions*. SAE Technical Paper 1999-01-1186. 1999 (cit. on p. 58).

[98] M. D. Bassett, D. E. Winterbone, and R. J. Pearson. *Modelling engines with pulse converted exhaust manifolds using one-dimensional techniques*. SAE Technical Paper 2000-01-0290. 2000 (cit. on p. 58).

[99] G. Montenegro, A. Onorati, F. Piscaglia, and G. D'Errico. *Integrated 1d-multid fluid dynamic models for the simulation of ice intake and exhaust systems*. SAE Technical Paper 2007-01-0495. 2007 (cit. on p. 58).

[100] A. Onorati, G. Montenegro, G. D'Errico, and F. Piscaglia. *Integrated 1d-3d fluid dynamic simulation of a turbocharged diesel engine with complete intake and exhaust systems*. SAE Technical paper 2010-01-1194. 2010 (cit. on p. 58).

Chapter 3

Numerical method

Contents

3.1 Introduction **70**
3.2 Staggered-grid scheme **72**
3.3 The Courant-Friedrichs-Lewy stability criterion adaptation **76**
3.4 Momentum diffusion term **77**
3.5 Flux corrected transport **78**
3.6 Total variation diminishing **79**
3.6.1 Davis total variation diminishing scheme 80
3.6.2 Adaptation of TVD to a staggered-grid 81
3.7 Shock-tube problem **82**
3.8 Summary and conclusions **88**
Chapter 3 bibliography **93**

3.1 Introduction

As it was anticipated in section 1.1, engine modelling has become an essential tool in the design of internal combustion engines, allowing considerable reductions in development time and cost. Classical design methodologies are based on prototype manufacturing and trial-and-error tests, but currently, most of those tests have been replaced by numerical computations, so that only the most promising design options are actually tested on engine bench.

For years, 1D gas dynamics codes in the time domain [5] have offered sufficiently good solutions for modelling both engine performance and intake and exhaust noise. The choice of 1D models is justified because in most ducts present in engine intake and exhaust systems it can be assumed that there is only one flow direction. However, for a more demanding level of design, a 1D representation may not be sufficient to describe accurately the flow in certain elements. Payri *et al.* [7] stated that this is especially important in the case of silencers, where the 1D assumption can only be applied to simple geometries and, even in that case, Beam [101] proved that suitable results can only be obtained for frequencies below the cut-off frequency of higher order modes. In the case of duct junctions, Broatch [8] showed that it is the existence of complex 3D flow structures what sets the applicability limit for a simple zero-dimensional description [6]. In view of these limitations, the first option would typically be the use of a computational fluid dynamics (CFD) model; however, the application of such a model to a complete intake or exhaust system entails an excessive computational time.

A possible solution comes from the use of a 3D model only locally at those parts in which 3D effects are relevant, through the coupling between 1D and 3D models, as performed by Montenegro and Onorati [9]. Such coupling can be done directly in the time domain [10] or by means of time–frequency hybrid schemes [102] in which the element information is obtained from 3D or quasi-3D linear models [103], although the use of hybrid schemes is hampered by their very slow convergence.

An alternative compromise solution is given by quasi-3D models, in which the momentum equation is solved in a simplified way on a staggered mesh [104]. A good quasi-3D model should be able to offer almost as good results as a CFD tool, at least for the particular problem for which it was designed, while reducing greatly the computation time. Such solutions have become standard in commercial codes, and have been successfully applied to silencers with perforated tubes and/or absorbing material, both in the acoustic regime by Montenegro *et al.* [28], and in real engine conditions, by Morel *et al.* [12].

It is well known, however, that non-physical oscillations in the flow variables appear when those methods are used in their basic form, most notably at points where significant pressure gradients are present (as usual in the literature, such points will be referred to here as "discontinuities", even if the variations occur over a very small but finite spatial distance). In order to avoid such overshoots at discontinuities, different approaches have been proposed in the literature. The first solutions reported were based on the inclusion in the momentum equation of an additional term, which Morel *et al.* [104] first implemented as an equivalent friction force in or, in more recent developments by Montenegro *et al.* [28], a momentum diffusion term. An alternative to this solution was suggested by Torregrosa *et al.* [1], where a Flux Corrected Transport (FCT) methodology, commonly used in flow equations solved with finite differences schemes, was adapted to a staggered-grid scheme. This approach will be expanded in this chapter.

However, it was proved by Pearson [105] that, under some circumstances, FCT methods can distort the finite-differences solution and produce noticeable errors in mass conservation. Therefore, another option to be used as a flux limiter for the quasi-3D method could expand the applicability of the method. Flux limiters based on the total variation diminishing (TVD) criterion proposed by Harten [65] were developed for one-dimensional engine gas exchange applications [106] precisely with this objective. TVD methods are still an active research topic (see e.g. Galiano [107] and Kim [108]) and in this chapter, a TVD flux limiter will also be adapted to the staggered quasi-3D method here developed, following the work of Torregrosa *et al.* [2].

The main objective of this chapter is to provide a comprehensive evaluation of the process of developing a staggered-grid finite volume method that can be used to simulate complex fluid-dynamic problems with a quasi-3D approach both in the time and frequency domain, providing a solution that considers the three-dimensional effects at a low computational cost. First, the concept of a staggered-grid will be explained and the numerical method will be applied to that mesh, paying special attention to the simplifications adopted. Then, the different flux limiters considered and its implementation will be discussed, including the formulation and adaptations when needed. Subsequently, the shock-tube problem is used to test the stability and convergence of the method and the performance of the flux limiters. Finally, in the conclusions of the chapter are summarized.

3.2 Staggered-grid scheme

In section 2.2 it was extensively detailed the development of the governing equations traditionally used in solving fluid-dynamic problems in engines. However, in general it is not possible to obtain an analytical solution for the hyperbolic partial differential equation system form by the Euler equations. Hence, multiple numerical techniques have been developed, specially for the one-dimensional case. Basically, these numerical methods consist in a discretization of the governing equations to form a set of more simple algebraic relationship that will be resolved with a computer. The governing equations define the propagation of pressure waves, so the numerical method has to be able to resolve the wave-action phenomena in every element simulated.

The majority of numerical methods more extensively used in engine simulation are based in a one-dimensional approach, due to it simplicity and sufficiency to solve the wave-action phenomena in the engine pipes, where basically only the longitudinal dimension is representative of the problem. Nevertheless, when trying to simulate with high accuracy more complex systems, such as mufflers, after-treatment systems or even duct junctions, where three dimensional effects may be present, a one-dimensional approach is not enough and a CFD tool results in a excessively expensive solution.

Therefore, when considering the prediction of wave dynamics in intake and exhaust systems of internal combustion engines and, in particular, the effects produced by complex elements, a suitable compromise between the quality of the solution and the computational cost is provided by quasi-3D staggered-mesh finite volume models [11]. Such models have become standard in commercial codes, either as the core of the whole computation [12, 13], or used locally for complex elements exhibiting significant three-dimensional features [28].

The selected mesh [1] consists in the use of a staggered-grid where two types of basic elements are considered: volumes and connectors. The former contain information about scalar magnitudes such as pressure, density or temperature, and of course of the cell volume itself. The latter contain information on vector quantities (flow velocity or momentum), on their own orientation in space and some scalar information (the connector area). It is important to emphasize that a connector always connects two volumes, whereas a volume may be attached to as many connectors as required by the problem. In Figure 3.1, two volumes connected by a connector are shown schematically (volumes do not actually have any defined shape, in the same way as the connector is simply the flow area between the two volumes).

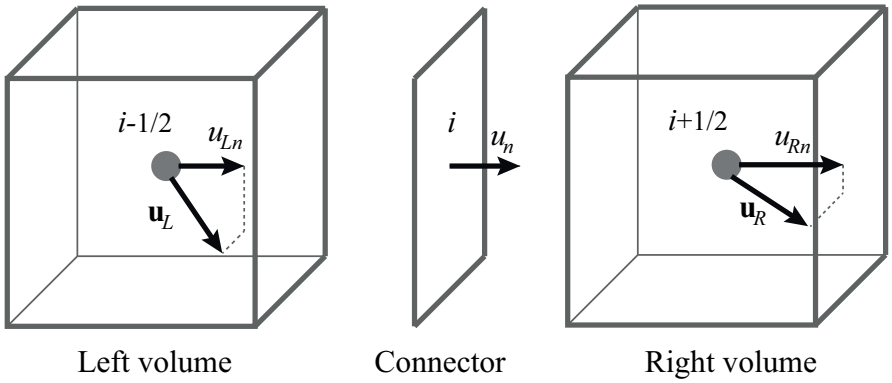

Figure 3.1: Basic mesh elements, definition of velocity projections and notation of volumes and connectors.

The starting point of the method are the widespread 3D Euler conservation equations without source terms:

$$\frac{\partial(\rho)}{\partial t} + \nabla \cdot (\rho \mathbf{U}) = 0 \tag{3.1}$$

$$\frac{\partial(\rho \mathbf{U})}{\partial t} + \nabla \cdot (\rho \mathbf{U} \times \mathbf{U}) = -\nabla p \tag{3.2}$$

$$\frac{\partial(\rho e_0)}{\partial t} + \nabla \cdot [(\rho e_0 + p)\mathbf{U}] = 0 \tag{3.3}$$

This system of equations is closed with the perfect gas equation of state.

$$p = \rho R T \tag{3.4}$$

However, in the current context, the key issue is where and how those equations are solved. The mass equation is solved in the volumes, so that its discretized expression is:

$$\rho^{n+1} = \rho^n + \frac{\Delta t}{V} \sum_{c=1}^{N_c} \rho_c^n u_c^n A_c \tag{3.5}$$

where ρ is the density and u is the flow velocity, the superscript n indicates the time step, Δt represents the time interval, V the volume of the cell, N_c the number of connectors and subscript c indicates that the variable is taken at the connectors (otherwise the variable is taken at the volumes).

A similar procedure is used then for the equation of energy, whose resulting discretized expression is

$$(\rho e_0)^{n+1} = (\rho e_0)^n + \frac{\Delta t}{V}\sum_{c=1}^{N_c} \rho_c^n e_{0c}^n u_c^n A_c + \frac{\Delta t}{V}\sum_{c=1}^{N_c} p_c^n u_c^n A_c \tag{3.6}$$

where, as stated before, p is the pressure of the gas and e_0 is the stagnation specific internal energy, which for a perfect gas is

$$e_0 = c_v T + \frac{u^2}{2} \tag{3.7}$$

The momentum equation is calculated at the connectors, and only in the direction orthogonal to the connector surface, by projecting the flow velocity in the connected volumes onto that direction, as depicted in Figure 3.1, where the velocity u_c in the connector, and the projections of the volume flow velocity, u_{Ln} and u_{Rn}, are shown. Based on this assumption, it follows that one can calculate the momentum in the connector from a one-dimensional momentum equation, whose discretization along the same lines as in the previous cases gives

$$(\rho_c u_c A_c)^{n+1} = (\rho_c u_c A_c)^n + \frac{\Delta t}{\Delta L}\left[(\rho u_n^2 + p)_L + (\rho u_n^2 + p)_R\right] A_c \tag{3.8}$$

Here, u_n denotes the velocity projection onto the direction orthogonal to the connector surface and subscripts R and L refer to the volumes at the right and left of the connector, respectively. It is worth noticing that, with this simplification, a one-dimensional equation for each connector must be solved, instead of three coupled equations for each volume, which significantly reduces the computation time. This quantity is then used in the mass and energy conservation equations for the next time step. In the case of the energy equation, some additional scalar terms from the connectors, such as density or pressure, are needed. These values are calculated by an upwind approach, so that they are taken from the right or left volumes, depending on the flow direction.

Finally, the momentum associated with the volumes is calculated by distributing the connector momentum between the two adjacent volumes according to their relative sizes. In uniform meshes, half the momentum of the connector is thus assigned to each volume. As the orientation of the connectors is also known, the momentum vector of each volume is obtained from the vector sum

$$(\rho \mathbf{u} V)_V^{n+1} = \frac{1}{2} \sum_{c=1}^{N_c} (\rho_c \mathbf{u_c} A_c \Delta L)^{n+1} \tag{3.9}$$

With the previous prescription, the method turns out to be a second-order accuracy method based on an explicit scheme with a staggered-grid, as shown in Figure 3.2

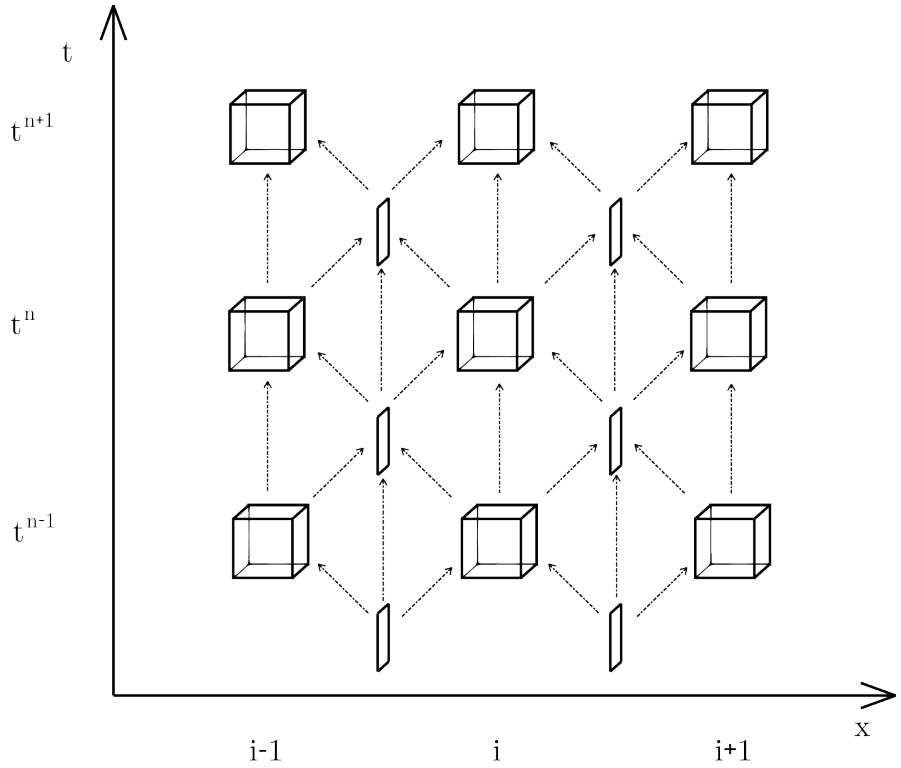

Figure 3.2: Scheme of the staggered mesh and the associated time marching.

Once the discretization has been stablish, the next step is to assure the stability of the method. In that regard, as in every fluid-dynamic scheme, the so-called CFL criterion needs to be accomplished. But in addition to that condition, the fact that the resulting scheme offers second-order accuracy, together with the simplifications adopted in the momentum equation, results in non-physical oscillations, especially in the vicinity of significant pressure gradients. This is a very common situation when simulating flows associated with engine gas exchange due to its pulsating behaviour. Since simulations

with unsteady mean flow or high amplitude pressure perturbations are one of the main goals of the method, a stabilization technique must be developed and applied to avoid spurious oscillations. However, most of the stabilization methods available are based on correcting the flux terms of the equations and have been developed for finite differences schemes, such as the Lax-Wendroff method [109]. In the following sections, the formulation of the three different flow limiters will be described, starting with the momentum diffusion term, MDT, as proposed by Montenegro [28]. In the case of the flux-corrected transport (FCT) and the total variation diminishing (TVD) techniques, a scheme developed for finite difference schemes will be chosen for each one, following the methodologies proposed by Torregrosa [1, 2], so that the methods will be adapted to be used in conjunction with the staggered-grid finite-volume method described above.

3.3 The Courant-Friedrichs-Lewy stability criterion adaptation

As previously explained in section 2.3.2, in a one-dimensional scheme, the value of the mesh size, Δx, used in a simulation, is previously determined by establishing a criterion which defines the compromise between accuracy and computational speed. The value of the time step, Δt, however, is subject to constraints imposed through stability considerations which arise from the criterion of Courant, Friedrichs and Lewy [49] (CFL). This criterion requires that information, in the form of disturbances, or waves, cannot travel more than one mesh length in one calculation time increment. This is expressed through the equation

$$\nu = \frac{\Delta t}{\Delta x} c^n_{max} \tag{3.10}$$

where

$$0 < \nu \leqslant 1 \tag{3.11}$$

and c^n_{max} represents the largest wave speed present in the entire solution domain at time level n. For non-linear problems, c^n_{max} can be estimated using the relationship

$$c^n_{max} = \max(a^n_i + |u^n_i|) \tag{3.12}$$

The parameter ν is known as the Courant, or CFL, number and clearly the time-marching procedure will be most efficient when the value of this parameter is close to 1. Although equation 3.12 will overestimate the the maximum wave speed in a particular cell if it is a shock wave, resulting in a stable solution, it can also lead to an underestimate of c^n_{max} in instances such as shock-tube calculations, where the flow is stationary at $t = 0$, so c^n_{max} would be only the local speed of sound. Therefore, it is an extended practice to use a conservative value for the Courant number, like $\nu = 0.9$, unless there are other constrains in the numerical value that impose a lower value.

When applying this criterion to a finite volume staggered-grid mesh, a slight modification has to be done to equation 3.10 to account for the fact that the mesh now consist of volumes, instead of finite lengths, resulting in

$$\nu = \frac{\Delta t \cdot A_c}{\Delta V} c^n_{max} \tag{3.13}$$

3.4 Momentum diffusion term

As previously pointed out, the quasi-3D method previously described does not satisfy the stability requirement, since non-physical oscillations may appear in cases where pressure gradients are significant. Also, in this numerical method, the solution of the momentum equation in the connectors is used to compute the fluxes required for the mass and energy equations in the volumes, whence the stabilization method should only be applied to the momentum equation. This fact will be taken into account when adapting stabilization methods originally developed for finite difference schemes into a staggered-grid method.

The basic concept of the MDT flux limiter is to add a diffusion term to the momentum equation so that the mass flux computed at the corresponding connector is conveniently limited. With this purpose, the momentum flux density tensor used in the momentum equation (3.2) can be modified, in a way similar to that used for incorporating viscosity effects, as follows

$$\frac{\partial(\rho \mathbf{U})}{\partial t} + \nabla \cdot (\rho \mathbf{U} \times \mathbf{U} + \mathbf{D}) = -\nabla p \tag{3.14}$$

where the tensor $\mathbf{D}$ is assumed to depend linearly on the local momentum gradients, i.e.:

$$\mathbf{D} = \epsilon \nabla(\rho \mathbf{U}) \tag{3.15}$$

where the scalar quantity ϵ has the dimensions of a kinematic viscosity and can thus be interpreted as a momentum diffusion coefficient. With this prescription, the contribution of the diffusion term $\nabla \cdot \mathbf{D}$ will only be relevant if significant gradients exist, and any resulting spurious oscillations will be damped.

Projection of equation (3.15) onto the direction of a connector and subsequent discretization in the same way as for equation (3.8) gives

$$(\rho_c u_c A_c)^{n+1} = (\rho_c u_c A_c)^n + \frac{\Delta t}{\Delta L}\left[(\rho u_n^2 + p)_L + (\rho u_n^2 + p)_R\right] A_c + \frac{\Delta t}{\Delta L}\left[\left(\tilde{D}_{Ln} - \tilde{D}_{Rn}\right)\right] \tag{3.16}$$

where $\tilde{D}_{Ln}$ and $\tilde{D}_{Rn}$ are the projections onto the connector direction of tensor

$$\tilde{\mathbf{D}} = \epsilon \nabla(\rho \mathbf{U} A_c) \tag{3.17}$$

which is computed in the two adjacent volumes. Following [28], the momentum diffusion coefficient is evaluated considering the mesh size and the time step in relation with the local flow velocity at the volume, as

$$\epsilon = \frac{|\mathbf{U}|}{2}(\Delta L - |\mathbf{U}|\Delta t) \tag{3.18}$$

and the gradient of mass flow rate $\nabla(\rho \mathbf{U} A_c)$ is computed from the projections of the mass flow rates of the adjacent connectors onto each direction.

3.5 Flux corrected transport

In this section, first a brief outline of the formulation of the method for finite differences schemes, which was detailed in section 2.4.1, will be described, following then with its adaptation to the quasi-3D method proposed.

When applied to a finite difference scheme, FCT consists of three stages [63]: a transport stage based on the scheme considered, a diffusion stage for reducing the numerical dispersion introduced in the transport stage, and an anti-diffusion stage to restore the accuracy of the scheme at cells with a smooth solution while preserving the diffusion operator accuracy in the vicinity of discontinuities. The transport stage is defined by the governing equations and its discretization, in this case the momentum equation (3.2). In the diffusion stage a linear operator is used, giving

$$\bar{\mathbf{W}}_i^{n+1} = \mathbf{W}_i^{n+1} + \mathbf{D}_i(\mathbf{W}_i^n) \tag{3.19}$$

Then, the anti-diffusion stage is applied, where the accuracy of the scheme used in the transport stage in those cells where the solution is smooth is restored. Using the non-linear operator A_j, the scheme ends as follows

$$\bar{\bar{\mathbf{W}}}_i^{n+1} = \bar{\mathbf{W}}_i^{n+1} + \mathbf{A}_i(\mathbf{W}_i^n) \tag{3.20}$$

The diffusion term can be calculated by using $\mathbf{W}_i^n$ or $\mathbf{W}_i^{n+1}$, and for the anti-diffusion stage, the two mentioned values or $\bar{\mathbf{W}}_i^{n+1}$ can also be used, giving different variants for the method.

The application of the FCT technique to a staggered-grid quasi-3D method poses some problems in the case of the mass and energy equations, as they both are calculated in the volumes, and it is not evident from which of the possible six connectors should the required data be taken. However, it is known that overshooting problems are related to the flux term of the discretization, which, for the mass and energy equations in this method, comes directly from the momentum equation, which is computed at the connectors. Since a connector always connects two volumes, the method can be adapted so that the FCT cells correspond to the connectors, and for the intermediate steps $i \pm 1/2$ the projection of the variables corresponding to the volumes connected by connector i are used. With this approach, for the staggered-grid $\mathbf{W}$ would only represent the momentum and it is a scalar instead of a vector, i.e., $W = \rho u_c A_c$. For instance, the equation for conservation of momentum with diffusion via damping would be as follows

$$(\overline{\rho u_c A_c})_i^{n+1} = (\rho u_c A_c)_i^{n+1} + D_i\left((\rho u_c A_c)_i^n\right) \tag{3.21}$$

and thus the diffusive term becomes

$$D_i(\rho u_c A_c) = \theta\left((\rho u_c A_c)_{i+1/2}\right) - \theta\left((\rho u_c A_c)_{i-1/2}\right) \tag{3.22}$$

where

$$\theta\left((\rho u_c A_c)_{i+1/2}\right) = \frac{\vartheta}{4}\left[(\rho u_c A_c)_{i+1} - (\rho u_c A_c)_i\right] \tag{3.23}$$

For the anti-diffusion stage, a similar procedure can be followed, so that the FCT technique can be readily adapted to the staggered-grid quasi-3D model.

3.6 Total variation diminishing

The total variation diminishing property of a scheme was discussed in section 2.4.2, along with its formulation. In this section, different TVD schemes

will be considered, choosing the more suitable one for a staggered-grid scheme. Finally, the adaptation of the chosen TVD scheme to the staggered-grid mesh method described in section 3.2 will be detailed.

3.6.1 Davis total variation diminishing scheme

Several TVD schemes have been developed for finite difference schemes, most notably by Harten [65], Sweby [62] and Davis [73]. A comparison of these methods was performed by Arnau [33] in a finite difference scheme, showing that all of them brought in a great improvement when compared to the Lax-Wendroff scheme. Specifically, both Davis and Harten TVD schemes gave the best results among the TVD schemes studied. However, regarding the increase in computational time with respect to the original Lax-Wendroff scheme, while the Davis TVD flux limiter needed only about twice the time, the Harten TVD flux correction method was increasing the computational time in around fifteen times the original, due to the calculation of the Jacobian matrix. In view of this, the Davis TVD flux limiter method was selected for its adaptation to the staggered-grid.

The method proposed by Davis [73] consists in using the following flux expression, based on the Lax-Wendroff scheme

$$\hat{\mathbf{F}}^n_{1/2} = \hat{\mathbf{F}}^{LW}_{1/2} + \frac{1}{2}\nu\left(1 - \frac{\Delta t}{\Delta x}\nu\right)\left(\psi(r_i^+) + \psi(r_i^-) - 2\right)\left(\mathbf{W}^n_{i+1} - \mathbf{W}^n_i\right) \quad (3.24)$$

where ν is the Courant number, as described in section 3.3 and the function ψ and variables $r_i^{\pm}$ depends on the value of $\mathbf{W}$ in the nearby cells. This limited flux provides artificial viscosity to the second order scheme, therefore avoiding numerical oscillations near the solution discontinuities.

In order to simplify the calculation, Davis replaces the one-step Lax-Wendroff scheme of the previous expression for the equivalent two-steps version. In this way, the scheme will be TVD just by adding the next expression to the second step:

$$\left[\bar{G}^+(r_i^+) + [\bar{G}^-(r_{i+1}^-)\right]\Delta\mathbf{W}^n_{i+1/2} - \left[\bar{G}^+(r_{i-1}^+) + [\bar{G}^-(r_i^-)\right]\Delta\mathbf{W}^n_{i-1/2} \quad (3.25)$$

where the function $\bar{G}^{\pm}$ is defined as

$$\bar{G}^+(r_i^+) = \frac{1}{2}C(\nu)\left[1 - \psi(r_i^{\pm})\right] \quad (3.26)$$

being $C(\nu)$ a function of the Courant number given by

$$C(\nu) = \begin{cases} \nu(1-\nu) & \nu \leqslant 0.5 \\ 0.25 & \nu > 0.5 \end{cases} \tag{3.27}$$

and finally

$$r_i^+ = \frac{[\Delta \mathbf{W}_{i-1/2}^n, \Delta \mathbf{W}_{i+1/2}^n]}{[\Delta \mathbf{W}_{i+1/2}^n, \Delta \mathbf{W}_{i+1/2}^n]},\ r_i^- = \frac{[\Delta \mathbf{W}_{i-1/2}^n, \Delta \mathbf{W}_{i+1/2}^n]}{[\Delta \mathbf{W}_{i-1/2}^n, \Delta \mathbf{W}_{i-1/2}^n]} \tag{3.28}$$

Here, $[\,.\,,\,.\,]$ denotes the inner product of two vectors and $\Delta \mathbf{W}_{i+1/2}^n = \mathbf{W}_{i+1/2}^n - \mathbf{W}_i^n$.

Regarding the limiter used in equation (3.24), Davis proposed the following expression

$$\psi(r) = \min(2|r|, 1) \tag{3.29}$$

which admits a Courant number of up to 0.95.

3.6.2 Adaptation of TVD to a staggered-grid

Considering the specific structure of the equations discretized on the staggered-grid, where the solution of the momentum equation in the connector is used to compute the fluxes for the mass and energy equations in the volumes, avoiding the numerical oscillations in the momentum equation is enough to stabilize the method. Therefore, the flux limiter should only be added to me momentum equation, using the required variables from the neighbour connectors. The momentum in the connectors will then be modified by adding the term:

$$\bar{W}^{n+1} = W^{n+1} + \left[\bar{G}^+(r_i^+) + [\bar{G}^-(r_{i+1}^-)\right] \Delta W_{i+\frac{1}{2}}^n - \left[\bar{G}^+(r_{i-1}^+) + [\bar{G}^-(r_i^-)\right] \Delta W_{i-\frac{1}{2}}^n \tag{3.30}$$

where $W = \rho_c u_c A_c$ a scalar value representing the momentum calculated with equation (3.8). The rest of the terms are calculated as described by Davis in equations (3.26) to (3.29), with the difference that here $\Delta W_{i\pm 1/2}$ is a scalar magnitude, since the term is only applied to the momentum equation. Most notably the $r^\pm$ expressions (3.28) is the only part where vector variables are used, since there is an inner product of two vectors formed by the conservative variables

$$\Delta \mathbf{W}^n_{i+\frac{1}{2}} = \begin{bmatrix} \Delta\rho_c^n \\ \Delta(\rho_c u_c A_c)^n \\ \Delta(\rho_c e_{0c})^n \end{bmatrix} \tag{3.31}$$

Despite the mass and energy equations being evaluated at the volumes, for the sake of consistency, their values for the $\Delta W^n_{i+1/2}$ vector must be taken from the connectors, for which again an upwind approach will be adopted, although other more complex methods could be explored.

The only issue when trying to adapt the Davis flux limiter method to a staggered-grid is dealing with end-volumes. As seen in equation (3.28), conservative variables of neighbour connectors from both sides are needed to compute the flux limiter of each connector. Furthermore, equation (3.25) uses the terms r^-_{i+1} and r^+_{i-1}, which are computed from the conservative variables of two neighbour connectors on each side. This is not a serious problem in a 1D model, since only two cells of each side of the modelled duct will be affected by this issue and it can be solved by taking the values of the variables of the non-existent neighbour cells as the same as the end-cell. This approximation has been used in 1D models with good results. However, when modelling a more complex geometry with a 3D mesh, many end-volumes may appear and the effect of the simplifications adopted can be much more significant.

In the method developed, the solution adopted consists of using the value of the conservative variables of the end connector, inverting the sign of the momentum so that the resultant momentum in the wall is zero. This approximation has given good results when applied to meshes with a sufficiently large number of cells in each direction, although the solution tends to be more diffusive.

3.7 Shock-tube problem

As a first validation of a numerical method capabilities, it is commonplace to consider the shock-tube problem [110]. In this problem, two gases with different thermo- and fluid-dynamic states separated in a tube are put into contact at $t = 0$. In Figure 3.3(a) an outline of the initial state of the problem is shown. As time progresses, a contact discontinuity travels with the flow velocity, whereas a shock wave propagates in the same direction at a velocity corresponding to the addition of the speed of sound and the flow velocity, and a rarefaction wave whose propagation velocity is the speed of sound minus the flow velocity travels in the opposite direction. These perturbations

define four zones with different thermo- and fluid-dynamic states, as shown in Figure 3.3(b). Since all kinds of possible propagating perturbations (contact discontinuity, and shock and rarefaction waves) are present and easy to identify in the solution, this problem is often used in the literature.

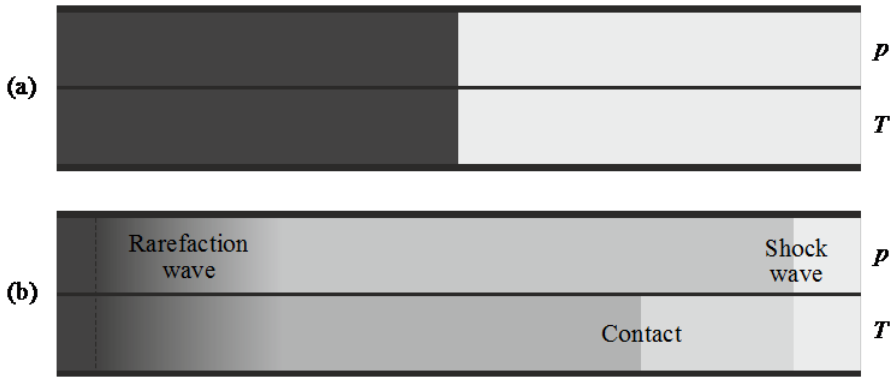

Figure 3.3: Initial state of the shock-tube problem (a) and scheme of the solution structure after a certain time (b).

After securing the CFL condition as shown in section 3.3, the staggered-mesh finite-volume method was applied to the shock-tube problem. The initial conditions chosen were: $p_1 = 3.5$ bar, $p_4 = 0.5$ bar, $T_1 = 2800$ K, $T_4 = 300$ K, and $u_1 = u_4 = 0$ m/s. A 1D mesh was used, with 250 volumes 4 mm long, and the simulation was stopped at $t = 3\dot{1}0^{-4}s$.

In Fig. 3.4 comparison is given between the analytical solution provided in [110] and the results obtained with the raw method without any flux limiter and with those obtained by including the momentum diffusion term. A noticeable overshooting associated with the propagation of the shock wave can be clearly seen in the basic solution, whereas it can be observed that those overshoots have been successfully removed by the inclusion of the momentum diffusion term. This appears to be the only point in which, as expected, this procedure produces significant changes in the solution, as the other features worth noticing are present in the two solutions shown: the smoothing effect on the trailing side of the leftwards-moving rarefaction wave, which is specially clear in the pressure and velocity plots, and a certain deviation from the analytical solution around $x = 0.65$ m in the pressure and velocity plots. Such deviation, that appears as an overestimation of the pressure value and an underestimation of the velocity magnitude, occurs precisely at the position of the contact discontinuity in the analytical solution for density and tem-

perature (the deviations observed in the density and the temperature will be commented later).

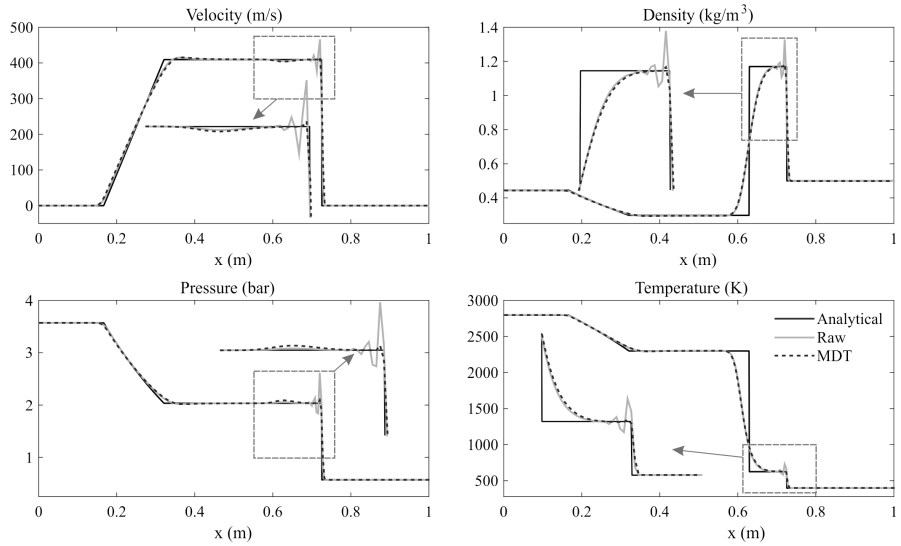

Figure 3.4: Comparison of solutions of the shock-tube problem: analytical, obtained with the original (raw) method and with the momentum diffusion term (MDT).

In Fig. 3.5, the same representation is given for the results obtained with the FCT method and the TVD scheme presented in this section. Again it can be observed that any overshoots have been suitably removed by the FCT method and, to a lesser extent, by the inclusion of the additional TVD terms, and that in both cases the smoothing effect on the trailing side of the leftwards-moving rarefaction wave is apparent.

Regarding the deviation noticed above at the theoretical position of the contact discontinuity, it can be observed that, regardless of the correction method used, the contact discontinuity spreads in space, and thus the methods are introducing some diffusion at this point due to the procedure used for the solution of the mass and energy equations. When this information is fed back to the momentum equation the deviations observed in pressure and velocity are produced, as the flat profiles observed in the analytical solution are only compatible with a real discontinuity. Additionally, it can be observed that a small perturbation appears in the TVD solution for pressure and velocity that might indicate that, even if the density and the temperature seem to be correctly computed, the effect of the spread contact discontinuity on the momentum equation has not been properly handled.

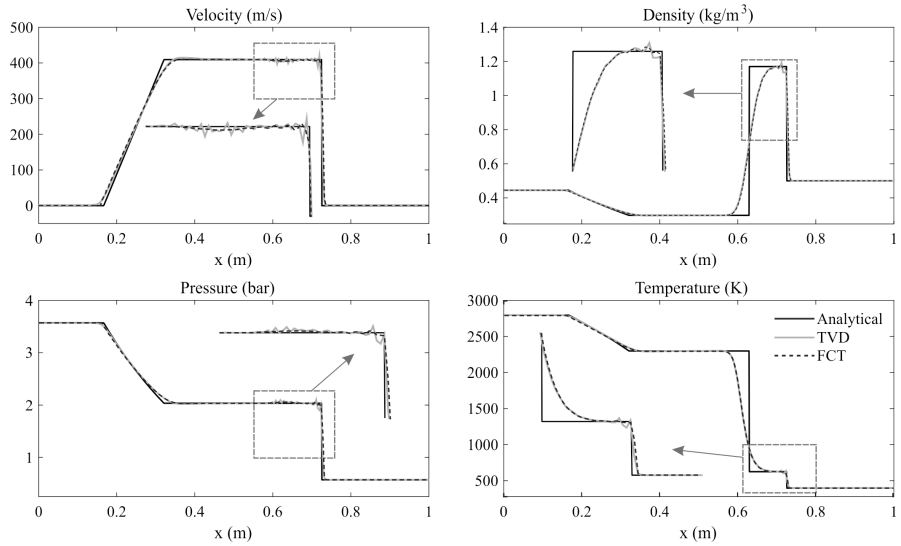

Figure 3.5: Comparison of solutions of the shock-tube problem: analytical, obtained with the TVD method and the FCT method.

While the spreading of the contact discontinuity could be considered as a serious shortcoming for the description of actual shock waves, this will not in general be the case in practical engine applications, as actual discontinuities occurring in those flow situations are much less abrupt. Additionally, one should expect that this issue should be strongly dependent on the discretization used, and this is confirmed by Figure 3.6, where density and pressure results obtained by using 250, 500 and 1000 volumes with the three correction methods considered are shown. As expected, the results for both magnitudes are closer to the analytical solution as the number of volumes increases. It is also worth mentioning that the perturbation observed in the pressure obtained with the TVD method is reduced, even if it has not totally disappeared, while the rest of the methods exhibit a smooth behaviour that even improves when increasing the number of volumes.

In order to quantify the previous considerations, the L^2 and L^∞ norms of the deviation of all the variables corresponding to the cases represented in Figure 3.6 were computed. These norms are defined as

$$L^2 = \sqrt{\sum_{i=1}^{N_v} x_i^2} \tag{3.32}$$

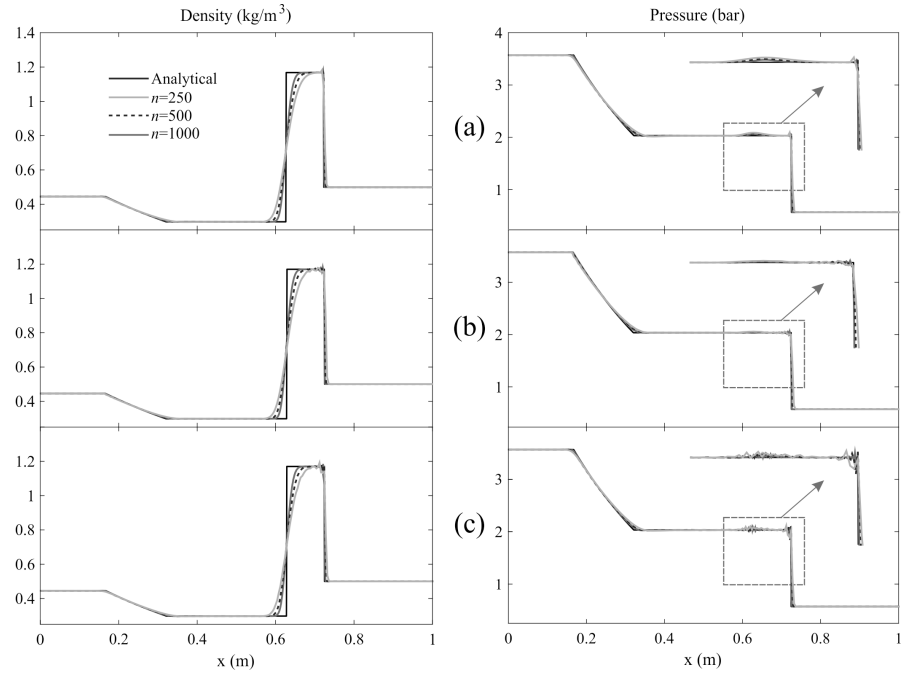

Figure 3.6: Effect of the discretization used on the description of the contact discontinuity for the three flux limiters considered: (a) MDT, (b) FCT, (c) TVD.

$$L^{\infty} = \max(|x_i|) \tag{3.33}$$

where x_i is the deviation between the analytical solution and the model prediction in each volume or connector, depending on the variable to which it is applied. These two norms were chosen because the L^2 norm provides a mean global assessment of the deviation obtained, which is complemented by the local view provided by the L^{∞} norm.

The results are shown in Table 3.1, 3.2 and 3.3 for different mesh size where, in order to make the results comparable, the L^2 norm was divided by the number of volumes N_v used in each case. Consistently with the results shown in Fig. 3.6, the results for L^2 improve when increasing N_v for the three methods. This is not the case, however, for L^{∞}, with a rather erratic behaviour and tendencies that change with the magnitude and the method considered. Therefore, increasing N_v produces an overall improvement in the solution, but significant local differences may still occur.

Considering now the comparison between the three methods, it can be observed that, for a sufficiently high number of volumes ($N_v = 1000$), the

performance of the three methods is comparable, except in the case of the velocity, in which the momentum diffusion term provides significantly lower values for both norms. In the intermediate case of $N_v = 500$ the results are again comparable both in terms of L^2 and L^∞, as none of the methods provides the lowest value for all the magnitudes: the best result for pressure is given by the FCT technique whereas the best result for velocity is that obtained with the MDT method, but all of them within the same order of magnitude. This situation is somehow reversed in the case $N_v = 250$, for which the best result for pressure is given by the MDT technique whereas the best result for velocity is that obtained with the FCT method.

Table 3.1: Comparison of the L^2 and L^∞ norms of the deviation between the analytical shock-tube solution and the different correction methods used with 250 cells.

$\mathbf{N_v = 250}$				
		FCT	**TVD**	**MDT**
$\mathbf{L^2/N_v}$	u	0.9949	1.6172	1.502
	ρ	0.0043	0.0042	0.00415
	p	0.0038	0.0026	0.0023
	T	21.499	21.698	21.823
$\mathbf{L^\infty}$	u	220.49	363.01	342.85
	ρ	0.4218	0.4092	0.4158
	p	0.8965	0.5422	0.4322
	T	1566.1	1573.2	1581.1

Table 3.2: Comparison of the L^2 and L^∞ norms of the deviation between the analytical shock-tube solution and the different correction methods used with 500 cells.

$\mathbf{N_v = 500}$				
		FCT	**TVD**	**MDT**
$\mathbf{L^2/N_v}$	u	0.4839	0.50147	0.4399
	ρ	0.0022	0.00227	0.0023
	p	0.0007	0.0008	0.00093
	T	14.621	14.651	14.719
$\mathbf{L^\infty}$	u	223.56	231.27	196.51
	ρ	0.4056	0.4146	0.416
	p	0.1408	0.1922	0.3097
	T	1588.4	1578.9	1590.3

Table 3.3: Comparison of the L^2 and L^∞ norms of the deviation between the analytical shock-tube solution and the different correction methods used with 1000 cells.

$\mathbf{N_v = 1000}$				
		FCT	**TVD**	**MDT**
$\mathbf{L^2/N_v}$	u	0.3151	0.3038	0.267
	ρ	0.0014	0.0014	0.0014
	p	0.0007	0.0006	0.0005
	T	9.8141	9.845	9.88
$\mathbf{L^\infty}$	u	236.59	213.26	181.22
	ρ	0.4131	0.4217	0.424
	p	0.6596	0.4812	0.364
	T	1601.1	1600.9	1606.7

3.8 Summary and conclusions

In this chapter a quasi-3D model which makes use of a non-linear second-order time and space discretization based on finite volumes staggered-grid has been developed. The goal of the method is to be able to provide a solution that takes into account the three-dimensional effects present in more complex geometries while maintaining a low computational cost, much lower than a CFD model. The computational cost should be comparable to a one-dimensional model and

the connexion between codes should be simple.

The model is based on a staggered-grid mesh approach, what means that there are two differentiated elements in the mesh, the calculation of some variables take place in one of them and the rest in the other one. In the model proposed, these elements are the volumes, where the scalar magnitudes are calculated, like pressure or density; and the connectors, which can be visualized as the surface linking two volumes, and store the vector values, like flow velocity or its own orientation in space. It is important to remark that a connector will always link two volumes, while a volume can have attached as many connectors as required.

The equations used in the method are the Euler conservation equations in its three-dimensional form. The mass and energy conservation equations are solved in the volumes, with a standard discretization, whereas the momentum equation is calculated in the connectors. In a regular three-dimensional scheme, the momentum is usually the most expensive equation to solve, since its a vector equation and that involves solving a system of three coupled equations for every cell. This quasi-3D method, however, makes use of the staggered-grid distribution and the fact that the connectors are represented as flat surfaces linking two volumes. Therefore, the momentum can be seen as a one-dimensional magnitude going through the connector with its direction orthogonal to that surface. This way, the momentum equation can be simplified to a one-dimensional equation to be solved in each connector and, although in general there would be more connectors than volumes, since all the momentum equations are decoupled, the computational time is greatly decreased compared to the standard approach. Finally, the momentum calculated in the connectors is distributed between the two volumes that it links, proportionally to their size, taking into account the orientation of the momentum in the mesh. By doing the vector sum of the momentum in the volumes, all the variables are calculated for the current time step and the method can proceed to the next one.

As any second-order scheme, this staggered-mesh finite-volume model is affected by the occurrence of non-physical overshoots in the vicinity of discontinuities in the flow variables. In order to remove those overshoots, two flux limiters commonly used in finite differences schemes have been considered: a Flux Corrected Transport (FCT) technique and a Total Variation Diminishing (TVD) method, along with a momentum diffusion term (MDT). It was found that the FCT method with dissipation via damping together with the phoenical form of the anti-diffusion term produces the best results when adapted

to the staggered-mesh finite-volume model. In the case of the TVD methods, different formulations have been analysed, and finally the Davis method was chosen for its adaptation in view of its relatively modest computational cost and its acceptable performance. Finally, a momentum diffusion term as described by Montenegro *et al.* [28] has been successfully applied.

The resulting method was checked in the case of the well-known shock-tube problem with the different flux limiters adapted. It was found that all the cases were comparably successful in removing the overshoots associated with the propagation of the shock wave. Additionally, they all exhibited a certain smoothing of the trailing side of the leftwards-moving rarefaction wave, and a considerable spreading of the contact discontinuity that in turn produces an overestimation of the pressure and an underestimation of the velocity at that point. In the case if the TVD method, these deviations were accompanied by spurious fluctuations, that did not get to disappear completely even when the mesh was improved in order to provide a better description of the contact discontinuity. The performance of the method with the different flux limiters will be tested and validated in the next chapters in order to find out the strengths and weakness of each one in the time and frequency domain.

Chapter 3 Bibliography

[1] A. Torregrosa, A. Broatch, F. Arnau, and M. Hernández. "A non-linear quasi-3D model with Flux-Corrected-Transport for engine gas-exchange modelling." *Journal of Computational and Applied Mathematics* 291 (2016), pp. 103–111 (cit. on pp. xi, 71, 72, 76, 179).

[2] A. Torregrosa, A. Broatch, F. Arnau, and M. Hernández. "On the effect of different flux limiters on the performance of an engine gas exchange gas-dynamic model." *International Journal of Mechanical Sciences* (2017) (cit. on pp. xi, 71, 76, 179).

[5] D. E. Winterbone and R. J. Pearson. *Design techniques for engine manifolds: wave action methods for IC engines*. Professional Engineering Publishing, 1999 (cit. on pp. 3, 31, 56, 70).

[6] F. Payri, E. Reyes, and J. Galindo. "Analysis and modeling of the fluid-dynamic effects in branched exhaust junctions of ICE." *Journal of engineering for gas turbines and power* 123(1) (2001), pp. 197–203 (cit. on pp. 3, 56, 70).

[7] F. Payri, A. Torregrosa, and M. Chust. "Application of MacCormack schemes to IC engine exhaust noise prediction." *Journal of Sound and Vibration* 195(5) (1996), pp. 757–773 (cit. on pp. 3, 70).

[8] A. Broatch, J. Serrano, F. Arnau, and D. Moya. "Time-domain computation of muffler frequency response: comparison of different numerical schemes." *Journal of sound and vibration* 305(1) (2007), pp. 333–347 (cit. on pp. 3, 70).

[9] G. Montenegro and A. Onorati. "A coupled 1D-multiD nonlinear simulation of IC engine silencers with perforates and sound-absorbing material." *SAE International Journal of Passenger Cars-Mechanical Systems* 2(2009-01-0305) (2009), pp. 482–494 (cit. on pp. 4, 70).

[10] J. Galindo, A. Tiseira, P. Fajardo, and R. Navarro. "Coupling methodology of 1D finite difference and 3D finite volume CFD codes based on the Method of Characteristics." *Mathematical and Computer Modelling* 54(7) (2011), pp. 1738–1746 (cit. on pp. 4, 70, 101).

[11] G. Montenegro, A. Onorati, and A. Della Torre. "The prediction of silencer acoustical performances by 1D, 1D–3D and quasi-3D non-linear approaches." *Computers & Fluids* 71 (2013), pp. 208–223 (cit. on pp. 4, 59, 72, 151).

[12] T. Morel, J. Silvestri, K.-A. Goerg, and R. Jebasinski. *Modeling of engine exhaust acoustics*. SAE Technical Paper 1999-01-1665. 1999 (cit. on pp. 4, 59, 70, 72).

[13] S. M. Sapsford, V. C. Richards, D. R. Amlee, T. Morel, and M. T. Chappell. *Exhaust system evaluation and design by non-linear modeling*. SAE Technical Paper 920686. 1992 (cit. on pp. 4, 59, 72, 122).

[28] G. Montenegro, A. Della Torre, A. Onorati, and R. Fairbrother. "A nonlinear Quasi-3D approach for the modeling of mufflers with perforated elements and sound-absorbing material." *Advances in Acoustics and Vibration* 2013 (2013) (cit. on pp. 5, 70–72, 76, 78, 90, 179).

[33] F. J. Arnau. *Métodos numéricos para el modelado unidimensional del proceso de renovación de la carga*. Reverté, 2009 (cit. on pp. 15, 80).

[49] R. Courant, K. Friedrichs, and H. Lewy. "Über die partiellen Differenzengleichungen der mathematischen Physik." *Mathematische annalen* 100(1) (1928), pp. 32–74 (cit. on pp. 31, 76).

[62] P. K. Sweby. "High resolution schemes using flux limiters for hyperbolic conservation laws." *SIAM journal on numerical analysis* 21(5) (1984), pp. 995–1011 (cit. on pp. 49, 54, 80).

[63] J. P. Boris and D. L. Book. "Flux-corrected transport. I. SHASTA, a fluid transport algorithm that works." *Journal of computational physics* 11(1) (1973), pp. 38–69 (cit. on pp. 50, 78).

[65] A. Harten. "High resolution schemes for hyperbolic conservation laws." *Journal of computational physics* 49(3) (1983), pp. 357–393 (cit. on pp. 53, 71, 80).

[73] S. F. Davis. "A simplified TVD finite difference scheme via artificial viscosity." *SIAM journal on scientific and statistical computing* 8(1) (1987), pp. 1–18 (cit. on pp. 55, 80).

[101] R. M. Beam and R. F. Warming. "An implicit finite-difference algorithm for hyperbolic systems in conservation-law form." *Journal of computational physics* 22(1) (1976), pp. 87–110 (cit. on p. 70).

[102] F. Payri, J. Desantes, and A. Torregrosa. "Acoustic boundary condition for unsteady one-dimensional flow calculations." *Journal of Sound and Vibration* 188(1) (1995), pp. 85–110 (cit. on pp. 70, 98, 100).

[103] A. Torregrosa, A. Broatch, A. Gil, and D. Moreno. "Analysis of acoustic networks including cavities by means of a linear finite volume method." *Journal of Sound and Vibration* 331(20) (2012), pp. 4575–4586 (cit. on pp. 70, 120, 122, 129).

[104] T. Morel, R. Keribar, and P. N. Blumberg. *A new approach to integrating engine performance and component design analysis through simulation*. SAE Technical Paper 880131. 1988 (cit. on pp. 70, 71).

[105] R. Pearson and D. Winterbone. "The simulation of gas dynamics in engine manifolds using non-linear symmetric difference schemes." *Proceedings of the type of Mechanical Engineers, Part C: Journal of Mechanical Engineering Science* 211(8) (1997), pp. 601–616 (cit. on p. 71).

[106] M. Vandevoorde, J. Vierendeels, E. Dick, and R. Sierens. "A new total variation diminishing scheme for the calculation of one-dimensional flow in inlet and exhaust pipes of internal combustion engines." *Proceedings of the type of Mechanical Engineers, Part D: Journal of Automobile Engineering* 212(5) (1998), pp. 437–448 (cit. on p. 71).

[107] S. J. Galiano and M. U. Zapata. "A new TVD flux-limiter method for solving nonlinear hyperbolic equations." *Journal of Computational and Applied Mathematics* 234(5) (2010), pp. 1395–1403 (cit. on p. 71).

[108] H.-D. Kim, Y.-H. Kweon, and T. Setoguchi. "A study of the weak shock wave propagating through an engine exhaust silencer system." *Journal of sound and vibration* 275(3) (2004), pp. 893–915 (cit. on p. 71).

[109] P. D. Lax and B. Wendroff. "Difference schemes for hyperbolic equations with high order of accuracy." *Communications on pure and applied mathematics* 17(3) (1964), pp. 381–398 (cit. on p. 76).

[110] G. A. Sod. "A survey of several finite difference methods for systems of nonlinear hyperbolic conservation laws." *Journal of computational physics* 27(1) (1978), pp. 1–31 (cit. on pp. 82, 83, 101).

Chapter 4

Boundary conditions

Contents

4.1 Introduction **96**
4.2 Independent boundary conditions **97**
4.3 One-dimensional collocated scheme connection **100**
4.4 Preliminary results and discussion **104**
4.5 Summary and conclusions **108**
Chapter 4 bibliography **111**

4.1 Introduction

During the development of a new numerical method, it is common to think about the conception and implementation of the numerical scheme as the only work that has to be performed. Nevertheless, there are some other fields that are usually overlooked because they are not as visible but they prove to be just equally important to the final performance of the method. One of these tasks is the development of boundary conditions, without which the numerical scheme cannot even be properly validated. This chapter is dedicated to the boundary conditions that have been conceived in order to, on the one hand, be able to validate the numerical method and, on the other hand, perform the eventual connection with a one-dimensional collocated scheme.

With this purpose, an extensive description of the boundary conditions formulation and implementation process is presented, paying special attention to the role of each of the elements of the staggered grid mesh. This kind of mesh is much less frequent in the literature, so much more work has to be developed or adapted from collocated mesh solutions. As it will be seen, the most promising techniques for the stand-alone boundary conditions reside in the use of the Method of Characteristics, while for the connection with a collocated scheme, the implementation of virtual cells offer more advantages.

Finally, some preliminary results obtained when testing all the mentioned boundary conditions will be shown and discussed. It is worth noticing that the cases that have been selected to test the boundary conditions implementation are usually simple geometries in a one-dimensional environment. This simplified first approach is intentional, since these simulations assure that any misbehaviour that may be detected would be only due to issues in the implementation of the boundary conditions and not introduced by other elements. More complex examples will have to be simulated and validated in future work to ensure the completely correct functioning of the model in any situation, but for this stage of the development process, these results can be used as a preliminary step, mainly for the more extensive validation performed in the following chapters, where the pulse inlet boundary condition is used, and to test that the connection with a one-dimensional model in a collocated grid is possible and feasible.

4.2 Independent boundary conditions

First, there was the need of developing some boundary conditions that would allow some simple simulations with the code that was developed without the need of using it connected to the more developed code of OpenWAM. Although the ultimate objective is to perform such connection in order to be able to use the quasi-3D method as an additional tool included in the one-dimensional model, before performing the connection a lot of tests are needed and the quasi-3D model code is constantly changing in the development phase until the best solution is found. Therefore, some boundary conditions that allow those tests and the eventual validation process of the numerical scheme have to be developed first.

The boundary condition which will become the main focus is the inlet pulse since it offers the versatility of obtaining results which are meaningful in both the time domain and, with little extra calculations, in the frequency domain. Besides, if experimental measurements are needed and can be performed for validation, they are easily obtained with an impulsive test rig. Therefore, a pulse development simulation in the time domain is useful to observe the behaviour of the numerical oscillations and how the flux limiters act on them. After that, with the Fourier transform the sound pressure levels of the incident and transmitted wave can be calculated to study the acoustic behaviour of the system, with the possibility to also calculate the transmission loss of the device. In this regard, a white noise boundary condition is the usual boundary condition used in acoustic simulations, and it might give more suitable results for acoustic characterisation, but it would be also much harder to obtain conclusions in the time domain and a longer simulation would be needed, potentially reducing the number of tests that could be performed. For the reasons stated above, the inlet pulse boundary condition was the first one to be considered and it will be consistently used in the following chapters for the validation process.

The starting point for these boundary conditions come from the assumption that, according to Mucklow and Wilson [111], it is possible to know the total velocity of a fluid in the particular place and space at which two simple waves meet, one travelling rightwards and associated with the velocity u^+ and another one travelling backwards characterized by a velocity u^-, with the simple relationship

$$u = u^+ + u^- \tag{4.1}$$

On the other hand, the velocity and the pressure of a simple wave can be related as:

$$\frac{u^{\pm}}{a_{ref}} = \left(\frac{2}{\gamma - 1}\right)\left[\left(\frac{p^{\pm}}{p_{ref}}\right)^{\frac{\gamma-1}{2\gamma}} - 1\right] \tag{4.2}$$

where p is the pressure, a the speed of sound and the ref subscript indicates reference conditions. From here, it is also possible to decompose the flow variables in order to identify the information propagating in the forward, p^+, and backward, p^-, directions, as follows:

$$\left(\frac{p}{p_{ref}}\right)^{\frac{\gamma-1}{2\gamma}} = \left(\frac{p^+}{p_{ref}}\right)^{\frac{\gamma-1}{2\gamma}} + \left(\frac{p^-}{p_{ref}}\right)^{\frac{\gamma-1}{2\gamma}} - 1 \tag{4.3}$$

Under the assumption of isentropic flow, the pressure and the local speed of sound can be related with:

$$\frac{p}{p_{ref}} = \left(\frac{a}{a_{ref}}\right)^{\frac{2\gamma}{\gamma-1}} \tag{4.4}$$

Therefore, by substituting the isentropic relationship into equation (4.3), it can be written

$$a - a_{ref} = (a^+ - a_{ref}) + (a^- - a_{ref}) \tag{4.5}$$

where a^+ and a^- represent the local speed of sound associated to the forward and backward simple waves. Such decomposition was performed by Payi *et al.* [102] in order to use the acoustic characteristics of a given singularity as a boundary condition. An important conclusion to draw from these equations is that the total pressure of the volume is composed by the two travelling waves and hence, in the inlet boundary condition it will not necessary be the same as the generated pulse. Simply imposing the pressure of the pulse in the volume brings erroneous results, so a more elaborated method should be used.

The approach chosen to create the boundary condition is based in the Method of Characteristics following the same approach as García-Cuevas [112] to implement a similar incident pressure boundary condition. Therefore, assuming that the section where the pulse is generated is on the left side of the system, first the non-dimensional left-travelling characteristic for non-homentropic flow, β, is calculated in that volume

$$\beta = \left(\frac{a}{a_{ref}} - \frac{(\gamma - 1)}{2} \cdot \frac{u_{end}}{a_{ref}} \right) \frac{a_A}{a_{ref}} \tag{4.6}$$

where u_{end} is the local velocity of the flow from the duct into the boundary volume and the entropy level a_A has been used to account the entropy variations in the flow, which is defined as:

$$\frac{p}{p_{ref}} = \left(\frac{a}{a_A} \right)^{\frac{2\gamma}{\gamma - 1}} \tag{4.7}$$

Note that for the case of homentropic flow, the entropy level would correspond to the reference speed of sound. Now, according to García-Cuevas [112], the non-dimensional right-travelling characteristic, λ, can be calculated as follows:

$$\lambda = \left[2 \left(\frac{p_{pulse}}{p_{ref}} \right)^{\frac{\gamma - 1}{2\gamma}} - 1 \right] \frac{a_A}{a_{ref}} \tag{4.8}$$

where the pressure of the pulse has been imposed by p_{pulse}. This last equation can be used to calculate the entropy level, so that the only unknown variable left is the pressure p in equation 4.7, which corresponds to the actual pressure that the section at which the pulse is generated needs to have to impose the desired pulse travelling to the right.

Finally, the velocity of the flow and the speed of sound in the volume are given by the equations

$$\frac{u}{a_{ref}} = \frac{\lambda - \beta}{\gamma - 1} \tag{4.9}$$

$$\frac{a}{a_{ref}} = \frac{\lambda + \beta}{2} \tag{4.10}$$

From here, the rest of the variables needed for the quasi-3D method can be calculated.

Another boundary condition that was needed to work along with the pulse inlet was an anechoic termination. This boundary condition has the property of not allowing any reflection, acting like an endless duct and therefore avoiding the need of simulating a very long duct to elude the reflection, resulting in a faster simulation. This boundary condition is used in almost every acoustic simulation because otherwise the reflection of the transmitted wave at the end

of the system would contaminate the measurement of the transmitted wave itself, since the pressure obtained would be the addition of the two waves travelling in different directions. Another option is to use a long enough duct at the end of the system so that the reflected wave would not reach the point where the transmitted wave is measured, since it has a much longer distance to cover. The problem with this technique is that simulating the long duct will increase the computational time required for the simulation.

Taking a similar approach as with the inlet pulse, the method of characteristics can be used to implement an anechoic termination boundary condition, as shown by Torregrosa *et al.* [113]. In this case, it has to be imposed that there is no wave travelling backwards, assuming the same disposition as before, where the anechoic termination is in the right side end of the duct. Following the same approach as Payri *et al.* [102], the rightwards wave associated flow velocity can be expressed as:

$$u^+ = \frac{2}{\gamma - 1}(a^+ - a_{ref}) \tag{4.11}$$

Under the assumption of non-reflection conditions, there is no backward wave and $u^- = 0$, thus, according to equation (4.1), the flow velocity in the boundary condition is equal to u^+. Equation (4.11) can be rearranged and substituted into equation (4.6), obtaining that the non-reflecting condition is translated into the equality $\beta = a_A/a_{ref}$. Finally, the rightwards characteristic and the rest of variables of the anechoic termination can be calculated as indicated by equations (4.7), (4.9) and (4.10).

For the purpose of this work and its objective, no more independent boundary conditions have been developed, being the two described above sufficient for the validation process originally proposed in this work, as it will be explored in the following chapters.

4.3 One-dimensional collocated scheme connection

Besides the previously mentioned boundary conditions, a connection with the one-dimensional code OpenWAM will eventually be needed, and although it will be the final step of the project and this work focuses on the development and validation process of the numerical method, the final objective is to include it in the core of the one-dimensional method, so the work would not be completed unless the connection between codes was at least outlined and some preliminary tests were performed. Therefore, in this section the strategy

for the connection between the quasi-3D staggered method and a collocated finite volume method one-dimensional scheme is proposed, focusing in how to resolve the differences between meshes and where are the variables calculated.

Another issue to address is the fact that the quasi-3D numerical method has been originally written in a different programming language than OpenWAM and translating the new code would not feasible at this stage of the project. Therefore, the approach that has been selected to test the viability of the connection between methods consist on creating first a simple one-dimensional code in the same programming environment as the quasi-3D method an then proceeding with the connection.

The one-dimensional method selected for this purpose is based on the first order Godunov scheme, as it was described in section 2.3.5, which is similar enough to the modern one-dimensional methods to obtain meaningful results, but does not require a heavy investment in development time, needing a rather simple code, specially in its first order form. These reasons make the first order Godunov method the best candidate to test the connection between methods.

In order to test the numerical method the shock-tube problem [110] has been simulated once again. As it was explained in section 3.7, this problem consist in simulating the evolution in time of the properties of a tube in which two gases with different thermo- and fluid-dynamic states separated in a tube are put into contact. In Figure 4.1 the results for the shock-tube obtained using the first order Godunov scheme are compared to the analytical results. In this case, the initial conditions for the left side are $p_1 = 5$ bar and $T_1 = 1200$ K, and for the right side, $p_2 = 1$ bar and $T_2 = 300$ K. The initial velocity of the flow in both sides is zero. Finally, the geometry used consist in a one metre duct of 5 cm of diameter meshed with 200 volumes and the simulation was stopped at $t = 0.0005$ seconds.

The results obtained with the first order Godunov method correspond with the ones expected, showing the characteristic dissipative behaviour of a first order scheme, specially noticeable in the contact zone discontinuity in the density and temperature plots. In any case, these results validate the one-dimensional method, since the values of the variables tend to the analytical solution. Therefore, the connection of numerical methods will be attempted between the quasi-3D method previously described and the first order Godunov method here appointed.

Despite the fact that there are several connection methods, like the approach followed by Galindo [10], based on the Method of Characteristics; the most suitable method for this case, taking into account the elements of the two

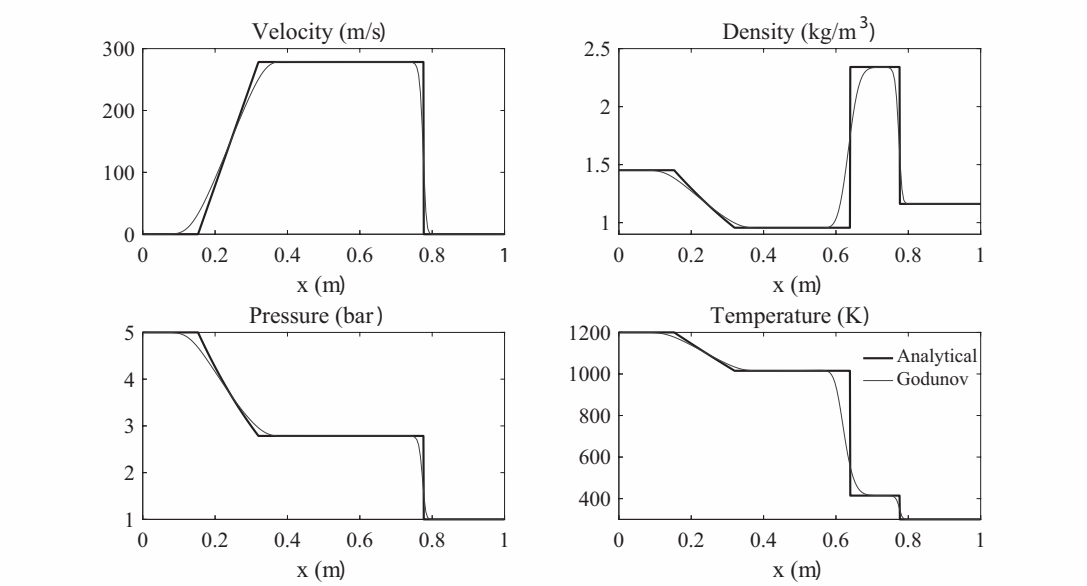

Figure 4.1: Shock-tube results with a one-dimensional first order Godunov scheme.

meshes and where the variables are calculated, lies in the use of virtual cells, based on its implementation by García-Cuevas [112]. On one hand, the cell of the quasi-3D method that will be connected to the one-dimensional scheme, which from now on will be called boundary cell, will need the values of the density and internal energy from the connected cell of the one-dimensional method, as well as the flow between the two cells in their contact surface. The way that the virtual cell works consists in connecting the boundary cell of the quasi-3D method to a virtual volume by means of a new connector which, by these standards, will be called virtual connector. Throughout the calculation of the variables in one time step, everything is performed as usual with the difference that in the next time step, the initial values of the variables of the virtual volume and the virtual connector that will be used to calculate the next time step are not the ones previously calculated by the quasi-3D method, but by the one-dimensional scheme in its boundary cell. Special attention has to be paid to the virtual connector, since it does not have a direct equivalent in the collocated mesh, so there are no variables calculated in its position. Therefore, an upwind approach is adopted, where the value of the flow may come either from the boundary cell of the collocated mesh or from the boundary cell of the staggered grid, depending on the direction of the flow in the previous

time step. The upwind approach has been chosen because it has already been used in the quasi-3D numerical method with good results.

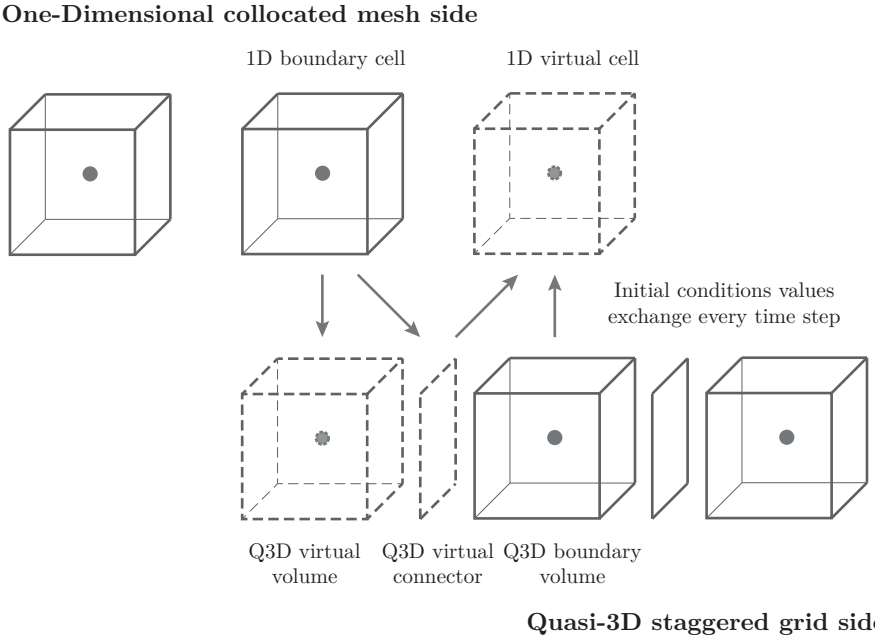

Figure 4.2: Schematic representation of virtual cells information exchange between one-dimensional and quasi-3D methods meshes.

On the other hand, a similar procedure will be followed in the one-dimensional side of the model. The boundary cell will be also connected to a virtual cell, whose initial values in each time step will come from the boundary cell for mass and energy equations, and from the virtual connector for the momentum equation. Figure 4.2 shows a schematic representation of the above explained procedure, connecting two one-dimensional ducts with different meshes by virtual cells.

It is worth remarking that these virtual cells are only there to translate the information between meshes and, even though every variable seems to fit in the other mesh after the translation, the way the flux is calculated and treated in each method is different, as it has been previously explained, with the staggered grid mesh calculating it in the connectors and the collocated mesh in the volume, so some unexpected behaviour could be found after the connection between codes.

4.4 Preliminary results and discussion

In this section some preliminary results obtained after the implementation of the previously described boundary conditions will be shown and discussed, along with the difficulties found when implementing them and the solutions adopted.

Inlet pressure and anechoic termination boundary conditions

First, to test the inlet pressure boundary condition, a simple geometry consisting of a one-dimensional duct 8.6 metres long has been meshed with 400 volumes, imposing a pressure pulse in one end of the pipe and studying how it propagates along the duct. Besides, at the end of the duct an anechoic termination will be placed so the two boundary conditions can be tested in the same simulation. In Figure 4.3 the measurements of a pulse generated in an impulsive test rig with a duct as the one modelled are represented, along with the results of the pressure obtained with the quasi-3D method in the volume connected directly with the boundary condition after imposing the measured pulse.

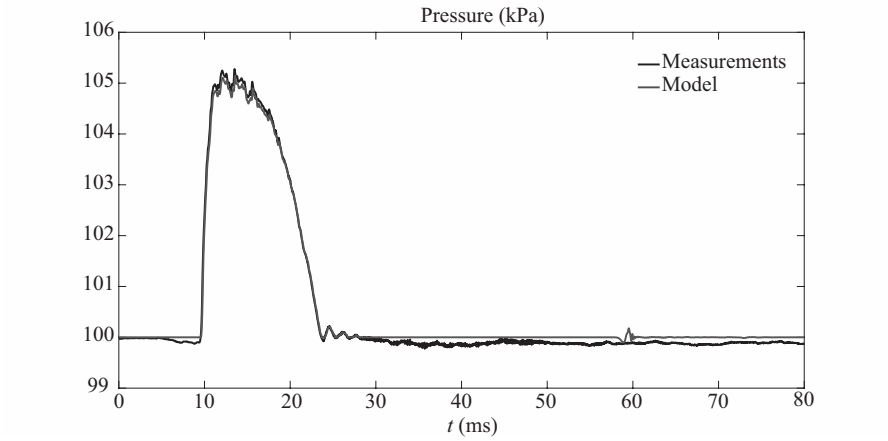

Figure 4.3: Plots of the pressure pulse generated and the pressure in the volume following the boundary condition in the mesh.

It can be seen that the boundary condition is able to reproduce almost exactly the pressure pulse, with a slightly lower amplitude. At around 60 ms, a small anomaly can be seen, which will be discussed later. The rest of differences, mainly the pressure level when there is no pulse, are due to the fact that there is a restriction that was added to the boundary condition that does

not allow the pressure to go below 1 bar. That is introduced to avoid possible measurement errors and to obtain somewhat cleaner results. Therefore, for the data points where the pressure is lower than 1 bar, the boundary condition automatically imposes 1 bar as outlet pressure.

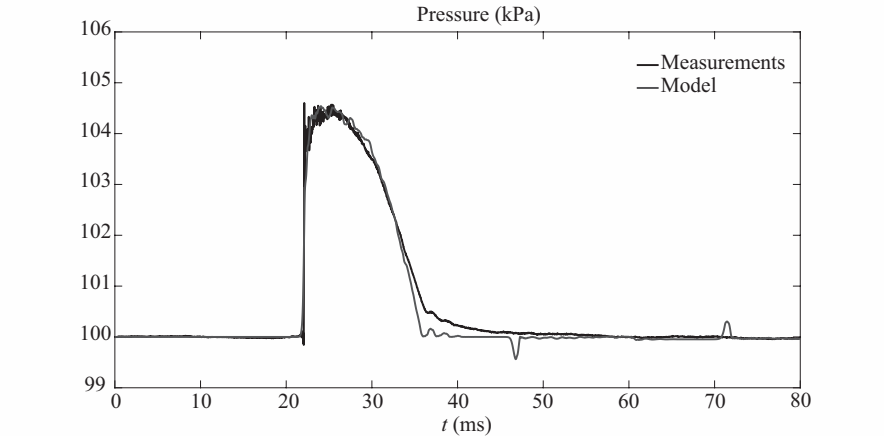

Figure 4.4: Plots of the pressure pulse measured and the pressure calculated at the middle of the duct.

The next step is to compare the results provided by the model, after the pulse has developed, with the measurements. Hence, Figure 4.4 shows the pulse predicted by the model and measured at the centre of the duct. The results show how the amplitude of the pulse is well represented, even though it is a litter higher than the measurements, while the generated was slightly lower. This means that the model has lower pressure losses, which is something to be expected since there is no friction model yet in the method. However, the ending part of the pulse does not drop as fast as the model predicts, but this could also be improved with a friction model, since the dissipation would be higher, affecting more the shape of the wave as it travels. More importantly, at around 47 ms there is a small anomaly in the pressure, which can only be a small reflection that the anechoic boundary condition has not been able to completely remove. It was already visible in Figure 4.3 in the generated pulse at 60 ms, since that point was further away from the anechoic end and the reflection took longer to reach it. The small pulse that can be seen at around 72 ms in Figure 4.4 is the result of the first reflection reaching the start of the duct and reflecting again.

Even though the anechoic termination is not completely anechoic, the re-

sults obtained show a very small amplitude reflection that for most of the acoustic applications should not introduce a big source of error, specially if using white noise as a source. However, when using an inlet pulse to characterize the acoustic behaviour of a system, the useful information is located in a much narrower space and a small deviation can be catastrophic for the final results. It is true that the reflection is really small and it would be easyly removable from the results as long as it is not in the pulse, but the same can be said of the reflection produced by a closed termination and since it has a much higher amplitude, it is easier to detect. Therefore, until this issue is resolved, it is not recommended to use the anechoic termination, at least with an inlet pulse, and in the validation process in the next chapters a longer ending duct to avoid reflections will be used instead.

The inlet pulse boundary conditions on the other hand fulfils the requirements and will be subsequently used in the validation process and different applications in the following chapters.

One-dimensional and quasi-3D connection

Finally, some tests will be performed on a model where two different meshes have been connected, a collocated one-dimensional first order Godunov scheme and a quasi-3D staggered grid, following the steps described in the previous section. With this objective, the same shock-tube problem considered in section 4.3 will be solved, with the exception that this time, the left half of the duct has been meshed with the quasi-3D staggered grid, and the right side with the 1D collocated scheme. The connection is therefore in the middle of the duct and initially each mesh will have different thermodynamics properties. Right at the beginning of the simulation, the contact surface, shock wave and the rarefaction wave will appear in the connection, thus assuring that all the relevant information goes through the connection and any issue can be detected.

As a reminder, the initial conditions for the left side are $p_1 = 5$ bar and $T_1 = 1200$ K, and for the right side, $p_2 = 1$ bar and $T_2 = 300$ K. The initial velocity of the flow in both sides is zero. Finally, the geometry used consist in a one metre duct of 5 cm of diameter meshed with 200 volumes and the simulation was stopped at $t = 0.0005$ seconds.

In Figure 4.5 the results of the shock-tube simulation can be seen, along with the analytical results as a reference. It can be observed that the simulation brings successful results with a good prediction of the variables in the four zones of the shock-tube and respecting the discontinuities, within the limits of each numerical scheme. The only alteration in the results that seems to

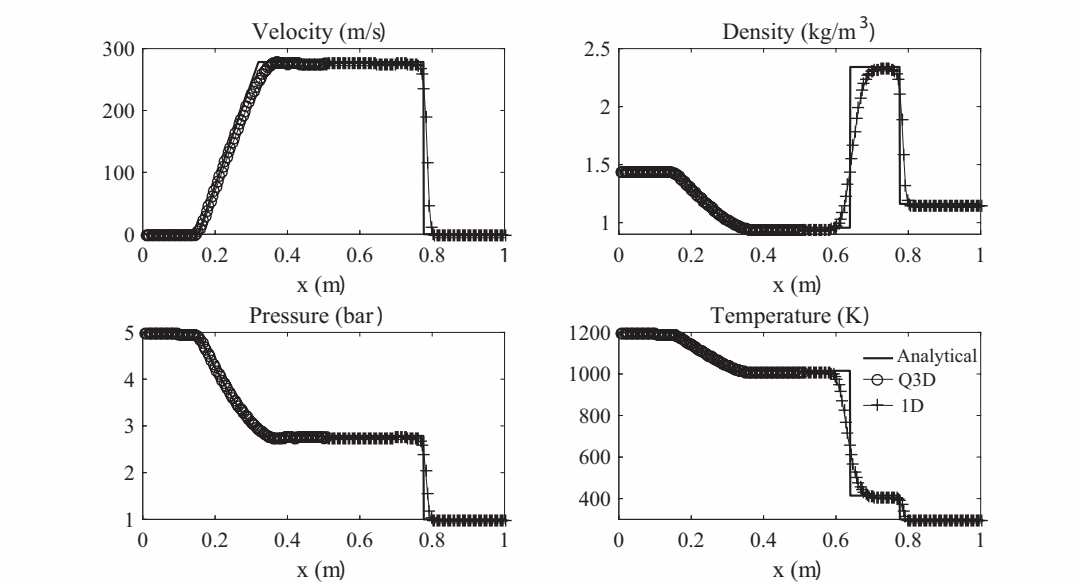

Figure 4.5: Shock-tube results with a staggered grid for the left side and a collocated scheme for the right side.

be produced by the connection can be located in the zones around the contact surface, with a not completely flat solution and some small oscillations in the transition to the rarefaction wave. In Figure 4.6, this region has been represented in more detail for the four variables, but the conclusions drawn from the shock-tube results are that the connection between meshes is possible and even if a slight distortion of the solution in the interface proximity can be expected, it would be of a very small magnitude, taking into account that the shock-tube test puts the numerical method into the most drastic situation with a large discontinuity between initial conditions. In engine simulations usually performed this severe steps are not expected, and so the behaviour of the connection between schemes is presumed to be even better.

As a final note for this section, it is worth clarifying that no flux limiter has been used in the quasi-3D numerical method for the boundary cell, while in the rest the MDT method has been used. The reason of this absence is the fact that their implementation increases the complexity of the connection, since for any of the flux limiters, information of at least the two neighbour cells for each connector is needed. These condition is even more problematic for the TVD method, since it needs information of two cells at each side of the

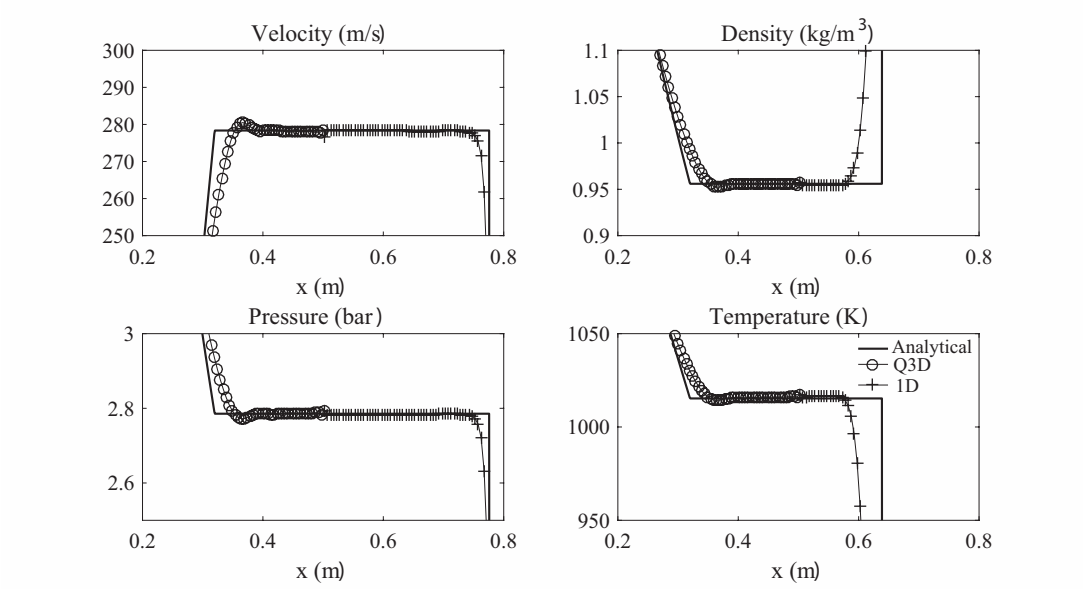

Figure 4.6: Detailed contact zone of the shock-tube results with a staggered grid for the left side and a collocated scheme for the right side.

connectors to properly work. The Momentum Diffusion Term flux limiter was tested with the current implementation of the connection, since is the most flexible method, but some spurious oscillations appeared near the connection, both in the quasi-3D and one-dimensional side. It is hard to detect where the oscillations are generated first, but another reason of this misbehaviour might come from the manipulation of the momentum in the connector that goes to the one-dimensional side, originating the numerical oscillations. In any case, some more test should be performed in the future, including the possibility of using two or more virtual cells in order to have extra-information for the flux limiters in the interface, but unfortunately these options could not be explored in this work due to time restrictions and because the original objective of this section was only to prove that the connection was possible and feasible, and show some preliminary results, as it has been achieved.

4.5 Summary and conclusions

This chapter has been dedicated to the important task of assuring that a connection between the staggered-grid quasi-3D numerical method here developed

and a collocated one-dimensional method is possible without having to sacrifice accuracy in the overall solution. This part is critical because the final objective of the model is to be added to a one-dimensional program to be used when required. Besides, some other boundary condition based on the Method of Characteristics have been developed, which will be particularly useful in the next chapters dedicated to the validation process.

Starting with the independent boundary conditions, the main efforts were focused on creating an inlet pressure pulse boundary condition, since the results obtained by simulating an impulsive test rig provide meaningful results in the time and frequency domains, after some calculations with the Fourier transform in the latter case. Another reason for the selection is that an impulsive test rig experiment is a simple test, opening the path to more experimental measurements to validate the results of the model.

A Method of Characteristics based approach was used to create the inlet pulse boundary condition and, following a similar strategy, the anechoic termination boundary condition, where the requirement was of course that there could not be any reflections. Having this boundary condition is particularly convenient because it can work along with the inlet pulse in the impulsive test rig simulation while avoiding the reflection of the pressure wave, thus allowing the use of a much shorter outlet duct and reducing the computational cost of the simulation.

To validate the boundary conditions, an impulsive test rig consisting on a pressure pulse travelling through a duct was modelled. For this problem, lots of experimental data are available, so a measured generated wave was imposed in the starting point of the duct so that the results of the model could be compared to the experimental test measurements at a certain point of the duct. First, the generated wave was compared with the pressure in the second volume of the model to ensure that the pulse is correctly transmitted by the boundary condition, as it was the case. Then, the pressure was measured at a certain distance from the inlet, coinciding with the experimental data available. This time, although the evolution of the wave was correctly captured by the model, with only some small differences in the ending part of the wave that can be due to some extra dissipation introduced by friction, the simulation results show a small reflection of the pulse that would introduce an error that could be significant in this kind of tests. Therefore, it is not recommended its use when simulating an impulsive test rig. However, it should be considered for other tests where the small reflection does not affect the final results.

Moving to the connection between different numerical methods, first a one-

dimensional method was proposed, based on a first order Godunov scheme in a collocated grid. The method was tested in the classical shock-tube problem, obtaining the expected results, which are a good approximation of the variables in the four zones created, but with a rather dissipative behaviour in the transition between zones, as it is characteristic of a first order numerical scheme. Godunov method was chosen due to its simplicity regarding the formulation and implementation, while offering accurate results. Besides, most modern one-dimensional schemes are based on the Godunov's method, so the strategy adopted to perform the connection between schemes in this chapter is much more likely to coincide with the one to finally be applied to any other modern numerical method.

For the connection method itself, a virtual cell approach was adopted, where a new cell is added to each of the meshes, right where the connection is planned. These couple of cells that will be connected to the virtual cell have been called boundary cells. The strategy to follow consists in the virtual cell inheriting the variables calculated in the boundary cell of the other mesh and using those variables as initial conditions for the following time step, process that will be repeated in every time step. The fact that the mesh elements used by each numerical method are different, with a collocated grid and a staggered grid with volumes and connectors, makes the traffic of information between meshes less obvious. The quasi-3D staggered grid uses a virtual volume and a virtual connector, obtaining the flow by an upwind approach. In the case of the collocated virtual cell, the information required comes from the boundary volume, for mass and energy, and from the virtual connector for the momentum.

In order to show some preliminary results, a one-dimensional duct was meshed with the objective to simulate a shock-tube once again, but this time using a staggered grid for the left side and a collocated mesh for the right side. In this way, all the relevant information goes through the connection. The results obtained are satisfactory, with the expected accuracy both in the final values of the variables in the zones as in the reproduction of the transition between them, according to the order of each numerical method. Only some small amplitude oscillations where detected near the rarefaction wave in the quasi-3D side, which may be caused by the connection or by the fact that no flux limiter was used, or even a combination of both. The reason of not using any flux limiter comes from the increase in complexity of implementation, and satisfactory preliminary results had been already achieved. In any case the quality of the results obtained is promising, specially considering the extreme

conditions imposed in the shock-tube problem. Therefore, it is concluded that the connection between the quasi-3D staggered grid scheme and a one-dimensional collocated method is possible and feasible, even if still some work has to be performed in adapting the flux limiters.

Chapter 4 Bibliography

[10] J. Galindo, A. Tiseira, P. Fajardo, and R. Navarro. "Coupling methodology of 1D finite difference and 3D finite volume CFD codes based on the Method of Characteristics." *Mathematical and Computer Modelling* 54(7) (2011), pp. 1738–1746 (cit. on pp. 4, 70, 101).

[102] F. Payri, J. Desantes, and A. Torregrosa. "Acoustic boundary condition for unsteady one-dimensional flow calculations." *Journal of Sound and Vibration* 188(1) (1995), pp. 85–110 (cit. on pp. 70, 98, 100).

[110] G. A. Sod. "A survey of several finite difference methods for systems of nonlinear hyperbolic conservation laws." *Journal of computational physics* 27(1) (1978), pp. 1–31 (cit. on pp. 82, 83, 101).

[111] G. Mucklow and A. Wilson. "Wave-Action in Gases: The Attenuation and Reflection of Compression Waves Propagated in Pipes: Part I-Wave Attenuation; Part II-Wave Reflection." *Proceedings of the Institution of Mechanical Engineers* 169(1) (1955), pp. 69–82 (cit. on p. 97).

[112] García-Cuevas González, Luis Miguel. "Experiments and Modelling of Automotive Turbochargers under Unsteady Conditions." PhD thesis. 2015 (cit. on pp. 98, 99, 102).

[113] A. Torregrosa, P. Fajardo, A. Gil, and R. Navarro. "Development of non-reflecting boundary condition for application in 3D computational fluid dynamics codes." *Engineering Applications of Computational Fluid Mechanics* 6(3) (2012), pp. 447–460 (cit. on p. 100).

Chapter 5

Application to mufflers and other three-dimensional systems

Contents

5.1 Introduction **114**
5.2 Meshing techniques **115**
5.3 Linear acoustics **120**
5.4 Parallelepiped shape muffler **125**
5.5 Reversal chamber **135**
5.6 General shape muffler **141**
5.7 Summary and conclusions **143**
Chapter 5 bibliography **146**

5.1 Introduction

Traditionally, even the acoustic behaviour of the devices where more three-dimensional effects occur has been successfully modelled with a one-dimensional approach up to not too high frequencies by using different techniques. However, as more complex geometries are needed to fulfil the increasingly restrictive regulation, one-dimensional models start being an insufficient tool either because the traditional techniques cannot be used or because higher frequencies need to be accurately modelled. It is possible in this case to use a three-dimensional CFD (computational fluid-dynamics) model, but that would imply investing a significantly higher amount of time in modelling and calculating, which is something that manufacturers cannot afford in early stages of the design. These are the reasons why quasi-3D methods are an increasingly interesting tool in the design of internal combustion engines in general, and specifically in the case of after-treatment systems and mufflers.

The non-linear quasi-3D numerical method that was developed in chapter 3 has as the most remarkable asset the ability of taking into account three-dimensional effects while maintaining a low computational cost. This is achieved by assuming some simplifications in the momentum conservation equation, as seen in chapter 3. Nevertheless, it is important to validate the numerical method by comparing the results obtained with either experimental measurements or with the results offered by other already validated and established codes modelling the same problem. While this is true for any new model under development, it is specially critical for models where strong assumptions are made, as is this case, with a one-dimensional momentum equation approach in a three-dimensional model.

Therefore, the most appropriate way of validation of the model appears to be the simulation of the three-dimensional devices to which the code is likely to be applied more often when modelling an engine, which are the mufflers. Mufflers, also known as silencers, are systems used to reduce the noise produce by the engine. Depending on its shape, distribution of inlet and outlet ducts and other properties, like the presence of absorbent materials, the muffler can be designed to act in a certain range of frequencies. A good design will reduce the noise only for the desired frequencies to avoid an unnecessary increase of the back pressure and hence, a decrease of the engine efficiency.

In this chapter, the above mentioned validation of the quasi-3D method is performed in different geometries and configurations. Before, a meshing technique has been implemented in order to facilitate the simulations and it has been detailed to further understand the implementation of the method into

the code. As the main comparison instrument, an existing linear acoustics tool is described. The main purpose of this tool is to serve as a reference solution by comparing the transmission loss obtained with the two different methods. As a general rule, a correct prediction of the non-linear quasi-3D method will follow the same curve as that given by the linear acoustics tool, only seeing certain differences at higher frequencies, where the three-dimensional effects may influence the transmission loss. Ideally, experimental results should be also available for the validation, but given the numerous devices and configurations that should be manufactured, most of them without any real application (they would only be used for that particular test), this has been discarded in this section. Therefore, the validation will consist in studying the improvements that the non-linear quasi-3D method brings when compared to a standard linear acoustics tool.

Furthermore, not only the acoustics prediction capabilities of the quasi-3D method and the effect of the simplifications adopted are validated, but the performance of the different flux limiters has been tested in every case to understand the advantages and disadvantages that each of them brings. The strategy that has been followed consists in the modelling and simulation of increasingly complex geometry devices with different inlet and outlet configurations. A pulse is generated upstream of the device and the incident and transmitted waves, one at each end of the main geometry, are taken to compute the transmission loss.

5.2 Meshing techniques

One of the steps that cannot be overlooked when simulating is the meshing of the problem which, although not as complex as the physical phenomenon, can be critical to obtain proper results. This is specially important when simulating three-dimensional elements, where the complexity of the mesh and the time needed to create it can represent an important part of the total work. Even the most accurate and efficient numerical methods would be useless if there are no means to apply them to the problem under study. Similarly, an efficient and automated way of meshing will eventually need to be developed, otherwise, it will not be possible to test regular geometries and the usefulness of the method will be greatly reduced. As a result, an efficient three-dimensional meshing technique needs to be developed to validate the numerical method.

As it was pointed out in section 3.2, the mesh consist of a staggered grid with two types of basic elements: volumes and connectors. Besides, each of

those connectors will be the link between two volumes and those volumes can have as many connectors attached as needed. With this approach, a matrix representation of the connexions between the two kind of elements of the mesh comes naturally to mind. Therefore, a matrix with the total number of volumes as rows and the number of connectors as columns will be created and it will be called from now on *G matrix*. This matrix will only have values in the positions where a volume and a connector are linked in the mesh and the value will be 1 if the connexion goes from the volume to the connector or -1 if it goes in the opposite direction, according with the Cartesian coordinate system. Therefore, for a very basic example of three volumes connected along the X axis by two connectors as a duct, the G matrix will be the following

$$\mathbf{G} = \begin{bmatrix} 1 & 0 \\ -1 & 1 \\ 0 & -1 \end{bmatrix} \tag{5.1}$$

In this example, there are three volumes, so the G matrix has three rows, and there are two connectors, hence the two columns of the matrix. It can also be seen how the volume 1 is attached with the connector 1 and, since the value of the G matrix is positive, that means that the connector is positioned at a higher value of the X axis than the volume. With the usual representation of the axis, connector 1 would be at the right side of volume 1. Looking now at volume 2, it can be seen that it corresponds to the opposite situation, since the value in the G matrix is -1, connector 1 is at the left side of volume 2 with respect the X axis. Finally, another way of obtaining visual information of the G matrix is looking at the columns. The first column corresponds to connector 1 and it links volumes 1 and 2, since those are the only rows of the matrix with non-zero values. Connector 2 does the same with volumes 2 and 3. Since every connector can only link two volumes, there has to be only one set of 1 and -1 for each row. If there is more than one, that connector is linking too many volumes, if there is none, that connector is not needed, and if both values are positive or negative, that means that the volumes are not properly connected, since both volumes cannot be at the same side of the connector. This simple verification is the first one that should be done when meshing.

Although it has been stated that the selection of the sign of the values of the G matrix is decided considering if the link goes along or against the direction of the axis, it is actually an arbitrary criterion that might be useful for the one-dimensional case but not sufficient for higher dimensional problems. In a one-dimensional case the information of the signs can be used to determine

the position of the volumes at each side of the connector, since there is only one axis. However, when there are more axes, there is no information of the orientation in space of the connector. Therefore, a new matrix is needed that will specify the orientation of each connector. This new matrix will be denoted *Cn matrix* and will have as many rows as connectors are in the mesh and as many columns as dimensions are considered in the problem. Each row will be formed by the unit vector of the direction orthogonal to the surface of the corresponding connector. For the previous example of a three volumes duct with two connectors along the X axis, the Cn matrix is the following

$$\mathbf{Cn} = \begin{bmatrix} 1 & 0 & 0 \\ 1 & 0 & 0 \end{bmatrix} \tag{5.2}$$

where both connectors have the same orientation, which is along the X axis, hence the unit vector is $[1, 0, 0]$ for both of them. Making use of these two matrices facilitates the implementation of the operations of the numerical method.

Hereunder several techniques that have been developed to solve the problem of meshing three-dimensional geometries will be outlined, starting for the most simple cases and finishing with a tool to import externally generated meshes.

Constant section geometries

As a first approach, three-dimensional geometries with constant section will be considered. These geometries, although simple, are very common silencers, intercoolers, filters or catalysts, at least in an important part of the element. The strategy here would be starting with an easy-to-make mesh of the section of the element. Then, the direction for the extension and the number of volumes for its length have to be specified to the tool. With that information, the tool will start to scan the section, going through every volume and checking its connectors that are not in the longitudinal direction. The volume and the connectors will be then copied and moved in the longitudinal direction and added to the G matrix, expanding it. The same process will be followed for every volume, ignoring the connectors that have already been moved alongside with previous volumes. After going through the original section and creating the next one, the whole process is repeated for the newly created section and so on, until the desired length is achieved. In Figure 5.1 an extension of a generic section can be seen. Even if the real element is not as simple and only a part of it has constant section, the mesh created with this method would simplify the meshing process, since only the rest of the less regular geometry would have to be meshed by other means.

It is worth mentioning that this tool can also be easily applied to mesh ducts just by using a single volume as starting section.

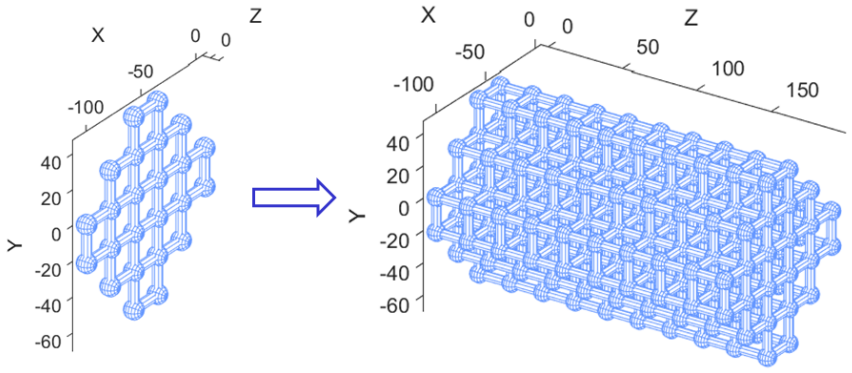

Figure 5.1: Constant section geometry mesh representation.

Geometries with parallel ducts

The next meshing technique developed consist in a variation of the constant section geometry meshing and it was thought specifically for meshing catalyst bricks and particulate filters. The main idea is to modify a constant section mesh created with the previously explained technique in such a way that the mesh is formed only by longitudinal parallel ducts. In order to obtain this mesh, an initial and ending section will be specified to the tool by selecting one volume of the initial section and one volume of the ending section. After that, the tool will check all the connections of the volumes between the specified sections and will remove all the connectors, except the longitudinal ones. Finally, the G matrix and the Cn matrix will be rewritten, excluding the removed connectors. The resulting mesh will be formed by parallel ducts in the longitudinal direction along the specified part of the element.

As mentioned above, these meshes are specially useful when simulating catalysts and particulate filters. Catalyst are formed by a great amount of channels to maximize the contact surface with the fluid and facilitate the chemical reactions and are traditionally simulated as a number of identical ducts, according to the cell density of the catalyst brick. In this way, only one duct has to be simulated, since every other one would offer the same results. This solution brings a low computational cost with good results, but it cannot take into account the different inlet conditions that the channels may have. With a complete 3D mesh, these effects can be simulated, but

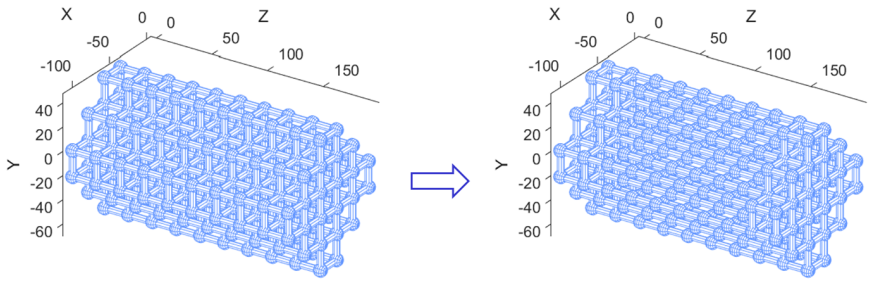

Figure 5.2: Parallel ducts geometry mesh transformation representation.

in order not to increase excessively the computational cost, all the channels should not be meshed. In Figure 5.2 the resulting mesh of applying the parallel ducts geometry transformation to the mesh of Figure 5.1 is shown. Here, the same effective one-dimensional approach to model catalyst can be used for the different ducts. This means that every duct should be treated as a certain number of identical ducts, so only one of them has to be simulated, but each set of identical ducts will have different inlet and outlet conditions, increasing thus the accuracy of the results by taking 3D effects into account, but without drastically increasing the computational time.

Complex geometries

Finally, more complex geometries will have to be meshed. This situation will be faced not only in the final steps of the validation process, but also when intending to use the quasi-3D method in real applications. Unfortunately, the development and implementation of a complete meshing tool is a task that would require too much time and it is not the main focus of this work. Nevertheless, the simulation of general shape geometries is eventually needed in the validation process, and therefore a temporary solution was elaborated until the final meshing tool is available.

The approach that was taken consist in building the mesh with a different source to export the data of the connections between cells. The only requirement for the source meshing tool is that it has to create an output file readable by a text editor with the information of the connections between cells and some kind of orientation in the three-dimensional plane. Knowing that every connector of the quasi-3D method will link two volumes and its orientation, it is possible to create the G matrix and the Cn matrix required for the calculations. In Figure 5.3 an example of the result of the above mentioned procedure is shown.

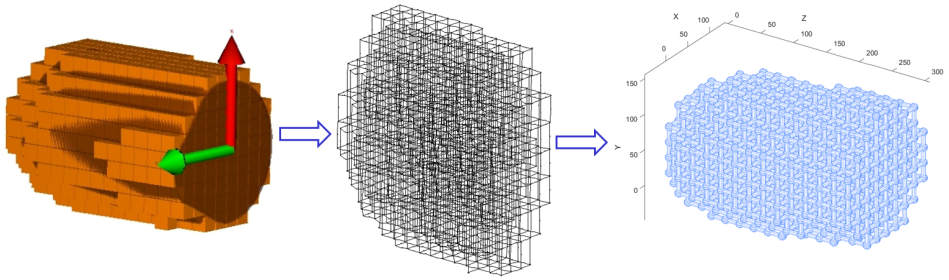

Figure 5.3: Complex geometry mesh importation process representation.

Although depending on an external tool for meshing complex geometries is not desired, it is a temporary solution that will make possible a more extensive validation of the non-linear quasi-3D numerical method. In future works, a reliable meshing tool will be developed.

5.3 Linear acoustics

The validation method selected for this section is based on the use of a linear acoustics tool. The tool used was described in [103] and has already been extensively validated with experimental measurements. The election of this linear acoustics tool makes sense because it allows the direct comparison between two tools with the same objectives but different approaches. On one hand one uses a non-linear approach and can obtain the acoustic response by the Fourier transform, while the other one can obtain the acoustic behaviour after linearizing the equations, as it will be detailed in this section. Both tools complement each other since both can be used to calculate the Transmission Loss of a system using the same mesh and compare the results, the linear tool with the advantage of being faster and the non-linear case with the advantages of also providing a time domain solution and, generally, a higher resolution in the frequency domain.

The numerical method used for the linear acoustics model is based on a linear version of finite volume method. The linearization procedure will be now described, showing how the linearized mass and momentum equations can be interpreted in terms of volume-related junctions connected by means of length- and area-related equivalent 2-ports.

In a similar fashion as the non-linear quasi-3D method, a staggered-mesh grid will be used, which also allows the use of the same G matrix for both

methods. Therefore, equations of mass and energy conservation are solved for each volume, and the momentum equation is solved for each interface between two volumes [114]. The energy equation will not be considered in this case, as the flow evolution in the volumes will be considered as isentropic, thus only the mass continuity equation and the momentum equation need to be solved. According to Morel [114], mass conservation in a given fluid volume can be expressed as:

$$\frac{\mathrm{d}m_n}{\mathrm{d}t} = \sum_i \dot{m}_n^{(i)} \tag{5.3}$$

where m_n is the mass contained in the n-th volume, and $\dot{m}_n^{(i)}$ represents the mass flow corresponding to the i-th opening connecting the n-th volume to any other volumes. Assuming that the evolution inside the volume is isentropic, one may introduce the pressure p_n inside the volume, thus getting

$$\frac{\mathrm{d}m_n}{\mathrm{d}t} = \frac{V_n}{c_0^2}\frac{\mathrm{d}p_n}{\mathrm{d}t} = \sum_i \dot{m}_n^{(i)} \tag{5.4}$$

Here, c_0 is the speed of sound and V_n is the volume. Now, writing all the variables as the addition of a mean value and a fluctuating part ($p \to p_0 + p$, etc.), and assuming harmonic time-dependence for the fluctuating parts, it is obtained that

$$\mathrm{j}\,\omega\frac{V_n}{c_0^2}p_n = \sum_i v_n^{(i)} \equiv v_n \tag{5.5}$$

where $\mathrm{j} = \sqrt{-1}$, ω is the angular frequency and v_n represents the mass velocity fluctuation, i.e. the fluctuating part of the mass flow rate. Therefore, in the pressure-mass velocity representation, the behaviour of the volume regarding mass conservation may be represented by considering a multi-port with a passive impedance given by:

$$Z^{(n)} = \mathrm{j}\,\frac{c_0^2}{\omega V_n} \tag{5.6}$$

which is the impedance corresponding to the compliance V/c_0^2 of a cavity of volume V [115]. Secondly, according to reference [114], the momentum equation at the interface between volumes can be written as

$$\frac{\mathrm{d}(mu)}{\mathrm{d}t} + \sum \dot{m}u = -A\Delta p \tag{5.7}$$

where u is the flow velocity and A is the cross-section area at the interface, whereas Δp represents the pressure difference between the two volumes. Now, if equation (5.7) is referred to the unit volume one gets

$$\frac{\mathrm{d}(\rho u)}{\mathrm{d}t} + \sum \frac{\rho u^2}{l} = -\frac{\Delta p}{l} \tag{5.8}$$

where l is a characteristic length. Following a linearization procedure similar to that used to obtain equation (5.5), for the case without a mean flow one obtains

$$\rho_0 \frac{\mathrm{d}u}{\mathrm{d}t} = -\frac{\Delta p}{l} \tag{5.9}$$

Then, assuming harmonic time dependence for all the fluctuating variables and introducing the mass velocity $v = \rho A u$, gives:

$$\mathrm{j}\,\omega \frac{l}{A} v = -\Delta p \tag{5.10}$$

As equation (5.10) is a linear relation, it admits a simple representation in terms of a 2-port as a system relating the state variables of two different points. With that, the momentum exchange at the interface between two volumes can be actually represented by a 2-port defined by equation (5.10), which corresponds to the impedance associated with the lumped inertance l/A of a short duct [115]. In the cases with mean flow, equation (5.5) remains unaffected, but according to Amphlett [116], equation (5.10) must be substituted by

$$\left[\mathrm{j}\,\omega \frac{l}{A} + 2\frac{U_0}{A}\right] v = -\Delta p \tag{5.11}$$

where U_0 is the mean flow velocity across the interface, which can be obtained from a time domain steady flow computation performed with the same spatial discretization, as described by Sapsford [13].

As a summary, mass and momentum exchange between volumes may be represented by considering each volume as a multi-port, as defined by equation (5.5), and then connecting those multi-ports by means of 2-ports as defined by equation (5.10), or equation (5.11) in the presence of flow. In this way, any cavity may be represented by a network of zero-dimensional nodes connected by 2-ports, for which suitable solutions already exist.

In the one-dimensional case, both 2-ports and multi-ports can be represented by transfer matrices [103], but in the three-dimensional case the order

of the multi-ports can be higher than 2, making the transfer matrix representation no longer valid. In Figure 5.4 the different wave components propagating in the adjacent 2-ports of a multi-port are represented. Under the assumption of plane wave, these wave components are related to the pressure and mass velocity fluctuations by

$$v_n^{(i)} = \frac{1}{Z_n^i}(p_n^{i+} - p_n^{i-}) \;\; ; \;\; p_n^{(i)} = p_n^{i+} + p_n^{i-} \;\; ; \;\; i = 1, \cdots m_n \tag{5.12}$$

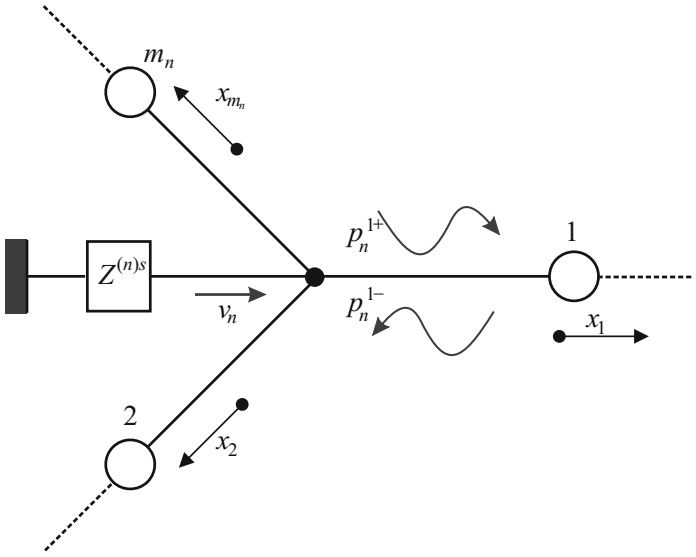

Figure 5.4: Schematic representation of a multi-port.

Here, $Z_n^i = c_0/A_i$ is the characteristic impedance of the 2-port i, A_i its cross-sectional area and m_n is the order of the multi-port. The total mass velocity fluctuation v_n across the multi-port can be written as

$$\sum_{i=1}^{m_n} \frac{1}{Z_n^i}(p_n^{i+} - p_n^{i-}) = v_n \tag{5.13}$$

Continuity of pressure across the multi-port gives

$$p_n^{i+} + p_n^{i-} = p_n \;\; ; \;\; i = 1, \cdots m_n \tag{5.14}$$

Therefore, from equations (5.5), (5.6), (5.13) and (5.14) it can be written

$$\left[\frac{1}{Z_n^1}+\frac{1}{Z^{n(s)}}\right]p_n^{1+}+\sum_{k=2}^{m_n}\frac{1}{Z_n^k}p_n^{k+}=\left[\frac{1}{Z_n^1}-\frac{1}{Z^{n(s)}}\right]p_n^{1-}+\sum_{k=2}^{m_n}\frac{1}{Z_n^k}p_n^{k-} \tag{5.15}$$

That can be written in matrix form as

$$\mathbf{S}_n^+\mathbf{p}_n^+=\mathbf{S}_n^-\mathbf{p}_n^- \tag{5.16}$$

Here, $\mathbf{S}_n^+$ and $\mathbf{S}_n^-$ are the positive and negative $m_n \times m_n$ scattering matrices for the multi-port n and $\mathbf{p}_n^+$ and $\mathbf{p}_n^-$ are m_n-vectors of travelling pressure amplitudes moving outwards from and towards the multi-port n. With this representation, the behaviour of the mass exchange between volumes can be expressed in a compact form.

According to equation (5.16), the best representation for these 2-ports is provided by the scattering matrix, as represented in Figure 5.5. Here, p^{1+}, p^{1-}, p^{2+} and p^{2-} are the travelling pressure amplitudes, whose values at each side of the 2-port are considered as state variables and are related by means of the scattering matrix $\mathbf{S}_m$ of the 2-port, as follows

$$\begin{bmatrix} p^{1-} \\ p^{2-} \end{bmatrix}=\mathbf{S}_m\begin{bmatrix} p^{1+} \\ p^{2+} \end{bmatrix} \tag{5.17}$$

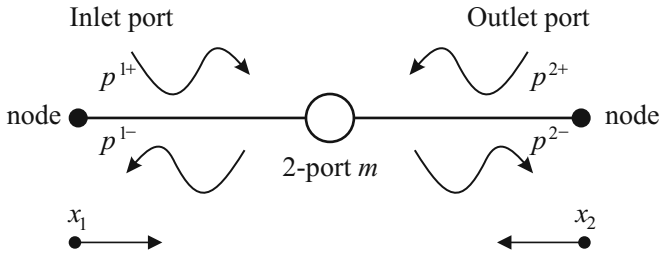

Figure 5.5: Scattering matrix formulation for 2-port.

The elements of the scattering matrix for the momentum-related 2-ports may be obtained from equation (5.10), resulting in the following form

$$\begin{bmatrix} 1 & \mathrm{j}\,\omega l/(2A) \\ 0 & 1 \end{bmatrix} \tag{5.18}$$

At this point, the conditions of mass and momentum conservation has been translated into the simultaneous solution of equation (5.16) for each multi-port

(volume) and of equation (5.17) for each 2-port (interface between volumes). Considering an acoustic network with M 2-ports, equations (5.16) and (5.17) give a total of $4M$ equations with $4M$ unknowns, so that it is possible to combine the multi-port equations (5.16) and the 2-port equations (5.17) to derive a single equation for the whole acoustic network. This complete network equation was written by Glav [117] as

$$\mathbf{A}\mathbf{p}_c^+ = \mathbf{B}\mathbf{p}_c^- \tag{5.19}$$

Here, $\mathbf{p}_c^+$ and $\mathbf{p}_c^-$ are $2M$-vectors containing the forward and backward pressure amplitudes at the endpoints of all the 2-ports in the network, and $\mathbf{A}$ and $\mathbf{B}$ denote the left and right network matrices, respectively, which are generated by using the characteristics of the 2-ports and the multi-ports. The complete procedure, which is basically creating a global incidence matrix equivalent to the G matrix of the quasi-3D method, was described by Glav [117]. Then, if $\mathbf{p}_c^+$ is known, $\mathbf{p}_c^-$ can be obtained. Hence, all the travelling pressure amplitudes are known and the complete acoustic state of the network is determined. From this overall representation, it is possible to compute the transfer matrix and the Transmission Loss between any two arbitrary multi-ports.

5.4 Parallelepiped shape muffler

Now that the meshing techniques and the validation tool have been explained, the method developed in chapter 3 will be applied to a parallelepiped shape muffler and then the results will be compared with the ones obtained by using the previously described linear acoustics tool. The three different flux limiters that were also described in chapter 3 will be compared, along with the raw method when possible. But before proceeding with the simulation of the three-dimensional case, a one-dimensional problem has to be considered, as a way to easily obtain results that will support and complement the 3D case. This consisted in the consideration of the propagation in a straight duct, with the same dimensions as the inlet and outlet ducts of the muffler, of a finite amplitude pressure pulse whose characteristics (amplitude and duration) were chosen so as to guarantee a sufficient frequency resolution in the frequency range of interest as well as a sufficient excitation level at all the relevant frequencies, i.e. a substantially flat spectrum [118]. The very same pulse will be later used in the simulation of the 3D muffler. Also, such a simple case as this one allows to a rather simple validation with an experimental test.

The experimental set-up is shown in Figure 5.6 together with an approximate representation of the pulse propagation in the (x,t) plane.

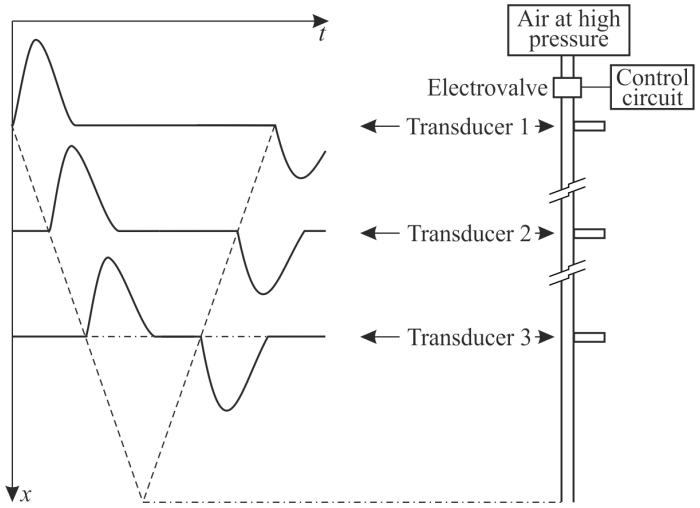

Figure 5.6: Experimental set-up and representation of pressure pulse propagation.

The pulse was generated through the controlled discharge from a high-pressure tank into the duct, making use of a fast-operation electrovalve [119]. Then, the resulting pulse was recorded 15 m downstream of the valve (transducer 1 in Figure 5.6), at a second station 10 m downstream of the first one (transducer 2) and at a third station 10 m downstream of the second one and separated 15 m from the downstream open end (transducer 3). In this way, proper development of the pulse into a weakly non-linear perturbation is allowed, and it is possible to avoid any overlap with the pulse reflected by the open end, as indicated in Figure 5.6. The pulse recorded by transducer 1 and its frequency spectrum are shown in Figure 5.7, where it can be observed that actually the pulse at this position is not yet fully developed, as indicated by the features present in the spectrum.

The results obtained at the two other measurement stations are shown in Figure 5.8 for the different flux limiters considered (the results of the raw method exhibited very large oscillations and have been omitted for clarity). It is apparent in the time domain representation of Figure 5.8(a) that any overshoots associated with the original method appear to be substantially removed by the three methods, except in the vicinity of the rising ramp of the pulse. In this case, only the TVD method is able to damp the pressure oscillations and produce a result closer to the measurement. Apart from this,

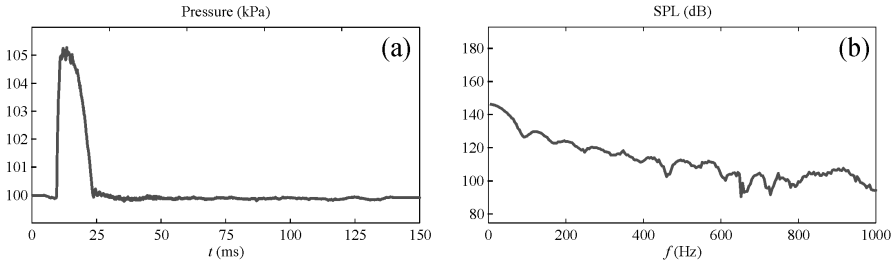

Figure 5.7: Pressure pulse recorded at first measurement station, and later used as boundary condition for the computations: (a) time domain, (b) frequency domain.

all the methods reproduce the overall shape of the pulse, except in the decay zone, where differences between the different methods are negligible, but none of them accounts for the gradual decay observed in the measurement.

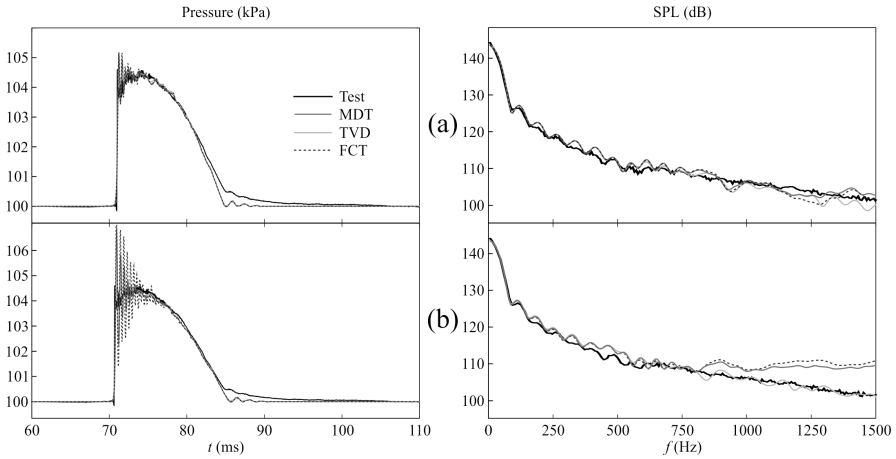

Figure 5.8: Pressure pulse as recorded at the second (a) and third (b) measurement stations, and results produced by the different methods.

In the frequency domain representation given in Figure 5.8(a), one may first notice that the experimental pulse is now properly developed, as a relatively smooth and almost flat spectrum is observed for frequencies above 200 Hz. Secondly, it is apparent that all the methods reproduce quite faithfully the experimental behaviour for frequencies below 500 Hz.

For frequencies above 500 Hz the results are more erratic, but in general the FCT and MDT methods predict a sound pressure level higher than that predicted by the TVD method. It is likely that this behaviour is related with

the non-physical oscillations retained by those methods. This would also be confirmed by the fact that this tendency is especially clear at the highest frequencies represented. In any case, it appears that none of the methods produces any severe suppression of the medium-to-high frequency content of the signal, contrary to the results shown by Fauconnier and Dick [120], which seem to point out that all non-linear schemes should suffer from large dissipation in combination with the generation of spurious oscillations throughout the entire wavenumber spectrum.

When considering the results obtained at the position of transducer 3, shown in Figure 5.8(b), all these effects are even more noticeable. As a result of the additional propagation, the residual oscillations previously shown by the MDT and FCT methods in the vicinity of the pulse ramp have grown dramatically, especially in the case of the FCT method, whereas the TVD results still follow quite closely the measured pressure trace. In the frequency domain a certain degradation of the quality of the results can be observed below 500 Hz for the three methods, and the agreement is somehow better than for transducer 2 between 500 and 750 Hz. However, the main differences are found for frequencies above 800 Hz: it is here where the effect of the spurious oscillations in the MDT and FCT methods becomes apparent, with an almost linear increase of the sound pressure level with frequency that produces a significant deviation with respect to the measured spectrum. At the same time, the TVD method produces a very good approach to the measurements in these high frequencies. Even if such long propagation distances do not occur in engine exhaust systems, these results point to a certain superiority of the TVD method from a frequency-domain point of view.

Once the performance of the different methods was assessed in detail in the one-dimensional case with the pulse propagation problem, the three-dimensional version of the method was applied to a simple but representative geometry, whose acoustic response cannot be properly accounted for by means of any one-dimensional model.

The geometry considered is shown in Figure 5.9: it is a rectangular expansion chamber, with dimensions $129 \times 258 \times 344$ mm^3, meshed into cubes with 43 mm of side (for clarity, these are represented as spheres). The location of the inlet and outlet ducts was chosen so that a significant number of higher order modes should be excited. The transmission loss was obtained by simulating the improved impulse method proposed by Payri *et al.* [119], in which the chamber is excited by a pressure pulse similar to those shown in Figure 5.8(a). In this way, there is significant content at all the relevant frequencies, and the

transmission properties are directly obtained from the pulse transmitted by the chamber.

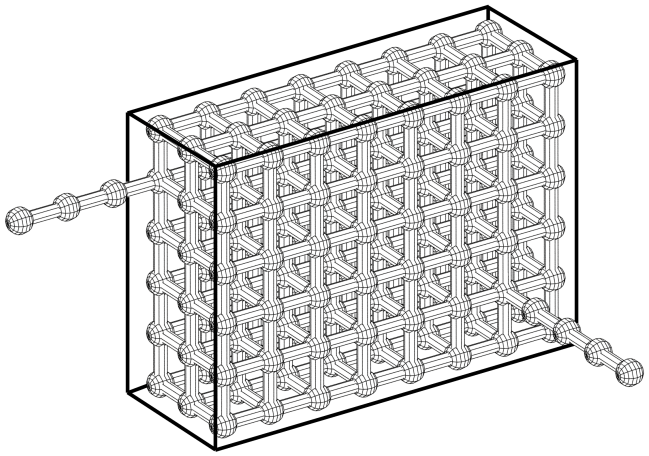

Figure 5.9: Geometry considered and mesh used.

It is worth noticing that with this simulation it is difficult to acquire the incident wave, since the simulation will offer the composed wave, where the incident and the reflected wave are mixed. Therefore, a rather simple solution consist in simulating the same generated wave in a long duct with the exact same geometry and mesh as the one used in the muffler simulation, hence obtaining the unadulterated incident wave.

The results are shown in Figure 5.10, both for the transmitted pulses in the time domain and the resulting transmission loss in the frequency domain. In this last case, the transmission loss computed with the linear frequency-domain counterpart of the present method, which was described and validated by Torregrosa *et al.* [103], is also included as a reference.

In the time domain representation, it can be observed that the results of the original method are severely affected by spurious oscillations that extend along the whole decay of the pulse. In all the other cases, such oscillations have been substantially removed. However, there are significant differences between the behaviour observed for the MDT and FCT methods, on one side, and for the TVD method on the other side. In the first case, some remaining oscillations persist, which are likely to be related with the actual wave dynamics inside the chamber, as multiple internal reflections occur, whereas in the case of

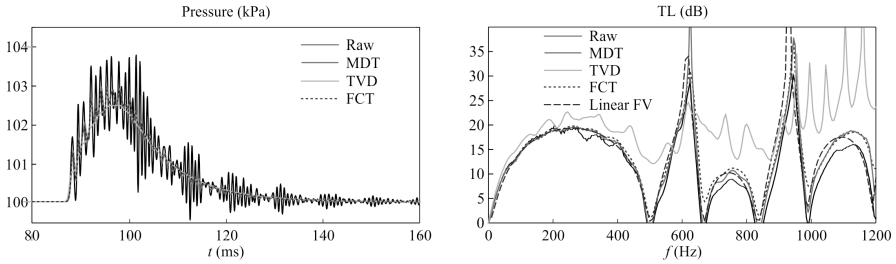

Figure 5.10: Pressure pulse transmitted by the chamber, and corresponding transmission loss, produced by the different flux limiters.

the TVD method it appears that all the oscillations, both non-physical and possibly physical, have been suppressed, and thus some essential dynamics of the system may have been lost.

This is confirmed by the transmission loss plots shown in Figure 5.10, where it can be observed that the results obtained with the TVD method depart significantly from the behaviour predicted by the linear model, which is fully consistent with the geometry of the chamber and the position of the inlet and outlet ducts, whereas all the essential features present in the linear transmission loss have been reproduced by all the other methods, included the raw method without any flux limiter. In particular, the pass-bands observed are precisely related with the period of the oscillations retained by the FCT and the MDT methods, and obviously also present in the results of the original method, even if masked by the high-frequency non-physical oscillations, whose associated frequency is above the frequency range represented.

However, it is obvious from Figure 5.10 that those non-physical oscillations have contaminated to some extent also the mid frequencies. This is particularly clear in the vicinity of the first three pass-bands, where instead of a zero value the original method predicts a negative transmission loss, i.e. some numerical noise is produced inside the chamber. At frequencies far from the pass-bands this may not be apparent, except for the fact that the original method gives everywhere, except at the resonant spikes, attenuation values lower than those corresponding to the linear solution, and thus this effect becomes visible only at the pass-bands themselves. This issue is also present in the results obtained with the MDT method, which might indicate that the expression of the momentum diffusion coefficient given by equation (3.18) in section 3.4 is not the most convenient one for these particular flow conditions.

The results of the FCT method give a fair reproduction of the linear so-

lution, without any negative values but with some clearly dissipative effects in some of the pass-bands and in the narrow-band resonant spikes, which are partially suppressed. Such dissipation is partly due to the use of the FCT technique, but it is also the expected behaviour when a pulse of relatively high amplitude (approximately 50 mbar in this case) is used as the excitation [119]. It can also be observed that the solution obtained starts to deviate quantitatively from the linear solution for frequencies above 1000 Hz, which is consistent with the size of the mesh used.

The rather strange behaviour exhibited by the TVD results will now be examined in some detail, as the results obtained in the one-dimensional case suggested that the frequency-domain performance of this method compared favourably to the other ones in a one-dimensional case. The bad results obtained in the three dimensional case indicate that, as pointed out in section 3.6.2, the problem may lie in the treatment of end-volumes. While the solution adopted may give fair results when a mesh with a sufficiently large number of cells in each direction is used, this may not be the case for the relatively modest mesh used here. However, instead of increasing the number of volumes, what would penalize significantly the computational cost, a modification of the method aiming to reduce the effect observed was attempted.

The modification introduced consisted in introducing a parameter ξ in equation 3.26 in the Davis TVD scheme, as follows

$$\bar{G}^{+}(r_i^{+}) = \xi C(\nu)\left[1 - \psi(r_i^{\pm})\right] \tag{5.20}$$

whose suggested value for a one-dimensional case is 1/2. As this choice has a direct impact on the results of the method the flux limiter in the momentum equation, the effect of considering smaller ξ values was studied. Such a change should reduce the influence of the additional TVD terms and consequently the effects of the *ad hoc* assumption at the end-volumes.

The results obtained are shown in Figure 5.11, again for both the transmitted pulses and the resulting transmission loss. It is apparent in the time domain representation that when reducing the value of ξ the physically meaningful oscillations associated with the internal wave dynamics of the chamber are recovered. This indicates that the original value might have been optimal for a one-dimensional case, but too diffusive for this application. This is confirmed by the transmission loss results, in which it can be observed that the TVD predictions are closer to the linear solution the lower is the value of ξ used. In fact, for $\xi = 0.05$ the agreement with the linear solution is very good for frequencies below 1 kHz, the results being even better than those produced

by the FCT method and shown in Figure 5.10. For frequencies above 1 kHz, the results are almost indistinguishable from those obtained with the FCT or the MDT methods. It is likely that lower ξ values would lead to negative transmission losses as those produced by the original and the MDT methods.

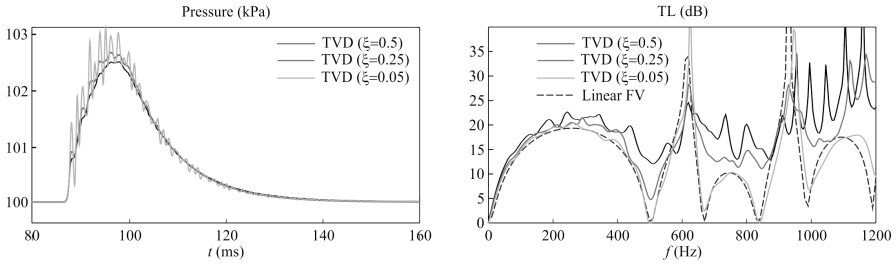

Figure 5.11: Effect of parameter ξ in equation (5.20) on the pressure pulse transmitted by the chamber and the corresponding transmission loss obtained with the TVD method.

In any case, this analysis would not be complete if the influence of such a change in ξ were not evaluated in the one-dimensional cases previously considered. The influence on the results of the shock tube problem can be observed in Figure 5.12, where an expanded view of the most relevant part of the pressure and velocity results is shown. For clarity, only the two extreme values of ξ have been considered.

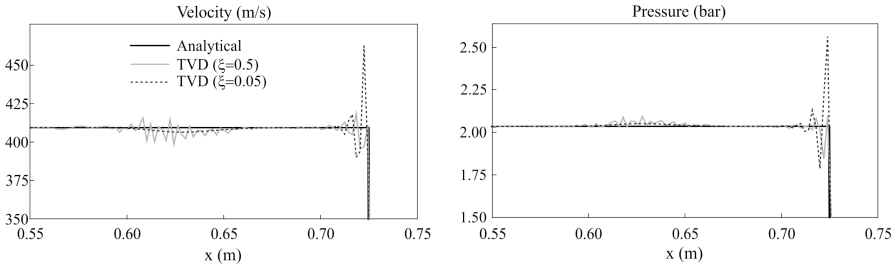

Figure 5.12: Effect of parameter ξ in equation (5.20) on the pressure and velocity results of the shock-tube problem: detail at the contact discontinuity and the shock front.

It is clear that lowering the value of ξ eliminates the spurious fluctuations previously noticed in the vicinity of the contact discontinuity, so that the results are now comparable to those obtained from the MDT and the FCT methods. However, this is achieved at the cost of a clearly insufficient removal

of the spurious oscillations occurring at the shock wave front. Therefore, the use of such a small value for ξ is not advisable in this particular problem.

The influence of ξ on the TVD results for the pulse propagation problem can be checked in Figure 5.13, where the pulses recorded after propagation along 20 m and their corresponding spectra are shown. It is apparent that the advantages previously exhibited by the TVD method regarding the absence of spurious oscillations and the good reproduction of the signal frequency content have been lost, the results being very similar to those provided by the MDT or the FCT methods.

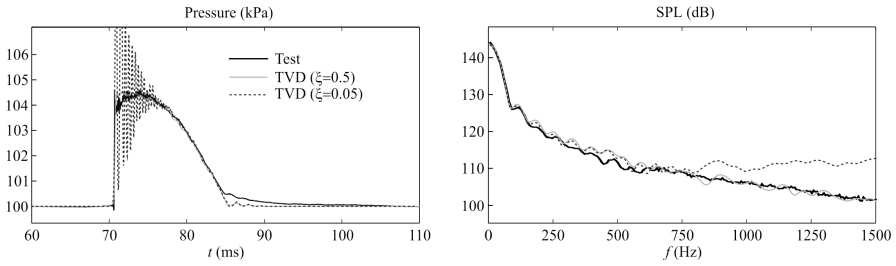

Figure 5.13: Effect of parameter ξ in equation (5.20) on the pressure pulse as recorded at the third measurement station.

It appears thus that this new formulation of the TVD method is especially well suited for the analysis of the acoustics of cavities, but in any other of the conditions considered here its performance is clearly worse than that of the MDT and FCT methods.

The next device that will be modelled is based on the same mesh, but the inlet and outlet ducts are in a different position, as shown in Figure 5.14. This allows the study of the influence of the position of the inlet and outlet ducts in the solution obtained as well as the three-dimensional effects present even in a distribution that might seem more one-dimensional. Furthermore, both the inlet and outlet ducts have been extended the distance equivalent to two volumes, as can be visible in Figure 5.14 if paying attention to the lack of transversal connectors in the first two volumes following the inlet and outlet ducts. Taking this new effect into consideration will increase the validation of the method.

The same impulsive test rig as before has been simulated, imposing an incident pulse at the inlet and comparing it to the transmitted pulse to observe the acoustic behaviour. The transmitted wave obtained using the three different flux limiters developed for the quasi-3D model are compared in Fig-

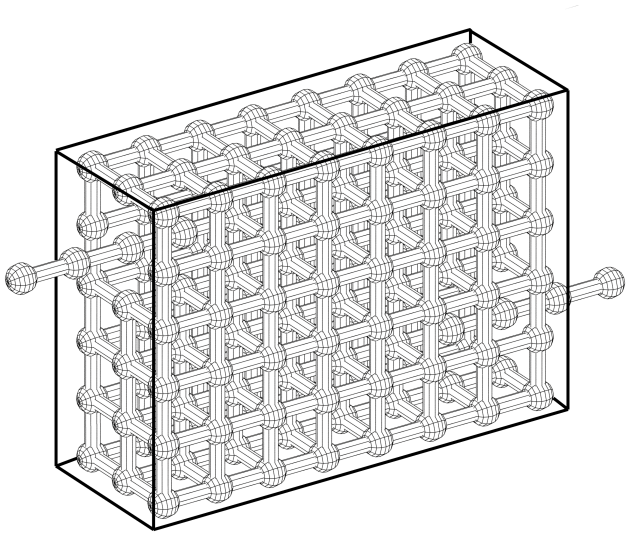

Figure 5.14: Geometry with extended ducts considered and mesh used.

ure 5.15, along with the transmission loss obtained with the three variations of the method and the linear acoustics solutions obtained with the previously explained tool. The parameter ξ of the TVD method was set to 0.15, since it seemed to provide the best results for the transmission loss without bringing too many oscillation in the time domain solution.

The results obtained follow similar tendencies as the previous case. In the time domain, the transmitted wave predicted by the three methods has the same shape, with small differences in the amplitude of the higher frequency oscillations, being lower for the FCT curve and slightly higher for the TVD case, although these oscillations are highly influenced by the parameters of the flux limiters. In the frequency domain, the transmission losses obtained with the different methods are also comparable, finding only significant differences in the pass band levels, with the MDT method being more accurate. When comparing the three non-linear curves with the linear acoustics solution, the same shape of the curves can be found, with slight differences in the local maximum between pass bands.

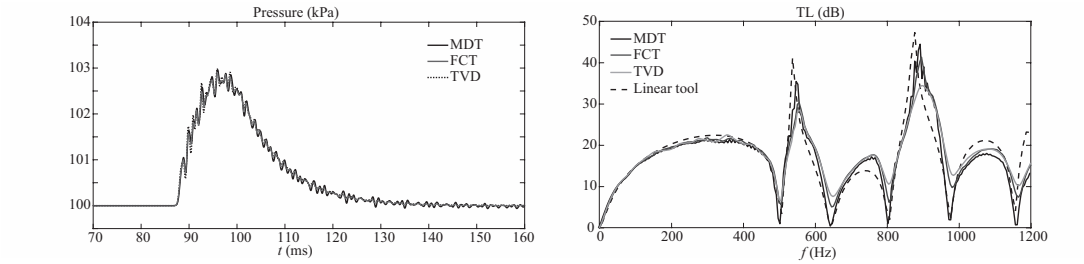

Figure 5.15: Pressure pulse transmitted by the chamber, and corresponding transmission loss, produced by the different flux limiters.

5.5 Reversal chamber

The next system used for the validation consists in a symmetric reversal chamber. The geometry selected is similar to the one showed in Figure 5.16 and although at first glance it might seem just a constant section geometry which would give similar results to a parallelepiped muffler, this geometry offers other issues worth studying in order to validate the numerical method.

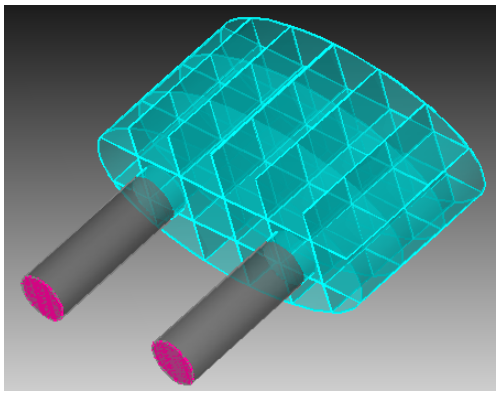

Figure 5.16: Symmetric reversal chamber representation.

In order to properly represent the geometry as accurate as possible, either a really fine mesh with a great number of identical volumes has to be used, or the equal cells concept has to be abandoned. The former implies a more difficult meshing process and a much higher calculation time, without guaranteeing

significantly better results. Therefore, the second option was adopted, creating a mesh of 3×6×3 volumes of 33 mm length, where the most external volumes have half those dimensions, as schematically show in Figure 5.17. This simple representation should be enough to properly reproduce the results obtained with the linear acoustics tool, even when it uses a more detailed mesh.

The results obtained are shown in Figure 5.18, where the same experiment was simulated and the momentum diffusion term was used as a flux limiter as the first option for the analysis. The results obtained with the model developed have been compared with the ones obtained with the linear tool described before in this chapter, but some differences were detected. In order to determine if these differences correspond to a more accurate description of the problem and the three-dimensional effects or, on the contrary, a worse behaviour of the new model, another validation tool was needed. Therefore, a commercial program with extensive validation in acoustic and engine simulation was used, which also could provide a non-linear solution and takes into account 3D effect until some extent. The very same mesh was created, imposing the same incident pulse after a long duct to avoid reflections.

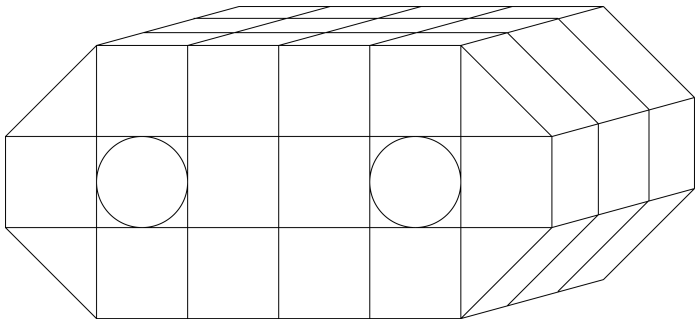

Figure 5.17: Symmetric reversal chamber schematic representation of the mesh used in the quasi-3D method.

The results shown in the time domain show some differences between codes, with the commercial code showing a higher dissipation after the long duct and the reversal chamber. This dissipation was purposely avoided in the developed model because of the long duct used, where too much dissipation could adulterate the results or at least make more difficult the comparison between them with the different flux limiters and the oscillations produced. The commercial code does not allow for such option. Even considering that difference, the shapes of the pulses are similar, although the commercial code produces less oscillations, which could probably be because of the higher dissipation. On the

other hand, in the frequency domain, both non-linear simulations give almost identical results up to almost 2000 Hz, which serves as a good validation of the new model. The linear transmission loss also validates the non-linear results, with only differences in its level above 1200 Hz, due to the complete absence of dissipation in the linear model.

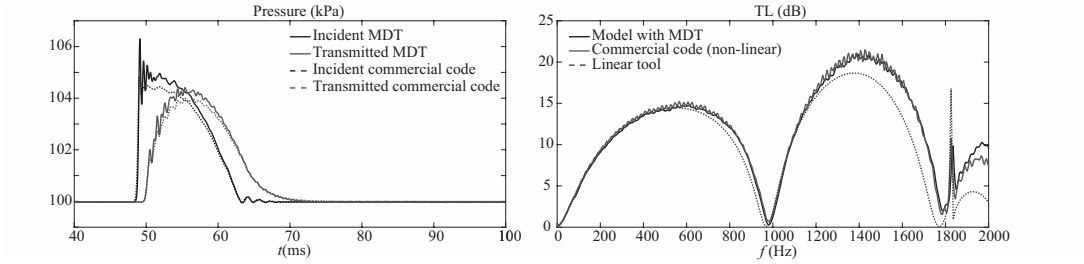

Figure 5.18: Incident and transmitted pressure pulses in the symmetric reversal chamber and corresponding transmission loss with MDT and a commercial code.

In Figure 5.19 the results obtained with the different flux limiters are shown, where the value of the parameters for the TVD used was $\xi = 0.15$, since it seemed to provide the best balance between time and frequency domain results. It can be seen that although the time domain results are almost identical to the point where the curves can almost not be distinguished, the quality of the results in the frequency domain is indeed different. As it can be seen, the MDT curve is the cleanest, followed by the FCT curve, which has lower values above 1200 Hz, and finally the TVD curve has higher amplitude oscillations and a general behaviour closer to the linear values. The conclusion that can be obtained from here is that the MDT flux limiter would give a better prediction of the 3D effects than the FCT flux limiter, and finally the TVD method is not recommended to be used in this case, with a more simple mesh with a lot of end-volumes, which, as seen in section 3.6, is usually a problem for the TVD formulation used.

The same reversal chamber geometry but with different positioning of the inlet and outlet duct might be interesting to make visible other three-dimensional effects and how they are influenced by this inlet and outlet ducts positioning. Furthermore, the more cases are correctly simulated the better the validation of the quasi-3D method would be. With this goal, the geometry shown in Figure 5.20 is considered, where the inlet duct has been moved to an upper position, whereas the outlet duct has been displaced down, resulting in a skew-symmetric distribution.

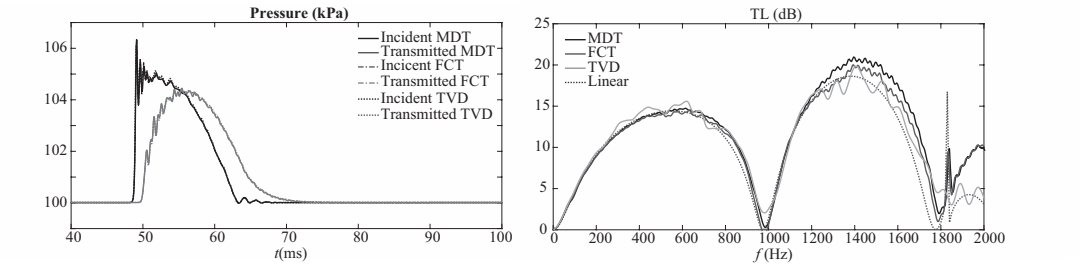

Figure 5.19: Incident and transmitted pressure pulses in the symmetric reversal chamber and corresponding transmission loss with the different flux limiters.

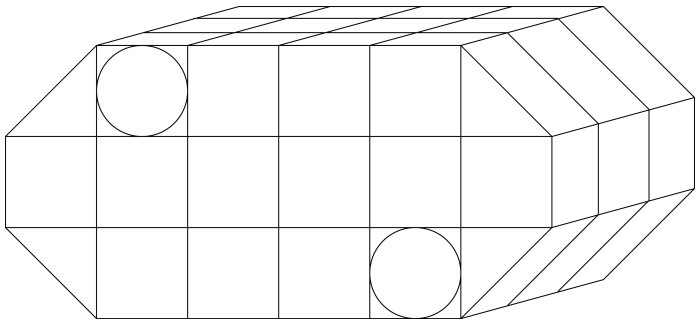

Figure 5.20: Skew-symmetric reversal chamber schematic representation of the mesh used in the quasi-3D method.

Once again, the mesh has been evaluated using the developed quasi-3D method, the linear tool and the non-linear commercial code that will allow to compare non-linear and linear acoustics results to further validate the model. The results obtained simulating the incident wave going through the system are shown in Figure 5.21. It can be seen that in the time domain similar amplitude discrepancies appear, due to the different treatment of the dissipation, but in the frequency domain, the three transmission losses predicted are consistent with each other, with only small differences in the level of the linear acoustics curve. It is worth noticing that at higher frequencies, from 1000 Hz, the transmission loss is much higher than in the symmetrical case shown in Figure 5.18.

The results obtained using the three different flux limiters considered are now compared in Figure 5.22, where the same conclusions as in the symmetric reversal chamber can be stated: virtually the same results in the time domain, but in the frequency domain the TVD solution is much worse from about 1200

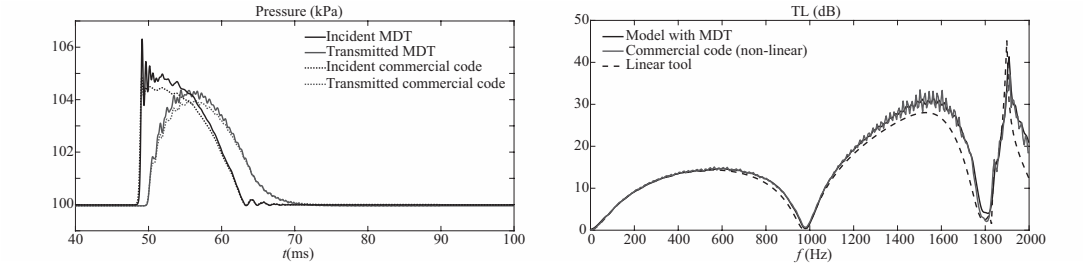

Figure 5.21: Incident and transmitted pressure pulses in the skew-symmetric reversal chamber and corresponding transmission loss with MDT and a commercial code.

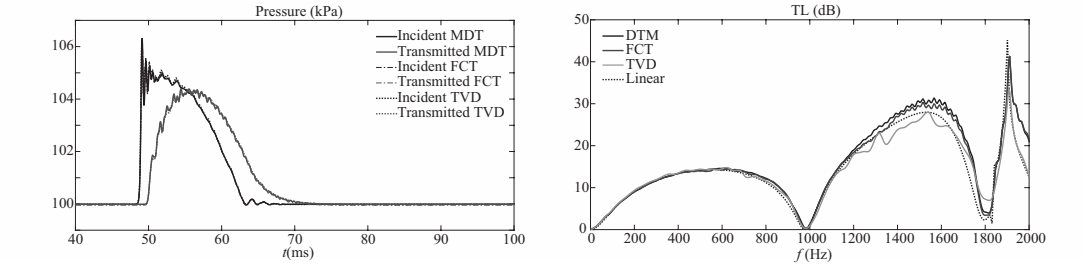

Figure 5.22: Incident and transmitted pressure pulses in the skew-symmetric reversal chamber and corresponding transmission loss with the different flux limiters.

Hz, with small differences between the MDT and FCT solutions.

Finally, an asymmetric distribution of the inlet and outlet duct has been evaluated. For this case, both the inlet and outlet duct have been displaced one volume to the left, as shown in Figure 5.23.

The same simulation has been performed with the non-linear quasi-3D method and the also non-linear commercial code previously used to obtain the transmission loss and this results have been compared with the ones obtained using a linear acoustics tool, as shown in Figure 5.24. It can be observed that this case keeps the same tendencies as the previous ones, with a lower amplitude in the waves of the time domain solution offered by the commercial code due to its higher dissipation, and similar results in the transmission loss with the three approaches, while it is true that the solution offered by the

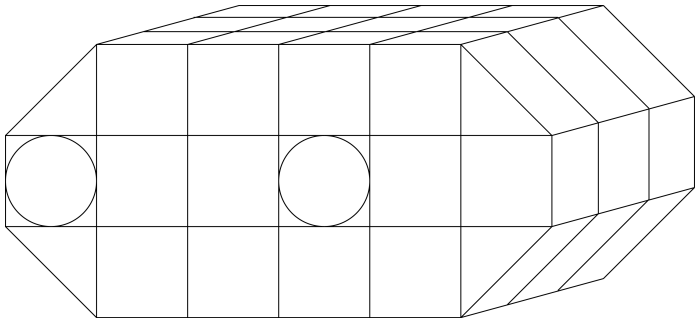

Figure 5.23: Asymmetric reversal chamber schematic representation of the mesh used in the quasi-3D method.

commercial code in the range between 1200 Hz and 1700 Hz approximately has some spurious oscillations and it is in general a lower quality prediction of the transmission loss curve. It can be also seen that in this case an even higher transmission loss is obtained for higher frequencies, what remarks the importance of using a model able to accurately predict high frequencies, since up to 1000 Hz, the transmission loss of the three devices are similar. However, when going to higher frequencies, huge differences can be observed, making one distribution more suitable for a given problem. In this case, with a very simple device, the transmission loss obtained with the linear tool matches the one predicted with the other non-linear approaches, but in general that could not be the case and another complementary tool would be needed to validate the acoustics results, specially if tests cannot be performed.

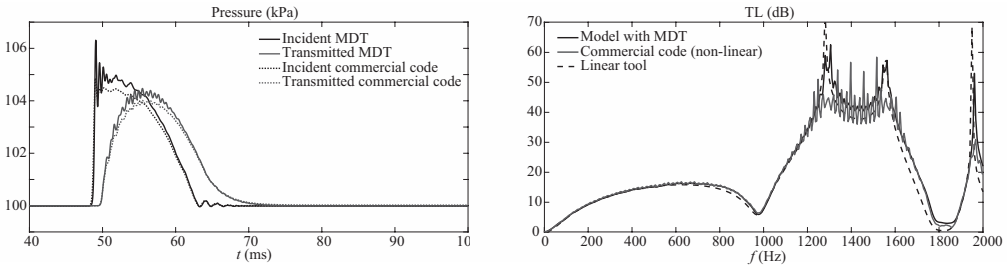

Figure 5.24: Incident and transmitted pressure pulses in the asymmetric reversal chamber and corresponding transmission loss with MDT and a commercial code.

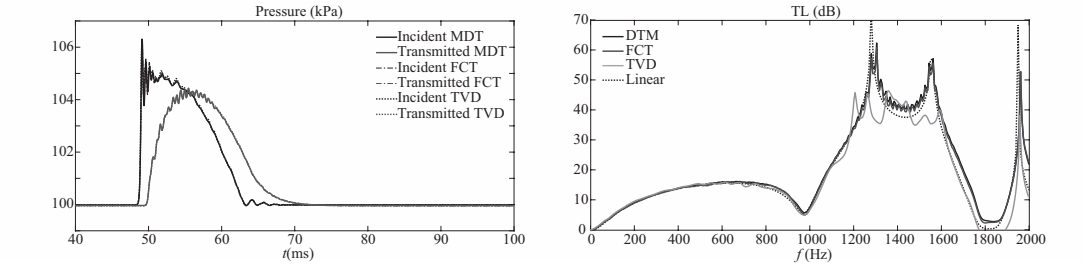

Figure 5.25: Incident and transmitted pressure pulses in the asymmetric reversal chamber and corresponding transmission loss with the different flux limiters.

Finally, the results obtained using the three different flux limiters are shown in Figure 5.25, where the same conclusions as for the rest of the cases are obtained, remarking the bad prediction of the transmission loss in the frequency domain for the TVD case from 1200 Hz.

5.6 General shape muffler

In the previous sections, the quasi-3D method developed in this work has been tested and validated using simple geometries as starting point, mixing different distributions of inlet and outlet ducts or extended ducts to increase the range of the validation. However, the validation would not be complete without considering a more general case, closer to the shape of a real muffler. In order to perform this test, the geometry represented in Figure 5.26 has been considered. This geometry offers a more general shape that will also put to a test the meshing techniques developed, and an internal baffle close to the middle of the muffler with an orifice in its centre of 40×40 mm.

As in the previous geometries, a long duct was connected to the inlet and another one to the outlet of the muffler to avoid reflections. Both ducts have a section of 20×20 mm and in the extreme of the inlet duct a pulse is generated. The pulse, as for the other cases, will travel through the ducts and through the muffler so that the waves in the inlet and outlet duct will be measured, close to the device.

In Figure 5.27 the results obtained using the momentum diffusion term for the quasi-3D model developed are compared with the results offered by a commercial non-linear program, as it was performed for the reversal chamber

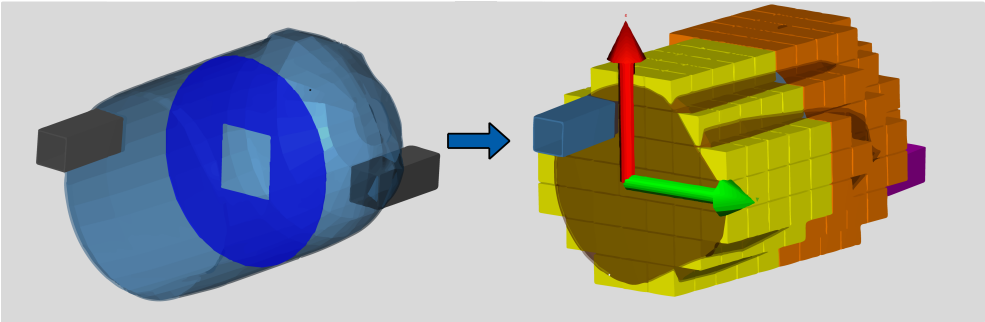

Figure 5.26: General shape muffler geometry and mesh considered in this section.

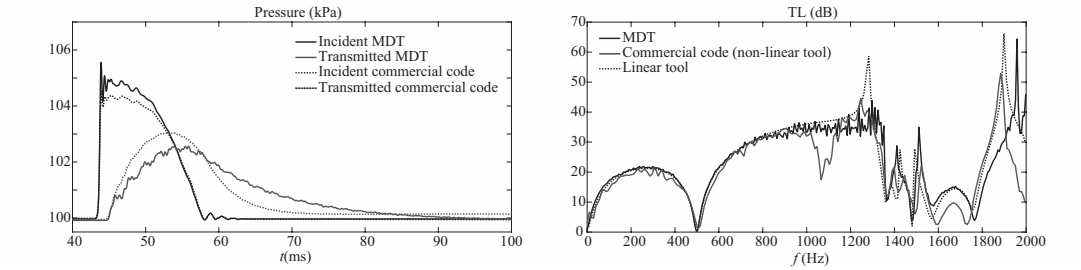

Figure 5.27: Incident and transmitted pressure pulses in the general shape muffler and corresponding transmission loss with MDT and a commercial code.

cases. This external tool is needed in order to evaluate the capabilities of the quasi-3D model, since by only using the linear acoustics tool as a comparison, it will not be possible to determine the better solution if differences are detected.

As opposed to the reversal chamber simulations, the time domain results obtained by the two non-linear codes for the muffler are unmistakably different. At first glance, the commercial code results seems to be incorrect ones, since the shape of the transmitted wave is too smooth and the initial pressure is not recovered after the wave has passed. This suspicions are proved true once the transmission loss is calculated. The curve obtained for the transmission loss using the commercial code waves were only able to correctly predict the first dome, until about 500 Hz. After this frequency, at around 600 Hz the curve became a flat line at 30 dBs, which is clearly a erroneous prediction of the transmission loss. Given these results, another tool offered by the commercial code was used to obtained a non-linear transmission loss curve.

Since apparently the commercial code is not able to properly simulate the travelling pulse for this geometry, a different approach was used, where white noise is generated by a speaker at the inlet and the pressure at the inlet and outlet of the device is compared to obtain the transmission loss. These are the results that have been finally shown for the commercial tool in the frequency domain.

Being able now to compare the three transmission loss curves it is possible to see that the quasi-3D model with the MDT flux limiter offers similar results as the linear acoustics tool, except the peak at 1300 Hz and small frequency shift at around 1900 Hz. The commercial code show a good agreement too, with some issues at 1100 Hz and a lower dome at 1700 Hz.

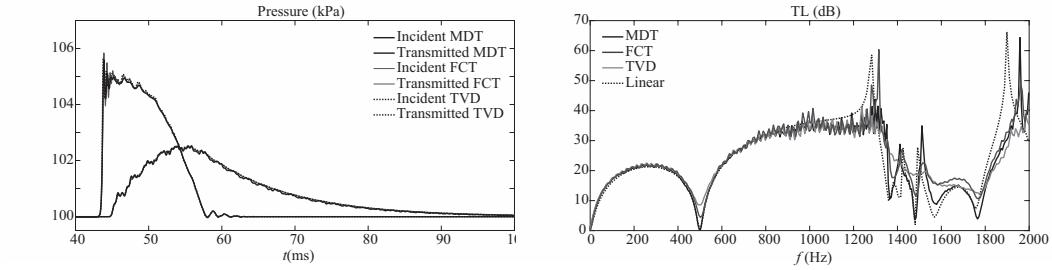

Figure 5.28: Incident and transmitted pressure pulses in the general shape muffler and corresponding transmission loss with the different flux limiters.

Finally, in Figure 5.28 the results obtained with all the flux limiters available for the quasi-3D model are shown. The tendencies identified for the previous cases are also present in this device. In the time domain, the correct solution is predicted with all the flux limiters with small differences, namely a slightly higher amplitude in the oscillations for the FCT method, and slightly lower for the TVD method, when compared with the MDT solution. In the frequency domain, all the predicted transmission loss are similar in shape until about 1300 Hz, after this point the MDT method seems to better reproduce the acoustic behaviour of the device according to the linear acoustics tool. Both the FCT and the TVD flux limiters present a more dissipative solution, specially in the case of the TVD method.

5.7 Summary and conclusions

In this chapter the main validation process of the non-linear quasi-3D method developed in this work was performed. With that purpose, it was decided that

a set of different mufflers would be modelled and an impulsive test rig would be simulated.

The first step was to develop a meshing technique where a given geometry could be meshed with the volumes and connectors needed. The so called *G matrix*, with the information of which couple of volumes are attached by each connector, and the *Cn matrix*, indicating the orientation of the connectors, are created from the mesh so they can be used for the calculations. Different techniques have been developed, from extending a section of the geometry to exporting the data of the mesh from other source for more complex geometries. After that, the linear acoustics tool that would be used as a reference solution during the validation process was extensively detailed.

The first device modelled was a simple parallelepiped shape muffler. An impulsive test rig was simulated, where a pulse was generated upstream of the device and the incident and transmitted wave, one in each side of the device, were computed. Although the time domain results are comparable between flux limiters, after calculating the transmission loss it was detected that the results provided by the TVD method where significantly worse than the ones using the MDT and FCT flux limiters. The reason for this departure seems to be the complete suppression of the oscillations in the time domain solution, *i.e.* the TVD method is too dissipative. This rather strange behaviour of the TVD method was further examined in more detail, concluding that a modification of the parameter ξ was needed. The value recommended for that parameter in the one-dimensional case is $1/2$, but it was to be lowered for the quasi-3D method in order to obtain a satisfactory solution. The following device modelled was a similar parallelepiped muffler, but with a different distribution of inlet and outlet ducts, which where also extended inside the device. After adjusting the parameters, the results obtained with the different flux limiters were similar in the time and frequency domains, with a more dissipative transmission loss for the FCT method, and even slightly more for the TVD method. When compared to the linear acoustics solution, only small differences appear when incrementing the frequency, presumably due to the absence of any dissipation in the linear model.

The next set of systems consist in a reversal chamber with different distribution of inlet and outlet ducts. It is worth mentioning that some of the volumes of the mesh have a different size, testing hence this feature with this geometry. Symmetric, skew-symmetric and asymmetric distribution were tested, significantly varying the shape of the transmission loss for each case, but obtaining a good match between linear and non-linear models each time.

For these cases, a commercial program also able to model three-dimensional geometries with a non-linear approach was used in order to further validate the new quasi-3D method. The conclusion is that in the time domain there are some differences in the amplitude of the pulses since the dissipation cannot be tuned down that much in the commercial program, but in the frequency domain the agreement is satisfactory. When comparing the solution provided by the different flux limiters, a similar conclusion as with the previous device can be reached: the MDT offers the best solution, the TVD is the most dissipative and the FCT is in between.

Finally, a general shape muffler was modelled which also included a baffle with an orifice in the middle. After simulating the impulsive test rig with the quasi-3D method and the commercial code, it could be seen that the latter was not able to properly predict the transmitted wave, and therefore, the transmission loss. If another tool of the commercial code that calculated the transmission loss from a white nose signal was used, better results were obtained. Regardless, the quasi-3D method offered a more reliable solution with only a shift in the curve at really high frequencies when compared to the linear solution. Following the tendencies detected in the previous cases and as a conclusion, although the three tested flux limiters prove to be proficient in removing the non-physical oscillations present in the quasi-3D numerical scheme, the momentum diffusion term approach has consistently arose as the better choice when analysing the acoustic behaviour. The flux corrected transport and the total variation diminishing ended offering a more dissipative solution, specially for the latter method, as could be observed in the frequency domain at higher frequencies. But in any case, the objective of validating the acoustics capabilities of the quasi-3D method with three-dimensional systems has been fully accomplished.

Chapter 5 Bibliography

[13] S. M. Sapsford, V. C. Richards, D. R. Amlee, T. Morel, and M. T. Chappell. *Exhaust system evaluation and design by non-linear modeling.* SAE Technical Paper 920686. 1992 (cit. on pp. 4, 59, 72, 122).

[103] A. Torregrosa, A. Broatch, A. Gil, and D. Moreno. "Analysis of acoustic networks including cavities by means of a linear finite volume method." *Journal of Sound and Vibration* 331(20) (2012), pp. 4575–4586 (cit. on pp. 70, 120, 122, 129).

[114] T. Morel, J. Morel, and D. A. Blaser. *Fluid dynamic and acoustic modeling of concentric-tube resonators/silencers*. SAE Technical Paper 910072. 1991 (cit. on p. 121).

[115] M. L. Munjal. *Acoustics of ducts and mufflers with application to exhaust and ventilation system design*. John Wiley & Sons, 1987 (cit. on pp. 121, 122).

[116] S. Amphlett, P. C. Niven, F. Payri, and A. J. Torregrosa. *Linear acoustic modelling using 1-D flow systems which represent complex 3-D components*. SAE Technical Paper 2011-01-1524. 2011 (cit. on p. 122).

[117] R. Glav and M. Åbom. *A general formalism for analyzing acoustic 2-port networks*. 1997 (cit. on p. 125).

[118] J. Galindo, J. Serrano, F. Arnau, and P. Piqueras. "High-frequency response of a calculation methodology for gas dynamics based on Independent Time Discretisation." *Mathematical and Computer Modelling* 50(5) (2009), pp. 812–822 (cit. on p. 125).

[119] F. Payri, J. Desantes, and A. Broatch. "Modified impulse method for the measurement of the frequency response of acoustic filters to weakly nonlinear transient excitations." *The Journal of the Acoustical Society of America* 107(2) (2000), pp. 731–738 (cit. on pp. 126, 128, 131, 150).

[120] D. Fauconnier and E. Dick. "Spectral analysis of nonlinear finite difference discretizations." *Journal of Computational and Applied Mathematics* 246 (2013), pp. 113–121 (cit. on p. 128).

Chapter 6

Application to duct junctions

Contents

6.1 Introduction **148**
6.2 Statement of the validation method **149**
6.3 Experimental procedure **151**
6.4 1D method with pressure loss-based junction model **153**
6.5 Results and discussion **154**
6.5.1 Experimental results 154
6.5.2 Assessment of modelling approaches considering a 0D description of the junction 159
6.5.3 Assessment of a modelling approach with a quasi-3D description of the junction 168
6.6 Summary and conclusions **174**
Chapter 6 bibliography **176**

6.1 Introduction

The importance of a correct modelling of junctions was already remarked in chapter 2.5, where the different approaches followed in the literature are reviewed and discussed. The application of the quasi-3D method to junctions comes naturally due to the 3D behaviour of the problem and the apparently simple mesh needed. When considering using a one dimensional scheme, some additional model needs to be used trying to account for the three dimensional effects that may appear. The simplest approach consists of the use of a constant pressure model, as described in [83], where the pressure at the end of all branches of the junction is assumed to be the same at any time. A more complex approach is described in [84], where the pressure differences existing between the different branches are incorporated in a quasi-steady manner with steady pressure loss coefficients and energy change coefficients.

A more direct approach would be the use of a three dimensional tool, which would be able to take into account all the 3D effects present in the junctions. However, that would imply a much more detailed meshing for every component, or at least every junction, and given the nature of the problems where simulation is useful, having to redo the mesh for every iteration of the design might be unattainable. Even if only the junctions are modelled with a 3D tool and the rest of the engine uses a 1D approach, the meshing process and the computational time needed may be just too high.

It is in these type of problems, where a 1D approach is too simple and a 3D approach is too expensive, where the compromise solution provided by a quasi-3D approach can become optimal. Making changes in the mesh becomes a trivial process where only a couple of parameters need to be adjusted, like the angle between the pipes or where they connect. On the other hand, the calculation time needed does not dramatically increase when compared to 1D codes and a connection to one of such codes is usually easier than a 3D to 1D connection since they often share a more similar numerical method. When a quasi-3D method on a staggered grid is applied to a junction, typically only one volume is used to represent the junction, taking also into account the effective areas and characteristic lengths for each connection with the adjacent ducts. This connections contain the vector information, including the orientation of the duct with respect to the junction, what makes it possible taking into account the effects of the junction on the flow when solving the momentum equation, without the need of adding pressure loss coefficients. This represents an advantage when modelling junctions, since some three dimensional effects can be taken into account without the need of specific measurements.

Additionally, a better acoustic representation of the problem can be expected.

This chapter has precisely as objective to establish the potential of these ideas as a way to improve the description of the effect of simple duct junctions on an otherwise one-dimensional flow system, as the intake or exhaust of an internal combustion engine. Specific experiments have been performed in order to obtain precise and reliable results on the propagation of pressure pulses across junctions. The results obtained have been compared to simulations performed with different versions of a staggered mesh finite volume method and different meshes and, as a reference, also with the results of a more conventional pressure loss-based model.

6.2 Statement of the validation method

Two junctions, shown schematically in Figure 6.1, were manufactured. A T-junction and a Y-junction were considered, in order to allow the analysis of the effect of the angle of the side branch. An internal diameter of 51 mm was used in all the branches of the junctions.

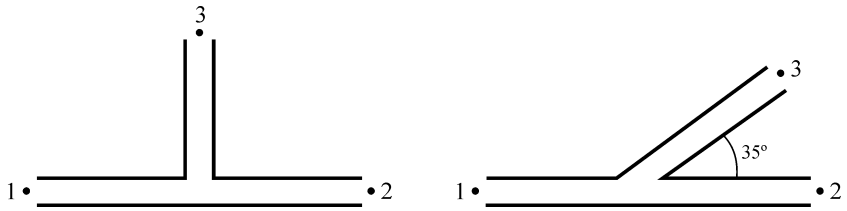

Figure 6.1: Junctions considered in the study.

While several formalisms may be used for the representation of the transient response of a system, the most intuitive one for the present case of a junction is that based on the consideration of wave components, so that the junction is actually regarded as a multi-port. In this framework, for a junction such as that represented in Figure 6.1, one has three excitations and three responses, and writing the relations between them directly in matrix form in the frequency domain, one has:

$$\begin{bmatrix} B_1 \\ B_2 \\ B_3 \end{bmatrix} = \begin{bmatrix} R_1 & T_{21} & T_{31} \\ T_{12} & R_2 & T_{32} \\ T_{13} & T_{23} & R_3 \end{bmatrix} \begin{bmatrix} A_1 \\ A_2 \\ A_3 \end{bmatrix} \tag{6.1}$$

where, as indicated in Figure 6.2, A_i represents the wave component moving towards the junction in port i and B_j represents the wave component moving away from the junction in port j. Regarding the matrix elements, R_i denotes the reflection coefficient as seen from port i whereas T_{ij} denotes the transmission coefficient between ports i and j. All these magnitudes are functions of the frequency f.

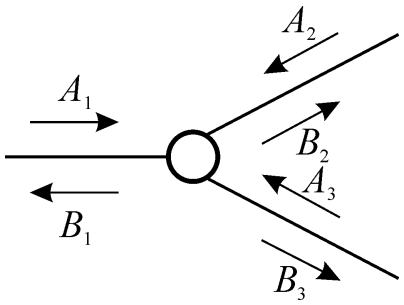

Figure 6.2: Wave components acting on a multi-port.

In this way, one has a reflection coefficient for each of the pipes arriving at the junction, and transmission coefficients for all the possible transmission paths, indicated by the corresponding subscripts. The experimental setup and the corresponding measurement procedure are described in detail in [119, 121], and here a brief overview is given in section 6.3.

Two different modelling approaches were evaluated: a staggered mesh finite volume method and, as a reference, a more conventional pressure loss-based model. The staggered mesh finite volume method used is described in detail in chapter 3, along with the different flux limiters developed to suppress the spurious oscillations of the numerical method.

The pressure loss-based model uses a conventional one-dimensional finite volume model with a collocated mesh, derived from the code available in [122]. The junction is modelled as a small volume with three connections to which different pressure loss coefficients are assigned, and in which the mass and energy conservation equations are solved. For the connection to the duct where the incident pressure pulse propagates it has been assumed that the total pressure loss is zero, whereas for the other two connections their corresponding pressure loss coefficients are computed following the expressions given in [89, 90].

6.3 Experimental procedure

Making reference to the notation in Figure 6.2, the determination of the transmission and reflection coefficients defined in Equation (6.1) requires the three following measurements:

- Excitation in duct 1, with anechoic terminations in ducts 2 and 3, so that $A_1 \neq 0$ and $A_2 = A_3 = 0$, and thus,

$$R_1 = B_1/A_1 \; ; \; T_{12} = B_2/A_1 \; ; \; T_{13} = B_3/A_1 \tag{6.2}$$

- Excitation in duct 2, with anechoic terminations in ducts 1 and 3, so that $A_2 \neq 0$ and $A_1 = A_3 = 0$; then,

$$R_2 = B_2/A_{21} \; ; \; T_{21} = B_1/A_2 \; ; \; T_{23} = B_3/A_2 \tag{6.3}$$

- Excitation in duct 3, with anechoic terminations in ducts 1 and 2, so that $A_3 \neq 0$ and $A_1 = A_2 = 0$, so that,

$$R_3 = B_3/A_1 \; ; \; T_{31} = B_1/A_3 \; ; \; T_{32} = B_2/A_3 \tag{6.4}$$

In order to perform the above-indicated tests, the modified version of the impulse method described in [11] was used, since pressure components, which all the previous developments are based upon, are directly obtained in the time domain with a simple procedure, and the consideration of three-port elements is straightforward. In Figure 6.3 both the experimental setup used and the relevant pressure waves recorded are illustrated.

The test performed was similar to the one explained in section 5.4, with an incident pulse generated by a high speed electrovalve and several transducers to measure the pulses in the desired position. However, in this case the junction introduces some differences in the layout, as it can be seen in figure 6.3. Since there are now two transmitted waves, one for each branch, one more transducer is needed. Besides, at the position indicated for transducer 1 in Figure 6.3, it is clear that this transducer records the addition of the incident and the reflected pulses, as illustrated in the figure. In order to surpass this difficulty, the solution adopted is the same as in chapter 5: the incident pulse on the junction at section 1 (whose Fourier transform will give the complex amplitude of the A_1 component) will be estimated from an additional test performed without any element, using the pressure recorded by transducer 0 only to

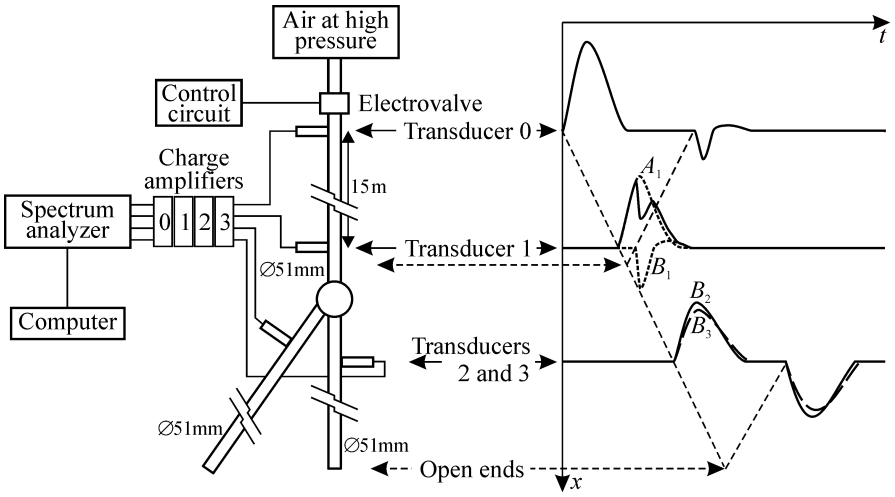

Figure 6.3: Experimental setup used.

check the comparability of the excitations used in both types of tests (with and without junction).

The incident pulse is generated by means of a high speed electrovalve that controls the discharge from a high-pressure tank. A proper choice of the opening time ensures that the spectrum associated with the incident pulse is essentially flat. The length of the ducts placed between the valve and transducer 0, transducer 0 and the junction, and the junction and the open ends is chosen so that no windowing is necessary in order to isolate the incident, the reflected, and the transmitted pulses, as indicated in Figure 6.3. Transducer 0 was located 15 m away from both the valve and the junction, and transducers 2 and 3 were placed 0.15 m downstream of the junction, and 15 m away from their corresponding open end.

At the position indicated for transducer 1 in Figure 6.3, it is clear that this transducer records the addition of the incident and the reflected pulses, as illustrated in the figure. In order to surpass this difficulty, the solution adopted is to estimate the pulse incident on the junction at section 1 (whose Fourier transform will give the complex amplitude of the A_1 component) from an additional test performed without any element, using the pressure recorded by transducer 0 only to check the comparability of the excitations used in both types of tests (with and without junction).

6.4 1D method with pressure loss-based junction model

In this case, a collocated one-dimensional finite volume method is used for all the calculations inside the pipes. The Euler equations of fluid dynamics simplified for one-dimensional flow in a straight uniform duct can be expressed as:

$$\frac{d\overline{\mathbf{W}}_\mathbf{i}}{dt} = \frac{d}{dt}\begin{pmatrix} \rho \\ \rho u \\ \rho e_0 \end{pmatrix}_i = \frac{A(\mathbf{F}_{i-1,i} - \mathbf{F}_{i,i+1})}{V_i} \tag{6.5}$$

Here, $\overline{\mathbf{W}}_\mathbf{i}$ is the cell-averaged state vector of cell i, $\mathbf{F}_{i-1,i}$ and $\mathbf{F}_{i,i+1}$ are the inter-cell fluxes between cells $i-1$ and i and between i and $i+1$, respectively, and the other symbols refer to the same magnitudes as in chapter 3, with u being now the axial velocity of the flow. The inter-cell fluxes are computed by an approximate solution of the Riemann problem as described by Toro et al. [61]. The state vector is extrapolated to the cell boundaries to compute the fluxes by means of a Monotonic Upstream-Centered Scheme for Conservation Laws (MUSCL) approach as described in [123], while the solution is propagated in time using Heun's method, leading to a second order in time and space, total variation diminishing scheme.

While the main one-dimensional flow inside the ducts is simulated, the effects of the geometry of the junction are modelled. The connections of the ducts to the junction are solved using an auxiliary small zero-dimensional element. Each of the one-dimensional branches is connected to that zero-dimensional element making use of the Riemann variables to compute the fluxes at their corresponding boundary. At each connection, it is assumed that a certain amount of stagnation pressure is lost, depending on the angle of the junction and of the ratio between the outflow mass flow $\dot{m}_{out}$ passing through the branch of interest and the inflow mass flow $\dot{m}_{in}$. The pressure loss coefficients are computed following the expressions given in [89] and [90], and are defined as the ratio of the difference in stagnation pressure between the outflow branch and the inflow branch to the dynamic pressure ($\rho u^2/2$) of the inflow branch. Finally, the total pressure loss coefficient K for a three-branch junction with the same section in all the branches can be estimated as:

$$K = \left(\frac{\dot{m}_{out}}{\dot{m}_{in}}\right)^2 - \frac{3}{2}\frac{\dot{m}_{out}}{\dot{m}_{in}} + \frac{1}{2} \tag{6.6}$$

when the branch is collinear with the inflow branch, and,

$$K = \left(\frac{\dot{m}_{out}}{\dot{m}_{in}}\right)^2 - 2\frac{\dot{m}_{out}}{\dot{m}_{in}}\cos\left(\frac{3}{4}\theta\right) + 1 \tag{6.7}$$

for the lateral branch, when the flow is split between a collinear and a lateral branch. In this case, θ is the angle between the lateral branch and the axial outflow branch, so that 0 degrees means that both outflow branches are parallel. The same expression applies when the inflow branch is not parallel to any of the outflow branches: in that case, the angle θ is measured between the inflow branch and the other outflow branch.

In the auxiliary zero-dimensional element, the gas is again considered as a perfect gas, and the mass and energy equations are solved:

$$\frac{dm}{dt} = \sum \dot{m} \tag{6.8}$$

$$\frac{d(mc_vT)}{dt} = \sum \dot{m}h_0 \tag{6.9}$$

where m is the mass trapped in the zero-dimensional element, $\dot{m}$ is the mass flow, positive when it enters the element, and h_0 is the specific stagnation enthalpy associated with the mass moving inside or outside of the element. These two equations set an additional limitation to the maximum possible time step.

6.5 Results and discussion

In this section, first the experimental results obtained will be analysed, both in the time and the frequency domains. Then, the performance of the different modelling approaches will be discussed, first in the case in which the junction itself is represented by a zero-dimensional element, and secondly in the case in which the staggered mesh method is used to provide a quasi-3D description of the junction.

6.5.1 Experimental results

The results for the T-junction in the time domain are shown in Figure 6.4. Ports are denoted as in Figure 6.1, and it is apparent that when the junction is excited at port 1 the pulse transmitted through port 2 (i.e., in the main propagation direction) has a higher amplitude than that transmitted through port 3 (the branched duct), as could be intuitively expected. It is also apparent, and equally expectable, that when the junction is excited at port 3, the

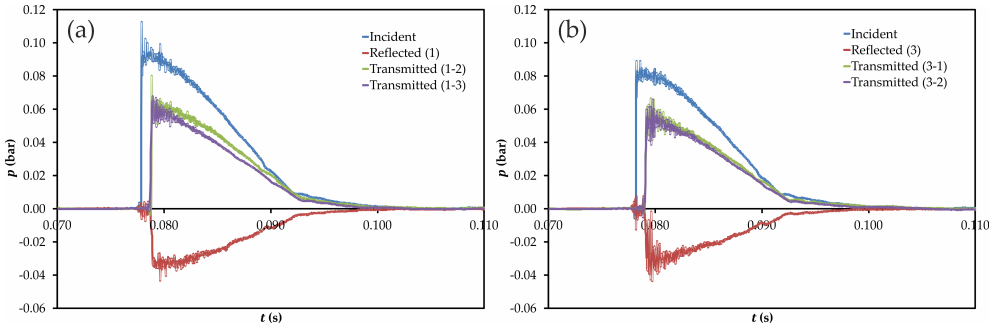

Figure 6.4: Experimental results for the T-junction in the time domain. (a) Excitation at port 1; (b) excitation at port 3. Ports are denoted as in Figure 6.1.

pulses transmitted through ports 1 and 2 are very similar, the small differences observed being attributable to manufacturing issues.

Differences in the reflected pulses recorded at ports 1 and 3 are also apparent, even if the incident pulses do not have the same amplitude. The reflected pulse recorded at port 3 is noisier, and its amplitude is comparable to that of the reflected pulse recorded at port 1, while the corresponding incident pulse has a lower amplitude. This indicates that reflection is more intense when the junction is excited at the branch duct, as it is also intuitively reasonable in terms of the interaction of the incident pulse with the wall of the main duct. Of course, none of these effects, regarding both transmission and reflection, can be accounted for by a constant pressure model, and this is the reason why such a model will not be considered in the subsequent discussion.

The results for the Y-junction are shown in Figure 6.5. Here the trends observed confirm those found for the T-junction regarding the difference between the main duct and the branch duct, but with additional issues related with the branch angle. Comparison of Figures 6.5a and 6.5b indicates that the difference in amplitude between the two pulses transmitted is more important when the branch direction is against that of the incident pulse (i.e., when the junction is excited at port 2), in which case the results are rather similar to those shown in Figure 6.4a for the T-junction. Regarding the reflected pulses recorded at ports 1 and 2, some differences may be observed mostly in the last part of the pulse, which suggests some difference in the dynamic behaviour of the junction.

These statements are supported by the results obtained with the excitation at port 3, shown in Figure 6.5c. Here, it appears that again the amplitude of the transmitted pulse is higher when there is no significant change in direction

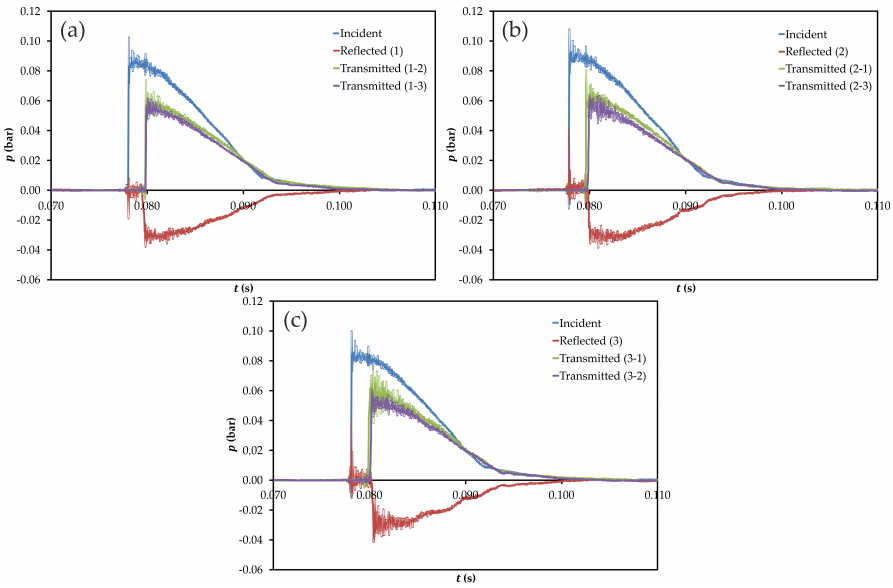

Figure 6.5: Experimental results for the Y-junction in the time domain. (a) Excitation at port 1; (b) excitation at port 2; (c) excitation at port 3. Ports are denoted as in Figure 6.1.

along the transmission path (in this case, from port 3 to port 1). However, the differences are not as apparent as those seen in Figure 6.54b, which is reasonable considering that here there is some change in direction in the two transmission paths. It is also worth noticing the clear differences observed between the reflected pulse recorded at port 3 and those recorded at the other two ports. A much more complex time evolution can be observed in the case of port 3, which again suggests that wave dynamics inside the junction depend significantly on the port at which the junction is excited.

In the frequency domain, the results obtained for the transmission and reflection coefficients defined in Equation (6.1) are analysed. For brevity, only the modulus of these coefficients will be considered, as this contains significant information about the overall energetic behaviour of the junction. The results for the T-junction are shown in Figure 6.6, where it can be observed that the values obtained in the very low frequency range (below 200 Hz) are fully consistent with the time domain results shown above in Figure 6.4: when exciting the junction at port 1, it is seen that $|T_{12}|$ is systematically larger than $|T_{13}|$ in this frequency range, whereas when the excitation is at port 3 the differences between $|T_{31}|$ and $|T_{32}|$ are significantly smaller.

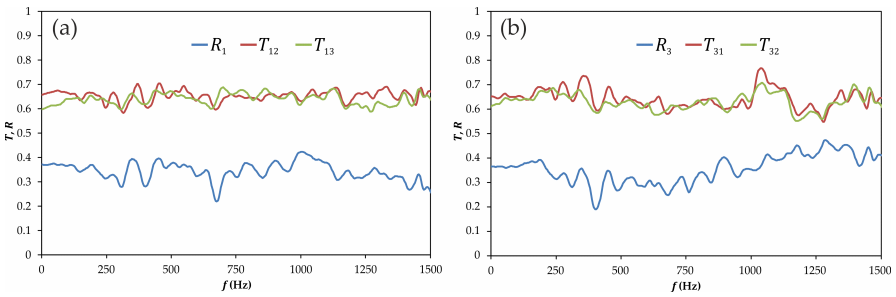

Figure 6.6: Experimental results for the T-junction in the frequency domain. (a) Excitation at port 1; (b) excitation at port 3. Ports are denoted as in Figure 6.1.

At higher frequencies, above 200 Hz, it can be seen that the behaviour of $|T_{12}|$ and $|T_{13}|$ is essentially flat around mean values of 0.65 and 0.64, respectively, with a maximum deviation from the mean of 0.065 in $|T_{12}|$ and of 0.05 in $|T_{13}|$. On the contrary, in the case of $|T_{31}|$ and $|T_{32}|$ their mean values are very similar to those of $|T_{12}|$ and $|T_{13}|$ (0.64 and 0.63, respectively) but some relevant acoustic features can be detected in both coefficients between 1000 and 1250 Hz, mostly in the case of $|T_{31}|$ where the deviation from the mean value reaches a maximum of 0.125, while $|T_{32}|$ follows the same trend but with a maximum deviation from the mean of 0.08 . This confirms, on one hand, that when the junction is excited at port 3 the two propagation paths are substantially equivalent and, on the other hand, that their behaviour is different from that obtained when exciting the junction at port 1.

This second statement is fully supported by the spectra of the reflection coefficients $|R_1|$ and $|R_3|$: it is apparent that $|R_3|$ is overall larger than $|R_1|$ for frequencies below 200 Hz, as suggested by the results shown in Figure 6.5, but now without any uncertainty due to the difference in amplitude between the incident pulses used in each test. Additionally, the trend observed is rather different for frequencies above 200 Hz, and most notably above 1000 Hz, where $|R_1|$ shows a certain decreasing tendency whereas $|R_2|$ increases with frequency.

The corresponding results for the Y-junction are shown in Figure 6.7. Again, results below 200 Hz confirm the time domain tendencies observed in Figure 6.5. In this frequency range, it is seen that while $|T_{12}|$ is only slightly higher than $|T_{13}|$, when exciting at ports 2 or 3 one finds that the transmission coefficient corresponding to a smaller change in direction (that is, $|T_{21}|$ when exciting at port 1 and $|T_{31}|$ when exciting at port 3) is significantly larger than the other one, and that this effect is more noticeable the larger is the change

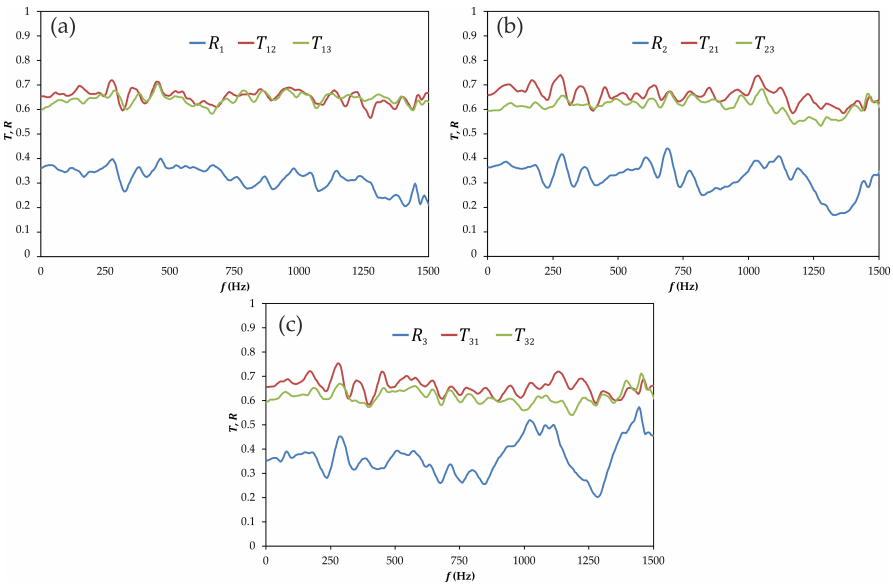

Figure 6.7: Experimental results for the Y-junction in the frequency domain. (a) Excitation at port 1; (b) excitation at port 2; (c) excitation at port 3.

in direction.

When considering frequencies above 200 Hz, noticeable differences are also observed between the case with excitation at port 1, for which results very similar to those shown in Figure 6.6a are obtained, with small differences between $|T_{12}|$ and $|T_{13}|$ and an almost flat behaviour with little dependency on frequency, and the other two cases, in which the transmission coefficients corresponding to the propagation path with the smallest change in direction ($|T_{21}|$ and $|T_{31}|$) are significantly and systematically higher than those implying an important change ($|T_{23}|$ and $|T_{32}|$, respectively) except at the highest frequencies represented.

However, it is in the reflection coefficients where the effect of the change in the excitation port is more apparent. In fact, the results for R_1 do not differ substantially from those obtained for the T-junction and shown in Figure 6.6a, neither in the low frequency values nor in the high frequency trend. On the contrary, the high frequency behaviour seen in R_2 and R_3 is a clear indication of the change produced in the dynamic characteristics of the junction when the excitation port is changed, an effect that could be guessed from the time domain results of Figure 6.5 but now is fully confirmed. Actually, a well-defined trend of picks and troughs can be observed in both cases, with similar

shape but a clear frequency shift, which provides a sort of acoustic signature of the dynamic behaviour of the junction. The fact that such a behaviour is not apparent in the spectrum of R_3 for the T-junction shown in Figure 6.6b indicates that such dynamic issues are suppressed by the symmetric nature of the excitation through a perpendicular branch.

6.5.2 Assessment of modelling approaches considering a 0D description of the junction

In this section, modelling approaches in which the junction itself is regarded as a 0-dimensional element, while the flow in the adjacent ducts is assumed to be one-dimensional, will be evaluated. In the context of the staggered mesh finite volume method, this corresponds to the case in which the junction is regarded as a single volume and the adjacent ducts are meshed only in the axial direction. The pressure loss-based model used here falls also within this category since the junction branches are connected through an auxiliary 0D element.

Once again, separate analyses for the time and the frequency domains are presented.

Starting with the time domain, in Figure 6.8, direct comparison between the experiments and the method with the momentum diffusion term (MDT) as flux limiter is given for the case of the T-junction. The figures at the top provide a direct representation of the results obtained, whereas in the figures at the bottom the differences between the experimental and numerical results are represented (these are labelled as ΔR and ΔT for reflected and transmitted pulses, respectively). In general, the model reproduces the experimental results within reasonable limits, but with a superimposed oscillation due to the development of the pulse from station 0 to station 1 (refer to Figure 6.3) and which is a consequence of the way in which the inlet boundary condition has been set. The scale of the vertical axis in the differences plots has thus been chosen so as to allow proper comparison for the times not affected by those oscillations.

From the differences plots, it is apparent that the numerical results tend to underestimate the actual measured values in the trailing part of the pulses, for $t > 0.85$ s, the differences being larger in general for the case of the reflected pulse. The situation is rather more complex for the previous instants, with different trends observed for the transmitted and reflected pulses, and with a noticeable influence of the port at which the junction is excited.

The results obtained for the rest of the modelling approaches considered

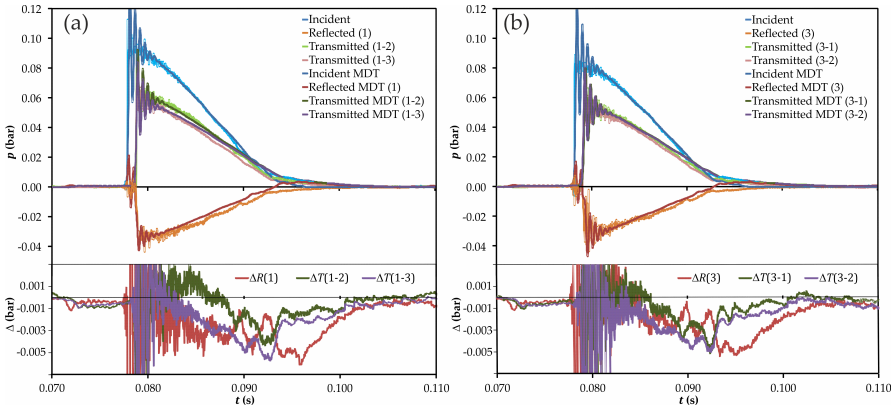

Figure 6.8: Experimental vs. modeled results for the T-junction: raw data (top) and differences (bottom) in the time domain, momentum diffusion term (MDT) method. (a) excitation at port 1; (b) excitation at port 3.

are compared in Figure 6.9, where for clarity the experimental results are not shown in the top figures, but the bottom figures have been expanded to allow proper analysis of the behaviour observed in each of the propagation paths. It is apparent that the conventional pressure loss method (labelled 1D in the figure) is much less dispersive than any of the staggered-grid methods, and thus better suited for this particular calculation setting. This is particularly true in the case of the reflected pulses, where the conventional method approaches the measured values considerably earlier. It is also apparent that while no significant differences can be found between the MDT and the FCT methods in the reflection seen from port 1, this is not the case when the junction is excited at port 3: the FCT method exhibits larger differences, except in the last part of the reflected pulse.

Regarding the different transmission paths, it can be observed that, while relatively small differences between all the methods are seen in the case of transmission from port 1 to port 2 (the performance of the conventional method being slightly better), significant differences appear at intermediate times in all the cases in which port 3 is involved. There is a clear trend in the results obtained in these cases, in the sense that the conventional method produces the lowest values, the FCT method the highest values, and those produced by the MDT method lie in between. However, the maximum differences are observed at time instants in which the amplitude of the transmitted pulses is relatively high.

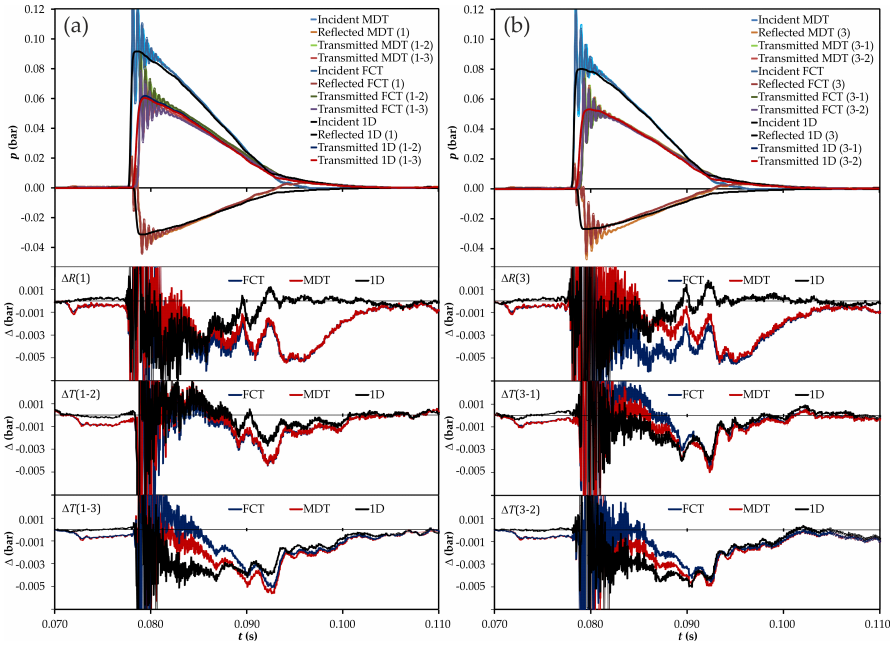

Figure 6.9: Comparison between the different models for the T-junction: raw data (top) and differences (bottom plots) in the time domain. (a) excitation at port 1; (b) excitation at port 3.

As an additional criterion for the comparison of the performance of the different modelling approaches, the mean quadratic error corresponding to the differences shown in Figure 6.9 was computed. A time window with $0.82 < t < 0.95$ was chosen to avoid the large oscillations and to focus on those times for which the differences between the methods are more apparent.

The values obtained for the mean quadratic errors are summarized in Table 6.1, where it is confirmed that the best values for the reflection coefficients are those provided by the conventional method, while the FCT method gives the best approach to the transmission coefficients.

Table 6.1: Values of the mean quadratic error: T-junction.

Path	**MDT**	**FCT**	**1D**
R_1	1.514×10^{-4}	1.842×10^{-4}	1.448×10^{-4}
R_3	1.102×10^{-4}	2.046×10^{-4}	1.019×10^{-4}
T_{12}	1.005×10^{-4}	9.932×10^{-5}	6.926×10^{-5}
T_{13}	1.609×10^{-4}	1.298×10^{-4}	1.774×10^{-4}
T_{31}	1.121×10^{-4}	1.094×10^{-4}	1.114×10^{-4}
T_{32}	1.554×10^{-4}	1.245×10^{-4}	1.833×10^{-4}

Similar comments can be made about the comparison shown in Figure 6.10 for the case of the Y-junction. Again, the conventional method reproduces better the behaviour of the reflected pulses, regardless of the excitation port, and the MDT and the FCT methods exhibit significant differences only when the junction is excited at port 3, following the same trend as for the T-junction.

The trend is also very similar for the different transmission paths. Transmission between ports 1 and 2 is acceptably reproduced by all the modelling approaches, regardless of the exciting port, again with a slightly better performance of the conventional model. In those cases in which port 3 is included in the transmission path, the tendency observed is again the same when the junction is excited at ports 1 or 2, with a small difference with respect to the T-junction when the excitation comes from port 3: in this case, the lowest values are those provided by the MDT method, most notably in the transmission from port 3 to port 2.

Again, the mean quadratic errors were calculated, and the corresponding results shown in Table 6.2 confirm the previous comments.

From these results, it is apparent that the conventional pressure loss model, while is not able to account for all the differences observed between the two transmission paths studied in each test, could still provide a sufficient approx-

Table 6.2: Values of the mean quadratic error: Y-junction.

Path	**MDT**	**FCT**	**1D**
R_1	1.575×10^{-4}	1.915×10^{-4}	1.273×10^{-4}
R_2	1.992×10^{-4}	2.172×10^{-4}	1.681×10^{-4}
R_3	1.648×10^{-4}	1.369×10^{-4}	9.186×10^{-5}
T_{13}	1.514×10^{-4}	1.322×10^{-4}	1.742×10^{-4}
T_{21}	1.992×10^{-4}	2.172×10^{-4}	1.681×10^{-4}
T_{23}	1.336×10^{-4}	1.296×10^{-4}	1.141×10^{-4}
T_{31}	1.669×10^{-4}	1.949×10^{-4}	1.355×10^{-4}
T_{32}	2.117×10^{-4}	1.516×10^{-4}	1.751×10^{-4}

imation to the real situation if the focus of the problem is on the reflection properties of the junction and only time domain issues are relevant for the problem under study (for instance, the eventual influence of a reflection at an intake junction on the volumetric efficiency on the engine). The staggered mesh finite volume method appears to be more sensitive to the relative directions of the different branches, mostly when the excitation comes from the side branch (port 3), as should be expected since the momentum equation is actually solved, albeit in an approximate way, at the junction, whereas in the conventional model such effects are included only through their influence on the pressure loss coefficients.

As already detected when describing the experimental results, it is in the frequency domain where the benefits of the staggered mesh finite volume method are more apparent. Consider first the results corresponding to the T-junction, shown in Figure 6.11 in the case of the reflection coefficients. Here, using either MDT or FCT as flux limiter, the staggered mesh finite volume method produces results for the reflection coefficients which overestimate dynamic effects when the excitation is at port 1, but produces a suitable approximation up to 1000 Hz when the excitation is at port 3 and the FCT flux limiter is used. In comparison with this, it is apparent that the conventional pressure loss model (again labelled as 1D in the figure) is unable to fully capture the dynamic features of the results, while still providing a sort of suitable average value, even if all the dynamic issues are lost, as an unavoidable consequence of the quasi-steady assumption underlying the calculation.

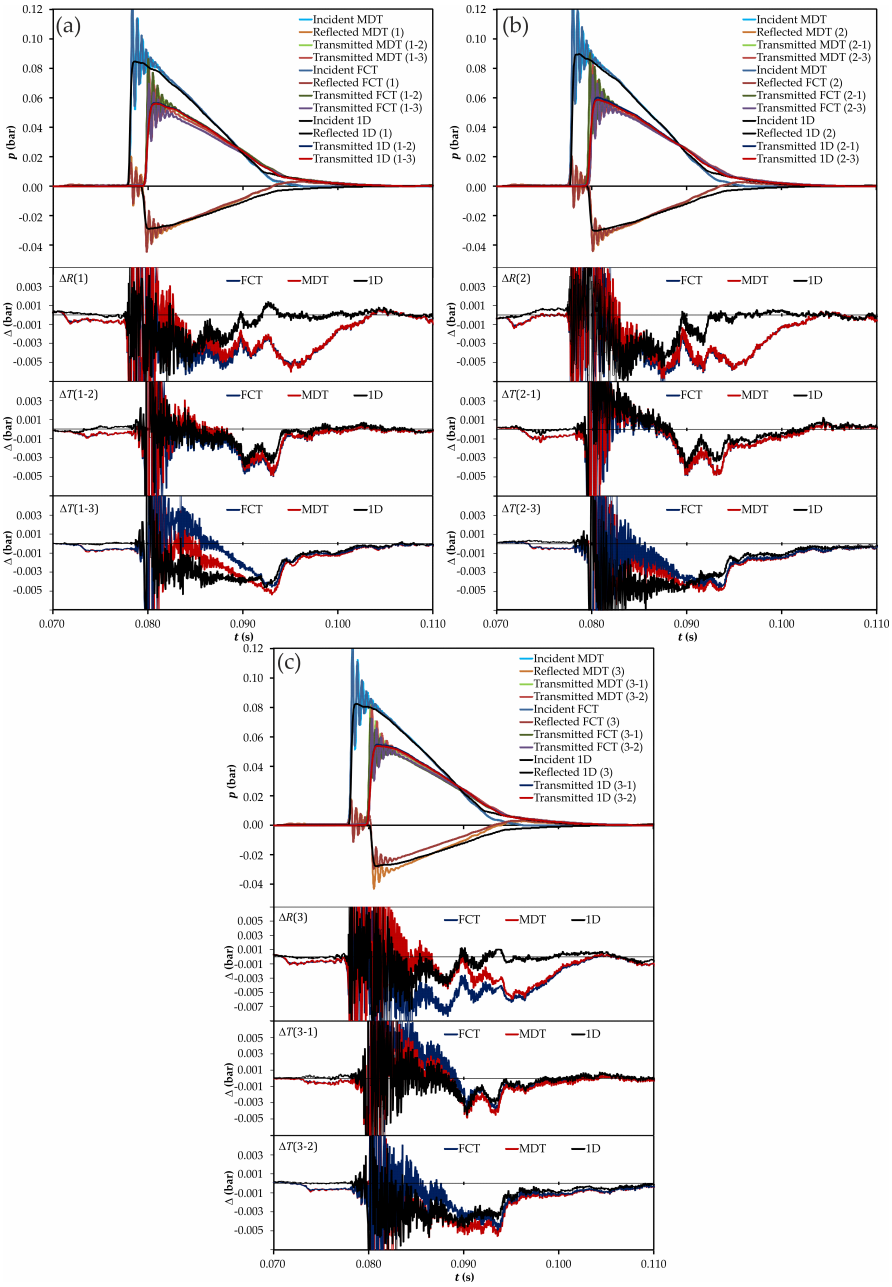

Figure 6.10: Comparison between the different models considered for the Y-junction (time domain): (a) excitation at port 1; (b) excitation at port 2; (c) excitation at port 3.

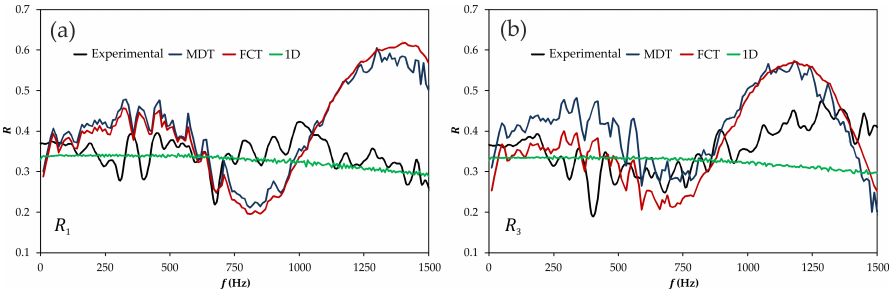

Figure 6.11: Comparison between the experimental results and the different models for the reflection coefficients of the T-junction (frequency domain): (a) excitation at port 1; (b) excitation at port 3.

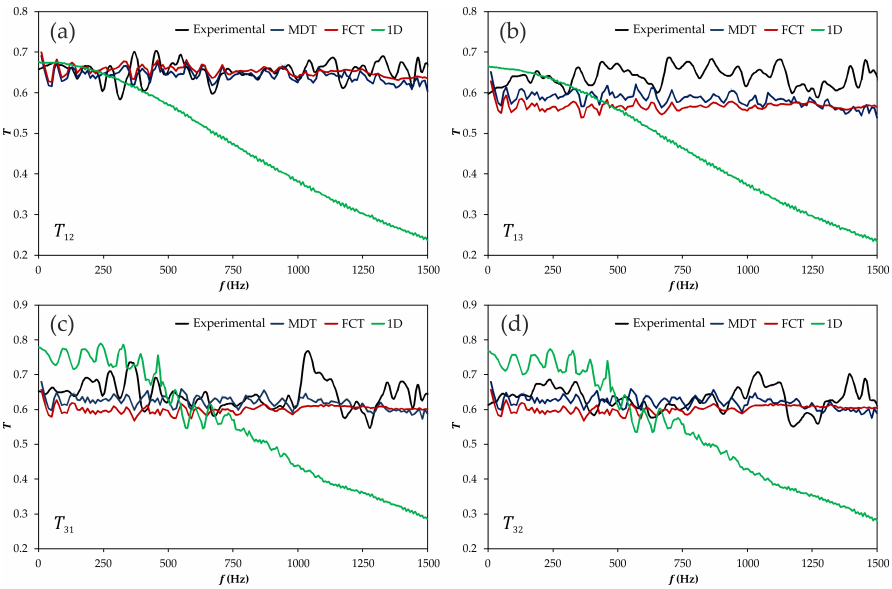

Figure 6.12: Comparison between the experimental results and the different models for the transmission coefficients of the T-junction (frequency domain): (a) excitation at port 1, transmission through port 2; (b) excitation at port 1, transmission through port 3; (c) excitation at port 3, transmission through port 1; (d) excitation at port 3, transmission through port 2.

The corresponding transmission coefficients are shown in Figure 6.12, where it can be observed that the staggered mesh finite volume method produces results that follow the overall trend of the experimental results, with two exceptions: when the excitation is at port 1 the method underestimates the

transmission to port 3, and when the excitation is at port 3 the method is unable to capture the behaviour observed between 1000 and 1250 Hz. In the case of the conventional model, it is apparent that in this case it is fully unable to reproduce neither the level nor the dynamic features of the measured data, the only acceptable results being produced when the excitation is at port 1 and that only for very low frequencies.

This essential difference between the two modelling approaches considered is even more apparent in the case of the Y-junction, whose results are shown in Figures 6.13 and 6.14 for the reflection and transmission coefficients, respectively. In this case, the results provided by the conventional model are rather similar regardless of the port at which the junction is excited. In all the cases, an acceptable value of the transmission coefficient in the very low frequencies is produced in those propagation paths with smaller change in direction, and also a suitable average value for the reflection coefficient as seen from any of the exciting ports. However, differences in transmission between the two propagation paths are not reproduced in any case and, moreover, the results start to decrease monotonically at about 200 Hz and reach totally unrealistic values for frequencies above 750 Hz in all the cases.

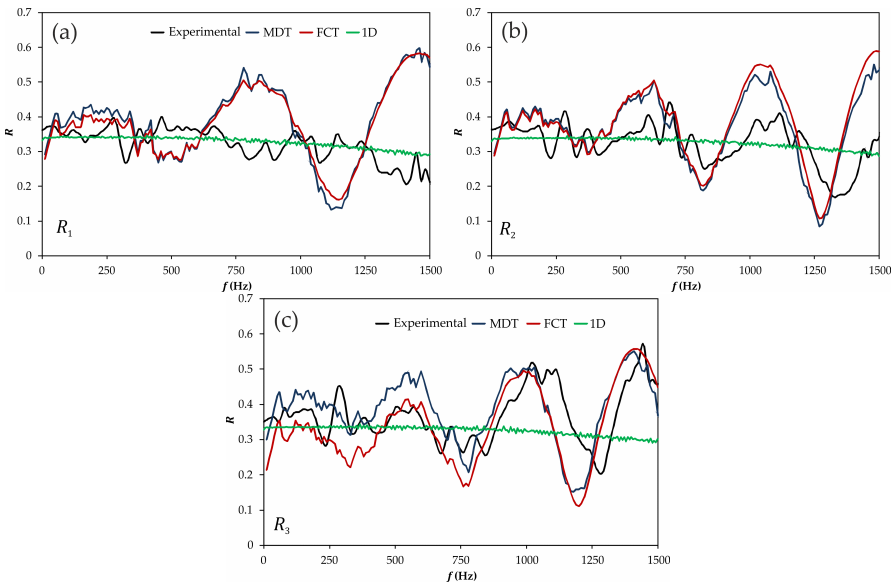

Figure 6.13: Comparison between the experimental results and the different models for the reflection coefficients of the Y-junction (frequency domain): (a) excitation at port 1; (b) excitation at port 2; (c) excitation at port 3.

On the contrary, the staggered mesh finite volume method reproduces quite fairly the overall dependency with frequency, but tends to overestimate the influence of the change in direction of the propagation path on the transmission coefficients (and thus to underestimate the value of the corresponding coefficient). With this geometry, this effect is especially evident in the results obtained with the FCT flux limiter for $|T_{13}|$, $|T_{23}|$, $|T_{31}|$ and $|T_{32}|$, i.e. all the cases in which the side branch (port 3) is involved. On the contrary, the results of the FCT method are affected by a certain overestimation when transmission through the main branch is considered ($|T_{12}|$ and $|T_{21}|$). Accordingly, with the description given in chapter 3, this difference in behaviour between the FCT and the MDT methods can only be due to the effect of the application to the junction itself of the different ways used to handle the information of the neighbouring volumes when limiting the flow.

In the case of the reflection coefficients, the overestimation of the junction dynamics already observed in the T-junction is also present here when the junction is excited at port 1, but the measured dynamics are quite successfully reproduced when the junction is excited at ports 2 and 3. The characteristic frequencies governing the reflection coefficient are not exactly captured, but the overall amplitude and the influence of the exciting port are reproduced by the numerical results.

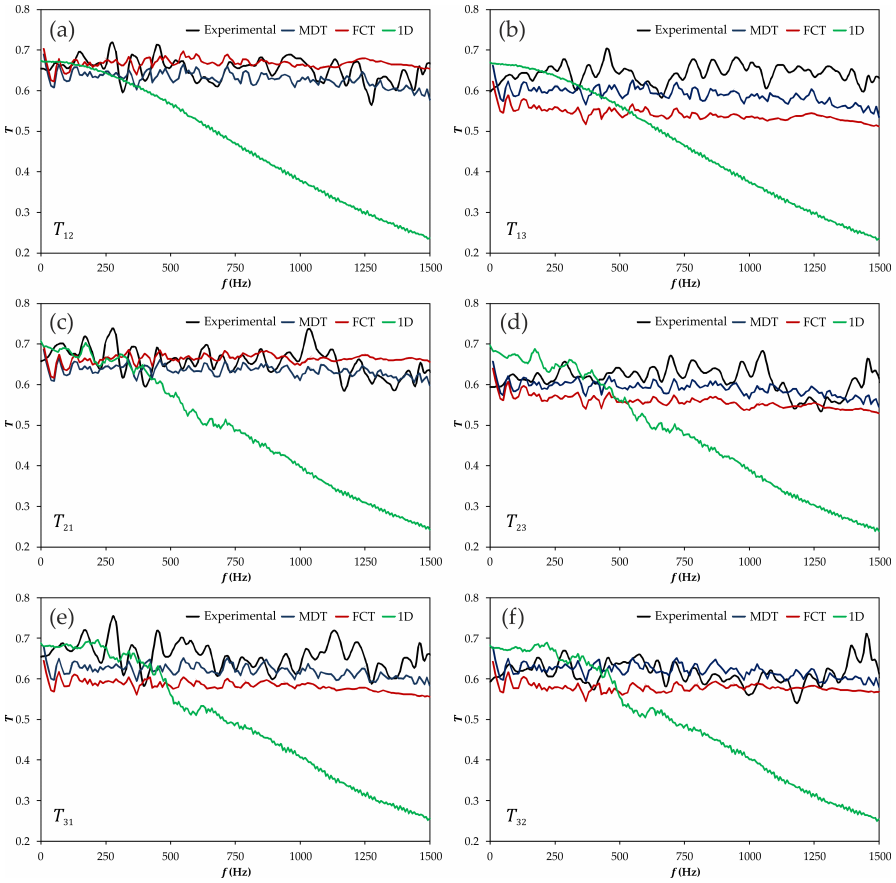

Figure 6.14: Comparison between the experimental results and the different models for the transmission coefficients of the Y-junction (frequency domain): (a) excitation at port 1, transmission through port 2; (b) excitation at port 1 , transmission through port 3; (c) excitation at port 2, transmission through port 1; (d) excitation at port 2, transmission through port 3 (c) excitation at port 3, transmission through port 1; (d) excitation at port 3, transmission through port 2.

6.5.3 Assessment of a modelling approach with a quasi-3D description of the junction

In order to explore the additional potential offered by the staggered mesh method regarding the approximate solution of the three-dimensional flow field inside the junction, such an approach was finally considered. In Figure 6.15 the mesh used is shown together, for reference, with that used in the previous

subsections. The four volumes at the endpoints of the part shown are then connected to a single volume, thus providing the connection with the one-dimensional computation at the ducts. The mesh chosen is relatively modest, in order to keep the computation time at reasonable values, but sufficient to show any potential advantages of this description.

Additionally, in view of the previous results, only the MDT method will be used as a flow limiter, since overall it has appeared to be more robust and consistent, and only the case of the T-junction will be analysed in the following, as no new qualitative issues have been identified in the Y-junction that were not present also in the T-junction.

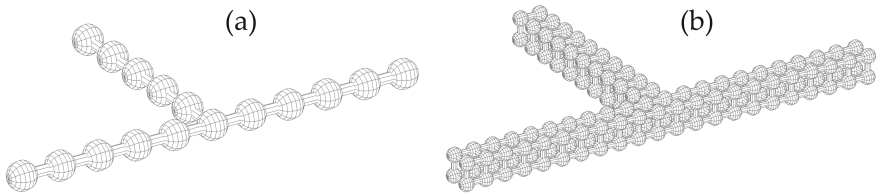

Figure 6.15: Meshes used in the staggered-grid method: (a) a 0D description of the junction; (b) a quasi-3D description.

In Figure 6.16 the results obtained in the time domain with the quasi-3D description of the junction (labelled MDT Q3D) are compared with those previously shown in Figure 6.8 corresponding to the MDT with 0D description of the junction. Again the plots on top represent the raw results, whereas the bottom plots show the differences with respect to the experimental values. It can be seen that, in all the cases, a certain improvement is achieved when using the quasi-3D junction, improvement which is more apparent when the junction is excited at port 3, this is, at the side branch, which is intuitively reasonable.

Again, the mean quadratic errors were computed, as shown in Table 6.3.

These results indicate that, while the reflection coefficients exhibit a similar mean error, there is a substantial improvement in the transmission coefficients, thus confirming the previous analysis.

However, the improvement achieved is not sufficient to produce results comparable to those shown in Figure 6.9 for the conventional model in the case of the reflection coefficient, and the differences in the transmission coefficients are clearly significant only when the junction is excited at the side branch. Therefore, while it appears that further refinement of the mesh at the junction should improve further the quality of the results, this might produce in turn

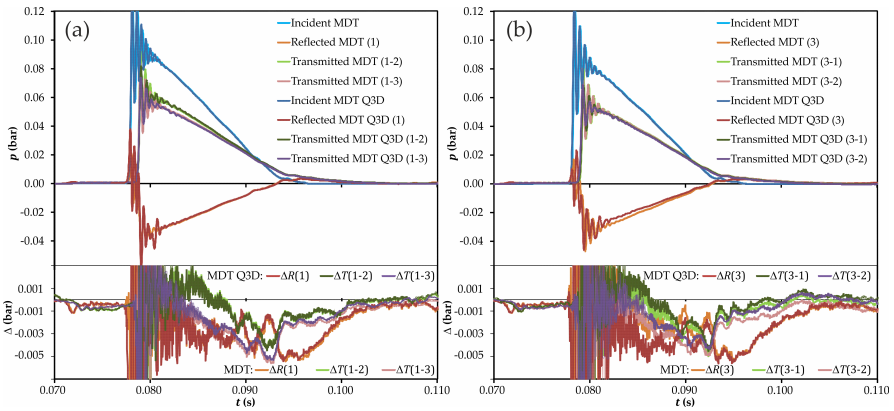

Figure 6.16: Influence of the description of the junction in the time domain, MDT method: raw data (top) and differences with measurement (bottom). (a) Excitation at port 1; (b) excitation at port 3.

Table 6.3: Values of the mean quadratic error: T-junction.

Path	**MDT**	**MDT Q3D**
R_1	1.514×10^{-4}	1.513×10^{-4}
R_3	1.102×10^{-4}	1.809×10^{-4}
T_{12}	1.005×10^{-4}	1.018×10^{-5}
T_{13}	1.609×10^{-4}	1.469×10^{-4}
T_{31}	1.121×10^{-4}	1.044×10^{-4}
T_{32}	1.554×10^{-4}	1.249×10^{-4}

a noticeable increase in the computation time.

Quite unexpectedly, when first looking at the results in the frequency domain, the improvements just commented did not have a translation. Both the reflection and transmitted coefficients were even showing a certain degree of degradation in the quality of the results, with the abnormally high values achieved at higher frequencies, specially when the junction was excited at port 1. After further research, it was detected that some spurious high-frequency oscillations was being generated at the interface between the quasi-3D junction and the 1D elements of the adjacent ducts, due to the virtual merging of four volumes into a single one. The pressure data was precisely being taken from the volume next to the interface and it was also found out that the spurious oscillation had a really low amplitude and it rapidly dissipated when moving away from the interface.

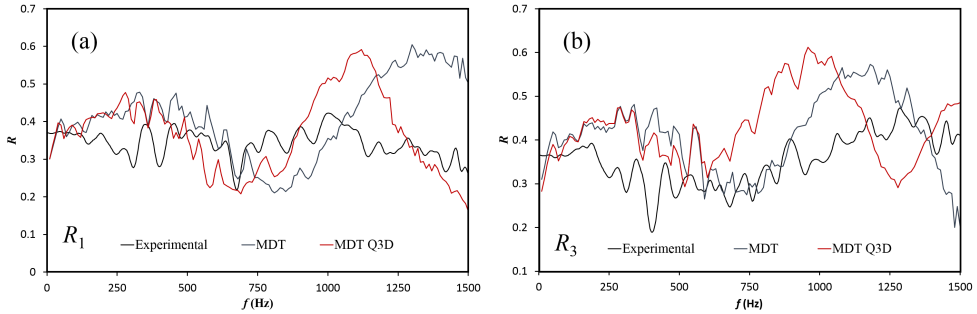

Figure 6.17: Influence of the description of the junction on the reflection coefficients (frequency domain), MDT method. (a) Excitation at port 1; (b) excitation at port 3.

Therefore, the solution adopted was to take the data from a volume several cells away from the interface, thus avoiding any degradation in the quality of the frequency domain results. The reflection coefficients are shown in Figure 6.17, where it can be seen that the new results offer a similar behaviour to simpler mesh ones, with a noticeable shift in frequency. This effect was, on the other hand, expected, since this shift in frequency in the reflection coefficient depends directly on the distance at where the measurements have been taken, shifting to lower frequencies the further from the device. In any case, at low frequency, the two predicted curves almost overlap for both configurations.

The same approach was followed for the transmission coefficients shown in Figure 6.18, with the data taken several cells away from the interface. The results offered by the more detailed mesh follow a similar trend when compared to the simple mesh, specially in the lower frequency. Some differences in level can be seen at some regions, with a less flat behaviour of the quasi-3D mesh. It is hard to tell which of the two methods offer better results, since neither of them can completely follow the transmission coefficient experimental results, but it can be concluded that in this case, the quasi-3D description of the junction does not provide significant improvements for the acoustic characterization.

Besides, it is possible that, even after taking the results at a safe distance from the interface between the quasi-3D junction and the one-dimensional ducts, some residual degradation of the results is still present in the coefficients shown, resulting in the small level differences discussed. In order to clarify this point, the whole system was meshed as shown in Figure 6.15b for the junction, and the results are shown in Figure 6.19, only for the case in which the junction is excited at port 1. It is apparent that a significant

improvement in the quality of the transmission coefficients is achieved, now showing a more realistic influence of the change in direction. In the case of the reflection coefficients the improvement is not so apparent, but the shape of the curve is smoother, what indicates that further refining of the mesh could lead to substantially improved results. However, that would be impractical, since the computation time increases substantially when the whole system is meshed in this way. Another possibility to be address in future work comes from developing a more complex technique for the connection between meshes able to avoid the unexpected spurious oscillations found, for example, using a virtual volume in a similar fashion as it was presented in section 4.3.

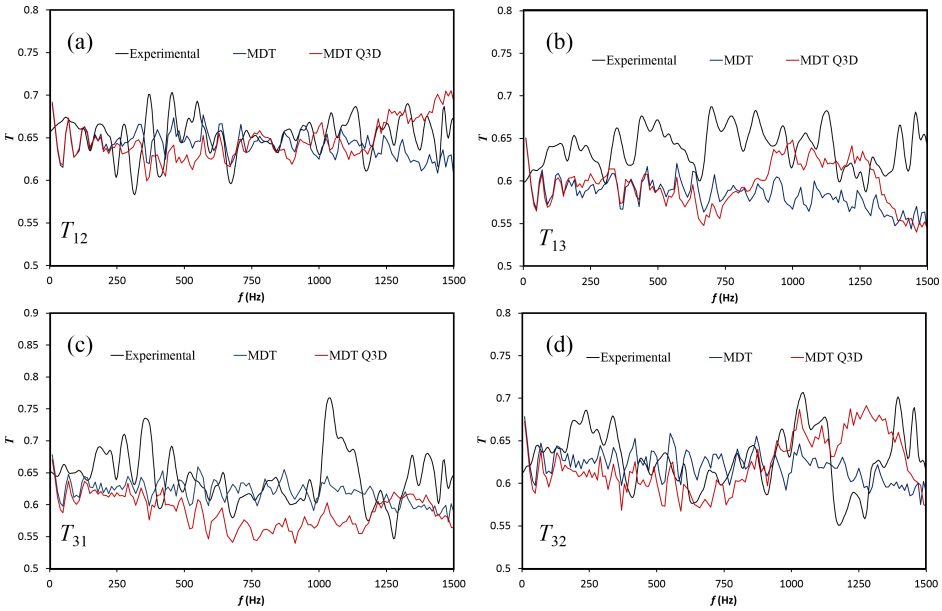

Figure 6.18: Influence of the description of the junction on the transmission coefficients (frequency domain), MDT method. (a) Excitation at port 1, transmission through port 2; (b) excitation at port 1, transmission through port 3; (c) excitation at port 3, transmission through port 1; (d) excitation at port 3, transmission through port 2.

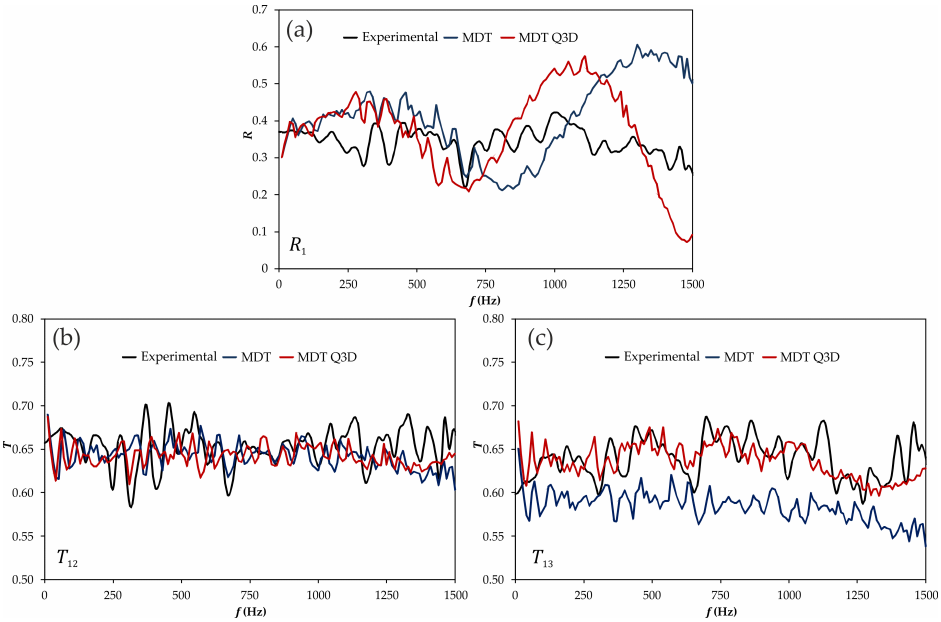

Figure 6.19: Influence of using a quasi-3D approach for the whole system on the reflection and transmission coefficients (frequency domain). MDT method, excitation at port 1. (a) Reflection at port 1; (b) transmission through port 2; (c) transmission through port 3.

6.6 Summary and conclusions

The objective of this chapter was to establish the potential of staggered mesh finite volume models as a way to improve the description of the effect of simple duct junctions on an otherwise one-dimensional flow system, as the intake or exhaust of an internal combustion engine. With that purpose, specific experiments were performed making use of a modified impulse method, in which two different junctions were characterized as a multi-port, and that provided precise and reliable results on the propagation of pressure pulses across junctions.

The experimental procedure was detailed, explaining how three measurements are needed for each case. Those three measurements consist on imposing an excitation in one of the ducts with anechoic terminations in the other two ducts, repeating the process for every duct. The incident pulse is generated by means of a high speed electrovalve that controls the discharge from a high-pressure tank.

The results obtained were then compared to numerical results obtained from different methods, both in the time and the frequency domains. First, methods assuming a zero-dimensional description of the junction were assessed, including the staggered mesh finite volume method with different flux limiters and, as a reference for comparison, a more conventional pressure loss-based model. Then, the potential of using the staggered mesh finite volume method in order to produce a quasi-3D description of the junction, to be coupled with the one-dimensional description of the adjacent ducts, was explored.

As an overall conclusion of the results found, one may state that none of the modelling approaches considered is able to reproduce totally the observed behaviour. However, the performance of the different models is such that a suitable choice seems to be possible depending on which is the actual focus of the problem under study: situations in which a suitable time domain description may be sufficient may be addressed either with the conventional quasi-steady pressure loss model (most notably when the focus is on the reflection properties of the junction) or with the staggered mesh model with quasi-3D junction description (in this last case, when the main interest is on transmission, and given that the lengths involved in the problem will not be as long as to give rise to spurious oscillations due to the dispersive character of the method).

When the focus is on the frequency domain and on the dynamic behaviour of the junction, it is the staggered mesh method the one that provides the most suitable results, at least from a qualitative point of view, as a consequence

of the fact that momentum conservation across the junction is accounted for. However, due to spurious oscillation arising in the interface proximity from the method used to couple a quasi-3D junction to the 1D ducts, no substantial improvements were found in using a quasi-3D description of the junction, since very similar results with a lower computation time have been obtained with the zero-dimensional description of the junction, and with a full quasi-3D description of the whole system, even though the quality of the results was noticeably improved, the increase in computational cost usually makes this last option unacceptable in practice. It is thus clear that further work is needed in this case in order to find the optimal settings for the calculation, most notably in the connection between the quasi-3D and the 1D regions.

Finally, it should be recalled that no empirical information has been included in the staggered mesh method used; the incorporation of such information in terms of effective sections and characteristic lengths and the evaluation of their potential could be additional topics for further research.

Chapter 6 Bibliography

[11] G. Montenegro, A. Onorati, and A. Della Torre. "The prediction of silencer acoustical performances by 1D, 1D–3D and quasi-3D non-linear approaches." *Computers & Fluids* 71 (2013), pp. 208–223 (cit. on pp. 4, 59, 72, 151).

[61] E. F. Toro, M. Spruce, and W. Speares. "Restoration of the contact surface in the HLL-Riemann solver." *Shock waves* 4(1) (1994), pp. 25–34 (cit. on pp. 47, 153).

[83] J. Corberán. "A new constant pressure model for N-branch junctions." *Proceedings of the type of Mechanical Engineers, Part D: Journal of Automobile Engineering* 206(2) (1992), pp. 117–123 (cit. on pp. 57, 148).

[84] B. Schmandt and H. Herwig. "The head change coefficient for branched flows: Why "losses" due to junctions can be negative." *International Journal of Heat and Fluid Flow* 54 (2015), pp. 268–275 (cit. on pp. 57, 148).

[89] M. Bassett, D. Winterbone, and R. Pearson. "Calculation of steady flow pressure loss coefficients for pipe junctions." *Proceedings of the type of mechanical engineers, part C: Journal of Mechanical Engineering Science* 215(8) (2001), pp. 861–881 (cit. on pp. 57, 150, 153).

[90] W. Hager. "An approximate treatment of flow in branches and bends." *Proceedings of the type of Mechanical Engineers, Part C: Journal of Mechanical Engineering Science* 198(1) (1984), pp. 63–69 (cit. on pp. 57, 150, 153).

[119] F. Payri, J. Desantes, and A. Broatch. "Modified impulse method for the measurement of the frequency response of acoustic filters to weakly nonlinear transient excitations." *The Journal of the Acoustical Society of America* 107(2) (2000), pp. 731–738 (cit. on pp. 126, 128, 131, 150).

[121] A. Torregrosa, A. Broatch, T. Fernández, and F. Denia. "Description and measurement of the acoustic characteristics of two-tailpipe mufflers." *The Journal of the Acoustical Society of America* 119(2) (2006), pp. 723–728 (cit. on p. 150).

[122] OpenWAM. CMT - Motores Térmicos. Universidad Politécnica de Valencia. URL: `http://www.OpenWAM.org` (cit. on pp. 150, 179).

[123] B. Van Leer. "Towards the ultimate conservative difference scheme. V. A second-order sequel to Godunov's method." *Journal of computational Physics* 32(1) (1979), pp. 101–136 (cit. on p. 153).

Chapter 7

Concluding remarks and future work

Contents

7.1 Introduction **178**
7.2 Main contributions **178**
7.3 Limitations **181**
7.4 Future work **184**
Chapter 7 Bibliography **187**

7.1 Introduction

In this chapter, a critical review of the present work is performed. Main findings and contributions of the thesis are included in section 7.2, differentiating between the numerical method development phase and the validation process.

Section 7.3 is devoted to the enumeration of limitations of the model and the approach followed in this thesis, which includes the limitations intrinsic to the numerical method approach that was chosen and some other issues that were found and appointed in this work.

Finally, Section 7.4 covers potential improvements that may be explored to improve the applicability and general performance of the quasi-3D model.

7.2 Main contributions

The main contribution of this thesis is the development of a non-linear quasi-3D numerical method for fluid-dynamics to be used along with an existing one-dimensional code for engine simulations. This model is able to account for phenomena that escape a one-dimensional approach capabilities, due to their three-dimensional nature, whilst the computational cost is not greatly increased. These properties makes the method specially interesting for non-linear acoustics predictions in the core of a one-dimensional model.

Numerical method

The quasi-3D model here developed makes use of a non-linear second order time and space discretization based on a finite volumes staggered-grid. This so-called staggered grid mesh approach creates two different types of elements in the mesh, performing the calculation of some properties of the fluid in one of the element types and the rest in the other one. In this case, the mesh differentiates between volumes, where scalar magnitudes are calculated, and connectors, which can be seen as flat surfaces linking two volumes and store the vector variables, such as momentum or space orientation. The calculation of the conservative variables is made by using a discretization form of the Euler conservation equations in its three-dimensional form. Therefore, the mass and energy equations are solved in the volumes and the momentum equation, in the connectors. It is precisely in the discretization of the momentum equation when the simplification that designates the numerical method as a quasi-3D model appears, for this equation is treated as a one-dimensional momentum equation in the direction orthogonal to the surface of the connector, where it is solved. In this way, a single equation needs to be solved for each

connector, instead of the three coupled equations of a regular centred finite volume scheme for the momentum term in each volume. The fact that each connector has associated an orientation in space makes it possible to keep the three-dimensional modelling capabilities of the method with a still low computational cost.

As any second-order scheme, this quasi-3D model is affected by the occurrence of non-physical overshoots in the vicinity of discontinuities in the flow variables [57]. In order to remove those overshoots, two flux limiters commonly used in finite differences schemes have been adapted: a Flux Corrected Transport (FCT) technique [1] and a Total Variation Diminishing (TVD) method [2], along with the momentum diffusion term (MDT) described by Montenegro *et al.* [28], already applied to similar methods. The outcome method with the corresponding flux limiters was tested in the well-known shock-tube problem, succeeding in removing the over-oscillations associated with the propagation of the shock wave. Only in the TVD method some low amplitude oscillations were still present in the solution; however, a more extensive performance test and validation of the method and the flux limiters is performed in subsequent cases in order to obtain better conclusions.

Boundary conditions

Eventually, in order to secure that the final objective of connecting the quasi-3D staggered grid method to the one-dimensional collocated mesh method used in OpenWAM [122] is achieved, some tests have been performed, obtaining some promising preliminary results. Due to time restrictions, the full connection between methods was not feasible, but to assure that it could be performed in the close future, a one-dimensional collocated scheme based on Godunov's method [57] was implemented as a representative modern one-dimensional scheme to be connected to the quasi-3D method. The boundary condition developed is based on the virtual cell approach, where the cells that shall be connected, here called boundary cells, are actually connected to another cell that will inherit the values of the variables of the boundary cells from the other mesh and use them as initial conditions every time step. Although there are some issues that had to be solved due to the different elements and their positioning in the mesh, the results obtained after simulating the shock-tube problem, with each half of the duct using one method, are completely satisfactory, with the correct prediction in the values of the variables of the four zones and the transition between them, within the limitations of each method. Only some small oscillations were detected in the quasi-3D method solution, but mainly due to the use of no flux limiters for these preliminary

tests. Even though there is still some work to do for this task, the results are promising and assure that the connection is possible and feasible.

Applications and validation process

After the description of the quasi-3D numerical method and the set up of the boundary conditions, the model is almost ready to be used in its full potential. However, the development process would not be complete without an extensive validation of the model, whether to show its correct performance or to provide examples where it can be applied. With this goal, the quasi-3D method has been used to simulate a set of three-dimensional devices, modelling increasingly complex geometry systems with different distributions of inlet and outlet ducts to explore as many options as possible while searching for three-dimensional effects that a one-dimensional approach cannot predict. The experiment selected to be modelled is an impulsive test rig, where a pulse is generated at the beginning of the inlet duct and the incident and transmitted waves are measured, right before arriving the device and after traversing it, respectively. From these two waves it is possible to calculate the transmission loss of the device, providing a validation of the accuracy of the results in time domain and the non-linear acoustics prediction capabilities. As validation tool, a linear acoustics code was used and, in some cases where it was not enough to determine if the difference in the results between non-linear and linear approach were due to the influence of the three-dimensional effect or to inaccuracies, a commercial non-linear program performing exactly the same simulation was used.

The general trend followed by the results shows that, although the three flux limiters prove to be proficient in removing the non-physical spurious oscillations in the time domain results, the Momentum Diffusion Term consistently arises as the best option when analysing the acoustic behaviour of the system. The Flux Corrected Transport technique is a close second, with a somewhat more dissipative solution, and finally the Total Variation Diminishing flux limiter increases the dissipative behaviour, specially at higher frequencies. However, it could be concluded that performance of the quasi-3D method is satisfactory and the objective of validating its acoustics capabilities with three-dimensional systems has been fully accomplished.

A different but equally interesting application of the quasi-3D method is the modelling of duct junctions. The method developed offers a simple approach to the problem with the objective to provide an accurate and easy to use tool to model junctions, since it is able to account for the pressure loss associated to the change of flow direction of junctions only with the relative

orientation of the ducts and its section as input data [3]. With this purpose, two geometries were considered, a T-junction and Y-junction, which where also simulated in an impulsive test rig. In this case, the results obtained with the quasi-3D method, employing each one of the three flux limiters, were compared with the results of a one-dimensional approach with a pressure-loss junction model, used as a reference solution, and also specific experiments have been performed after manufacturing both junctions.

The results in the time domain show the better performance of the quasi-3D method regarding the prediction of the amplitude of the transmitted waves, giving a better agreement with the experimental results than the one-dimensional approach. The conventional pressure-loss model is not able to reliably capture the difference in amplitude between the two transmitted waves. It is however in the frequency domain when the superior modelling capabilities of the quasi-3D method are more evident. The one-dimensional method in frequency is only capable of giving a flat value for the reflection coefficient, although the average value could be a decent approximation, but for the transmission coefficient, the conventional model is completely unable to reproduce neither the level nor the dynamic features of the solution. The quasi-3D method, on the other hand, even though for some cases these dynamic effects can be overestimated, it is able to produce a much more suitable approximation in the frequency domain and follow the overall trends of the experimental results. It was also stated that using a more detailed grid for the junction can bring some improvements in the accuracy of the solution, but with a higher computational cost and it should be studied if that slight improvement in accuracy justifies the rather noticeable increase in computational cost. It is also worth mentioning that the results in the cells in close proximity to the transition zone between the detailed mesh and a one-dimensional duct can present a strange behaviour in the frequency domain for higher frequencies, as it was detected in some cases. As a conclusion, it can be stated that the overall results provided by the quasi-3D method offer a better description of the wave dynamics and the general frequency domain solution compared to the conventional models used in one-dimensional codes for duct junctions, while requiring only the knowledge of the geometry of the junction.

7.3 Limitations

Even though the main objectives presented in chapter 1 were accomplished, the model developed still presents some limitations that should be addressed.

- As it was explored in chapter 5, the behaviour of the acoustic solution obtained when using the TVD flux limiter was heavily influenced by the value of the parameter ξ. In the TVD schemes studied in the literature review, this parameter was stablish at the value of $\xi = 0.5$, as it was said to provide good results for a majority of cases without needing to tune it. However, when the TVD method was used for the parallelepiped muffler, the results obtained where unacceptably dissipative, to the point that the transmission loss calculated could only predict really low frequencies. It was proved that by reducing the value of the parameter, the results quality could be increased until appropriate levels. Even though it is true that the value set for the parallelepiped muffler proved to be also the most suitable for the rest of simulations performed in this work, that does not mean that it will always be the case. Therefore, it is possible that a suitable value of ξ will have to be found for different simulations, which might be at least inconvenient when deciding to use the method. The FCT technique is in a similar spot with the parameter ϑ, although it was not needed to fit it in any of the simulations performed in this work.

- Nevertheless, even after fitting the respective parameters, the TVD and FCT methods provided more dissipative results than when using the MDT flux limiter. As it was said above, reducing the value of those parameters bring a less dissipative solution, but reducing it too much might also result in the appearance of some instabilities. In chapter 5 it was also explored how the lowest value of ξ tested entailed more oscillations in the time domain solution and some negative values in the transmission loss calculated, which is not physically possible. After these issues, it might appear that there is no point in using a flux limiter different than the MDT method, however, the fact that it has usually provided a somewhat better solution does not mean that it will always be the case. There may be some simulations in which the MDT method fails to properly reproduce the behaviour of the system, whereas the FCT or TVD schemes give a good approximation. The conclusion that should be deduced here is that the MDT method should be the first option when simulating, and if the results are not satisfactory, the FCT and TVD methods should be used.

- In chapter 6 it was first implemented the connection between a more refined mesh with a merely one-dimensional mesh. That means that there

was a transition between a volume with four smaller volumes by means of four small connectors in the same direction. This did not represent any problem in the time domain solution, but in the frequency domain solution, a strange behaviour in the volumes in close proximity to the transition zone was detected in the form of high values of the transmission and reflection coefficients at medium frequencies. This anomalies disappeared when moving away from the transition zone a certain number of volumes, but it is something to take into account when modelling this kind of connections and will need more work to develop a proper connection.

- When testing the connection between the quasi-3D method and a collocated one-dimensional scheme by simulating the shock-tube problem, some small oscillations where detected in the quasi-3D side, close to the rarefaction wave. This low amplitude oscillations may come from the connection itself, due to the non-existent direct match between some elements and the variables in their position in the other mesh, as it is the case of the momentum in the connectors being translated into the collocated scheme. Additional tests are needed in this regard, since these perturbations are apparently too weak to disturb the final solution and are expected to further decrease once flux limiters are implemented, but still, it will have to be checked. Also, the anechoic termination boundary condition in not able to completely remove reflections, making it not usable for some applications.

- Finally, one limitation that has to be accounted for is the computational cost of the numerical method. From the beginning it was presented as an improvement of a one-dimensional scheme with three-dimensional modelling capabilities, but a computational cost comparable a one-dimensional model. With the simplifications adopted, it will always be much faster than a complete CFD three-dimensional code, but the truth is that when trying to model a reasonably detailed mesh, the computational time will be noticeably increased. Using a simplified version of the mesh would solve this, but in that case the accuracy might also suffer, so a compromise solution should be found. Although the increase in computational time is an evident consequence of modelling three-dimensional cases, since the number of cells and connections needs to be higher, it is something that needs to be taken into account when planning the simulations.

7.4 Future work

In this work, the basis of the numerical method with different options to guarantee its stability by means of flux limiters has been developed, as well as an extensive validation process. However, there are still some activities that need to be accomplished, or at least considered, before the final implementation in the main one-dimensional code.

- The first task that should be pursued is the complete translation of the code to the programming language in which OpenWAM is written, which is C++. The quasi-3D method, on the other hand, has been originally written in an interpreted programming language due to its easier implementation as an standalone tool. Nevertheless, a compiled programming language is always preferred for the final product, since it offers a much faster execution time. Therefore, the translation should be performed directly into OpenWAM project, which will also simplify their connection. It is worth noting that the fact that the code was first implemented in a interpreted programming language is the reason for which no specific computational times of the method have been provided through this work. The times needed for the simulation would have been misleading, since once the translation to a compiled language is performed, these values will be severely reduced.

- Additionally, further research is needed regarding the recommended values of the parameters ξ and ϑ for the TVD and FCT methods, respectively. As it was stated in chapter 5, these parameters directly influence the amount of dissipation of the method in such a way that reducing their values also reduces the dissipation in the solution, but if their values are too low, some other issues appear, like the inability of removing spurious oscillations or some negative values in the transmission loss calculated, which is physically not possible.

- In chapter 3, when describing the adaptation of the TVD method to a three-dimensional mesh, there was some issues that had to be faced, being the most important the treatment of the so-called end-volumes. The TVD method used needs information of two cells in each side for each direction, so when reaching an end-volume, which is not connected to enough volumes in some direction, some assumptions have to be made. In a one-dimensional scheme, this is not a big issue since only two volumes will need this special treatment, one on each end of the duct, but

in a three-dimensional case, the number of end-volumes is much higher, since all of the volumes in the surface will be in that situation. Therefore, the decision that was taken consist in assuming that the needed values for the TVD method in an end-volume from the side where there are no volumes will come from the opposite side, but inverting the sign of the flow. This means that if, for example, a volume is not attached to any other volume to its right side, the values for the TVD flux limiter for that volume will be taken from the left side volume, changing only the sign of the flow speed. This solution proved to work, but might be the responsible of the sometimes excessively dissipative behaviour of the quasi-3D method with the TVD flux limiter, hence some other options should be explored with the objective of reducing the dissipation of the method.

- In order to perform the validation process of the numerical method, there was no need of implementing source terms in the code, since they would not affect the solution. However, before adding the code to the one-dimensional program, the option of considering source terms should be implemented, like heat transfer between the fluid and the walls, as it is in the rest of the model. Another model present in OpenWAM that should eventually be part ot the quasi-3D method is an improved species model, capable of tracking the evolution of the composition of the fluid. This includes better models for the gas properties, like the heat capacity ratio as a function of the composition and the temperature.

- Moreover, in order to have a more competitive tool, some other features should be eventually included in the model. Some examples that have been considered include the option of modelling absorptive materials inside mufflers. This is a common practice among muffler manufacturers, so it might be an interesting addition. It was also considered to add the possibility of model a catalyst brick with the quasi-3D method. Some initial work was done in section 5.2 when describing the meshing techniques that have been developed in this work, particularly with the case of geometries with parallel ducts, just by adding a feature that allows to divide each parallel duct in a certain number of identical channels to simulate the inside geometry of a catalyst brick. The main idea is to calculate only one of the small channels for each one of the original parallel ducts and assume that the rest of small channels inside the duct have the same properties. This way, the computational cost would be the same,

since only one channel per duct is calculated. This strategy is usually used in one-dimensional models of catalysts, but in that case all the channels have the same properties. With the quasi-3D method instead, every set of channels in a duct will have the same properties, but the set will be different between them, giving three-dimensional resolution to the problem. The same approach can be followed for particulate filters, although the parallel ducts should be treated differently to model the behaviour of a particulate filter. This option for the modelling of after-treatment devices in engines is particularly interesting, since it would offer three dimensional resolution by adapting validated one-dimensional techniques and without heavily increasing the computational cost. Unfortunately, their implementation was not possible in this work because better meshing techniques were required.

- Finally, only the initial steps of the development of the boundary conditions has been fulfilled and there is still more work to perform in this regard. Besides, a more extensive validation of the connection between numerical schemes should be made once that connection is fully developed and established. The preliminary results are promising, but further testing will be needed to secure the proper functioning of the tool with all the flux limiters.

Chapter 7 Bibliography

[1] A. Torregrosa, A. Broatch, F. Arnau, and M. Hernández. "A non-linear quasi-3D model with Flux-Corrected-Transport for engine gas-exchange modelling." *Journal of Computational and Applied Mathematics* 291 (2016), pp. 103–111 (cit. on pp. xi, 71, 72, 76, 179).

[2] A. Torregrosa, A. Broatch, F. Arnau, and M. Hernández. "On the effect of different flux limiters on the performance of an engine gas exchange gas-dynamic model." *International Journal of Mechanical Sciences* (2017) (cit. on pp. xi, 71, 76, 179).

[3] A. J. Torregrosa, A. Broatch, L. M. García-Cuevas, and M. Hernández. "A Study of the Transient Response of Duct Junctions: Measurements and Gas-Dynamic Modeling with a Staggered Mesh Finite Volume Approach." *Applied Sciences* 7(5) (2017), p. 480 (cit. on pp. xi, 3, 181).

[28] G. Montenegro, A. Della Torre, A. Onorati, and R. Fairbrother. "A nonlinear Quasi-3D approach for the modeling of mufflers with perforated elements and sound-absorbing material." *Advances in Acoustics and Vibration* 2013 (2013) (cit. on pp. 5, 70–72, 76, 78, 90, 179).

[57] S. K. Godunov. "A difference method for numerical calculation of discontinuous solutions of the equations of hydrodynamics." *Matematicheskii Sbornik* 89(3) (1959), pp. 271–306 (cit. on pp. 42, 48, 179).

[122] OpenWAM. CMT - Motores Térmicos. Universidad Politécnica de Valencia. URL: `http://www.OpenWAM.org` (cit. on pp. 150, 179).

Bibliography

Amphlett, S., Niven, P. C., Payri, F., and Torregrosa, A. J.
Linear acoustic modelling using 1-D flow systems which represent complex 3-D components. SAE Technical Paper 2011-01-1524 2011 (cit. on p. 122)

Arnau, F. J.
Métodos numéricos para el modelado unidimensional del proceso de renovación de la carga. Reverté 2009 (cit. on pp. 15, 80)

Bassett, M., Pearson, R., Fleming, N., and Winterbone, D.
A multi-pipe junction model for one-dimensional gas-dynamic simulations. SAE Technical Paper 2003-01-0370 2003 (cit. on p. 58)

Bassett, M., Winterbone, D., and Pearson, R.
"Calculation of steady flow pressure loss coefficients for pipe junctions." *Proceedings of the type of mechanical engineers, part C: Journal of Mechanical Engineering Science* 215(8) (2001), pp. 861–881 (cit. on pp. 57, 150, 153)

Bassett, M. D., Winterbone, D. E., and Pearson, R. J.
Modelling engines with pulse converted exhaust manifolds using one-dimensional techniques. SAE Technical Paper 2000-01-0290 2000 (cit. on p. 58)

Beam, R. M. and Warming, R. F.
"An implicit finite-difference algorithm for hyperbolic systems in conservation-law form." *Journal of computational physics* 22(1) (1976), pp. 87–110 (cit. on p. 70)

Benajes, J., Lujan, J., Bermudez, V., and Serrano, J.
"Modelling of turbocharged diesel engines in transient operation. Part 1: insight into the relevant physical phenomena." *Proceedings of the type of Mechanical Engineers, Part D: Journal of Automobile Engineering* 216(5) (2002), pp. 431–441 (cit. on p. 5)

Benson, R. S.
Thermodynamics and Gas Dynamics of Internal Combustion Engines. Cambridge University Press 1982 (cit. on pp. 4, 25, 57)

Benson, R.
"The Effect of Excess Scavenge Air on the Pressure Drop in the Cylinder of a Two-Stroke Cycle Engine During Exhaust Blow down." *The Aeronautical Journal* 59(539) (1955), pp. 773–778 (cit. on p. 24)

Benson, R. and Woods, W.
"Wave action in the exhaust system of a supercharged two-stroke-engine model." *International Journal of Mechanical Sciences* 1(2-3) (1960), pp. 253–281 (cit. on p. 24)

Bingham, J. and Blair, G.
"An improved branched pipe model for multi-cylinder automotive engine calculations." *Proceedings of the type of Mechanical Engineers, Part D: Transport Engineering* 199(1) (1985), pp. 65–77 (cit. on p. 58)

Boris, J. P. and Book, D. L.
"Flux-corrected transport. I. SHASTA, a fluid transport algorithm that works." *Journal of computational physics* 11(1) (1973), pp. 38–69 (cit. on pp. 50, 78)

Broatch, A., Serrano, J., Arnau, F., and Moya, D.
"Time-domain computation of muffler frequency response: comparison of different numerical schemes." *Journal of sound and vibration* 305(1) (2007), pp. 333–347 (cit. on pp. 3, 70)

Colella, P.
"A direct Eulerian MUSCL scheme for gas dynamics." *SIAM Journal on Scientific and Statistical Computing* 6(1) (1985), pp. 104–117 (cit. on p. 55)

Colella, P. and Woodward, P. R.
"The piecewise parabolic method (PPM) for gas-dynamical simulations." *Journal of computational physics* 54(1) (1984), pp. 174–201 (cit. on p. 55)

Coquel, F. and LeFloch, P. G.
"An entropy satisfying MUSCL scheme for systems of conservation laws." *Numerische Mathematik* 74(1) (1996), pp. 1–33 (cit. on p. 56)

Corberán, J.
"Contribución al modelado del proceso de renovación de la carga en motores de combustión interna alternativos." PhD thesis. Tesis Doctoral, Universidad Politécnica de Valencia 1984 (cit. on pp. 4, 5)

Corberán, J.
"A new constant pressure model for N-branch junctions." *Proceedings of the type of Mechanical Engineers, Part D: Journal of Automobile Engineering* 206(2) (1992), pp. 117–123 (cit. on pp. 57, 148)

Corberán, J. and Gascón, M. L.
"New method to calculate unsteady 1-D compressible flow in pipes with variable cross section. Application to the calculation of the flow in intake and exhaust pipes of I. C. engines." *ASME, NEW YORK, NY,(USA).* 23 (1995), pp. 77–87 (cit. on pp. 23, 25)

Corberán, J. and Gascón, M. L.
"TVD schemes for the calculation of flow in pipes of variable cross-section." *Mathematical and computer modelling* 21(3) (1995), pp. 85–92 (cit. on p. 23)

Courant, R., Friedrichs, K., and Lewy, H.
"Über die partiellen Differenzengleichungen der mathematischen Physik." *Mathematische annalen* 100(1) (1928), pp. 32–74 (cit. on pp. 31, 76)

Courant, R., Isaacson, E., and Rees, M.
"On the solution of nonlinear hyperbolic differential equations by finite differences." *Communications on Pure and Applied Mathematics* 5(3) (1952), pp. 243–255 (cit. on p. 41)

Daneshyar, H.
One-Dimensional Compressional Flow. Peramon Press 1976 (cit. on p. 15)

Davis, S.
"Simplified second-order Godunov-type methods." *SIAM Journal on Scientific and Statistical Computing* 9(3) (1988), pp. 445–473 (cit. on p. 47)

Davis, S. F.
"A simplified TVD finite difference scheme via artificial viscosity." *SIAM journal on scientific and statistical computing* 8(1) (1987), pp. 1–18 (cit. on pp. 55, 80)

Desantes, J., Chust, M., and Llorens, J.
"Análisis comparativo de métodos numéricos para la resolución del flujo no estacionario en colectores de motores de combustión interna alternativos." In: *II Congreso de Métodos Numéricos en Ingeniería, F. Ambarina and M. Casteleiro, eds., c SEMNI* 1993 (cit. on p. 5)

Desantes, J., Torregrosa, A., and Broatch, A.
"Experiments on flow noise generation in simple exhaust geometries." *Acta Acustica united with Acustica* 87(1) (2001), pp. 46–55 (cit. on p. 57)

Dwyer, H., Allen, R., Ward, M., Karnopp, D., and Margolis, D.
"Shock capturing finite difference methods for unsteady gas transfer." In: *7th Fluid and PlasmaDynamics Conference* 1974, p. 521 (cit. on p. 25)

European Parliament, Council of the European Union.
"Regulation (EC) No 715/2007 of the European Parliament and of the Council of 20 June 2007 on type approval of motor vehicles with respect to emissions from light passenger and commercial vehicles (Euro 5 and Euro 6) and on access to vehicle repair and maintenance information (Text with EEA relevance)." *Official Journal of the European Union* (50) (June 2007), pp. 1–16 (cit. on p. 14)

European Parliament, Council of the European Union.
"Regulation (EC) No 595/2009 of the European Parliament and of the Council of 18 June 2009 on type-approval of motor vehicles and engines with respect to emissions from heavy duty vehicles (Euro VI) and on access to vehicle repair and maintenance information and amending Regulation (EC) No 715/2007 and Directive 2007/46/EC and repealing Directives 80/1269/EEC, 2005/55/EC and 2005/78/EC (Text with EEA relevance)." *Official Journal of the European Union* (52) (July 2009), pp. 1–13 (cit. on p. 14)

Fauconnier, D. and Dick, E.
"Spectral analysis of nonlinear finite difference discretizations." *Journal of Computational and Applied Mathematics* 246 (2013), pp. 113–121 (cit. on p. 128)

Ferrari, G. and Onorati, A.
"Determination of silencer performances and radiated noise spectrum by 1-d gas dynamic modelling." In: *VEHICLE AND ENVIRONMENT. 25TH FISITA CONGRESS, BEIJING 1994, VOL 3. TECHNICAL PAPER NO. 945135* 1994 (cit. on p. 25)

Galiano, S. J. and Zapata, M. U.
"A new TVD flux-limiter method for solving nonlinear hyperbolic equations." *Journal of Computational and Applied Mathematics* 234(5) (2010), pp. 1395–1403 (cit. on p. 71)

Galindo, J.
"Diseño de uniones de colectores de escape de motores alternativos." PhD thesis 1998 (cit. on p. 5)

Galindo, J., Serrano, J., Arnau, F., and Piqueras, P.
"High-frequency response of a calculation methodology for gas dynamics based on Independent Time Discretisation." *Mathematical and Computer Modelling* 50(5) (2009), pp. 812–822 (cit. on p. 125)

Galindo, J., Serrano, J., Climent, H., and Arnau, F.
"New one-dimensional fluid-dynamic model for automotive intercoolers." In: *Proceedings of EAEC 8th European Automotive Congress* 2001 (cit. on p. 5)

Galindo, J., Tiseira, A., Fajardo, P., and Navarro, R.
"Coupling methodology of 1D finite difference and 3D finite volume CFD codes based on the Method of Characteristics." *Mathematical and Computer Modelling* 54(7) (2011), pp. 1738–1746 (cit. on pp. 4, 70, 101)

García-Cuevas González, Luis Miguel
"Experiments and Modelling of Automotive Turbochargers under Unsteady Conditions." PhD thesis 2015 (cit. on pp. 98, 99, 102)

Gascón Martínez, M. L.
"Estudio de esquemas en diferencias finitas para el cálculo del flujo compresible unidimensional, no estacionario y no isentrópico." PhD thesis. Universitat Politècnica de València 1995 (cit. on p. 22)

Glav, R. and Åbom, M.
A general formalism for analyzing acoustic 2-port networks 1997 (cit. on p. 125)

Godunov, S. K.
"A difference method for numerical calculation of discontinuous solutions of the equations of hydrodynamics." *Matematicheskii Sbornik* 89(3) (1959), pp. 271–306 (cit. on pp. 42, 48, 179)

Goodman, J. B. and LeVeque, R. J.
"A geometric approach to high resolution TVD schemes." *SIAM journal on numerical analysis* 25(2) (1988), pp. 268–284 (cit. on p. 55)

Hager, W.
"An approximate treatment of flow in branches and bends." *Proceedings of the type of Mechanical Engineers, Part C: Journal of Mechanical Engineering Science* 198(1) (1984), pp. 63–69 (cit. on pp. 57, 150, 153)

Harrison, M., De Soto, I., and Unzueta, P. R.
"A linear acoustic model for multi-cylinder IC engine intake manifolds including the effects of the intake throttle." *Journal of Sound and Vibration* 278(4) (2004), pp. 975–1011 (cit. on p. 56)

Harten, A. and Zwas, G.
"Self-adjusting hybrid schemes for shock computations." *Journal of Computational Physics* 9(3) (1972), pp. 568–583 (cit. on p. 55)

Harten, A. and Zwas, G.
"Switched numerical Shuman filters for shock calculations." *Journal of Engineering Mathematics* 6(2) (1972), pp. 207–216 (cit. on p. 55)

Harten, A.
"High resolution schemes for hyperbolic conservation laws." *Journal of computational physics* 49(3) (1983), pp. 357–393 (cit. on pp. 53, 71, 80)

Harten, A. and Osher, S.
"Uniformly high-order accurate nonoscillatory schemes. I." *SIAM Journal on Numerical Analysis* 24(2) (1987), pp. 279–309 (cit. on p. 56)

Harten, A.
"The artificial compression method for computation of shocks and contact discontinuities. III. Self-adjusting hybrid schemes." *Mathematics of Computation* 32(142) (1978), pp. 363–389 (cit. on p. 55)

Harten, A., Lax, P. D., and Leer, B. v.
"On upstream differencing and Godunov-type schemes for hyperbolic conservation laws." *SIAM review* 25(1) (1983), pp. 35–61 (cit. on p. 45)

Hirsch, C. and Hirsch, C.
Fundamentals of numerical discretization. Wiley 1988 (cit. on p. 26)

Ikeda, T. and Nakagawa, T.
"On the SHASTA FCT algorithm for the equation = 0." *Mathematics of Computation* 33(148) (1979), pp. 1157–1169 (cit. on p. 51)

Jameson, A.
"Steacfy-State Solution of the Euler Equations for Transonic Flow." - (1982) (cit. on p. 55)

Jameson, A., Schmidt, W., Turkel, E., et al.
"Numerical solutions of the Euler equations by finite volume methods using Runge-Kutta time-stepping schemes." *AIAA paper* 1259 (1981), p. 1981 (cit. on p. 55)

Jenny, E.
"Unidimensional transient flow with consideration of friction, heat transfer and change of section." *Brown Boveri Review* 37(11) (1950), p. 447 (cit. on p. 24)

Karlsson, M. and Åbom, M.
"Aeroacoustics of T-junctions-An experimental investigation." *Journal of Sound and Vibration* 329(10) (2010), pp. 1793–1808 (cit. on p. 57)

Karlsson, M. and Åbom, M.
"Quasi-steady model of the acoustic scattering properties of a T-junction." *Journal of Sound and Vibration* 330(21) (2011), pp. 5131–5137 (cit. on p. 56)

Kim, H.-D., Kweon, Y.-H., and Setoguchi, T.
"A study of the weak shock wave propagating through an engine exhaust silencer system." *Journal of sound and vibration* 275(3) (2004), pp. 893–915 (cit. on p. 71)

Lax, P. D.
Hyperbolic systems of conservation laws and the mathematical theory of shock waves. SIAM 1973 (cit. on p. 33)

Lax, P. D. and Wendroff, B.
"Difference schemes for hyperbolic equations with high order of accuracy." *Communications on pure and applied mathematics* 17(3) (1964), pp. 381–398 (cit. on p. 76)

Lax, P. and Wendroff, B.
"Systems of conservation laws." *Communications on Pure and Applied mathematics* 13(2) (1960), pp. 217–237 (cit. on p. 37)

Lerat, A. and Peyret, R.
"Non-centred schemes and shock propagation problems." *Computers and fluids* (1974), pp. 35–52 (cit. on p. 40)

Liu, J., Schorn, N., Schernus, C., and Peng, L.
Comparison studies on the method of characteristics and finite difference methods for one-dimensional gas flow through IC engine manifold. SAE Technical Paper 960078 1996 (cit. on p. 23)

MacCormack, R. W.
"The effect of viscosity in hypervelocity impact cratering." *Frontiers of Computational Fluid Dynamics* (1969), pp. 27–44 (cit. on p. 39)

Montenegro, G., Della Torre, A., Onorati, A., and Fairbrother, R.
"A nonlinear Quasi-3D approach for the modeling of mufflers with perforated elements and sound-absorbing material." *Advances in Acoustics and Vibration* 2013 (2013) (cit. on pp. 5, 70–72, 76, 78, 90, 179)

Montenegro, G. and Onorati, A.
"A coupled 1D-multiD nonlinear simulation of IC engine silencers with perforates and sound-absorbing material." *SAE International Journal of Passenger Cars-Mechanical Systems* 2(2009-01-0305) (2009), pp. 482–494 (cit. on pp. 4, 70)

Montenegro, G., Onorati, A., and Della Torre, A.
"The prediction of silencer acoustical performances by 1D, 1D–3D and quasi-3D non-linear approaches." *Computers & Fluids* 71 (2013), pp. 208–223 (cit. on pp. 4, 59, 72, 151)

Montenegro, G., Onorati, A., Piscaglia, F., and D'Errico, G.
Integrated 1d-multid fluid dynamic models for the simulation of ice intake and exhaust systems. SAE Technical Paper 2007-01-0495 2007 (cit. on p. 58)

Montenegro, G., Della Torre, A., Onorati, A., Fairbrother, R., and Dolinar, A.
Development and application of 3D generic cells to the acoustic modelling of exhaust systems. SAE Technical Paper 2011-01-1526 2011 (cit. on pp. 4, 59)

Morel, T., Keribar, R., and Blumberg, P. N.
A new approach to integrating engine performance and component design analysis through simulation. SAE Technical Paper 880131 1988 (cit. on pp. 70, 71)

Morel, T., Morel, J., and Blaser, D. A.
Fluid dynamic and acoustic modeling of concentric-tube resonators/silencers. SAE Technical Paper 910072 1991 (cit. on p. 121)

Morel, T., Silvestri, J., Goerg, K.-A., and Jebasinski, R.
Modeling of engine exhaust acoustics. SAE Technical Paper 1999-01-1665 1999 (cit. on pp. 4, 59, 70, 72)

Mucklow, G. and Wilson, A.
"Wave-Action in Gases: The Attenuation and Reflection of Compression Waves Propagated in Pipes: Part I-Wave Attenuation; Part II-Wave Reflection." *Proceedings of the Institution of Mechanical Engineers* 169(1) (1955), pp. 69–82 (cit. on p. 97)

Munjal, M. L.
Acoustics of ducts and mufflers with application to exhaust and ventilation system design. John Wiley & Sons 1987 (cit. on pp. 121, 122)

Naeimi, H., Domiry, G. D., Gorji, M., Javadirad, G., and Keshavarz, M.
"A parametric design of compact exhaust manifold junction in heavy duty diesel engine using CFD." *Thermal Science* 15(4) (2011), pp. 1023–1033 (cit. on p. 57)

Onorati, A. and Ferrari, G.
Modeling of 1-D unsteady flows in IC engine pipe systems: numerical methods and transport of chemical species. SAE Technical Paper 980782 1998 (cit. on p. 25)

Onorati, A., Montenegro, G., D'Errico, G., and Piscaglia, F.
Integrated 1d-3d fluid dynamic simulation of a turbocharged diesel engine with complete intake and exhaust systems. SAE Technical paper 2010-01-1194 2010 (cit. on p. 58)

OpenWAM
CMT - Motores Térmicos. Universidad Politécnica de Valencia. URL: `http://www.OpenWAM.org` (cit. on pp. 150, 179)

Paul, J., Selamet, A., Miazgowicz, K., and Tallio, K.
Combining flow losses at circular T-junctions representative of intake plenum and primary runner interface. SAE Technical Paper 2007 (cit. on p. 58)

Payri, F., Benajes, J., Galindo, J., and Serrano, J.
"Modelling of turbocharged diesel engines in transient operation. Part 2: wave action models for calculating the transient operation in a high speed direct injection engine." *Proceedings of the type of Mechanical Engineers, Part D: Journal of Automobile Engineering* 216(6) (2002), pp. 479–493 (cit. on p. 5)

Payri, F., Benajes, J., and Reyes, M.
"Modelling of supercharger turbines in internal-combustion engines." *International Journal of Mechanical Sciences* 38(8) (1996), pp. 853–869 (cit. on p. 5)

Payri, F., Desantes, J., and Broatch, A.
"Modified impulse method for the measurement of the frequency response of acoustic filters to weakly nonlinear transient excitations." *The Journal of the Acoustical Society of America* 107(2) (2000), pp. 731–738 (cit. on pp. 126, 128, 131, 150)

Payri, F., Desantes, J., and Corberán, J.
"A quasi-steady model on gas exchange process, some results." *Motor Sympo'88* (1988) (cit. on p. 5)

Payri, F., Desantes, J., and Torregrosa, A.
"Acoustic boundary condition for unsteady one-dimensional flow calculations." *Journal of Sound and Vibration* 188(1) (1995), pp. 85–110 (cit. on pp. 70, 98, 100)

Payri, F., Galindo, J., and Serrano, J.
"Variable geometry turbine modelling and control for turbocharged Diesel engine transient operation." In: *Thermo-and Fluid-dynamic Processes in Diesel Engines: Selected Papers from the THIESEL 2000 Conference Held in Valencia, Spain, September 13-15, 2000*. Springer Verlag 2002, p. 189 (cit. on p. 5)

Payri, F., Reyes, E., and Serrano, J.
A model for load transients of turbocharged diesel engines. SAE Technical Paper 1999-01-0225 1999 (cit. on p. 5)

Payri, F., Torregrosa, A., and Chust, M.
"Application of MacCormack schemes to IC engine exhaust noise prediction." *Journal of Sound and Vibration* 195(5) (1996), pp. 757–773 (cit. on pp. 3, 70)

Payri, F., Reyes, E., and Galindo, J.
"Analysis and modeling of the fluid-dynamic effects in branched exhaust junctions of ICE." *Journal of engineering for gas turbines and power* 123(1) (2001), pp. 197–203 (cit. on pp. 3, 56, 70)

Pearson, R., Bassett, M., Batten, P., Winterbone, D., and Weaver, N.
Multi-dimensional wave propagation in pipe junctions. SAE Technical Paper 1999-01-1186 1999 (cit. on p. 58)

Pearson, R. and Winterbone, D.
"The simulation of gas dynamics in engine manifolds using non-linear symmetric difference schemes." *Proceedings of the type of Mechanical Engineers, Part C: Journal of Mechanical Engineering Science* 211(8) (1997), pp. 601–616 (cit. on p. 71)

Pérez-García, J., Sanmiguel-Rojas, E., Hernández-Grau, J., and Viedma, A.
"Numerical and experimental investigations on internal compressible flow at T-type junctions." *Experimental thermal and fluid science* 31(1) (2006), pp. 61–74 (cit. on p. 57)

Pérez-García, J., Sanmiguel-Rojas, E., and Viedma, A.
"New coefficient to characterize energy losses in compressible flow at T-junctions." *Applied Mathematical Modelling* 34(12) (2010), pp. 4289–4305 (cit. on p. 58)

Peters, B. and Gosman, A.
Numerical simulation of unsteady flow in engine intake manifolds. SAE Technical Paper 930609 1993 (cit. on p. 58)

Reyes, M.
"Contribución al Modelado del Proceso de Transferencia de calor en Colectores de Escape de Motores Alternativos." PhD thesis. Tesis Doctoral, Universidad Politécnica de Valencia 1993 (cit. on p. 5)

Richtmyer, R. D. and Morton, K. W.
"Difference methods for initial-value problems." *Malabar, Fla.: Krieger Publishing Co.,| c1994, 2nd ed.* (1994) (cit. on p. 39)

Riemann, B. et al.
Über die Fortpflanzung ebener Luftwellen von endlicher Schwingungsweite. Verlag der Dieterichschen Buchhandlung 1860 (cit. on p. 25)

Roe, P. L.
"Approximate Riemann solvers, parameter vectors, and difference schemes." *Journal of computational physics* 43(2) (1981), pp. 357–372 (cit. on p. 44)

Sakowitz, A., Mihaescu, M., and Fuchs, L.
"Turbulent flow mechanisms in mixing T-junctions by Large Eddy Simulations." *International Journal of Heat and Fluid Flow* 45 (2014), pp. 135–146 (cit. on p. 57)

Sapsford, S. M., Richards, V. C., Amlee, D. R., Morel, T., and Chappell, M. T.
Exhaust system evaluation and design by non-linear modeling. SAE Technical Paper 920686 1992 (cit. on pp. 4, 59, 72, 122)

Schmandt, B. and Herwig, H.
"The head change coefficient for branched flows: Why "losses" due to junctions can be negative." *International Journal of Heat and Fluid Flow* 54 (2015), pp. 268–275 (cit. on pp. 57, 148)

Serrano, J. R., Arnau, F. J., Martin, J., Hernandez, M., and Lombard, B.
Analysis of Engine Walls Thermal Insulation: Performance and Emissions. SAE Technical Paper 2015 (cit. on p. xii)

Serrano, J.
"Análisis y modelado del transitorio de carga en motores turboalimentados de encendido por compresión." PhD thesis. PhD thesis, Universidad Politécnica de Valencia, Spain 1999 (cit. on p. 5)

Shaw, C., Lee, D., Richardson, S., and Pierson, S.
Modelling the effect of plenum-runner interface geometry on the flow through an inlet system. SAE Technical Paper 2000 (cit. on p. 57)

Sod, G. A.
"A survey of several finite difference methods for systems of nonlinear hyperbolic conservation laws." *Journal of computational physics* 27(1) (1978), pp. 1–31 (cit. on pp. 82, 83, 101)

Steger, J. L. and Warming, R.
"Flux vector splitting of the inviscid gasdynamic equations with application to finite-difference methods." *Journal of computational physics* 40(2) (1981), pp. 263–293 (cit. on p. 42)

Sweby, P. K.
"High resolution schemes using flux limiters for hyperbolic conservation laws." *SIAM journal on numerical analysis* 21(5) (1984), pp. 995–1011 (cit. on pp. 49, 54, 80)

Tang, S.
"Sound transmission characteristics of Tee-junctions and the associated length corrections." *The Journal of the Acoustical Society of America* 115(1) (2004), pp. 218–227 (cit. on p. 56)

Toro, E. F., Spruce, M., and Speares, W.
"Restoration of the contact surface in the HLL-Riemann solver." *Shock waves* 4(1) (1994), pp. 25–34 (cit. on pp. 47, 153)

Torregrosa, A., Broatch, A., Arnau, F., and Hernández, M.
"A non-linear quasi-3D model with Flux-Corrected-Transport for engine gas-exchange modelling." *Journal of Computational and Applied Mathematics* 291 (2016), pp. 103–111 (cit. on pp. xi, 71, 72, 76, 179)

Torregrosa, A., Broatch, A., Arnau, F., and Hernández, M.
"On the effect of different flux limiters on the performance of an engine gas exchange gas-dynamic model." *International Journal of Mechanical Sciences* (2017) (cit. on pp. xi, 71, 76, 179)

Torregrosa, A., Broatch, A., Fernández, T., and Denia, F.
"Description and measurement of the acoustic characteristics of two-tailpipe mufflers." *The Journal of the Acoustical Society of America* 119(2) (2006), pp. 723–728 (cit. on p. 150)

Torregrosa, A., Broatch, A., Gil, A., and Moreno, D.
"Analysis of acoustic networks including cavities by means of a linear finite volume method." *Journal of Sound and Vibration* 331(20) (2012), pp. 4575–4586 (cit. on pp. 70, 120, 122, 129)

Torregrosa, A., Fajardo, P., Gil, A., and Navarro, R.
"Development of non-reflecting boundary condition for application in 3D computational fluid dynamics codes." *Engineering Applications of Computational Fluid Mechanics* 6(3) (2012), pp. 447–460 (cit. on p. 100)

Torregrosa, A. J., Broatch, A., García-Cuevas, L. M., and Hernández, M.
"A Study of the Transient Response of Duct Junctions: Measurements and Gas-Dynamic Modeling with a Staggered Mesh Finite Volume Approach." *Applied Sciences* 7(5) (2017), p. 480 (cit. on pp. xi, 3, 181)

Van Leer, B.
"Towards the ultimate conservative difference scheme I. The quest of monotonicity." In: *Proceedings of the Third International Conference on Numer-*

ical Methods in Fluid Mechanics. Springer 1973, pp. 163–168 (cit. on p. 55)

Van Leer, B.
"Towards the ultimate conservative difference scheme. V. A second-order sequel to Godunov's method." *Journal of computational Physics* 32(1) (1979), pp. 101–136 (cit. on p. 153)

Vandevoorde, M., Vierendeels, J., Dick, E., and Sierens, R.
"A new total variation diminishing scheme for the calculation of one-dimensional flow in inlet and exhaust pipes of internal combustion engines." *Proceedings of the type of Mechanical Engineers, Part D: Journal of Automobile Engineering* 212(5) (1998), pp. 437–448 (cit. on p. 71)

Wallace, F. and Boxer, G.
"Wave action in diffusers for exhaust-pipe systems, with special reference to the scavenging of two-stroke engines." *Proceedings of the type of Mechanical Engineers* 170(1) (1956), pp. 1131–1156 (cit. on p. 24)

William-Louis, M., Ould-El-Hadrami, A., and Tournier, C.
"On the calculation of the unsteady compressible flow through an N-branch junction." *Proceedings of the type of Mechanical Engineers, Part C: Journal of Mechanical Engineering Science* 212(1) (1998), pp. 49–56 (cit. on p. 58)

Winterbone, D., Pearson, R., and Zhao, Y.
"Numerical simulation of intake and exhaust flows in a high speed multi-cylinder petrol engine using the Lax-Wendroff method." *I Mech E, C* 430 (1991), p. 038 (cit. on p. 25)

Winterbone, D. E. and Pearson, R. J.
Design techniques for engine manifolds: wave action methods for IC engines. Professional Engineering Publishing 1999 (cit. on pp. 3, 31, 56, 70)

Winterbone, D. E. and Pearson, R. J.
Theory of engine manifold design: wave action methods for IC engines. Wiley-Blackwell 2000 (cit. on p. 15)

Zehnder, G.
"Calculating gas flow in pressure-wave machines." *Brown Boveri Review* 58(4-5) (1971), p. 172 (cit. on p. 25)